

Biochemical Studies of Cutaneous Damage in Mouse Models of Insulin Resistance and Obesity

Amgad Alhabian

Clore Laboratory
University of Buckingham

A thesis submitted in fulfilment of the requirements for the degree
Doctor of Philosophy

December 2014

DECLARATION

I hereby declare that this thesis is my own work and no part of it has been submitted previously anywhere for any other degree. I have received technical assistance from Mr Edward Wargent, Mr David Hislop during tissue's collection, and from Dr Mohamed Zaïbi during the *in vitro* phase. The sources of information in this thesis have been duly acknowledged.

Amgad Alhabian

December 2014

Acknowledgements

First and foremost, all thanks to Allah the Almighty for blessing me with the strength to achieve this goal.

I cannot find words to express my sincere gratitude to my first supervisor **Dr. Kenneth Langlands** for his guidance, understanding, patience, and editorial advice was essential to the completion of this thesis and has taught me innumerable lessons and insights on the workings of academic research in general, and most importantly, his friendship during these years.

I also gratefully acknowledge my second supervisor **Dr. Claire Stocker**. Without her encouragement and patience I would not have been writing this thesis. Her mentorship was paramount in providing a well-rounded experience, excellent guidance, caring, patience, and providing me with an excellent atmosphere for doing research.

I am most fortunate to have had the chance to carry out my thesis project with Professor Mike Cawthorne and highly thank him for his sincere assistance when he gave me the opportunity to work with one of the world's most respected research groups. It is not often that one finds such a great environment like the Clore laboratory where you meet both research advisors and colleagues that always find the time for listening to the little problems and roadblocks that unavoidably crop up in the course of performing research. Through the course of my DPhil there have been a number of unforgettable people who have helped me along the way, and I am very proud to work with them; Dr Joanne Selway, Mrs Parvathy Harikumar (for the great contribution in the histology method paper). I highly thank Mr Osman Osman, Dr Maysson Al-haj Ibrahim, Dr Hisham Al-Assam, Dr Malgosia Kępczyńska, Mr Avijit Guha Roy, Dr Jwan Razak Jaf, Dr Jacqueline O'Dowd, Professor Jon Arch, Miss Julie Cakebread, Mrs Anita Roberts, Mr David Hislop and Mr Edward Wargent for unique insights.

I would like to thank Dr Mohamed Zaïbi for his technical help *in vitro* studies, and Dr Mauricio da Silva Krause, and Professor Philip Newsholme from the Department of Physiology, Institute of Basic Health Sciences, Federal University of Rio Grande do Sul, Porto Alegre, Brazil for his generous donation of insulin receptor β -subunit antibody and preparing the western blotting experiment. I gratefully acknowledge the

Ministry of Higher Education in Syria for funding part of this project.

I thank my spiritual father **Muthanna** for his faith in me and allowing me to be as ambitious as I wanted. I would like to thank my family (mom and **Ahmad**, Eman, Farah, and Ibrahim) for having faith in the choices I have made. It was under their watchful eye that I gained so much drive and an ability to tackle challenges head on.

Finally, and most importantly, I would like to thank my beloved wife **Shaherah** for her understanding and love during the past few years, support, encouragement, quiet patience and unwavering love were undeniably the bedrock upon which the past ten years of my life have been built. Her tolerance of my occasional vulgar moods is a testament in itself of her unyielding devotion and love. She was always there cheering me up and stood by me through the good times and bad. Her support and encouragement was in the end what made this thesis possible and for her I dedicate this work.

Abstract

Mammalian skin is a highly-specialised organ, providing a robust barrier against environmental challenges. In order to maintain functional integrity and a healthy state, the skin's constituent tissues undergo continuous renewal, controlled by finely-controlled homeostatic mechanisms. Skin disease is incredibly common, ranging from debilitating (but not life threatening) disorders such as acne or eczema to increasingly aggressive, pernicious disorders like psoriasis, through to neoplasms such as carcinomas and melanoma. Importantly, the skin may present manifestations of systemic disease such as in diabetes, obesity, cardiovascular diseases (CVD) and metabolic syndrome (Azfar and Gelfand, 2008, Van Hattem et al., 2008, Nawale et al., 2006). Such cutaneous alterations could be the first signs of the disease, and may precede diagnosis by many years.

The integrity of the skin degrades with age, and numerous metabolic disorders lead to pathological conditions that exacerbate this process (Nikolakis et al., 2013). For example, the vast majority of individuals suffering from type 2 diabetes will experience skin complications during the natural history of their disease, especially with years of poorly- controlled plasma glucose (Romano et al., 1998, Levy and Zeichner, 2012). Problems range from the sub-clinical, such as neuropathy, chronic inflammation micro- and macrovascular damage and collagen disorganisation, which lead to potentially catastrophic events such as delayed wound healing, ulceration, infection and gangrene. Proactive control of the glycaemic state may prevent or delay many of these associated complications, but it may not reverse pathological changes once established.

Obesity and related risk factors in humans are associated with increased fat deposition, with many studies documenting the abnormal structure and function of dermal adipose tissue. Impaired fibroblasts function may contribute to many dermatological changes, such as the loss of dermis or fibrosis, via mechanisms related to insulin signalling (Rivera-Gonzalez et al., 2014). However, the dysfunction of dermal adipocyte which is characterised by adipocyte hyperplasia and hypertrophy, hypoxia, elevated inflammation, and adipokines signalling are now emerging as a potential mediator of insulin-resistance (Klötting and Blüher, 2014). Thus it is possible that the chronic exposure of fibroblasts to adipokines underlies their impaired function.

Although many reports describe the use of mouse skin to reveal insights into aspects of human disease pathology and aetiology, it remains a challenge to find a standard protocol that can create optimal sections, retaining the intrinsic structure of mouse skin effectively, and researchers tend to use human skin histology protocols. This is not necessarily acceptable when one considers the anatomical differences between human and mice (Treuting and Dintzis, 2011). Mouse skin is thinner and more fragile than human skin, and so loss of architecture during processing has implications for downstream applications. Obtaining good histology from diabetic mouse skin, and maintaining subcutaneous adipocytes architecture and the discrimination of components such as fine elastic fibres, present a considerable challenge. Therefore, great care must be taken when selecting the conditions, particularly fixative type, to ensure that meaningful conclusions may be drawn (Al-Habian et al., 2014). The skin sections from mouse models used in chapter 3 were prepared using best practice at the time for a retrospective study, but I was able to better histology at the cost of time and materials in sectioning and staining by using tissue macroarrays techniques. Thus, for prospective analysis of mouse skin histology I revised some histology methods. By evaluating the processing protocol and then four commonly used fixatives I enhanced IHC, and histomorphological analysis of normal mouse skin. Moreover, these histopathology techniques are applicable to different mouse tissues, and I recommend using these findings as a guideline not only for diabetic mouse skin histology but for many tissues derived from a variety of species.

The dermatologic sequelae of type 2 diabetes mellitus are manifold. Murine models of insulin resistance are useful in elucidating molecular mechanisms of impaired wound healing, but little is known of other pathophysiological changes in these models. A variety of histological and *in vitro* techniques were used in this thesis to study skin organisation in environmental (diet-induced obesity) and genetic (C57BL/6 *Lepob/Lepob* and C57BLKS/J *Leprdb/Leprdb*) models of insulin resistance, type 2 diabetes mellitus, and in chronological age. An expanded subcutis was accompanied by progressive dermal erosion in which the papillary dermis was spared at the expense of the deeper reticular layer as insulin resistance increased. Elastosis was also observed in our models, but damage was not accompanied by an increase in immune infiltration, nor an increase in advanced glycation end products. Altered epidermal differentiation was associated only with the most extreme obese phenotype.

Moreover, compromised fibroblast function was maintained *in vitro*, with C57BL/6 *Lepob/Lepob* cells displaying compromised growth and reduced collagen synthesis. While mouse skin does not necessarily model the range of cutaneous sequelae observed in human diabetic subjects, it is likely that underlying cellular mechanisms are shared. An improved understanding of the contribution of the layers of the skin, particularly the dermis during insulin resistance, and ageing and its pathological processes may provide new insights into the mitigation of damage. While impaired insulin signalling in skin is associated with disrupted skin homeostasis, and extra cellular matrix remodelling in ageing and type 2 diabetes mellitus (Nikolakis et al., 2013), a recent study has linked these changes to dermal fibroblast , and adipocyte dysfunction (Rivera-Gonzalez et al., 2014). Interestingly, our observation showed that both aged and *Lepob/Lepob* murine fibroblasts show lowered insulin receptor expression suggesting that this will be a fruitful area for future investigation for improving insulin sensitivity and glucose utilisation in the dermal layers could have important consequences for cutaneous health.

This thesis reports a specific pattern of cutaneous damage that is initiated before the onset of frank diabetes and is exacerbated with increasing insulin resistance. This work provides a new insight into the consequences of metabolic disease on skin structure. Finally, further insights into how dermal damage in genetically modified and environmentally adapted diabetic mouse models and vice versa are likely to subserve in detecting early signs of cutaneous insulin resistance and may likely offer better approaches to prevent or at least cure the dermatological sequelae of type 2 diabetes mellitus.

Abbreviations

α-ASMA	α -Smooth Muscle antibody
1°Ab	First antibodies
2°Ab	Secondary antibodies
ACM	Adipose conditioned medium
AF	Alcoholic formalin
AR	Antigen retrieval
AT	Adipose tissue
CD31	Cluster of differentiation 31
CD68	Cluster of differentiation 68
DEJ	Dermal-Epidermal Junction
DIO	Diet induced obesity
ECM	Extra cellular matrix
EGF	Epidermal growth factor
EtOH	Ethanol
FITC	Fluorescein isothiocyanate
G & O	Giemsa and orcein
GMCSF	Granulocyte macrophage colony-stimulatory factor
H&E	Haematoxylin and eosin
HIF1-α	Hypoxia-inducible factor 1- α
IFN	Interferon
IHC	ImmunoHistoChemistry
IL	Interleukins
K14	Keratin 14
MCP1	Macrophage chemo-attractant protein
MKC	Mouse keratinocyte-derived cytokine
MT	Masson Trichrome
NBF	Neutral buffered formalin
PAS	Periodic acid Schiff
PBS-T	Phosphate buffered saline with tween
PCNA	Anti-proliferating Cell Nuclear Antigen
PDGF	Platelet derived growth factor
PS	Picrosirius red
RAGE	Receptor for advanced glycation end products
RANTES	Regulated on activation, normal T cell expressed and secreted).
ROS	Reactive oxygen species
RT	Room temperature
SAT	Subcutaneous adipose tissue-
SC	Sub Cutaneous or subcutis
TGF	Transforming growth factor (TGF)
TIMP-1	Tissue inhibitors of metalloproteinases -1
TMA	Tissue macro arrays
TNF-α	Tumour necrosis factor - α
TRITC	Tetramethylrhodamine isothiocyanate
VEGF	Vascular endothelial growth factor
WAT	White adipose tissue
Wt	Wild-type
ZnF	zinc formalin

Table of Contents

1	Abstract	v
2	Abbreviations	viii
3	Table of Contents	ix
4	Table of Figures	xiii
5	Table of Tables.....	xvi
1	Chapter 1: Introduction	1
1.1	The skin in health and disease	2
1.2	The epidermis	2
1.2.1	The basal layer (or stratum basale)	5
1.2.2	The spinous layer (the stratum spinosum)	6
1.2.3	The granular layer	6
1.2.4	The clear layer (stratum lucidum)	6
1.2.5	The horny layer (stratum corneum).....	7
1.3	Other cells of the epidermis.....	7
1.3.1	Melanocytes	7
1.3.2	Merkel cells.....	7
1.3.3	Langerhans cells.....	8
1.3.4	The basement membrane or dermal-epidermal junction.....	8
1.4	The dermis	9
1.4.1	Dermal fibroblasts	11
1.4.2	Collagen	12
1.4.3	Elastic fibres.....	14
1.4.4	Other cells in the dermis	16
1.5	The hypodermis	17
1.6	Skin appendages	18
1.6.1	The hair	18
1.6.2	Sweat glands	19
1.6.3	Sebaceous glands	20
1.6.4	Cutaneous vasculature.....	20
1.6.5	Innervation	21
1.7	Obesity.....	21

1.7.1	Health complications.....	22
1.7.2	Diabetes mellitus.....	25
1.7.3	Underlying mechanisms in type 2 diabetes mellitus.....	26
1.7.4	Dermatological complications of type 2 diabetes, obesity and ageing	28
1.8	Hypothesis and aims of the thesis	35
2	Chapter 2: Material and Methods.....	38
2.1	Animals models and diet	39
2.1.1	C57B/6	39
2.1.2	Lepob/Lepob	39
2.1.3	Diet induced obesity model.....	40
2.1.4	Mouse models of ageing (old).....	40
2.1.5	C57BlKS/J (misty).....	40
2.1.6	<i>Leprdb/Leprdb</i>	40
2.2	Physiological measurements	40
2.2.1	Body weight	40
2.2.2	Body composition	41
2.2.3	Blood glucose.....	41
2.2.4	Plasma Insulin	42
2.2.5	Preparation of adipose tissue conditioned medium (ACM).....	42
2.2.6	Mesoscale.....	43
2.3	Histology methods.....	44
2.3.1	Tissue preparation and fixation.....	44
2.3.2	Tissue processing	44
2.3.3	Embedding	45
2.3.4	Sectioning.....	45
2.3.5	Tissue macro arrays (TMA) construction	45
2.3.6	Special histological stains	47
2.3.7	Morphology stain	47
2.3.8	Connective tissue stain.....	47
2.3.9	Elastic fibres and immune cells stain	49
2.3.10	Basement membrane and glycogen deposition.....	49
2.3.11	Chromogenic immunohistochemistry (IHC).....	50
2.3.12	Immunofluorescence	52
2.3.13	Antigen retrieval methods	54

2.4	ScanScope imaging protocol	55
2.5	Image capture and analysis.....	60
2.6	Preparation of dermal fibroblasts	61
2.6.1	Explant culture of dermal fibroblast	61
2.6.2	Enzymatic isolation of fibroblasts.....	62
2.6.3	Western blotting	62
2.6.4	Dermal fibroblast experiments	63
2.6.5	Statistical analysis	64
3	Chapter 3: Skin Histology of Mouse Models of Obesity and Type 2 Diabetes	65
3.1	Introduction	66
3.2	Materials and methods.....	67
3.2.1	Histology of diabetic mouse skin.....	67
3.3	Results	68
3.3.1	Murine models of obesity and diabetes.....	68
3.3.2	Cutaneous organizations in insulin resistance, obesity, and old mice models	69
3.3.3	Skin compartmental depth and body composition	70
3.3.4	ECM structure and immune infiltration	73
3.3.5	Epidermal differentiation markers	77
3.4	Discussion	79
4	Chapter 4: Optimising Histological Analysis of Normal Mouse Tissues	83
4.1	Introduction	84
4.2	Methods and results	86
4.2.1	Optimised processing of mouse tissues	86
4.2.2	Effect of fixation time and temperature	95
4.2.3	Reduction of endogenous peroxidases	99
4.2.4	Optimisation of primary antibody concentrations.....	100
4.2.5	Antigen retrieval.....	101
4.2.6	Effect of fixatives type on histological analysis	103
4.2.7	Elastic fibres and immune cells	106
4.2.8	Collagen fibre organisation	106
4.2.9	Immunostaining	108
4.2.10	Comparison of four fixatives for short and long time.....	113
4.2.11	Histological analysis of diabetic mouse skin fixed with AF.....	116

4.3	Discussion	119
5	Chapter 5: Cytokine Profiling and Dermal Fibroblast Culture	124
5.1	Introduction	125
5.2	Methods	127
5.2.1	Optimisation of dermal fibroblast culture protocol.....	127
5.3	Results	131
5.3.1	Plasma cytokine levels	131
5.3.2	Subcutaneous adipose conditioned medium	133
5.3.3	Epididymal adipose conditioned medium.....	134
5.3.4	Comparing cytokines profile from different cutaneous layers.....	135
5.3.5	Insulin receptor expression in normal and diabetic fibroblasts.....	138
5.3.6	Proliferation of <i>wt/wt</i> and <i>ob/ob</i> fibroblasts.....	138
5.3.7	Collagen production by <i>wt/wt</i> and <i>ob/ob</i> fibroblasts.....	140
5.3.8	Senescence in <i>wt/wt</i> and <i>ob/ob</i> fibroblasts.....	140
5.4	Discussion	141
6	Chapter 6: General Discussion and Future Work	146
6.1	General discussion.....	147
6.2	Conclusion.....	157
6.3	Future work	157
6.3.1	Dermal fibroblast physiology in insulin resistant models.....	157
6.3.2	The restoration of cutaneous insulin sensitivity and diabetic skin function 157	
6.3.3	Investigation of fibroblast/ keratinocyte interactions.....	159
6.3.4	Role of adipokine signalling in skin damage.	159
6.3.5	Studies of vasculature and epithelial appendages	160
7	References	161
8	Appendices.....	180

Table of Figures

Figure 1-11 Overview of skin organisation.	3
Figure 1-2 Haematoxylin and Eosin stained sections of human skin.	4
Figure 1-3 The layers of the epidermis.	5
Figure 1-4 Comparison between human skin sections stained with PAS and H&E to identify the DEJ.....	9
Figure 1-5 Human dermis stained with H&E.	10
Figure 1-6 Fibrotic plaque.....	12
Figure 1-7 Schematic diagram of collagen synthesis.....	13
Figure 1-8 Human skin sections stained for connective tissues.....	14
Figure 1-9 Elastic fibre organization of human skin.....	15
Figure 1-10 Elastic fibre organisation of human skin stained with Giemsa and Orcein.	16
Figure 1-11 Organization of the hair follicle.	19
Figure 1-12 Type 2 diabetes is characterized by three pathophysiological abnormalities.	27
Figure 1-13 Comparison of skin histomorphology from human and mouse stained with H&E.	30
Figure 2-1 Principle of the immunoassay with 7- spot microplate.	43
Figure 2-2 Tissue macro arrays (TMA) construction steps.	46
Figure 2-3 Schematic for the Imgescope™ software showing the scan area options setup.	56
Figure 2-4 Scanning and calibration optimizing steps with the Aperio Imagescope™ software.....	57
Figure 2-5 The scanning process.....	58
Figure 2-6 Snapshot review of a human skin sample at 1x magnification.	59
Figure 2-7 Human skin stained with G&O and scanned with the Aperio Imagescope.	60
Figure 3-1 Skin compartments and collagen changes from different mouse models.	70
Figure 3-2. Cutaneous phenotypes in animal models of insulin resistance.	72
Figure 3-3 Body composition of mouse models of obesity and diabetes, and age.	73
Figure 3-4 ECM organisation	74
Figure 3-5 Representative image for positive PAS stain in diabetic pancreas.	76
Figure 3-6 Representative images for expression of IHC with RAGE antibody.....	76
Figure 3-7 Macrophage infiltration, angiogenesis and epidermal maturation.	78
Figure 3-8 Involucrin immunoreactivity.....	79

Figure 4-1 H&E staining of tissues with standard and extended processing protocols. .	88
Figure 4-2 H&E staining of tissues prepared using the standard processing protocol. ..	90
Figure 4-3 H&E staining of tissues prepared with an extended processing protocol.	91
Figure 4-4 Antigen retrieval methods to reveal CD31 immunoreactivity	92
Figure 4-5 Representative images of immunofluorescent detection of CD31	93
Figure 4-6 Loss of sections from organ tissue arrays	94
Figure 4-7 Tissue macroarray overview	95
Figure 4-8 H&E staining of wt/wt skin fixed for 6 hours in 10%NBF at RT and 40°C.	96
Figure 4-9 PCNA immunoreactivity in <i>wt/wt</i> skin	97
Figure 4-10 Disrupted organisation in H&E stained <i>wt/wt</i> skin with 32 hour fixation. .	98
Figure 4-11 Effect of fixation time.	99
Figure 4-12 Endogenous peroxidase reduction skin from <i>wt/wt</i> mouse skin.	100
Figure 4-13 IHC detection of cutaneous markers.	103
Figure 4-14 H&E stained sections of mouse skin prepared with four different fixativ	104
Figure 4-15 Representative images of normal skin with PAS and G&O stained sections.	105
Figure 4-16 Collagen fibre organisation with different stains.	107
Figure 4-17 Immunodetection of K14 (A, B), involucrin (C, D) and PCNA (E, F) in mouse skin prepared with different fixatives.	109
Figure 4-18 H&E staining of wild-type mouse skin with four fixatives.....	113
Figure 4-19 Representative images of K14 immunohistochemistry after 6 hours (40°C) and 32 hour fixation in various solutions.....	114
Figure 4-20 Representative images of PCNA immunohistochemistry after 6 hours (40°C) and 32 hours fixation in various fixatives.....	115
Figure 4-21 Gross organisation of TMA sections with old and revised histological methods.	117
Figure 4-22 H&E stained sections of mouse skin.....	118
Figure 4-23 Different mouse models skin fixed in AF and stained with H&E.....	119
Figure 5-1 Mouse skin adipose tissue layers.	126
Figure 5-2 Explant culture of dermal fibroblasts from <i>wt/wt</i> mouse.	128
Figure 5-3 Preparation of dermal fibroblasts..	129
Figure 5-4 Use of collagen coated flasks to promote dermal fibroblast attachment and proliferation.....	130
Figure 5-55 Illustrative figure for outer and inner layer separation in <i>ob/ob</i> skin.....	135

Figure 5-6 Cytokine profiles from plasma and deferent skin compartment of <i>ob/ob</i> mice.	137
Figure 5-7 Insulin receptor (β -chain) expression in dermal fibroblasts.	138
Figure 5-8 Proliferation of normal and insulin resistance fibroblasts.	139
Figure 5-9 Proliferation of normal and insulin resistant fibroblasts.	139
Figure 5-10 Collagen production by <i>wt/wt</i> and <i>ob/ob</i> mice fibroblasts	140
Figure 5-11 Senescence assay in normal and insulin resistant fibroblasts.	141
Figure 6-1 Mouse collagen basket-weave structure prior to optimisation.	149
Figure 6-2 Improved collagen basket weave structure from mouse skin processed with the optimised techniques.	150
Figure 6-3 Signaling mechanisms leading to insulin resistance and endothelial dysfunction under obesity and type 2 diabetes	156
Figure 6-4 The effect of rosiglitazone on adipocyte size	159

Table of Tables

Table 1-1 Obesity-associated disorders.	23
Table 1-2 BMI classifications established by the WHO.	24
Table 1-3 Classifications of cutaneous manifestations associated with type 2 diabetes.	29
Table 1-4 Summary of the key differences between human and mouse skin.	31
Table 1-5 Reports describing common epidermal features in diabetic and ageing epidermis.	32
Table 1-6 Reports describing common features in diabetic and ageing dermis.	33
Table 1-7 Reports describing common features in diabetic and ageing hypodermis.	34
Table 2-1 Immunohistochemical chromogenic detection.	51
Table 2-2 Immunofluorescence protocol.	53
Table 2-3 Qualitative description of IHC images.	61
Table 3-1 Primary antibody dilution and antigen revival (AR) method.	68
Table 3-2 Body weight, fasting blood glucose and plasma insulin levels in murine models of obesity and type 2 diabetes.	69
Table 4-1 Optimised primary antibody dilutions, incubation conditions and antigen retrieval methods.	101
Table 4-2 Summary of special staining for 32 hour fixation.	111
Table 4-3 Summary of IHC results for 32 hours fixation.	112
Table 4-4 Optimisation of diabetic mouse skin histology and IHC.	121
Table 4-5 Recommended guidelines for diabetic mouse skin histology and IHC application.	123
Table 5-1 Critical parameters in primary dermal fibroblast culture.	128
Table 5-2 Plasma levels of cytokines from 3-4 animals per each group. Significant analysis was performed using unpaired two-tailed Student's t-test for each parameter.	132
Table 5-3 Cytokine profile from subcutaneous adipose conditioned medium (ACM) from 4 animals per each group. Significant analysis was performed using unpaired two-tailed Student's t-test for each parameter.	133
Table 5-4 Cytokine profile from epididymal adipose conditioned medium (ACM) from 4 animals per each group. Significant analysis was performed using unpaired two-tailed Student's t-test for each parameter.	134
Table 5-5 Summary of key cytokines in plasma, skin and adipose depots of <i>ob/ob</i> mice. Fold-change values compared to control animals are shown.	136

Chapter 1: Introduction

1.1 The skin in health and disease

Mammalian skin is comprised of three main layers; the outer epidermis, the dermis, and the deeper hypodermis, (Figure 1.1 and 1.2A). The skin contains a number of epithelial-derived structures, including sweat and sebaceous glands, and hair follicles, and is highly innervated and vascularised (Kanitakis, 2002). Moreover, the skin forms the integumentary system comprised of diverse tissue types. It is the largest mammalian organ, with many physiological, immunological and mechanical functions including, synthesis of vitamin D3, prevention of water loss, protection against the harmful effects of UV radiation, sensation, temperature control and immunological surveillance. It also makes a significant contribution to whole-body homeostasis (Machens et al., 2013), as well as having an important psychological and social role (Taylor et al., 1997). Therefore, an understanding of the sophisticated interplay of factors that maintain and repair the skin's integrity and function is essential if one is to gain meaningful insights into cutaneous physiology in health and disease.

Recent technological advances have revolutionised skin research, for example immunohistochemistry (IHC), confocal and electron microscopy, as well as molecular biology have yielded insights of both clinical and cosmetic relevance (Varghese et al., 2013). Not only has this led to a deeper understanding of cutaneous structure and function, but has also facilitated a more profound understanding of pathogenic mechanisms, with implications for the diagnosis and future treatment of dermatological diseases. It is useful to consider the individual structures of the layers of the skin, and these are described in the following sections.

1.2 The epidermis

The epidermis plays a vital role as it forms an external barrier with the environment, coordinating the inward/outward passage of water and electrolytes, controlling the loss of essential body fluids, limiting the penetration of toxic substances and preventing harmful effects of the sun and radiation (Cork et al., 2009). Microscopically, the epidermis consists of four distinct layers: the basal, spinous, granular and horny or cornified layers (as seen in Figure 1.2 B). It is separated from the underlying papillary dermis by a basement membrane (Ghadially, 2012).

The epidermis is comprised primarily of keratinocytes, and is in a constant state of self-renewal. Transit-amplifying cells progress from the basal epidermal layer to the surface, accompanied by a highly-regulated process of differentiation to create a new outer cornified layer every 28 to 30 days (Archer, 2004). This is associated with the production and assembly of a range intermediate filaments to produce a resilient barrier (Simon and Green, 1984). The epidermis is also populated by various migratory cell types that include pigmented melanocytes, dendritic Langerhans cells and sensory Merkel cells (described below). It remains, to an extent, enigmatic precisely how these cells proliferate, stratify and differentiate into such an organised tissue, but a complex network of cytokines are central to this process. Cytokines are also involved in mediating the inflammatory and immune responses in the skin (Ansel et al., 1990).

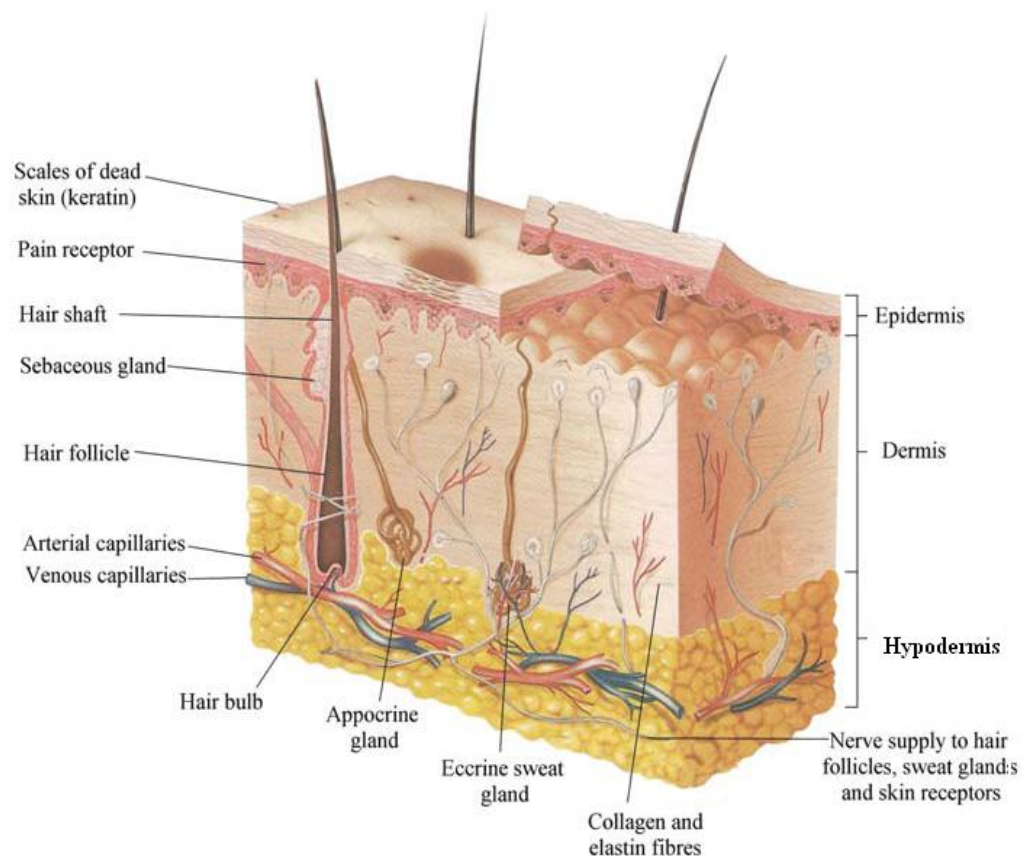


Figure 1-1 Overview of skin organisation.

Adapted from (Wang and Sanders, 2005).

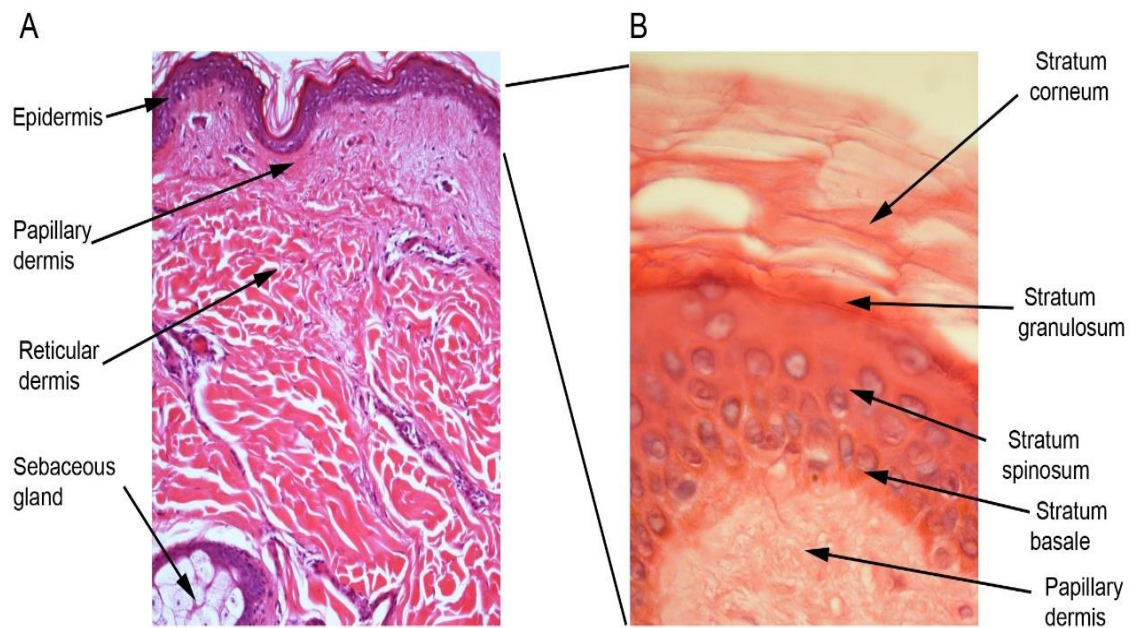


Figure 1-2 Haematoxylin and Eosin stained sections of human skin.

Images are shown at 20x original magnification (A), and at 50x original magnification (B) to highlight the epidermal layers.

Whilst a number of cell types in the epidermis are capable of secreting cytokines including Langerhans cells, melanocytes and Merkel cells (Wilhelm et al., 2010), keratinocytes are the major source of cytokines in the epidermis. These include interleukins (IL) -1, 6, 8, tumour necrosis factor (TNF)- α , transforming growth factor (TGF) - α and - β , fibroblast growth factor (FGF), epidermal growth factor (EGF), platelet derived growth factor (PDGF), interferon (IFN) - α and - γ , and granulocyte macrophage colony-stimulatory factor (GM-CSF) (Shiraki et al., 2006). The individual layers are described below.

1.2.1 The basal layer (or stratum basale)

This is the deepest layer of the epidermis, and forms a single layer of cells in normal mammalian skin, although this may increase in hyper-proliferative conditions (Lippens et al., 2000). Cells comprising this layer are relatively small, with a dense cytoplasm and nuclei (as seen in Figure 1.3). Compartmental integrity and cell-cell communication in the stratum basale are provided by desmosomes, while the basal cells are attached to the basement membrane and dermal extracellular matrix (ECM) via hemi-desmosomes (McMillan and Shimizu, 2001).

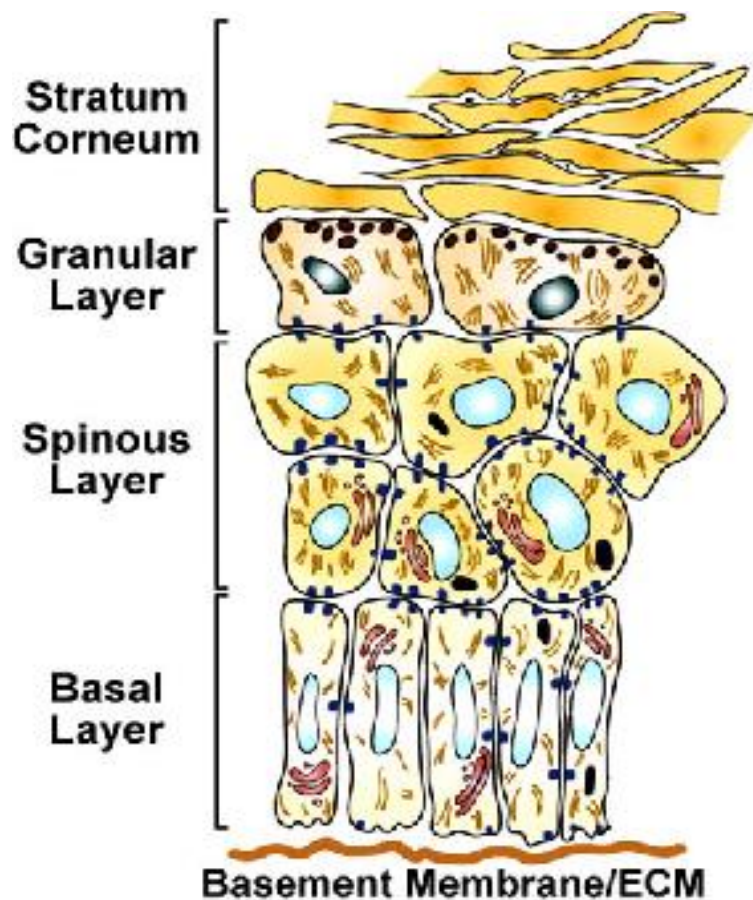


Figure 1-3 The layers of the epidermis.

Adapted from the University of New South Wales Embryology Web (embryology.med.unsw.edu.au).

The basal layer also harbours a population of stem cells that divide to form transit-amplifying cells with a limited proliferative capacity (Balaji et al., 2010). The maintenance of balance between proliferation and differentiation is critical to a

functional epidermal barrier, along with the maintenance of effective cell-cell contacts. For example, disorders such as epidermolysis bullosa sequela, degradation of collagen type VII, result in a failure to attach to the basement membrane causing severe blistering (Chen et al., 1997). The cytoskeleton of basal cells is characterised by the presence of keratins 5 and 14 (Haake et al., 2001).

1.2.2 The spinous layer (the stratum spinosum)

Above the basal layer is the spinous layer, which is generally 5-10 cell layers deep, with cells attached by desmosomes, as a consequence of the spiny extensions that appear to connect these cells in histological sections, it is called also called the 'prickle-layer'. The profile of intermediate filament expression is distinct with a progressive decrease in keratins K5 and K14, and an increase in keratins such as K1 and K10 (Wikramanayake et al., 2014).

1.2.3 The granular layer

The granular layer is 3-5 cells thick deep, and keratinocytes of this layer are characterised by intracellular granules of keratohyalin (irregular, amorphous granules filled with profilaggrin critical to the keratinization process in its cleaved form). Expression of proteins such as involucrin and loricrin, which are components of cornified envelopes are detectable in this layer. These cells are progressively characterized by a flattened shape and begin to lose their nuclei as they transit upwards. In addition to profilaggrin, the granules in this layer contain many compounds such as carbohydrates, various proteins, free sterols, lipids and hydrolytic enzymes. Basal phospholipids are gradually replaced by ceramides, which are the most abundant lipids in the outer layers, and play a crucial role in epidermal barrier function (Das et al., 2009). Pathological processes that disrupt to this layer can result from viral infection or chemical irritation (Baden et al., 1974) (Fernandez-Flores, 2009).

1.2.4 The clear layer (stratum lucidum)

This layer is most apparent in thick skin and is named after its translucent appearance, presenting a thin layer of flattened, non-nucleated eosinophilic cells containing densely packed cytoplasmic keratin filaments (Walli, 2009).

1.2.5 The horny layer (stratum corneum)

The stratum corneum is the outmost layer of the epidermis and is composed of 15-20 cell layers of corneocytes, which are terminally-differentiated keratinocytes. The upper layers are comprised of completely anucleate, keratinized cells, creating what is often referred to as the horny layer, the outer cells of which are eventually shed by the desquamation process. Under the electronic microscope, dead keratinocytes in the cornified layer appear to be filled with keratin filaments that are lined with a marginal band (the cornified cell envelope) (Burns et al., 2010). The main compounds of the cornified envelope are the proteins involucrin and loricrin, which are cross-linked by transglutaminase enzymes and filaggrin that promotes the condensation of intermediate filaments (Jain, 2012). The cornified cell envelope serves as a peripheral, resilient barrier against physicochemical factors and water loss from the body (Ghadially et al., 1995a).

1.3 Other cells of the epidermis

While 95% of the cells of the epidermis are keratinocytes, they also interact with migratory cells such as melanocytes, Langerhans cells and Merkel cells. These cells all play a fundamental role in orchestrating skin physiology as described below.

1.3.1 Melanocytes

Melanocytes originate from the neural crest (ectoderm)-derived dendritic cells, and are found randomly dispersed in the basal layer. Melanocytes produce the pigment melanin (Sturm et al., 1998). Under light microscopy with routine H&E staining (Figure 1.4.A arrow), melanocytes have small, dark nuclei and clear cytoplasm (Droste, 2007). Depending on the location of the melanocytes (for example interfollicular epidermis, hair or iris), pigmentation may vary from black to brown to yellow (Burns et al., 2010). Melanin is delivered to the growing hair shaft, and to adjacent interfollicular keratinocytes by mature melanosomes, and this aggregates to form an umbrella-like shape conferring protection from UV rays by the absorption and scattering of incident light, as well as by scavenging reactive oxygen species (Solano, 2014). Recently, melanocytes have emerging as active players, like keratinocytes, in cutaneous immune responses, due to their synthesis and sensitivity to a variety of cytokines (Plonka et al., 2009).

1.3.2 Merkel cells

Merkel cells are located in the basal layer, hair follicles and sweat ducts, with greater numbers in the fingers and oral mucosa (Burns et al., 2013). They are rarely visible under light microscopy, rather identification requires electron microscopy and immunostaining. Their full functions have not yet been elucidated in human skin, but there is growing evidence that they act as touch receptors, providing tactile information to the sensory nerves via neurotransmitter secretion after physical stimulation (Maksimovic et al., 2014).

1.3.3 Langerhans cells

Langerhans cells (LCs) are dendritic cells derived from bone marrow precursors that serve as antigen presenting cells (APCs). LCs are integral to immune surveillance in the skin due to their ability to initiate an immune response through antigen uptake, processing, migration and presentation to T cells (Bodey et al., 2004). Functionally, LCs are primarily responsible for capturing pathogenic factors that the skin encounters, and so provide a primary defence against infection. Ultra-structurally, LCs are migratory dendritic cells without tonofilaments, and cell attachment structures such as desmosomes, and are characterised by antigen containing tennis racquet shaped Birbeck granules (Shimizu, 2007).

1.3.4 The basement membrane or dermal-epidermal junction

The boundary between the epidermis and the dermis consists of a special aggregation of attachment molecules collectively known as dermal-epidermal junction (DEJ) or BM (basement membrane) zone (Rook et al., 1986). It serves as an important physical interface between the epidermis and the dermis, enhanced by a partial penetration of the BM into the papillary dermis via irregular finger-like projections known as the rete-ridges (Terstappen, 2008). These cone-shaped structures help in increasing the surface area of the epidermis, vasculature and lymphatics of the upper part of the dermis, and play a crucial role in controlling the exchange rate of nutrients and cell migration (Terstappen, 2008).

Interestingly, as a person ages, the convoluted rete-ridges of the DEJ flatten out, resulting in reduced contact with the dermal vasculature network, and a reduction in exchange of material. However, these changes not only take place in age but also in diseases such as diabetes where rete-ridges compromised, either by flattening or by extension deeper into the dermis. Other disorders, such as lentigo, impact the integrity

of the DEJ (Farage et al., 2009). DEJ cannot be observed using routine H&E staining (Figure 1.4.A) but rather with special staining protocols such as periodic acid Schiff (PAS) staining which interacts with glyco- proteins and mucopolysaccharides to reveal the DEJ as a thin purple band (Figure.1.4.B).

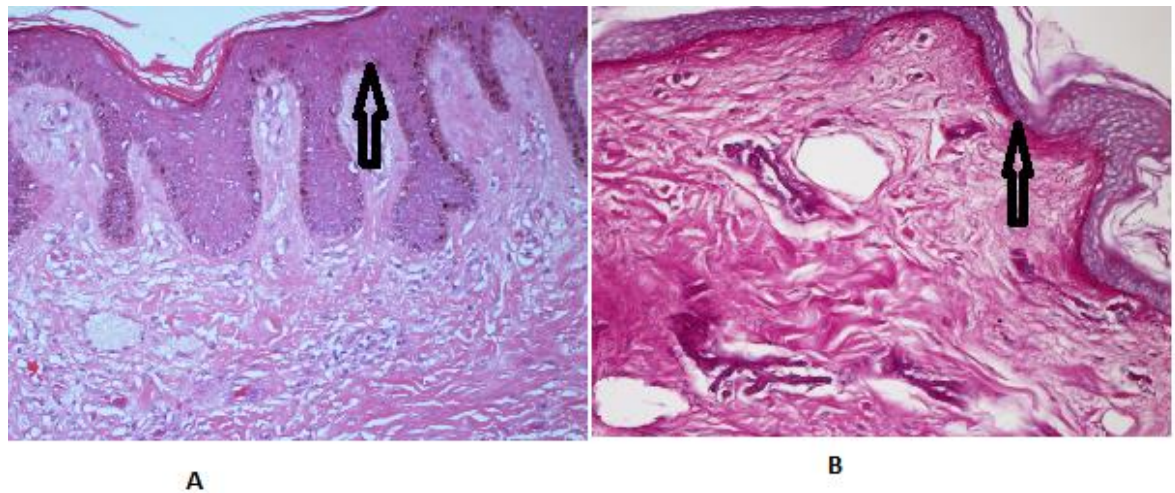


Figure 1-4 Comparison between human skin sections stained with PAS and H&E to identify the DEJ.

With H&E staining, the DEJ cannot be discerned (A). The arrow identifies the DEJ in part as shown in B. Both images were captured at 20x original magnification.

1.4 The dermis

The dermis is, by mass, the largest component of the skin in lean individuals. It varies in thickness from 5mm on the back to 1mm on the eyelids in man (James et al., 2011). The dermis consists primarily of an extracellular matrix comprised of unbranched collagens arranged in a basket-weave conformation, elastic fibres and “ground substance” (mainly glycosaminoglycans such as hyaluronan. The ECM is populated by dermal fibroblasts, and highly vascularised but, unlike the epidermis, this tissue is innervated and host to migratory cells of the immune system, notably mast cells, dendritic cells, macrophages, lymphocytes, eosinophils and plasma cells (Burns et al., 2010). It also is likely to host a variety of stem cells (McGrath et al., 2010). The mammalian dermis is organized into a thinner upper papillary layer comprised of fine fibres (Figure 1.5A), and a thicker lower reticular layer comprised of coarser fibres (Figure1.5 B). The superficial papillary dermis forms an uneven junction with the epidermis, and is mainly composed of fine

type III collagen and elastic fibres, with abundant capillaries to nourish not only the dermis, but also the epidermis. Type III fibres also characterise adnexal dermis (Rook et al., 1986). The deeper reticular dermis is comprised of thicker, predominantly type I collagen fibres and contains larger blood vessels (Ghosh et al., 1997).

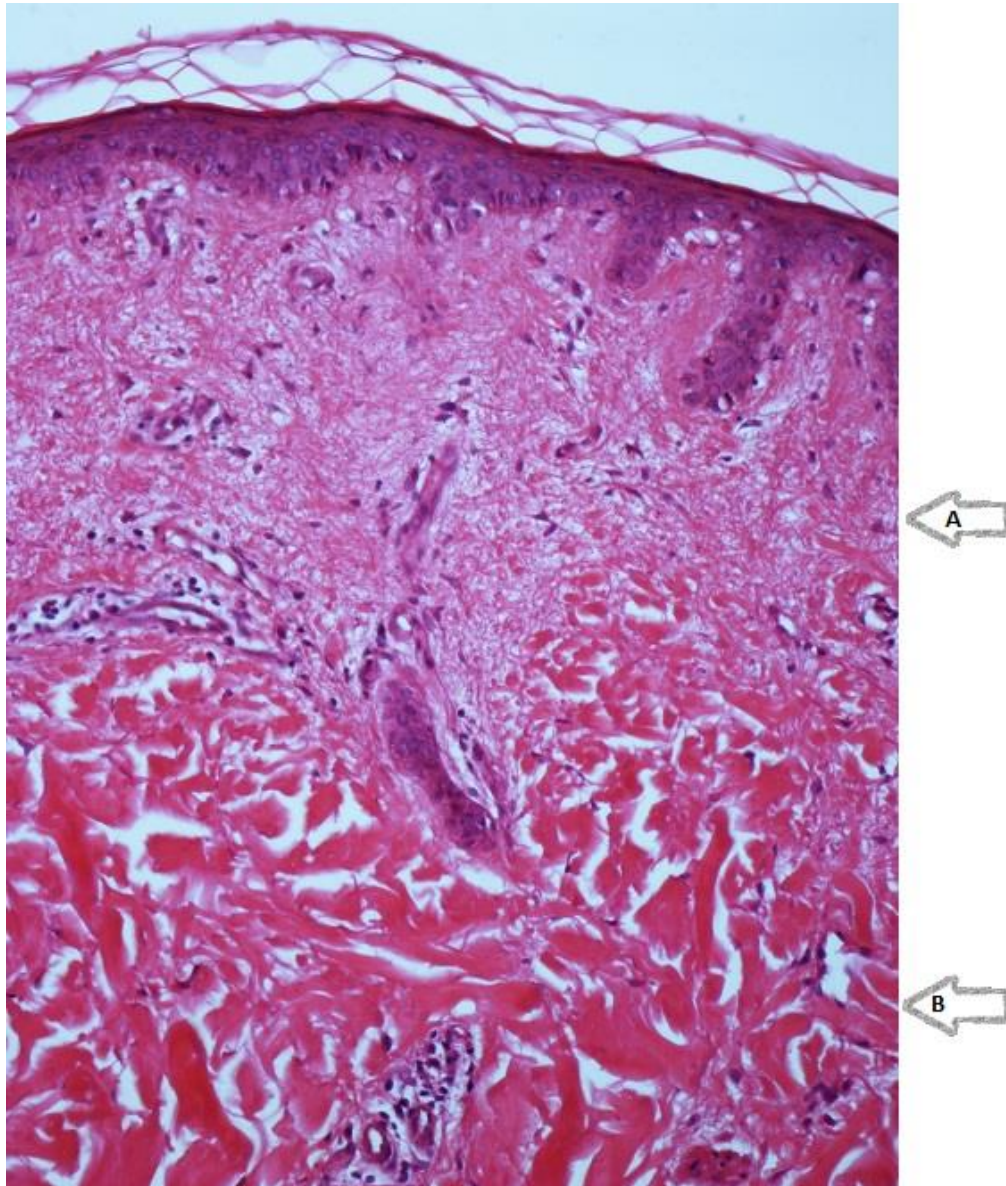


Figure 1-5 Human dermis stained with H&E.

Dermal layers; arrow A shows the papillary layer (with thin collagen fibres) and arrow B the reticular layer (with thicker collagen fibre). Original image captured at 40x magnification.

This compartment is in contact with the subcutaneous fat layer (the hypodermis), with slightly lower cellularity than the papillary layer. The dermis has many functions including: 1) interaction with epidermal cells to promote the development and maintenance of the epidermis and its appendages (which are supported within the dermis); 2) protection of internal organs from mechanical injury; 3) thermoregulation

and regulation of water retention (Reddi et al., 2012); and 4) supporting dermal fibroblasts and facilitating tissue repair and renewal (2007, Burns et al., 2010). The key dermal components are discussed in more depth below.

1.4.1 Dermal fibroblasts

Dermal fibroblasts produce the collagens that provide tensile strength (and constitute the majority of the dermis), elastins that provide elasticity and proteoglycan molecules that provide viscosity and retain water (Orgel et al., 2011). Dermal fibroblasts are involved in a variety of physiological processes including cytokine secretion and responses (including pro-inflammatory mediators), and the turn-over of structural components of the ECM (Sherwood and Toliver-Kinsky, 2004) (Clark et al., 2007). These functions vary according to location, for example, isolated papillary fibroblasts have a higher capacity to produce collagen type III and fibronectin than reticular dermal fibroblasts, and are smaller and proliferate at a higher rate (Sorrell and Caplan, 2004a) (Wang et al., 2008).

In healthy skin, fibroblasts appear as thin spindle shaped cells arranged along collagen fibres, as observed with H&E staining (Figure.1.5.A arrow). With advanced maturation, mature fibroblasts nuclei shrink and have reduced endoplasmic reticulum.

Fibroblasts have the capacity to differentiate into myofibroblasts, smooth muscle cells, chondrocytes, and osteoclasts, as demonstrated in developing or regenerating tissues (Lei et al., 2014). For example, under in certain chronic stimuli or disorders associated with hypertrophic scarring (resulting in the creation of fibrotic plaques), myofibroblasts are characterized by expression of α -SMA (alpha smooth muscle actin) (Wang et al., 2008). Figure1.6.A shows the immunodetection of α -SMA actin in a fibrotic plaque from a sample of irradiated human breast skin. Microscopically, with picrosirius staining, a fibrotic plaque can be observed under bright field microscopy (Figure.1.6.B). In contrast, under crossed-polar microscopy the plaque lacks the birefringence property of healthy collagen due to the loss of regular structure, and appears as a dark area (Nong et al., 2011) (Figure.1.6.C).

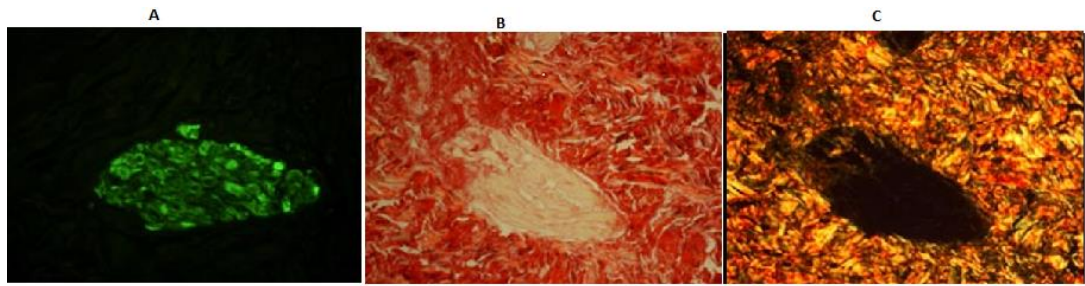


Figure 1-6 Fibrotic plaque

Immunofluorescent detection of α SMA expression (A); picosirius staining viewed under bright-field (B); and (C) picosirius staining viewed under crossed-polar microscopy. Images were captured at 20x original magnification.

1.4.2 Collagen

Collagen is the major component of the integument, accounting for 75% of the dry weight of the skin (Hookerman, 2014). It provides strength and support, with tensile strength being a function of collagen type and density. There are many types of collagen in the skin, and approximately 80-90% is type I (most commonly in reticular dermis), 8-10% type III (most common in the papillary dermis) and around 5% is type V (Shimizu, 2007). Skin collagen can be subdivided into fibrillar collagens (type I, II, III, V, and XI), non-fibrillar collagens (type IX, XI, XIV, and IV) and basement membrane collagen (type IV, VII, XVII). Procollagens are secreted by fibroblasts, which are processed and self-assembled into a triple helical structure, which results in three individual C-terminal peptides (Shimizu, 2007). This is followed by the intracellular ordering of helical binding between the C to the N termini of the three α chains via the modification of prolines within procollagen into hydroxyl-proline (which serves as stabilizing factor for the triple helix) (Boudko et al., 2002). In the extracellular space, the triple helices self-aggregate into irregular overlapping staggered fibres as seen in (Figure 1.7).

Two kinds of helices exist. The first contains a triple-helical collagenous domain, consisting of uninterrupted GLY-X-Y repeated sequences, forming fibrillar collagens. The second type of helical chains are found in FACIT collagens (fibril-associated-collagens with interrupted triple helices), which are non-fibrillar (Shimizu, 2007).

Images viewed under light microscopy with Picosirius staining (PS) do not reveal obvious collagen organization (Figure 1.6. A), while the birefringent properties of

highly regular collagen are revealed under polarized light, which readily allows assessment of collagen organisation (Figure.1.6. B) (Jones et al., 2002). A loss of organisation, particularly the basket-weave, is associated with many skin conditions and diseases such as ageing, scarring, and type 2 diabetes (Osman et al., 2013a). Many histological stains are available to identify collagen organisation including Masson's trichrome (Figure 1.8.B) and Herovici's stain (Figure.1.8.A), the latter distinguishes young, newly formed collagen fibres which appear blue; from the mature, dense collagen fibres, which appear red, making this stain a very useful tool in the investigation of collagen synthesis and organisation (Collins et al., 2011b, Al-Habian et al., 2014).

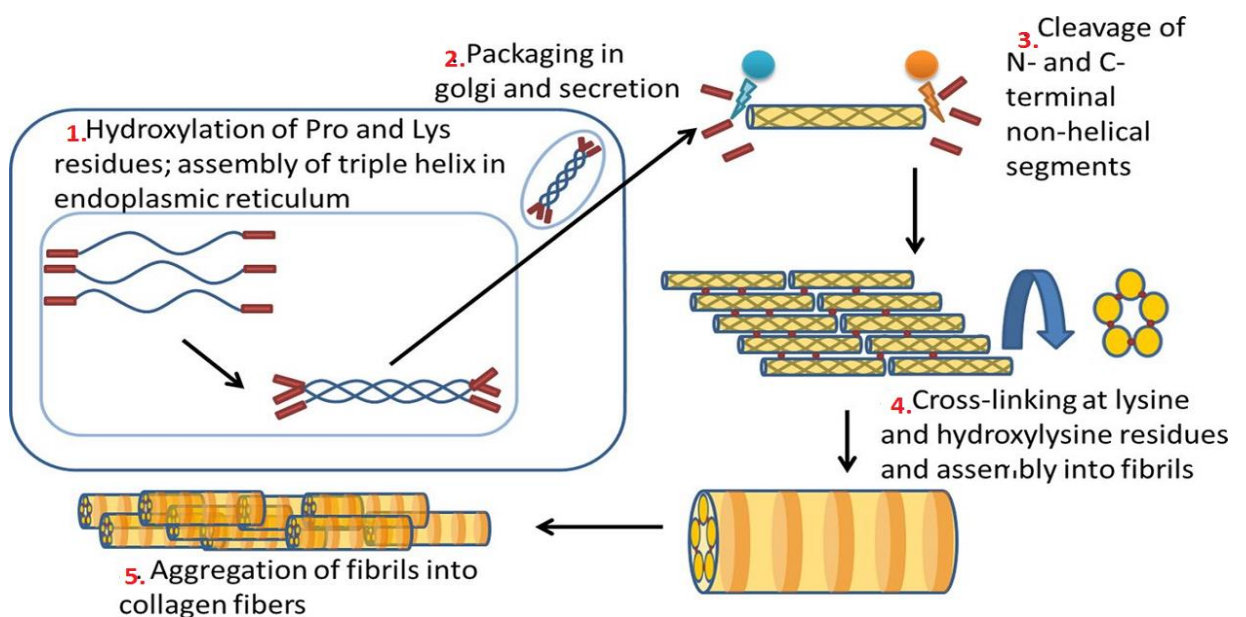


Figure 1-7 Schematic diagram of collagen synthesis.

Synthesis begins with the translation of collagen pro-chains in the rough endoplasmic reticulum. After these chains form a triple helix, the molecule is secreted from the cell, where it undergoes further processing and aggregation into fibrils and fibres adapted from (McKleroy et al., 2013).

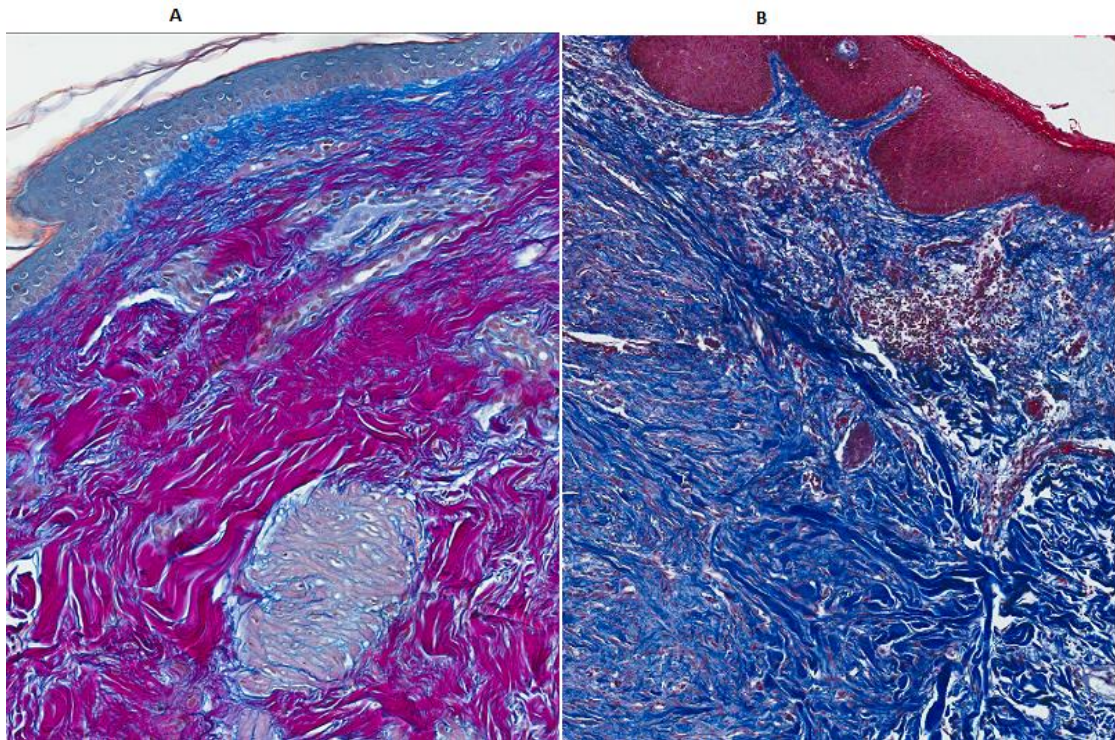


Figure 1-8 Human skin sections stained for connective tissues.

Herovici's stain (A) distinguishes young (blue) collagen fibres in the papillary dermis from mature (red) thick collagen fibres in the reticular dermis. Masson's trichrome (B) shows the differential staining of thin collagen fibres (light blue) in comparison to thick collagen (dark blue). Images captured at 20x original magnification.

1.4.3 Elastic fibres

Elastin is a connective tissue protein with extremely good elastic properties, but it is not as strong as collagen. Elastin is the predominant protein in the walls of blood vessels, lymph vessels, lungs and the skin as well as the other extensible tissues such as tendons. The extraordinary elasticity is attributed to the “rubbery” and amorphous structure of elastin, allowing the elastin molecules to stretch and recoil when any deforming force is withdrawn (Mithieux and Weiss, 2005). The precursors of elastic fibres (like collagen fibres) are synthesized and secreted by dermal fibroblasts in the skin, chondroblasts in the elastic cartilage and smooth muscle cells in the vascular walls. After secretion, elastin molecules are assembled extracellularly to form fibrils and fibres (Burns et al., 2010).

Histological examination of mammalian skin sections does not reveal the presence of elastic fibres when stained with H&E (Figure 1.5). Elastin fibres can be observed after

staining with special stains such as van Gieson (Lu et al., 2009) (Figure1.9.A) or with Giemsa and Orcein (Burns et al., 2010) (Figure1.9.B), where they appear as brownish black bundles (see Figure1.10 arrow), extending from the DEJ to the connective tissue of the subcutaneous fat layer (Kempf et al., 2008).

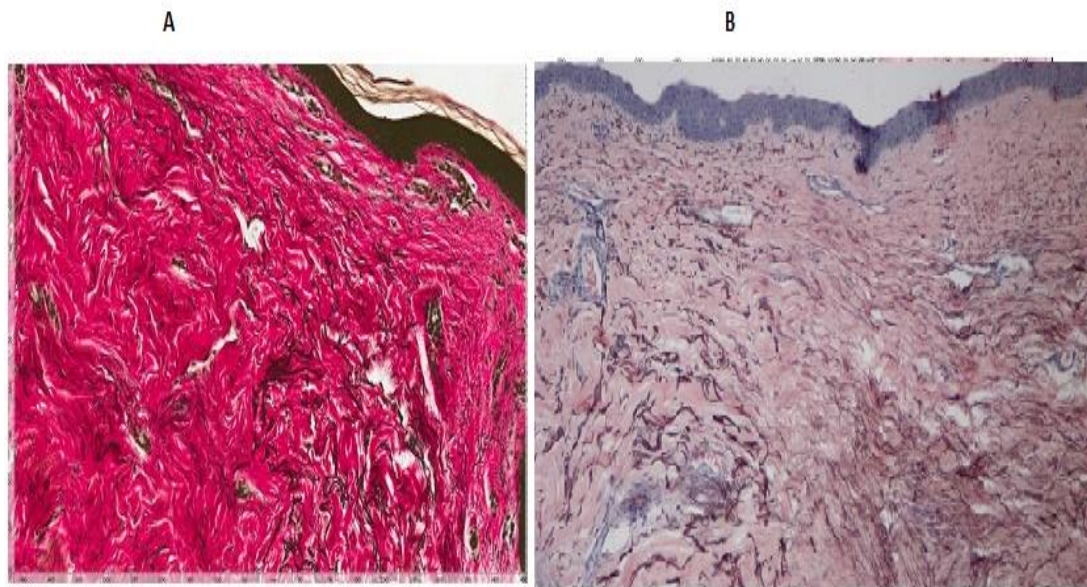


Figure 1-9 Elastic fibre organization of human skin.

Human skin section stained with van Gieson (A), and with Giemsa and Orcein (B). Elastic fibres appear as brownish black bundles scattered in the papillary (thin), and the reticular dermis (thicker) with both stains. Images captured at 20X original magnification.

Elastic fibres distributed between collagen fibres have a convoluted appearance. In the normal dermis, the closer the elastic fibres are to the papillary layer the thinner they appear, orientated in a perpendicular plane relative to the skin surface (Figure1.10). Ultra-structural analysis reveals that fibrillar components may exist as isolated filaments (oxytalan) or randomly integrated with variable amounts of elastin (elunin). In the papillary dermis, oxytalan fibres are found in large numbers in the primitive stage and extend vertically from the lamina densa of the DEJ to the junction between the papillary and reticular dermis. Oxytalan fibres are also connected to the lamina densa of glands, sweat ducts, smooth muscles, nerves and blood vessels (Burns et al., 2010). At the papillary-reticular junction, oxytalan fibres merge horizontally to form more mature fibres called elunin fibres, which form the major components of elastic fibres in the reticular dermis and are less flexible than the fibres of the papillary (Robinson et al., 2006).

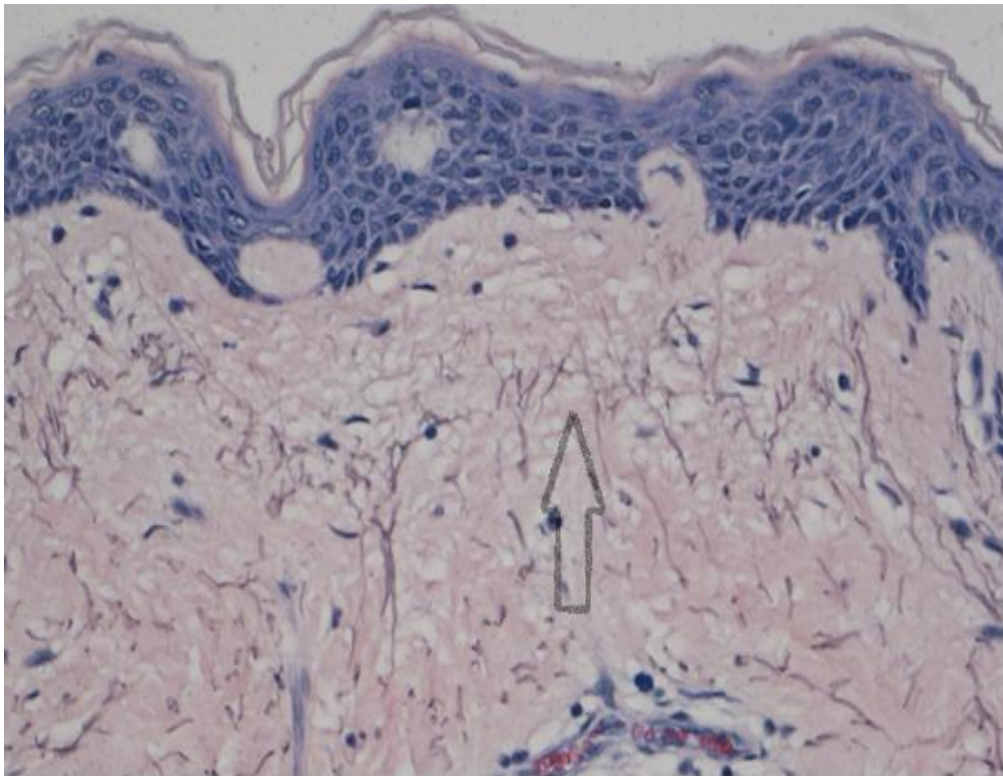


Figure 1-10 Elastic fibre organisation of human skin stained with Giemsa and Orcein.

Orcein stained elastic fibres appear as brownish black bundles (arrow), collagen as rose pink and nuclei as dark blue. Images were captured at 40x original magnification.

1.4.4 Other cells in the dermis

Beside the fibroblasts, the dermis also contains smooth muscle cells, axons and specialised nerve endings, pericytes, glomus cells, and mesenchymal stem cells. Furthermore, the dermis hosts various other cells including, mast cells, endothelial cells and variety of other hematopoietic cells such as macrophages, monocytes, lymphocytes, eosinophils, neutrophils and plasma cells (Rocken et al., 2012). Some of these cells are described briefly below.

1.4.4.1 Mast cells

Mast cells are derived from bone marrow CD34+ stem cells, which under the influence of the ECM and other cellular factors, undergo a multistage differentiation process to become active mast cells in the connective tissues of the body at the interface of an organ and the environment (Chantrain et al., 2008). In the skin, mast cells are found mostly in papillary dermis near the DEJ and in the sheaths of epidermal appendages.

They are also harboured around the blood vessels and nerves in the sub-papillary plexus, and in subcutaneous tissues.

Mast cells possess intra-cytoplasmic basophilic metachromatic granules containing mediators such as histamine, heparin, tryptase, chymase, carboxy-peptidase, and neutrophilic and eosinophilic cationic factors (Heib et al., 2008, Chugunova, 2004). They are identified under light microscope as spindle shaped cells with a round or oval nucleus and abundant cytoplasmic granules that do not stain with routine H&E stain. The cytoplasmic granules can be observed with colloidal iron, toluidine blue, methylene blue, and Giemsa and Orcein stains (Sams and Smith, 1961, Constantine, 1969). The mast cells population is elevated in many inflammatory dermatoses and they play a substantial role in the early phase of wound healing (Aroni et al., 2008).

1.4.4.2 Dermal mesenchymal cells

Dermal mesenchymal stem cells are anchored in the perifollicular connective tissue sheath and the papilla (Mercati et al., 2009). These cells have the capacity to differentiate into adipocytes, smooth muscle cells, osteocytes, chondrocytes, neurons, glia, hematopoietic cells of myeloid and erythroid lineages, and they are thought to be activated early in response to cutaneous injury (Brohem et al., 2013).

1.4.4.3 Dermal dendrocytes, macrophages, lymphocytes and plasma cells

Dermal dendrocytes, macrophages, lymphocytes and plasma cells exist only in small numbers in healthy skin, and most notably in the perivascular region. An increase in these cells characterises some pathogenic conditions (Bonamigo et al., 2011).

1.5 The hypodermis

The third layer of the skin is the hypodermis, also known as the subcutis (SC). The subcutaneous fat layer is found just beneath the dermis and is distinct from visceral fat, which is found within the peritoneal cavity. This layer is well vascularised and is primarily composed of adipocytes supported by a network of reticular fibres and connective tissues (Bennett, 2009).

Excess energy in the body is stored in the form of triglyceride in the SC layer, which also serves as an insulating pad and a cushion resisting mechanical forces. In addition, SC adipocytes have a vital endocrine function as they secrete a variety of cytokines

(adipokines) such as leptin, which provides a feedback signal for the regulation of fat mass and appetite through signalling to the hypothalamus (Kelesidis et al., 2010, Baskin et al., 1999).

The thickness of the SC layer varies considerably over the surface of the body, and also varies with age, sex, race, and endocrine and nutritional status (Bischof et al., 2013). The thickness of the SC has been widely linked to glucose metabolism, energy homeostasis, insulin resistance, hypertension, atherosclerosis and cancer (Karastergiou and Mohamed-Ali, 2010). In addition to changes in physiological function of the fat layer, there are structural changes that occur under these conditions, for example, collagen type VI plays a crucial role in metabolic disorders and is associated with metabolic disease via ECM remodelling and inhibiting adipocyte hypertrophy (Divoux and Clement, 2011, Khan et al., 2009).

1.6 Skin appendages

The skin has several appendages and accessory structures that lie in the dermis and project onto the surface through the epidermis. These include hair, nails (the cornified appendages) and sebaceous and sweat glands (the glandular appendages).

1.6.1 The hair

The hair is an important appendage of the skin. It grows from a sac-like extension of the epidermis called a hair follicle. It may be divided longitudinally into the infundibulum (neck), the shaft (containing a bulge region) and the hair bulb (Figure 1.11). Horizontal sections reveal the outer cuticle, the cortex, and the medulla. Hair grows all over the body with the exception of the glabrous skin of the palms and the soles (Oshima et al., 2001). More specifically, the hair follicle consists of many concentric cylinders of cell types, including the outer root sheath (ORS), the inner root sheath (IRS, comprised of Henley, Huxley and cuticle layers, and the innermost hair shaft (HS). The arrector pilus is a small smooth muscle containing numerous sensory fibres that enables the hair to stand erect in response to stimuli such as cold or emotions (Poblet et al., 2004). Pilosebaceous units include the sebaceous gland (described below).

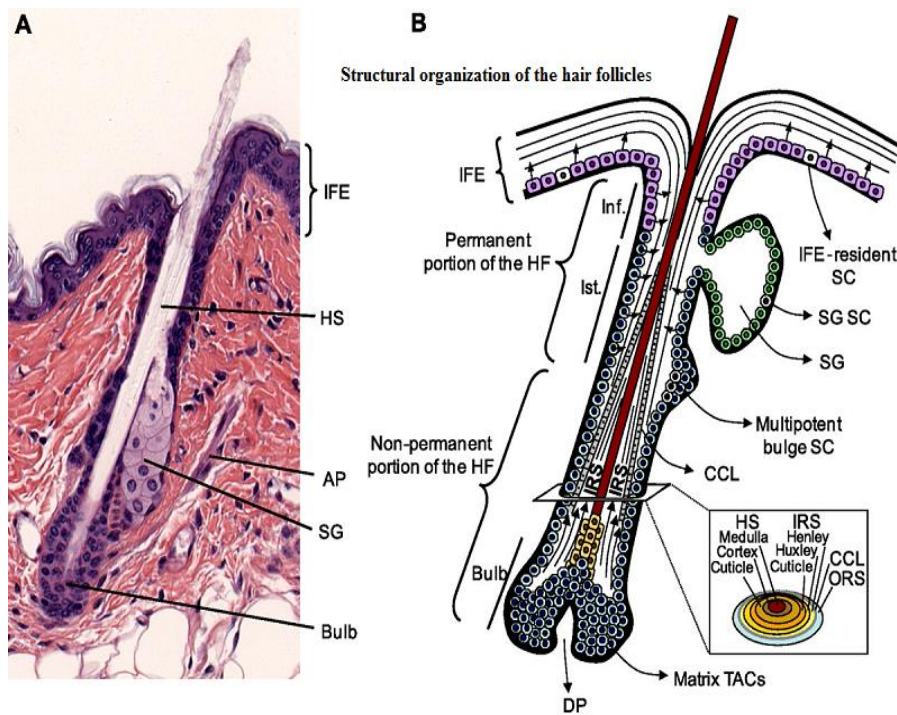


Figure 1-11 Organization of the hair follicle.

A) H&E staining of a hair follicle in late catagen/telogen phase from mouse back skin. B) Schematic representation of the hair follicle and location of the stem cell compartments in the epidermis. AP, arrector pili; CCL, companion cell layer; DP, dermal papilla; HF, hair follicle; HS, hair shaft; IFE, interfollicular epidermis; Inf, infundibulum; IRS, inner root sheath; Ist, Isthmus; ORS, outer root sheath, SC, stem cells; SG, sebaceous gland; TACs, transit-amplifying cells. Modified from (Margadant et al., 2010).

1.6.2 Sweat glands

Sweat glands are simple, highly coiled tubular glands located within the dermis over the majority of the body, and are divided into a coiled secretory region (located in the dermis), and an excretory duct that extends to the epidermis. Eccrine glands form a key part of the body's thermoregulatory system and are innervated by sympathetic (cholinergic) nerve fibres (with an estimated population of 250,000 glands per human foot) found over the palms, soles, axillae and the forehead (Wood and Kelly, 2010). Apocrine glands are fewer in number and have relatively bigger ducts, which deposit their contents into the upper part of the hair follicle (the infundibulum).

1.6.3 Sebaceous glands

Sebaceous glands are the third type of gland found in the dermis. They are derived from epidermal cells and have a close association with hair follicles, particularly those of the scalp, face, chest and back (Smith and Thiboutot, 2008). They produce an oily moisturizing sebum that contains various lipids, cholesterol esters, wax esters and triglycerides. Sebum, transits via the follicular canal to the skin surface and actively helps in maintaining epidermal barrier permeability, as well as having an acidic bactericidal function (with a pH of 4-6). Sebum may also offer protection from UV radiation and aid in the wound healing process (Makrantonaki et al., 2011). Peroxisome proliferator-activated receptors (PPARs) are well recognized as major players in lipid metabolism and adipogenesis. Furthermore, the agonists of PPARs (α , γ , δ , and pan-agonist) are potential drugs in dermatology via their effects on PPARs which are expressed in many cutaneous cellular elements (including keratinocytes (Mao-Qiang et al., 2004a), and fibroblasts (Ghosh et al., 2004b), and are much involved in many functions including epidermal growth and sebum production (Smith and Thiboutot, 2008).

1.6.4 Cutaneous vasculature

The skin has an extensive blood supply comprising of a vascular network of distributing and collecting channels and horizontal plexi. These form a connected microcirculatory meshwork composed of arterioles, venules, and capillaries. Most of the microvascular structure is localised in the papillary dermis, while the arterioles and the venules form two plexi in the dermis (Braverman, 2000). Both networks are physiologically important as they are involved in thermoregulation by controlling the blood flow in capillaries of the upper dermis via dilation or constriction of their capillary loops. Another important contributor to thermoregulation are the arteriovenous anastomoses (AVA), which are found most abundantly in the dermis, close to the level of the sweat glands. These assist in regulating blood perfusion by shunting blood directly from the arterial to the venous system, bypassing the capillary network (Burns et al., 2010).

Paralleling the blood supply of the skin is a lymphatic system that regulates interstitial fluids, as well as clearing the tissue of discarded proteins, lipids, microorganisms, cells and degraded materials from the extra-vascular components of the dermis. Lymphatic

vessels have a larger lumen and an more irregular shape in comparison to blood vessels, with a thinner endothelial vessel wall (Requena and Sangueza, 1997). The vasculature of the skin (the blood and lymphatic system) are implicated in many local and systemic disease such as atopic dermatitis, obesity, insulin resistance, and metabolic syndrome (Muris et al., 2013, Zraggen et al., 2013).

1.6.5 Innervation

Many sensory nerves transmit tactile, pressure, pain and temperature sensations via free nerve endings, Merkel cells and structures such as Meissner corpuscles (located in the papillary dermis), and pacinian corpuscles (located in deep dermal and SC layer) (Shimizu, 2007).

The autonomic nervous system supplies motor innervation via adrenergic fibres (sympathetic autonomic fibres distributed with sensory nerves in the dermis) until they branch (at which point they change from myelinated to non-myelinated fibres) to innervate vascular smooth muscle, the arrector pili muscle of the hair follicles, and apocrine glands, while the cholinergic fibres innervate eccrine sweat glands. The endocrine system regulates the sebaceous glands, which are not innervated by autonomic fibres (Gauglitz and Schaubert, 2013).

1.7 Obesity

Obesity is a heterogeneous clinical disorder. It can be developed as the chronic imbalance between energy intake and expenditure, and encompass both environmental and genetic factors and their interactions and many other factors (Nguyen and El-Serag, 2010). These factors might facilitate an excessive accumulation of fat as well as abnormal fat distribution (Despres, 2012). Obesity is thus considered as a medical condition not only characterized by the accumulation of excess body fat, but also by adverse effects on health (via its co-morbidities), leading to reduced life expectancy and increased health problems (according the World Health Organisation [WHO] report (Organization, 2009).

Approximately 65% of the world's population live in countries where overweight and obesity kill more people than malnourishment (Nigro et al., 2014). The prevalence of obesity is increasing at an alarming rate and it is recognized as one of the most serious public health issues of the 21st Century (Barnes et al., 2007). Studies indicate that 10-

27% of men and up to 38% in women are obese in Europe (Cases, 2006). In the United Kingdom almost 30% of adults are currently classified as obese, while around 3 in ten children aged 2-5 years are either overweight or obese (Weight, Dunton, 2011). The obesity rates in the US population are dramatically increasing across different age groups, including older adults, and is expected to rise from 40.2 million to 88.5 million by 2050 (Fakhouri and Statistics, 2012).

According to the WHO, there has been a 3-fold increase in the number of obese people in the last two decades globally. By 2015, 2.3 billion people will be overweight, and 700 million people will be obese. Moreover, chronic metabolic disorders affect more than 500 million adults and 43 million children under the age of five worldwide (Bumaschny et al., 2012).

The cumulative burden of the health care costs associated with the increasing prevalence of obesity is of particular concern (Lehnert et al., 2013). In the US it has been estimated that over 9.0% of annual medical expenditure relate to obesity, and in addition to the direct costs of treating obesity, the related disorders such as type 2 diabetes, hypertension, cardiovascular diseases and the other co-morbidities (listed in Table 1) account for 43% of the costs of health insurance (Kleinman et al., 2014). This is, therefore, an enormous problem of global reach.

1.7.1 Health complications

Table 1.1 summarises the most common diseases or disorders associated with obesity (adapted from (Cornier et al., 2011, Goran and Alderete, 2012a, Legro, 2012, Cameron et al., 2003, Boza et al., 2012).

Disorders associated with obesity	
Insulin resistance	Nutritional deficits
Glucose intolerance and dyslipidaemia	Cholecystitis
Fatty liver disease	Asthma & respiratory infections
Hypertension	Infertility
Cardiovascular complications	Increased risk of cancer
Type 2 diabetes	Depression and psychosocial problems
Type 1 diabetes	Early puberty
Metabolic syndrome	Orthopaedic alterations
Eating disorders	Lower pregnancy & live- birth rates
Renal alterations & and hyperuricemia	Obstructive sleep apnea (OSA)
Dermatological complications	Polycystic ovary syndrome

Table 1-1 Obesity-associated disorders.

Overweight and obese individuals are more prone to develop systemic inflammation, hypoxia, and hypo-perfusion, which may lead to multiple organ dysfunction syndrome. Many peripheral effects of systemic disease will necessarily be reflected in the skin, and obesity is known to exacerbate barrier damage, infection, (such as in intertrigo), pressure and diabetic ulcers, psoriasis, and delayed wound healing (Lowe, 2009).

There are several parameters to measure overweight and obesity. The most common method is body mass index (BMI). The formula for BMI reflects a range of body weight indices and is derived by dividing an individual's weight in kilograms by the square of their height in meters [weight (kg) / height (m²)] (Oka et al., 2013). Due to the broad range of body weights, the WHO classifies BMI into six categories as shown in Table 1.2.

BMI	Classification
< 18.5	Underweight
18.5–24.9	Normal weight
25.0–29.9	Overweight
30.0–34.9	Class I obesity
35.0–39.9	Class II obesity
≥ 40.0	Class III obesity

Table 1-2 BMI classifications established by the WHO.

There is, however, no strict cut-off from the physiological perspective and a sliding scale from a healthy BMI of 20, up to the morbidly obese >35 can be defined. This calculation for BMI is not accurate for children and adolescents if the impact of gender and physiological differences in body fat are not taken into account (Thompson et al., 2012). BMI scales are remarkably dependant on age, gender and ethnic groups (Maxwell and Cole, 2012). Moreover, it is important to recognize that BMI alone is a rather crude indicator of overweight or obesity since it fails to measure the amount of body fat in certain groups of individuals. For example, athletes may have a BMI that identifies them as overweight even though they do not have excess body fat. However, in the majority of cases, an increased mass of adipose tissue combined with an increased body weight is observed in the obese state. For this reason, many studies have included one or more specific parameters of body composition such as: body fat percentage, lean tissue, bone and fluid mass, fat distribution (by measuring waist to hip ratio (WHR), visceral to subcutaneous fat tissue ratio (VSR) and waist circumference (WC) (Gorman, 2011). Nevertheless, an assessment of adipose tissue only gives an approximate idea of general body fat distribution, and a more accurate measurement of these variables can be obtained by performing sophisticated analytical approaches such as bio-electrical

impedance, dual energy X-ray absorption (DEXA), computed tomography (CT), under water weighing and magnetic resonance imaging (MRI) (Bosello & Zamboni, 2000; Kuk et al., 2005; Gallagher et al., 2009, Bozzetto et al., 2010).

1.7.2 Diabetes mellitus

Diabetes mellitus DM is a serious endocrine disorder that is characterised by the disruption of intermediary metabolism when the pancreas does not produce enough insulin or when the body cannot effectively utilize the insulin produced, or both (Kolluru et al., 2012). Diabetes mellitus is commonly classified into types: type 1 diabetes mellitus (Type 1 diabetes mellitus, or insulin-dependent diabetes mellitus, IDDM), and type 2 diabetes mellitus (Type 2 diabetes, or non- insulin dependent diabetes mellitus, NIDDM). Approximately 10% of diabetics have type 1 disease, and around 90% have type 2 (Tuomilehto, 2013). Type 1 diabetes, was previously known as juvenile onset diabetes, as it predominantly occurs in children and adolescents. In this disorder, the pancreas does not produce sufficient insulin for blood glucose control due to an auto-immune destruction of pancreatic β -cells resulting in the inability to produce endogenous insulin. This type of diabetes can only be treated by life-long administration of regular insulin injections and careful monitoring of blood glucose concentration (Tchorsh-Yutsis et al., 2011). In contrast, type 2 diabetes is characterized by the inability of tissues to respond to normal levels of circulating insulin (Kolluru et al., 2012). The successful treatment for type 2 diabetes can be achieved through various approaches, which range from consistent physical activity, diet control and taking insulin sensitising and/or blood glucose suppressant medications (Inzucchi et al., 2012).

As the incidence of type 2 diabetes rises exponentially in the early part of the 21st Century, the global diabetes health care and financial burdens associated with this chronic disease was estimated to be \$376 billion in 2010, and expected to rise to \$490 billion in 2030 (Zhang et al., 2010). Type 2 diabetes is a chronic disease that we can treat but not completely cure. According to current estimates, there are around 350 million diabetics worldwide and the number is dramatically increasing (WHO, 2013 factsheet) (Bernat-Karpinska and Piatkiewicz, 2014). In the United Kingdom, the estimated number of type 2 diabetics is in the order of 2.2 million, with a further 500 thousand going undiagnosed (Information Centre Quality Outcomes Framework Data 2005/06). This figure is expected to reach 5 million by 2025. In 2009, the prevalence of

diabetes was about 5.4% in the UK (Daultrey et al., 2011), and in the United States its prevalence was estimated at 7.8% in 2007 (according to The National Institute of Diabetes and Digestive and Kidney Diseases,) (Control et al., 2011). In Europe, according to the International Diabetes Federation (IDF) estimates, 55 million adults have diabetes mellitus((both type 1 and type. 2), predicted to rise to 66 million in 2030.

1.7.3 Underlying mechanisms in type 2 diabetes mellitus

Diabetes mellitus is a major contributor to morbidity and mortality in industrialized countries. Increasing urbanization, obesity, increased consumption of fructose corn syrup and other relatively cheap or junk foods, increasing economic impact on families, decreasing physical activity and genetic factors all contribute to the development of this disease (Hu, 2011).

Insulin secretion in type 2 diabetes may ultimately be impaired as the pancreas becomes compromised following attempts to maintain glucose homeostasis by initially increasing insulin production, but at the outset impaired sensitivity to insulin-mediated glucose disposal (insulin resistance) is central to the disease process (Schwartz et al., 2013). While insulin has several metabolic and mitogenic functions (Rains and Jain, 2011), its key function is to stimulate glucose uptake in insulin-sensitive tissues, and so lower plasma glucose levels.

An overview of the pathophysiology of the disease is shown (Figure 1.12). Due to reduced glucose uptake in muscle and adipose tissue (which leads to increased lipolysis and non-esterified fatty acid [NIFA] production), blood glucose concentrations remain high even in a fasting state (Richter and Hargreaves, 2013). At this stage, the liver might exacerbate this condition by increasing glucose production via gluconeogenesis. Elevated levels of glucagon from islet α -cells are also detected in type 2 diabetes, which enhances glycogenolysis, lipolysis, gluconeogenesis and ketogenesis, whilst inhibiting lipogenesis and glycolysis (Rosen and Spiegelman, 2006). Elevated concentrations of blood glucose result in an increased rate of glucose reabsorption in the kidney and progressive insulin resistance in target tissues, which switch to fatty acid metabolism (Poudel, 2013). Chronically elevated insulin production by the pancreas acts as a compensatory step to restore glucose homeostasis, and this along with chronic high glucose levels may have a toxic effect on islet function and lead to further worsening of hyperglycaemia. In concert with lipotoxicity resulting from elevated level of free fatty

acids, these effects promote malfunction of pancreatic β -cells, islet hyperplasia and β -cell apoptosis (Kitamura, 2013).

In summary, the pathogenic processes of type 2 diabetes are characterised by a gradual decline of glucose homeostasis as a result of disruption to multifactorial metabolic pathways (Holst and Gromada, 2004). Thus, insulin resistance in peripheral tissues, increased glucose production in the liver, and eventual pancreatic β -cells failure results in hyperglycaemia which plays a key role in type 2 diabetes pathophysiology. Other corollaries of type 2 diabetes are cardiovascular disease, hypertension, stress, and metabolic syndrome (DeFronzo et al., 2013).

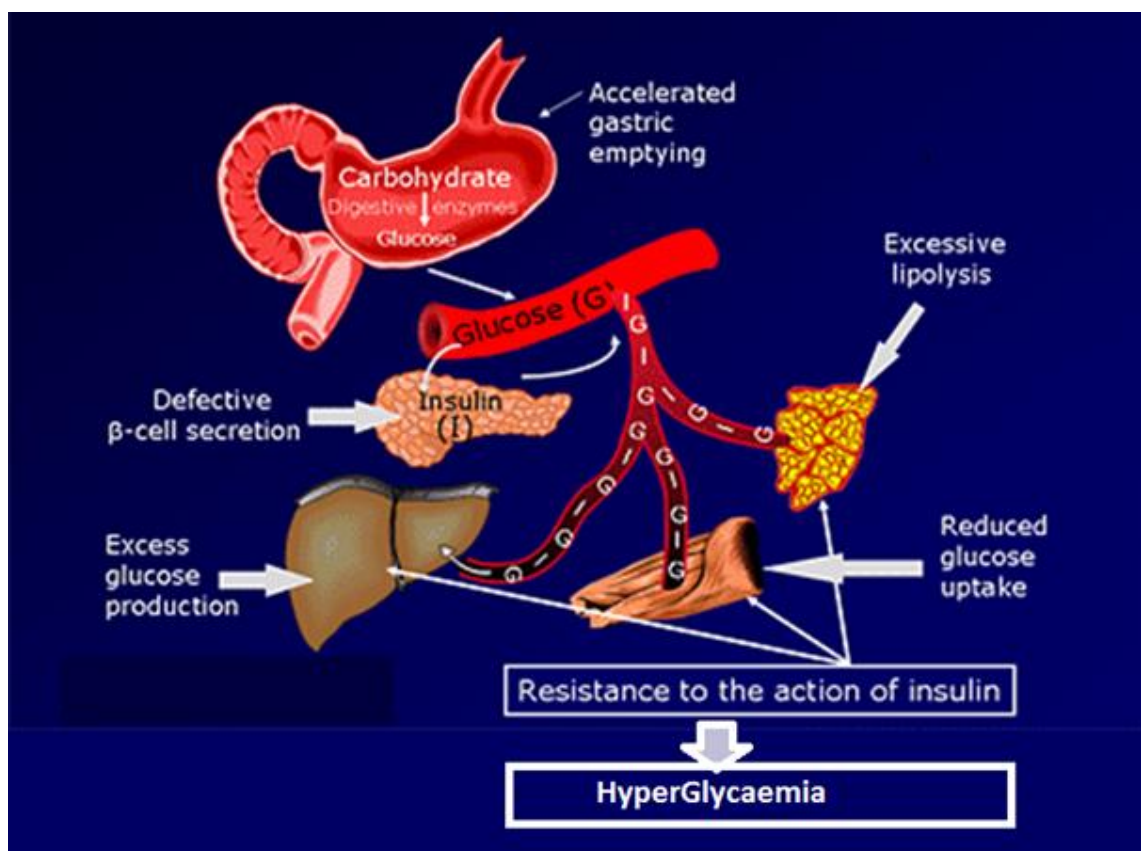


Figure 1-12 Type 2 diabetes is characterized by three pathophysiological abnormalities.

Impaired insulin secretion, peripheral insulin resistance and excessive hepatic glucose production. Adapted from (DeFronzo et al., 1992).

1.7.4 Dermatological complications of type 2 diabetes, obesity and ageing

Obesity is the most major risk for insulin resistant, and the development of type 2 diabetes, which is further stressed by chronological age, and other contributing factors such as cardio vascular disease, smoking, sedentary life style, unhealthy diet and if left uncontrolled, it may affect nearly all the body organs system (Yosipovitch et al., 2007). The skin largest organ in the body. Therefore, the majority of individuals suffering from type 2 diabetes will experience skin complications of varying severity during their lifetime (Baloch et al., 2008). Likewise, obesity and ageing is associated with a range of cutaneous complications. There are very common dermatological disorders associated with type 2 diabetes, which include (but are not limited) to necrobiosis lipoidica diabetorum (NLD), granuloma annulare, diabetic dermopathy, acanthosis nigricans, vitiligo, psoriasis, lichen planus, and microangiopathy, which in conjunction with neuropathy lead to foot ulcers, delayed wound healing and infection (LeRoith et al., 2004, Van Hattem et al., 2008). The appearance of some of these lesions may provide early signs of type 2 diabetes, notably acanthosis nigricans, lichen planus, skin tags, and dermopathy, which are seen in hyperglycaemia or/and euglycemic dysfunction (Rasi et al., 2007, Baloch et al., 2008, Thoenes, 2012). Skin manifestations are commonly described in both types of diabetes mellitus, and there are no distinctive classifications for dermatological complications related to type 2 diabetes. Thus grouping them under the following headings will give a better understanding of clinical dermatoses or complications associated with this disease (Table 1.3).

Skin lesions associated with type 2 DM	Cutaneous infection associated with type 2 DM
Pruritus	Fungal
Acanthosis nigricans	Bacterial
Diabetic thick skin	Viral
Cutaneous Xanthomas	Cutaneous manifestations related to diabetic complications
Diabetic dermopathy	Macroangiopathy
Skin tags	Microangiopathy
Rubeosis faciei	Diabetic neuropathy
Diabetic bullae	Diabetic foot
Lichen planus	Antidiabetic therapy complications
Granuloma annulare	Sulphonylurea-related skin lesions
Diabetic xerosis	Insulin lipo-atrophy
Vitiligo	Insulin lipo-hypertrophy
Acquired perforating dermatoses	
Necrobiosis lipoidica diabetorum	

Table 1-3 Classifications of cutaneous manifestations associated with type 2 diabetes.

Adapted from (Baloch et al., 2008, El-Khalawany and Mahmoud, 2014).

However, it is still enigmatic whether the cutaneous complications are caused directly by the pathogenesis of type 2 diabetes or it is merely an epiphenomenon of metabolic interference of various metabolic disorders such as obesity, CVD, metabolic syndrome (Baloch et al., 2008, Berlanga-Acosta et al., 2012). Studying early markers of diabetes in human subjects is difficult for both ethical and practical reasons: people may not wish to know they are prediabetic, and routine biopsy is difficult to justify. This is confounded by heterologous skin presentations. Therefore, mouse models of obesity and diabetes are widely used to study human disease, but relatively little evaluation of diabetic associated murine skin pathology have been performed, other than studies of impaired wound healing (Trousdale et al., 2009). Whilst many attempts have been undertaken by researchers to model a variety of human skin diseases such as fibrosis, psoriasis and cancer in mice using transgenic or environmental models, xenografting, or

other forms of genetic manipulation of target genes, progress is limited (Wagner et al., 2010, Khavari, 2006). Animal models are attractive surrogates for human diseases with the ability to manipulate, and control the environmental and the genetic variables, allowing detailed histopathological and molecular studies to be performed. However, one must take account the anatomical differences between humans and mice (Table 1.4 and Figure 1.13). One key difference is that mouse skin is much thinner than human skin, which complicates the preparation of good histology sections, particularly in the diabetic state (Al-Habian et al., 2014). Thus, obtaining good mouse skin histology is a key factor in achieving meaningful morphological analysis (Treuting and Dintzis, 2011). Critically, *in vivo* models also provide a system for evaluating therapeutic remediation of diabetic phenotypes. The most common histological and molecular findings of skin layers in obesity, type 2 diabetes, and ageing are summarised in (Table 1.5, 6, and 7).

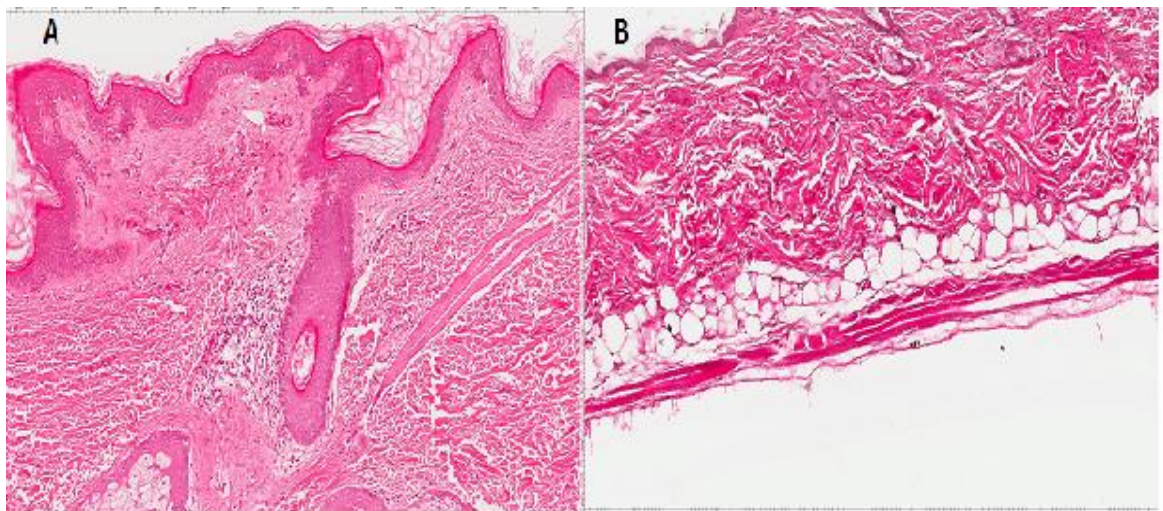


Figure 1-13 Comparison of skin histomorphology from human and mouse stained with H&E.

Mouse skin layers (B) are thinner and less distinctly separated than in human skin (A). In particular, the two dermal layers (papillary and reticular) clearly seen in human skin (A). Images were captured by an Aperio ScanScope scanner at 5x magnification.

	Human	Mouse
Epidermal layers	Relatively thick, with distinct layers (particularly the stratum spinosum can be seen to be composed of multiple layers of keratinocytes)	Thinner, with less discrete layers
Keratohyalin granules	Consist of filaggrin in human interfollicular epidermis	Consist of filaggrin and loricrin proteins.
Epithelial architecture	Rete ridges present	No rete ridges
Dermis	Thick, good distinguish between papillary and reticular dermis	Thinner, lesser discrimination between papillary and reticular dermis
Vasculature	Highly vascularised	Poorly vascularised compared to human dermis
Apocrine sweat glands	Present in axilla, inguinal, and perianal skin regions	Not present in mouse skin, extensive in mammary glands
Hypodermal thickness	Consistent between body sites	Variable with age, body site, and murine strains
Biomechanical properties	Thick, relatively stiff, adherent to underlying tissues	Thin, compliant, loose.

Table 1-4 Summary of the key differences between human and mouse skin.

Modified from (Wong et al., 2010, Treuting and Dintzis, 2011).

	Human epidermis	Mouse epidermis	Ageing mammalian epidermis
Reduced keratinocyte proliferation	(Terashi et al., 2005)	(Sakai et al., 2003, Lamers et al., 2011)	(Rook et al., 1986)
Hyperkeratosis	(Lowe, 2009) (Levy and Zeichner, 2012, Plascencia Gómez et al., 2014)	(Grice et al., 2010)	(Bitter, 2000)
Impaired epidermal barrier function	(Lowe, 2009)	(Taylor et al., 2011)	(Ghadially et al., 1995b)
Atrophy	(Sakai et al., 2005)	(Taylor et al., 2011)	(Waller and Maibach, 2005)
Increased rate of infection	(Levy and Zeichner, 2012, Bandaru et al., 2013)	(Bandaru et al., 2013)	(Scheinfeld, 2005)
Irregular pigmentation	(Levy and Zeichner, 2012)	(Salton et al., 2000)	(Mine et al., 2008)
Delayed wound epithelialisation	(Schmidt and Horsley, 2013)	(Frank et al., 2000)	(Bennett et al., 2008)

Table 1-5 Reports describing common epidermal features in diabetic and ageing epidermis.

	Human dermis	Murine dermis	Ageing mammalian dermis
Reduction in Type I/III collagen synthesis	(LeRoith et al., 2004, Lateef et al., 2004)	(Lerman et al., 2003a, Schmidt and Horsley, 2013)	(Mine et al., 2008, Varani et al., 2006a) Mine et al., 2008)
Loss of collagen organisation	(LeRoith et al., 2004, Ren et al., 2013)	(Osman et al., 2013a) (Morris et al., 2013)	(Mine et al., 2008)
Increased MMP expression	(LeRoith et al., 2004, Lateef et al., 2004)	(Morris et al., 2013) (Ibuki et al., 2012) Morris et al., 2013)	(Mine et al., 2008)
Increased RAGE expression/ glycation	(LeRoith et al., 2004, Nawale et al., 2006)	(Giacco and Brownlee, 2010) Ibuki et al., 2012)	(Nawale et al., 2006)
Changes in inflammatory cell infiltration	(LeRoith et al., 2004, Bandaru et al., 2013)	(Maruyama et al., 2007)	(Bennett et al., 2008)
Microvasculature complications	(LeRoith et al., 2004, Nawale et al., 2006)	(Maruyama et al., 2007, Kanasaki and Koya, 2011)	Decreased. (Nawale et al., 2006)
Elastic fibre disorganisation/ loss of elasticity	(LeRoith et al., 2004) (Ye et al., 2010, Ezure and Amano, 2011)	(Ezure and Amano, 2011)	(Rook et al., 1986, Lavker et al., 1987) (Mine et al., 2008)
Fibrosis	(LeRoith et al., 2004, Osman et al., 2013a)	Not reported	(Osman et al., 2013a, Watt and Fujiwara, 2011)
Flatting of DEJ	Not reported	(Taylor et al., 2011)	(Mine et al., 2008, Janovska et al., 2013)
Altered fibroblast shape	(Schmidt and Horsley, 2013)	(Langevin et al., 2005)	(Varani et al., 2006a)

Table 1-6 Reports describing common features in diabetic and ageing dermis.

	Human subcutis	Mouse subcutis	Ageing mammalian subcutis
Loss of elasticity	(Lowe, 2009)	(Ezure and Amano, 2011)	(Sherratt, 2009)
Altered collagen deposition	(Van Hattem et al., 2008) (Lowe, 2009)	(Khan et al., 2009)	(Sherratt, 2009)
Increased MMP expression	(O'Hara et al., 2009)	(Ibuki et al., 2012)	(Sherratt, 2009)
increased macrophage infiltration	(O'Hara et al., 2009)	(Xu et al., 2003) (Trayhurn, 2013a)	(Tchkonia et al., 2010)
Increase fat cells size and number	(Goossens, 2008)	(Xu et al., 2003, Ezure and Amano, 2011)	(Watt and Fujiwara, 2011)
Vascular dysfunction	(Van Hattem et al., 2008) (Goossens, 2008)	(Ibuki et al., 2012)	(Nawale et al., 2006)
Increase in pro-inflammatory cytokines (particularly TNFα and IL-6)	(Tchkonia et al., 2010)	(Xu et al., 2003) (Trayhurn, 2013a)	(Tchkonia et al., 2010)
Adipocyte necrosis and or apoptosis	(Tchkonia et al., 2010)	(Murano et al., 2008). (Khan et al., 2009)	(Tchkonia et al., 2010)

Table 1-7 Reports describing common features in diabetic and ageing hypodermis

In summary, a range of cutaneous pathological changes are associated with insulin resistance and type 2 diabetes complications such as delayed wound healing, diabetic foot ulcers, neuropathy, and vascular problems (Van Hattem et al., 2008). Many attempts to investigate mechanisms of skin complications in murine models of insulin resistance and diabetes have been reported (Seitz et al., 2011). It is, however, noteworthy that not all secondary diabetic cutaneous signs can be modelled accurately in the mouse due to physiological and anatomical variation. Nevertheless, it is likely that there exist many common mechanisms at the cellular and molecular levels in diabetic human and mouse skin. Furthermore, using either genetically altered mouse models of obesity, insulin resistance (notably *Lepob/Lepob* mice lacking leptin) and diabetes (*leprdb/leprdb* mice lacking the leptin receptor), or environmental models (dietary induced obesity [DIO])(Seitz et al., 2011) will allow more effective analysis of the various stages of skin disease, which are not practicable (or ethical) in human subjects.

1.8 Hypothesis and aims of the thesis

Previous studies of peripheral lesions in metabolic disease include insulin resistance, obesity, and type 2 diabetes mellitus have focussed on the role of hyperglycaemia, glycation (in particular the formation of advance glycation end products), hypoxia, adipose tissue-driven inflammation and cytokine action as drivers of disease pathology (Van Hattem et al., 2008, Barrientos et al., 2008, Seitz et al., 2011). Keratinocytes and fibroblasts have active insulin-dependent glucose transport systems (Shen et al., 2000, Howard et al., 1979). The integrity of the skin is maintained by a continuous programme of renewal, and it is possible that progressive insulin resistance and hyperglycaemia will have a profound effect on cutaneous homeostasis and function. Herein, I seek to use animal models of human disease in order to investigate the complex mechanisms underlying cutaneous changes associated with insulin resistance and type 2 diabetes(Wong et al., 2010).

My first hypothesis is that insulin resistance itself plays an important role in dermatological changes. I tested this hypothesis in a pre-diabetic (insulin resistance),

and hyperinsulinaemic (diabetic) animal model by evaluating skin phenotypes in paraffin sections of tissue derived from environmental C57BL/6 mice maintained on a high fat diet, genetic models of obesity and insulin resistance (*Lepob/Lepob*), and models of type 2 diabetes (*leprdb/leprdb*). I sought to achieve this by using a range of special histological stains to evaluate structural changes in the skin. This work was extended by the use of immunohistochemical (IHC) methods with antibodies recognising a range of key proteins including markers of proliferation (PCNA), epidermal maturation (K14, involucrin, profilaggrin), endothelium (CD31) and immune infiltration (CD68).

Dermal damage, and overall skin fragility in insulin resistant and obese murine models is associated with an expansion of subcutaneous adipose tissue (Ibuki et al., 2012) and it was notable from my work that the tissue layer adjacent to the expanded subcutis (i.e. the reticular dermis) sustained the greatest damage, which is consistent with chronic exposure to locally produced adipokines in human studies (Khan et al., 2009). Thus my second hypothesis is that chronic exposure to paracrine inflammatory signals released from an expanded subcutis underlies some of the peripheral effects of insulin resistance or type 2 diabetes on mouse skin compartments. In this regard, measuring the systemic (plasma), and local (subcutaneous adipose tissue) cytokines production was undertaken to elucidate their contribution to dermatological sequelae related to insulin resistance and type 2 DM. My third hypothesis is that insulin-resistant dermal fibroblasts are impaired in their ability to secrete and organise collagen. Therefore, their function from fibroblasts isolated from *Lepob/Lepob* and normal C57BL/6 animals was assessed. The receptors for both insulin-like growth factor1 and insulin are highly expressed by both basal keratinocytes and dermal fibroblasts (Hodak et al., 1996). Their chronic activation resulting from hyperinsulinaemia may have pathological consequences. Thus, evaluating insulin receptor expression in isolated dermal fibroblasts would help in investigating a role for local insulin resistance in type 2 diabetes skin lesions. By using a range of histological techniques, IHC, and *in vitro* methods, I sought to achieve the following aims:

- 1) Rigorous evaluation of histological differences in skin isolated from different mouse models of insulin resistance and diabetes.
- 2) Assessment of cutaneous molecular characteristics associated with increasing insulin resistance via immunohistochemistry analysis of some cutaneous maturation and function biomarkers.
- 3) Investigation of a role for adipokine signalling in skin damage.
- 4) Evaluation of insulin signalling mechanisms in cutaneous fibroblasts.

Chapter 2: Material and Methods

2.1 Animals models and diet

Over the last decade several animal models have been used to investigate the metabolic syndrome. Rodents are commonly used models to study human disease in part through their similarity in mammalian anatomy, their genome is well characterised, their fast reproduction rates (making them cost effective), and the wide availability of biological markers and assays (Spence, 1999) make them attractive research tools. Various mouse models have been developed to study obesity and type 2 diabetes, including genetically modified; transgenic or polygenic models, and environmental models for example streptozotocin treatment, partial pancreatectomy, or exposure to a high fat diet (Buckingham et al., 2012).

Male C57BL/6, *Lepob/Lepob*, *Leprdb/Leprdb* and Misty mice were purchased from (Charles River, Manston, UK) at 5-6 weeks of age. All experiments were conducted in accordance with the University of Buckingham Home Office licence and ethical review process. Animals were housed in solid-bottomed, sawdust-filled cages with access to tap water and fed a standard chow diet (10% kcal fat, 70% kcal carbohydrates, 20% kcal protein; (Beekay Diets, New Brunswick, NJ, USA)) or a high fat diet (40% calories are provided by fat) (Western diet, Special Diets Services, Witham, UK). The fat in the high fat diet was derived predominantly from milk (other source: corn oil, cholesterol) while the source of fat in the chow diet was soybean oil. Mice were maintained at a controlled temperature of $23\pm1^{\circ}\text{C}$, on a 12 hour light-dark cycle (7.00 until 19.00 hours).

2.1.1 C57BL/6

The C57B/6 mouse (here after referred to as wild type (*wt/wt*), or lean mice) inbred strain was used in this study (Garcia-Menendez et al., 2013). The C57BL/6 mouse was used for the diet induced obesity (DIO) and ageing models.

2.1.2 *Lepob/Lepob*

C57BL/6 *Lepob/Lepob* (here after referred to as *ob/ob* or insulin resistance model). These mice lack circulating leptin because they are lacking a functional leptin gene. Leptin is a key regulator of satiety and energy homeostasis, and these mice show post-natal weight gain and progressive insulin-resistance (moderate hyperglycaemia with compensating hyperinsulinemia) (Clee et al., 2005). Feeding *ob/ob* mice a 40%-60%

high fat diet (here after referred to as *ob/ob* HFD) results in an increase in body weight, glucose intolerance and progressive insulin insensitivity (Kennedy et al., 2010, Koch et al., 2014).

2.1.3 Diet induced obesity model

The diet induced obesity model (DIO) was produced in C57BL/6 wild-type animals maintained on a high fat diet (in which 40% or more of their calories are provided by fat) from 6-7 weeks of age for a total of 45 weeks feeding. DIO mice become obese and are mildly insulin resistant (but not diabetic), allowing for the investigation of the early effects of insulin resistance (Wargent et al., 2013).

2.1.4 Mouse models of ageing (old)

This model was introduced in C57BL/6 wild-type animals maintained on a chow diet until 20 months of age.

2.1.5 C57BLKS/J (misty)

The C57BLKS/J strain (here after referred to as KSJ or Misty) is closely related to C57BL/6, but the strains are phenotypically distinct. C57BLKS/J with a leptin knockout receptor will be homozygous for the diabetes *Leprdb/Leprdb*. The Misty strain was used as the control strain for *Leprdb/Leprdb* (Mao et al., 2006) .

2.1.6 *Leprdb/Leprdb*

Leprdb/Leprdb (here after referred to as *db/db* or diabetic mouse) mice fail to respond to leptin. A dysfunctional leptin receptor in *db/db* in mice on the C57BLKS/J background results in excessive, rapid post-natal weight gain, obesity, glucose intolerance and insulin resistance, accompanied with a deterioration in pancreatic islet function from 6-7 weeks of age leading to hyperglycemia and hyperinsulinemia and frank diabetes. This strain shows impaired wound healing, and is thus considered a good model to study the associated complications of type 2 diabetes on skin function (Trousdale et al., 2009).

2.2 Physiological measurements

2.2.1 Body weight

The body weight of the mice was measured weekly. Each animal was placed in a small bowl on an electronic scale (Adventurer TM Pro, Ohaus Corporation, Pine Brook,

USA). Readings were taken over a 5 second period and averaged by the scales in order to allow for the animal's movements.

2.2.2 Body composition

Body fat content, lean mass, and bone density were measured by the Dual Emission X-ray Absorptiometry (DEXA) densitometer (LUNAR PIXImus™, LUNAR Europe N.V, Brussels, Belgium). DEXA passes two X-ray beams through the subject and measures the amount of X-ray absorbed by the tissue. One beam is of high intensity and the other of low intensity, so the relative absorbance of each beam is an indication of the density of the tissue it has passed through. The higher the tissue density, the greater is the reduction in X-ray intensity. The DEXA densitometer was calibrated for bone mineral density and percent fat content by scanning a 'phantom mouse' supplied with the machine. The phantom mouse measurement for bone mineral density and percent fat must be within 2% of the expected quality control values in order to proceed with animal scans. Prior to the measurement of body composition, mice were weighed and anaesthetised with an isoflurane/nitrous mix (Isoba, Schering-Plough Limited, Welwyn Garden City, UK), (1.5% flow with 1 litre/minute N₂O and 0.5 litre/minute O₂) and transferred ventral side down onto a specimen tray whilst being maintained under anaesthesia. Mice were positioned on the DEXA densitometer so that the entire body and base of tail were measured in the scan. The DEXA scanning of each animal was performed and finalised by image acquisition and analysis using the PIXImus2™ 1.46 software (GE Medical Systems, Bedford, UK).

2.2.3 Blood glucose

Blood glucose measurements were determined using the Infinity™ Glucose (Oxidase) Liquid Stable Reagent (Thermo Fisher Scientific Inc., Middletown, USA). 10µl of blood drawn from the tail vein was mixed with 390µl of haemolysis reagent (50mg/l digitonin, 100mg/l maleimide) before 20µl was transferred to a 96-well plate in duplicate. A set of glucose standards (at 5.56, 16.67 and 44.4mmol/l) were included. 180µl Trinders reagent (Thermo Fisher Scientific) was added to each well before incubation for 30 minutes in the dark. Absorbance at both 505 and 575nm were measured using a spectrophotometer (Spectramax, Molecular Devices, CA, USA). A linear regression calculation from the glucose standards provided glucose concentrations using Prism 5.0 (GraphPad™ Software, LA Jolla, CA, USA).

2.2.4 Plasma Insulin

Mice were fasted for 5 hours and blood was collected into EDTA coated tubes (Sarstedt, Nümbrecht, Germany) and plasma prepared by centrifugation for 5 minutes at 3000g in a microfuge. Plasma insulin was measured using a 96-well ELISA kit mouse insulin enzyme-linked immunosorbant assay ELISA (Crystal Chem., Illinois, USA) according to the manufacturer's recommendations (sensitivity 0.1ng/ml, CV≤10%). Prior to the first reaction, 5µl of the plasma samples and mouse insulin standards (0-10ng/ml) were dispensed in duplicate onto a microplate coated with the mouse anti-insulin monoclonal antibody. 95µl of guinea pig anti-insulin antibody was added and the plate was incubated for 16 hours at 4°C. Following this three washes with phosphate buffered saline with tween 20 (PBS-T) (PBS-0.01% Tween-20) was carried out to remove unbound antibodies, the mouse anti-insulin monoclonal antibody/guinea pig anti-insulin antibody complex was detected by the addition of the horseradish peroxidase (HRP) labelled anti-guinea pig antibody (100µl). Prior to the enzymatic reaction, after 3 hours incubation at room temperature and five washes with PBS-Tween-20, to each well 3,3',5,5'-Tetramethylbenzidine (TMB) substrate solution (100µl) was added. After 30 minutes incubation in the dark, the reaction was stopped by adding 1N sulphuric acid (10µl) to each well. The absorbance was measured at wavelengths of 492nm (measuring wavelength) and 630nm (subtracting wavelength). The insulin concentration in each sample was interpolated from a standard curve generated in Prism 5.0 (GraphPad™ Software, LA Jolla, CA, USA) using the standard concentrations and corresponding absorbance values.

2.2.5 Preparation of adipose tissue conditioned medium (ACM)

At the time of dissection approximately 0.2g of epididymal and subcutaneous fat from lean, *ob/ob*, *db/db*, misty were collected from each of three mice into 24 well plates (Sigma Aldrich, Gillingham, UK) containing pre-warmed Krebs-Ringer-HEPES buffer pH7.4 and 1% endotoxin free bovine serum albumin (Sigma-Aldrich, Gillingham, UK). Adipose tissue samples were then transferred into a fresh plate containing 0.5ml of DMEM/F-12 and Ham's medium (1:1) supplemented with L-glutamine, 15mM HEPES and 0.5% BSA (Gibco, Life Technologies, Paisley, UK) and chopped into small pieces. The samples were incubated at 37°C using a plate shaker for 90 minutes at 450rpm (Heidolph Titramax, Germany). The culture medium was collected and frozen at -80°C prior to analysis of secreted cytokines.

2.2.6 Mesoscale

The Meso Scale Discovery TM (MSD TM MesoScale Discovery, Gaithersburg, USA) technology uses chemiluminescent detection of substances in either single or multiplex assays, where one or more analytes are detected during one immune-based assay. It involves the use of Sulfo-Tag (N-Hydroxysuccinimide) NHS ester- labelled detection antibodies which emit light under the electrochemical stimulation of an electrode attached to the surface of the microplate well (Gowan et al., 2007). The plate is analysed in a Sector Imager 2400 reader (MesoScale Discovery, Gaithersburg, USA). During the measurement, a voltage applied to the plate electrodes causes the labels bound to the electrode surface to emit light. The instrument measures the intensity of emitted light as a quantitative measure of the cytokines present in the sample (Figure 2.1).

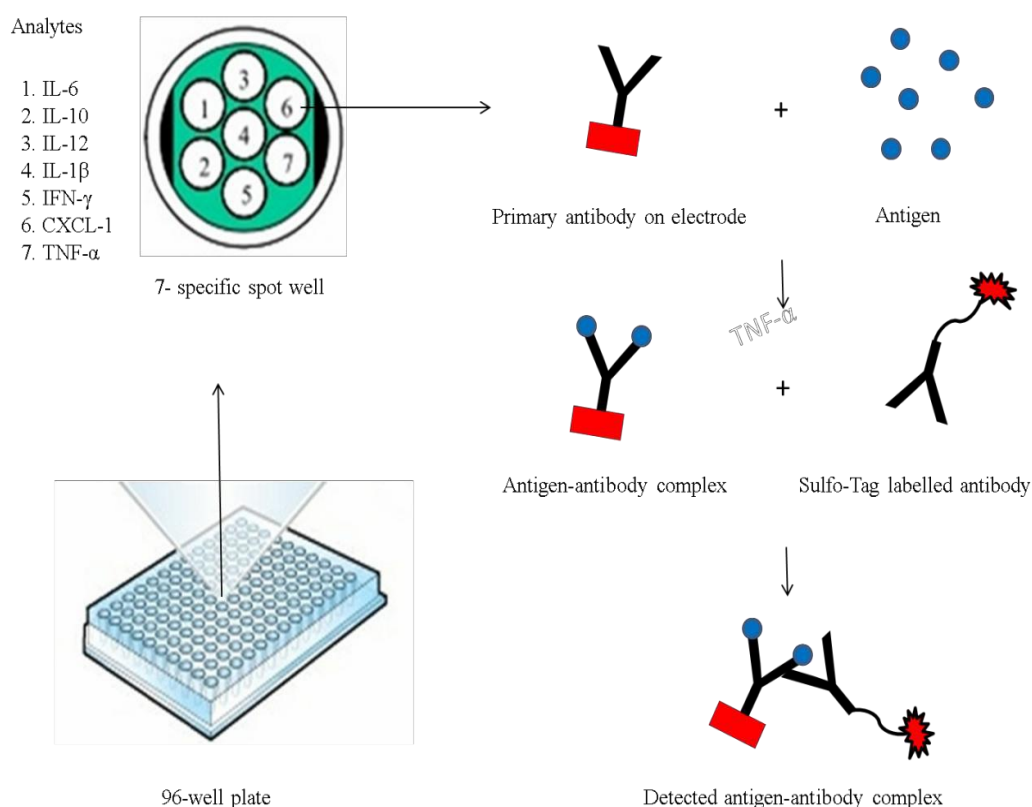


Figure 2-1 Principle of the immunoassay with 7- spot microplate.

In each spot different cytokines are detected. Antigen binds to the primary antibody on the working electrode and the antigen-antibody complex is detected by a Sulfo-Taq labelled antibody. Adapted from Meso Scale Discovery, Gaithersburg, USA.

Cytokine levels were measured in plasma and subcutaneous or epididymal adipose conditioned medium from *wt/wt*, *ob/ob*, *misty*, and *db/db* mice, at 3 months and 20 months of age. Specific cytokines were measured in conditioned medium prepared from skin compartments isolated from both the hypodermis and the outer layers of the skin (comprising the dermis and epidermis) in chow-fed wild-type and in *ob/ob* mice. Cytokine levels were quantified using the MesoScale™ ultra-sensitive mouse pro-inflammatory 3 and 7-plex assay measuring MCP1, RANTES, KC, IFN- γ , IL-1 α , IL-6, IL-10, IL-12, GM-CSF and TNF- α . Antibodies for the specific protein targets are coated onto 7 spots (or electrodes) in the same well. Plates were run as per manufacturer's recommendation, briefly, a blocker solution (150 μ l) was added into each well of the microplate. The plate was incubated at room temperature on a shaker for 1 hour (Heidolph Titramax, Heidolph Instruments GmbH & Co, Schwabach, Germany) at 300–1000rpm and then washed with PBS-0.05% Tween. Diluent (40 μ l) and either sample (25 μ l) or a serially diluted mouse standard (0-10000pg/ml) was then dispensed in duplicate into each well. The plate was incubated under the same conditions for a further two hours and then washed. The anti-mouse goat polyclonal secondary has a unique sulpho tag, and 25 μ l was added, with a further incubation for 1 hour. After washing, read buffer (150 μ l) was dispensed into each well and the plate was analysed in the Sector Imager 2400 reader.

2.3 Histology methods

2.3.1 Tissue preparation and fixation

The dorsal area of each mouse was shaved using electrical clippers prior to the dissection of the skin samples. Skin from each mouse was sliced into small pieces 5x10 mm (to allow for better penetration of fixative), and then placed into histological cassettes (VWR International Ltd, Milton Keynes, UK) prior to fixation for 3 days in 10% neutral buffered formalin (10% NBF) (BDH, VWR International Ltd, Lutterworth, UK) at room temperature. This fixation method was used historically with all mouse models in our laboratory, including in this study, but has later been revised as described in detail in Chapter 4.

2.3.2 Tissue processing

Cassettes were transferred to a Leica TP1020 tissue processor (Leica Microsystems, Milton Keynes, UK) for automated dehydration, clearing and wax impregnation using

the protocol detailed in Appendix 1. This processing protocol was routinely used for processing of the skin samples but has been revised in Chapter 4.

2.3.3 Embedding

Skin tissue samples were embedded using an embedding station (Leica EG1150H) for 30 minutes in a mould in the correct orientation to prepare paraffin blocks. Skin specimens were oriented in warm (60°C) metal histological cassettes filled with hot (65°C) paraffin wax (Leica, Milton Keynes, UK), so that sections were taken at an angle perpendicular to the epidermis. This was followed by transfer to a cold plate (Leica EG 1150C). Once the paraffin had solidified, the mould was filled with more molten wax and the base of the histological cassette was placed on top to create a support, which was subsequently filled with more wax. Blocks were kept on the cooling plate for one hour before separating the paraffin blocks to ensure complete solidification.

2.3.4 Sectioning

After the blocks had hardened, a Leica RM 2125 rotary microtome was used to cut 4µm thick sections. A room temperature of 15°C was maintained, to minimise softening of the wax and reduce sectioning artefacts, and sections were cut at an angle of 45°. Sections were then transferred to a Leica HI1210 water bath at 40°C, and floated onto positively-charged 76x26mm microscope slides (Star Frost, Waldemar Knittel Glasbearbeitungs, Germany) before drying on a hot plate (RA Lamb, Eastbourne, UK) at 35°C for several hours. Finally, the slides were dried overnight at 37°C.

2.3.5 Tissue macro arrays (TMA) construction

The tissue macro arrays (TMA) technique is a high throughput analysis technique used to achieve experimental uniformity (less variability) (Kampf et al., 2012). A 12x4mm core multiple tissue array was used to study the four mouse models in triplicate, and representative tissue from each mouse was presented on a single slide from four fixatives to evaluate the duration and fixative choice for later experiments. The TMA block was made up from 12 regular paraffin blocks of skin samples or multiple mouse tissues (brain, brown adipose tissue (BAT), epididymal fat, heart, pancreas, skin, kidney, liver, small intestine, soleus muscle, lung, and spleen. Briefly, a 12 steel tube custom mould (Figure 2.2A) was used to match the punch pen diameter of 4mm to create the recipient block with 12 cores. After keeping the 12 donor blocks, and one

recipient block at 37°C for 3-5 minutes to soften samples were obtained from each paraffin-embedded biopsy specimen by using 4mm punches merged to the 12 holes recipient paraffin block as seen in (Figure 2.2 C) with maintaining the embedding orientation to the recipient block. The TMA blocks were flattened by keeping them in the oven at 37°C for 20 minutes upside down on a glass slide and then applying gentle load or pressure in order to achieve full adherence and integration to the recipient block. The TMA block was attached to a glass slide and placed on a cooling plate prior to sectioning and staining (Figure 2.2 D).

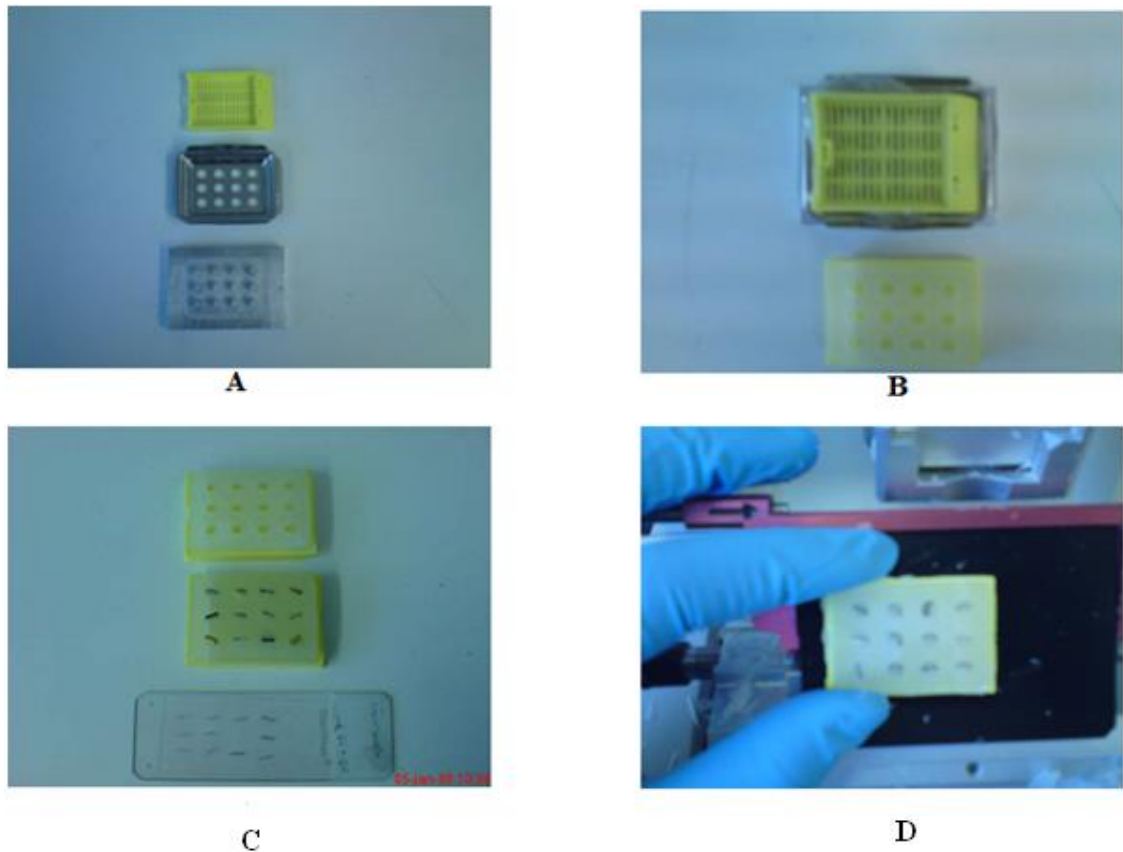


Figure 2-2 Tissue macro arrays (TMA) construction steps.

Custom mould (A), recipient block (B). A single TMA was created containing tissue from 3 different mice (columns), each was treated with the four different fixatives (rows) (C); recipient, arrayed paraffin block and multiple tissue arrayed slide (C and D).

2.3.5.1 TMA sectioning procedures

The hard cutting surface of the TMA blocks was as a result of the heterogeneity of multiple samples from different models and different mouse tissues. Thus it required many attempts to achieve good sectioning outcomes which included; sectioning at low

temperature, frequent blade changing, chilling blocks on ice and tissue paper soaked with softening agents for 2-5 minutes (see formulation in Appendix 4).

2.3.6 Special histological stains

Four μm paraffin sections were stained using a variety of histological stains informative for cutaneous organisation. The initial steps for all the histochemical stains and immunohistochemistry involved de-waxing the slides in an oven at 60°C for 15 minutes followed by rehydration (Histo-Clear™ II, National Diagnostics, UK) twice for 2 minutes each, then in graded ethanols (100%, 90%, 70%; each for 1 minute for each step, with a final rinse under running tap water). Staining was then carried out using solutions for each staining as described below. At the end of each staining procedure, sections were dehydrated using graded ethanols (100% and 90%; 30 seconds each), Histo-Clear™ II (30 seconds) and then mounting in VectaMount™ permanent Mounting Medium (Vector Laboratories, Peterborough, UK) and coverslipping.

2.3.7 Morphology stain

2.3.7.1 Haematoxylin and Eosin (H&E)

Haematoxylin and Eosin stain is the most common histologic stain used to study the general morphology of any tissue. Haematoxylin is a basic dye with affinity for nucleic acids (blue), while Eosin Y stains the cytoplasmic elements (pink) and the red blood cells (red). It is prepared from 7g/L Haematoxylin Solution, Harris Modified and Eosin Y, 0.5% (w/v) in acidified 90% ethanol. Routine H&E staining was performed according to Gamble (Gamble, 2008) (Appendix 6). Briefly, slides were immersed in Harris' haematoxylin for 8 minutes followed by rinsing in water, 30 seconds in 1% HCl in 70% ethanol (v/v) (differentiation), 1 minute rinsing in water, 30 seconds in 0.1% (w/v) sodium bicarbonate (blueing), 5 minutes rinsing in water and then in eosin Y 0.5% (w/v) in acidified 90% ethanol for 3 minutes.

2.3.8 Connective tissue stain

2.3.8.1 Masson Trichrome

The Masson Trichrome stain is a very common connective tissue stain which distinguishes collagen fibres (blue) from muscle fibres (red) and cell nuclei (black). It can also indicate the collagen content in the tissue (Yamamoto et al., 2012). The Masson trichrome stain kit (Sigma, HT15) contains aniline blue solution, Biebrich scarlet-acid fuchsin solution, phosphotungstic acid and phosphomolybdic acid. This kit

was used according to the manufacturer's recommendation, briefly slides were incubated in preheated Bouin's solution for 15 minutes, followed by Weigert's iron haematoxylin solution (5 minutes), Biebrich scarlet-acid fuchsin (5 minutes), dipped in phosphotungstic/ phosphomolybdic acid solution and aniline blue, with a final wash in 0.5% (v/v) acetic acid. A running tap water rinse was carried out between each step.

2.3.8.2 *Herovici*

Herovici's stain for young and mature collagen was adapted from Herovici (Herovici, 1963). This stain consists of Weigert's iron haematoxylin solution, Herovici solution (50ml solution A (100ml Picric acid [saturated aqueous]), 10ml acid fuchsin, 1% (w/v) aqueous solution, 50ml methyl blue (0.05% (w/v) aqueous), 10ml glycerol and 0.5ml saturated aqueous lithium carbonate. The first step of the protocol was nuclear staining with an acid-resistant nuclear stain (Weigert's iron haematoxylin) for 1 minute followed by a 2 minute incubation in Herovici staining solution (50ml Solution A (100ml Picric acid [saturated aqueous], 10ml acid Fuchsin, 1% aqueous solution), 50ml methyl blue (0.05% aqueous), 10ml glycerol, 0.5ml saturated aqueous lithium carbonate) followed by rinsing in tap water (Friend, 1963). Slides were then immersed in 1% (v/v) acetic acid for 1 minute.

2.3.8.3 *van Gieson*

The elastic stain kit (Sigma, HT25) is also known as Verhoeff Van Gieson stain (Pieraggi et al., 1985). This kit was used to study elastic fibres which stained nuclei (black), and collagen (red) and other tissue elements (yellow). This kit is composed of a working elastic solution (20ml Haematoxylin solution, 3ml ferric chloride solution, 8ml Weigert's iodine solution and 5ml deionised water) and a working ferric chloride solution (3ml ferric chloride and 37ml deionised water). The Van Gieson counter stain solution (acid fuchsin, 0.05% (w/v) in 95% saturated picric acid solution) was used according to the manufacturer's recommendation. Firstly, slides were incubated in elastin stain solution for 10 minutes. After rinsing in tap water, slides were differentiated in ferric chloride solution followed by a tap water rinse. Slides were transferred to 95% ethanol for 1 minute and then incubated in Van Gieson stain for 2 minutes (Hayashi et al., 2004).

2.3.8.4 *Picrosirius*

The Picrosirius stain contains Sirius red (Direct Red 80) and Sirius Red 0.1% (w/v) in saturated picric acid (see Appendix 7). Collagen fibres are stained to different degrees with this stain depending upon their thickness from green (thin), yellow, orange, to red (thick) under crossed polar microscopy as they align parallel to the transmission axis of the filter (Rich and Whittaker, 2005). This stain was performed as described previously (Junqueira et al., 1979, Sweat et al., 1964, Puchtler et al., 1973). Briefly, slides were incubated in 0.1% (w/v) of direct Red 80, which was prepared in saturated picric acid for 1 hour at room temperature, followed by differentiation in 0.5% (v/v) acetic acid (Junqueira et al., 1979).

2.3.9 Elastic fibres and immune cells stain

2.3.9.1 *Giemsa and orcein (G and O)*

This stain was used to identify immune cell infiltration, and in particular mast cells (dark purple) and elastic fibres (black) (Harikumar et al., 2014)(see Appendix 8). Slides were incubated at room temperature in 0.5% (w/v) Orcein solution for 10 minutes. After rinsing in tap water for 10 minutes, the slides were incubated in 1ml Giemsa stock solution (diluted in 45ml H₂O) for 1 hour at 50°C in a water bath. Giemsa solution was prepared by dissolving 7.36g Giemsa in 500ml warm glycerol (~50°C) for 30 minutes with occasional mixing, cooling and 500ml methanol added. The solution was filtered before use and stored at room temperature (Pinkus, 1944, Pinkus and Hunter, 1960). After rinsing in tap water for 5 minutes, slides were incubated in 0.4% (95% ethanol/eosin Y solution) for 2-3 minutes until the collagen fibres stained pink (as observed by microscopy).

2.3.10 Basement membrane and glycogen deposition

2.3.10.1 *Periodic acid Schiff*

The periodic acid Schiff (PAS) stain kit (Sigma, 395B) contains Haematoxylin Solution (Gill No.3), periodic acid solution and Schiff's reagent. This kit was used according to the manufacture's recommendation. It is a very common stain used to identify non-enzymatic glycation (when glucose binds to the amino groups of proteins without enzymatic action). Schiff's reagent interacts with glycol and leads to the formation of aldehyde groups (appearing as red-purple) which mostly occurs in the basement membrane and to a lesser extent in collagen fibres (Singh et al., 2014). Slides were incubated in periodic acid reagent for 5 minutes, followed by a tap water rinse and

incubation in Schiff's reagent for 15 minutes. The slides were then rinsed in water and counterstained with Harris' haematoxylin.

2.3.11 Chromogenic immunohistochemistry (IHC)

A list of all antibodies used in this thesis are listed in (Appendix 5), herein only the antibodies with positive signal are shown in the method section. An evaluation of antigenicity was performed using IHC with antisera raised against the following proteins: CD68 (SC-9139 Santa Cruz Biotechnology Inc, Santa Cruz, CA, USA), CD31 (Cellworks, Caltag Medsystems Ltd, Buckingham, UK Cat No ZHA-1225), rabbit anti-involucrin (1/50 dilution; PRB-140C; Covance, Maidenhead, UK), rabbit anti-keratin 14 (K14) (1/500 dilution; stock: 1mg/ml; PRB-155P; Covance), RAGE IHC antibody ready to use (IW-PA1069 IHC World, LLC, Woodstock, USA) and mouse anti-proliferating cell nuclear antigen (PCNA) (1/100 dilution; P8825; Sigma), Hypoxia-inducible factor 1-alpha HIF1- α (1/50 dilution; Santa Cruz, USA). Tissue sections were deparaffinised and hydrated (Table 2.1). Prior to antibody incubation, endogenous peroxidases were inactivated by treatment with 3% hydrogen peroxide in methanol (v/v) for 10-30 minutes, followed by a wash in PBS-T containing 0.1% (v/v) Triton X-100 (PBS-T). A 15-30 minute 5% goat serum block in PBS preceded incubation with primary antibodies for 90 minutes at RT (all diluted in PBS). Subsequently, slides were incubated with species-appropriate HRP-conjugated secondary antibodies (all used at 1/200 dilution in PBS for 1 hour). After washing in PBS-T, slides were developed using chromogenic detection (DAB Peroxidase (HRP) Substrate (Vector Laboratories, Peterborough, UK)) and counterstained with Harris' haematoxylin for 8 minutes followed by rinsing in water, 30 seconds in 1% HCl in 70% ethanol (v/v) (differentiation), 1 minute rinsing in water, 30 seconds in 0.1% (w/v) sodium bicarbonate (blueing), 5 minutes rinsing in water, then dehydrated and cleared as routine for special stains, and mounted in Vectashield™ hardset Mounting Medium (Vector Laboratories, Peterborough, UK).

STAGE	REAGENT	DURATION	NOTES
1	Xylene	2x 2 min	Dewaxing
2	100% EtOH	2x1 min	Rehydration
	90% EtOH	1 min	
3	0.3% H ₂ O ₂ (in methanol, optional)	20 min	Blocking of the endogenous peroxidase activity.
4	PBS-T	3 min	Wash
5	Pressure cooking in citrate buffer (optional)	10 min	Antigen retrieval
6	PBS-T	3 min	Wash
7	Running tap water	1 min	Rinse
8	5% serum block in PBS-T	20 min	Blocking
9	1° antibody at empirically determined dilution	60 min to overnight (RT to 4°C)	First layer
10	PBS-T	3 min	Wash
11	2° antibody (HRP labelled) (1/200 dilution).	30 min (RT)	Second layer
12	PBS-T	3 min	Washing
13	Chromagen	2-10 min (determine empirically)	Detection
14	Running water	1 min	Rinse
15	Dehydrate, clear and mount		

Table 2-1 Immunohistochemical chromogenic detection.

2.3.12 Immunofluorescence

Some of the biomarkers investigated in this study have been tested using fluorescence IHC. In this method the antibody-mediated antigen interaction can be visualised by fluorescence (FITC, TRITC) tagged secondary antibodies. This protocol has fewer steps than for the IHC enzymatic method because there is no need for a substrate to activate the enzyme (blocking endogenous and enzyme activation steps were omitted). Instead, organic fluorophores are conjugated to the secondary antibody which can then be detected under a fluorescent microscope. Different antigen retrieval (AR) methods (Table 2.2) were applied with some antibodies to unmask the antigen site for antibody binding action. Briefly, after the dewaxing and rehydration steps, the sections underwent blocking nonspecific background staining by a 15-30 minute incubation with the 5% serum from the species, used to create secondary antibodies (2°Ab). Then slides were incubated for 1 hour at RT with the primary antibodies (diluted according to manufacturer's recommendation or optimised to the optimal dilution), before incubation in FITC or TRITC-conjugated anti- IgG anti-sera for 30 to 60 minutes at RT following a PBS-T wash. After a second wash, slides were mounted in VectaShield™ Mount containing the nuclear stain DAPI (Vector Laboratories) and viewed using the fluorescence Nikon microscope (Nikon Eclipse 80i, Nikon Corporation, Japan).

STAGE	REAGENT	DURATION	NOTES
1	Incubator	To melt the wax heat at 60 °C in the oven.	15 to 30 min
2	Rehydrate tissues	2x HistoClear (2 min), 100%, 90%, 75% EtOH (1 min each), running water.	
3	0.1% trypsin	Enzymatic or heat antigen retrieval in the pH 6-9 solution.	30 min, 10 min 37 °C /120 °C
4	0.2% glycine in PBS, tap water rinse	5min RT to Stop enzyme, cooling slides for 10 mins.	0.2% glycine in PBS, rinsing
5 Optional	PBS-T	Wash	Rinse RT
6	5% serum in PBS	Block stage. Use serum from the species used to create 2°Ab.	20 min RT
7	1°Ab in PBS / 2% serum	Dilution: according to the manufacturer's recommendation	1h.30.min RT
8	PBS-T		3 min
9	2°Ab in PBS / 2% serum	FITC or TRITC-conjugated anti- IgG anti-sera at 1/400 dilution.	1 hr RT
10	PBS-T		3min
11	Mount	Use hard setting mounting media with DAPI.	

Table 2-2 Immunofluorescence protocol.

2.3.13 Antigen retrieval methods

Poorer immunostaining occurs with formalin-fixed tissues as compared to frozen sections, due to the cross-linking of proteins (antigens) during the fixation process. This can render the epitopes (antibody-binding locations) of antigens inaccessible to many antibodies (epitope masking), preventing detection by several immunohistochemical methods. A number of methods were assessed to unmask antigens, including enzymatic treatment (e.g. trypsin), heat-based methods in citrate buffer of varying pH (using a microwave) or a combination of pressure and heating (steamer or pressure cooker). The process of protein cross-linking is progressive i.e. the longer the fixation time, the stronger the cross-linking. This is enhanced by increasing the temperature, which also leads to a reduction in immunochemical detection (Webster et al., 2009). Antigen retrieval was performed as described below. Briefly, sections were de-waxed (by placing the slides for 5 minutes in the oven) and rehydrated. Sections were then treated with 0.1% trypsin (PBS/ tween 20) for 30 minutes at 37°C, followed by 5 minutes in 0.2% glycine/ PBS-T to stop the enzymatic action and then processed according to the standard IHC protocol (as discussed above). The different antigen retrieval methods included;

2.3.13.1 Microwaving

A 800-watt microwave oven was used to preheat 400–600ml of citrate buffer to 95°C before incubation of the de-waxed and rehydration of the slides. Sections were then maintained at 95°C for 10 minutes (ensuring that the buffer covered all the sections). Slides were allowed to cool in the buffer for a minimum of 30 minutes before washing in PBS-T prior to IHC.

2.3.13.2 Steaming

A steamer filled with 1l of citrate retrieval buffer (pH 6.0), was preheated to 80°C, and then the slides were placed in a metal jar filled with the buffer, and heated for 30 minutes, followed by cooling for 15 minutes.

2.3.13.3 Pressure cooking

The citrate buffer was preheated to 120°C (10 minutes on a hotplate) before immersing the sections in a metal rack and securing the pressure cooker lid. Once the cooker had reached the full pressure (approximately 5-10 minutes) the pressure cooker was placed

in an empty sink after releasing the pressure valve and cold water was run over the cooker for 3-5 minutes. Slides were left to cool for an additional 5 to 10 minutes after opening the lid before IHC staining.

2.4 ScanScope imaging protocol

All chromogenic IHC, and most of the histology stained sections were scanned by a digital scanner (CS2, Aperio, Vista, USA) under x40 magnification. Images scanning the entire tissue were saved as 'Cis' files, viewed and analysed using ImageScope™ software. This software provides powerful viewing analysis tools to scan the entire slide with high resolution images and various image analysis options (Olson, 2013). The operation and calibration steps were followed according to manufacturer's recommendations. Briefly, a series of critical calibration steps were carried out using the Aperio Scanscope, and some illustrative figures referring to the screen shots of these calibration steps shown below.

In the five options of the first window (Start, Scan area, Focus Points, Calibrate, Scan) which influence the image results (as seen in Figure 2.3), there options have to be adjusted to give a better image quality. In the scan area window option, choosing (20x doubled magnification, with narrow stripes) gave better images quality (particularly with big specimens). However, choosing 40x doubled magnification with wide stripes was not applicable when scanning multiple tissues (TMA) to generate good resolution of whole samples.

The number of focus points, and the location of the blue point into the clear area out from the focus point rectangle will affect the clarity of the scanned tissue and background noise ratio (Figure 2.4 and 2.5 respectively). Before running the analysis for the whole slide after setting these parameters, one has to get quick snapshots and review them, making sure they are clear from air bubbles, debris, and that the focal point is located correctly by visualizing clear tissue with less background staining density (Figure 2.6). By following these steps high quality images were obtained which improved the analysis of skin structure (Figure 2.7).

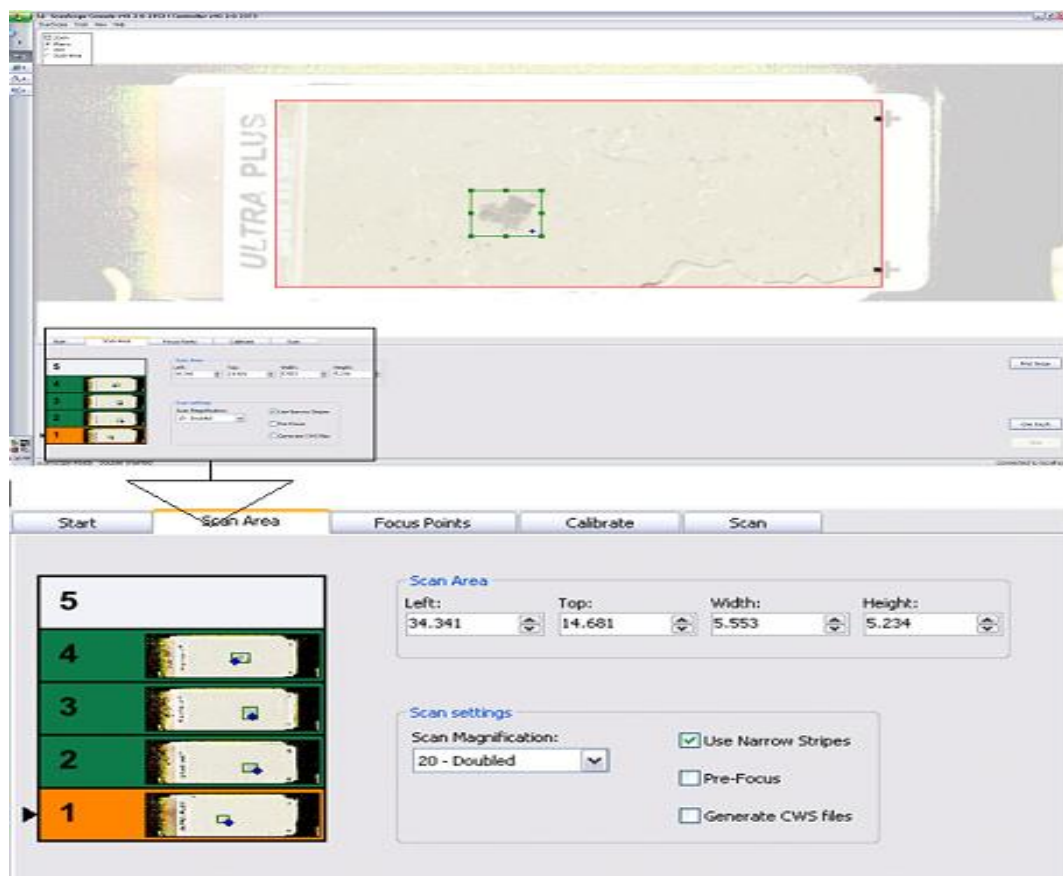


Figure 2-3 Schematic for the Imgescope™ software showing the scan area options setup.

The image was scanned at 20x magnification and narrow strips option.

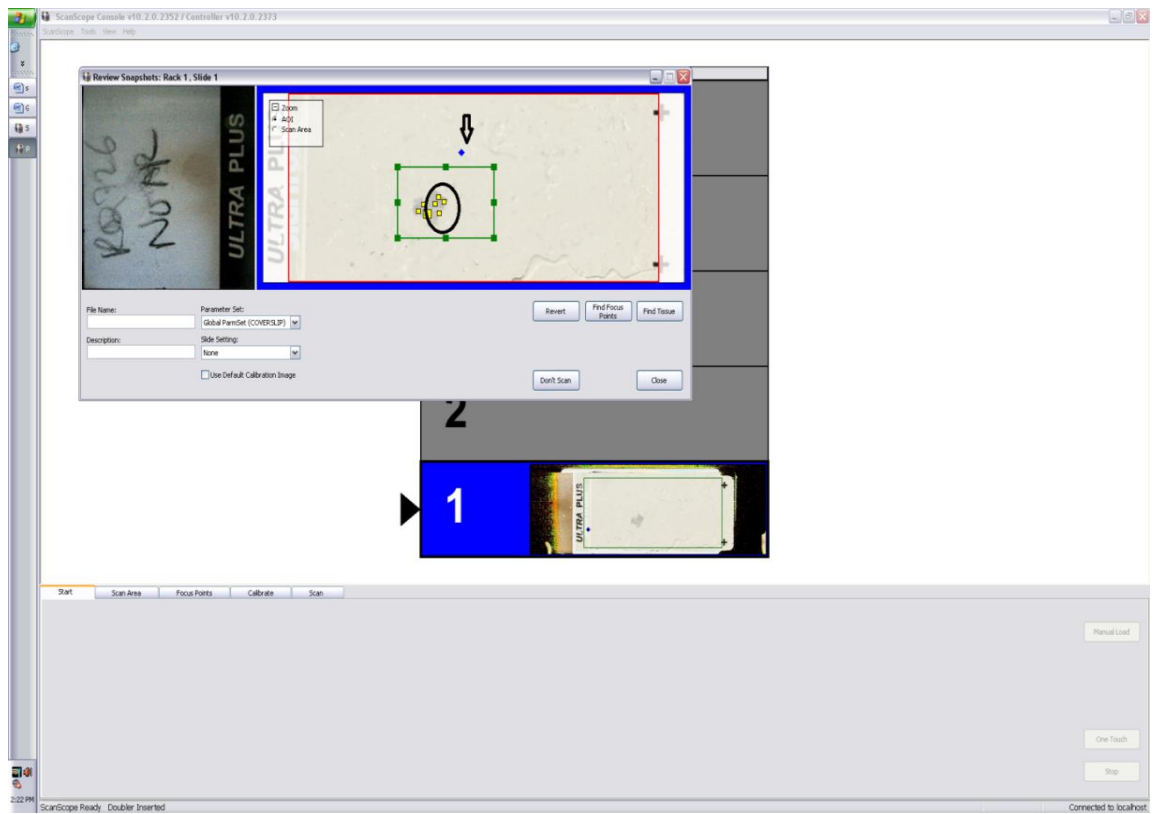


Figure 2-4 Scanning and calibration optimizing steps with the Aperio Imagescope™ software.

Setting up the focus points (circle) inside the calibrated area, and locating the blue diamond point (arrow) outside the scanned rectangle in a clean background.

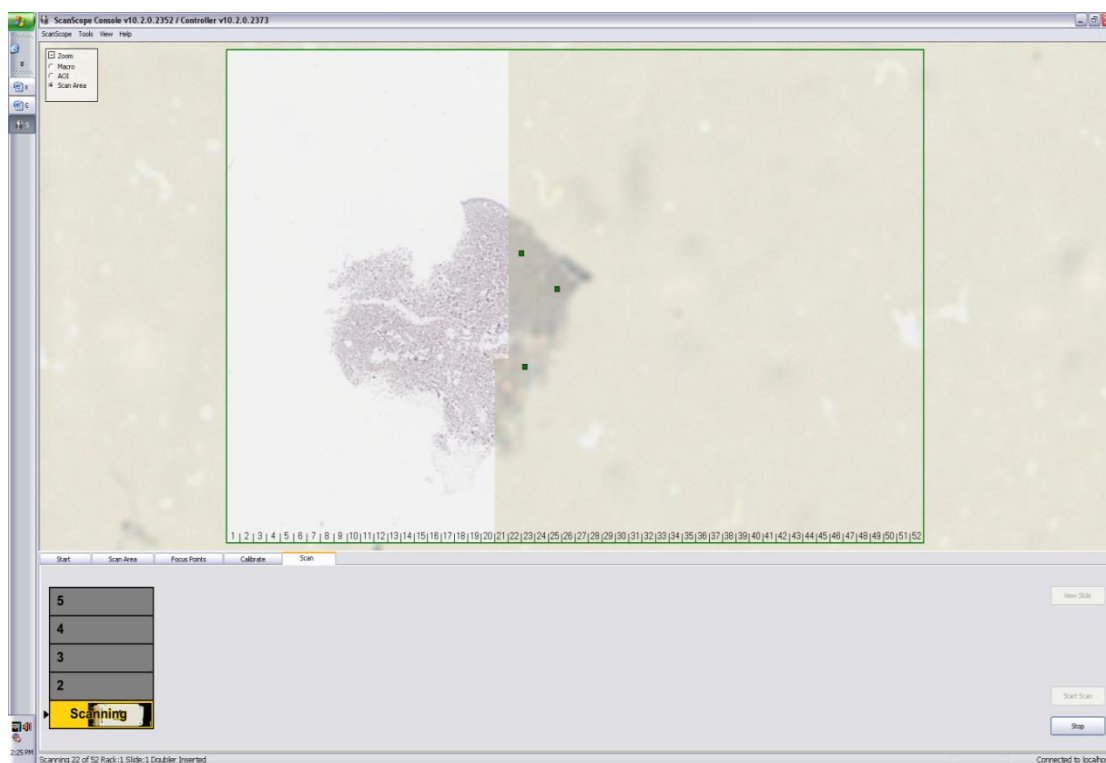


Figure 2-5 The scanning process.

Applying the narrow strips option from a skin sample scanned with the Aperio Imagescope™ software. The image was scanned at 20x magnification.

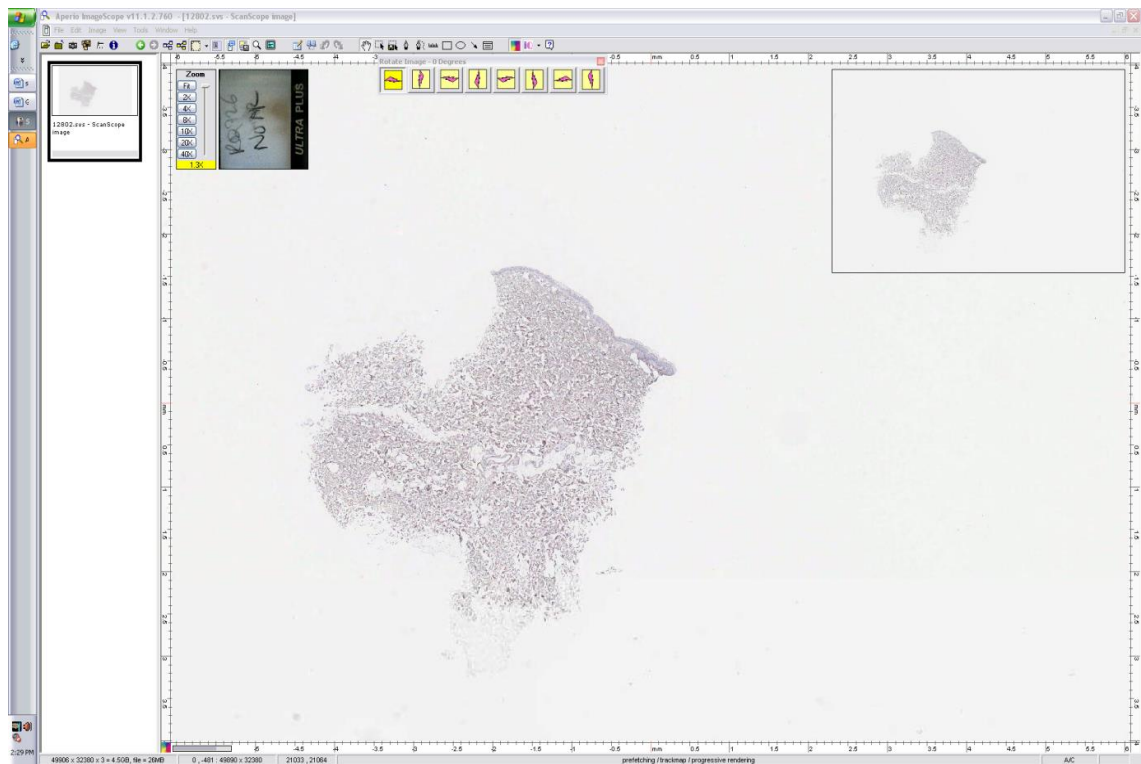


Figure 2-6 Snapshot review of a human skin sample at 1x magnification.

This step was used to evaluate the calibration setting.

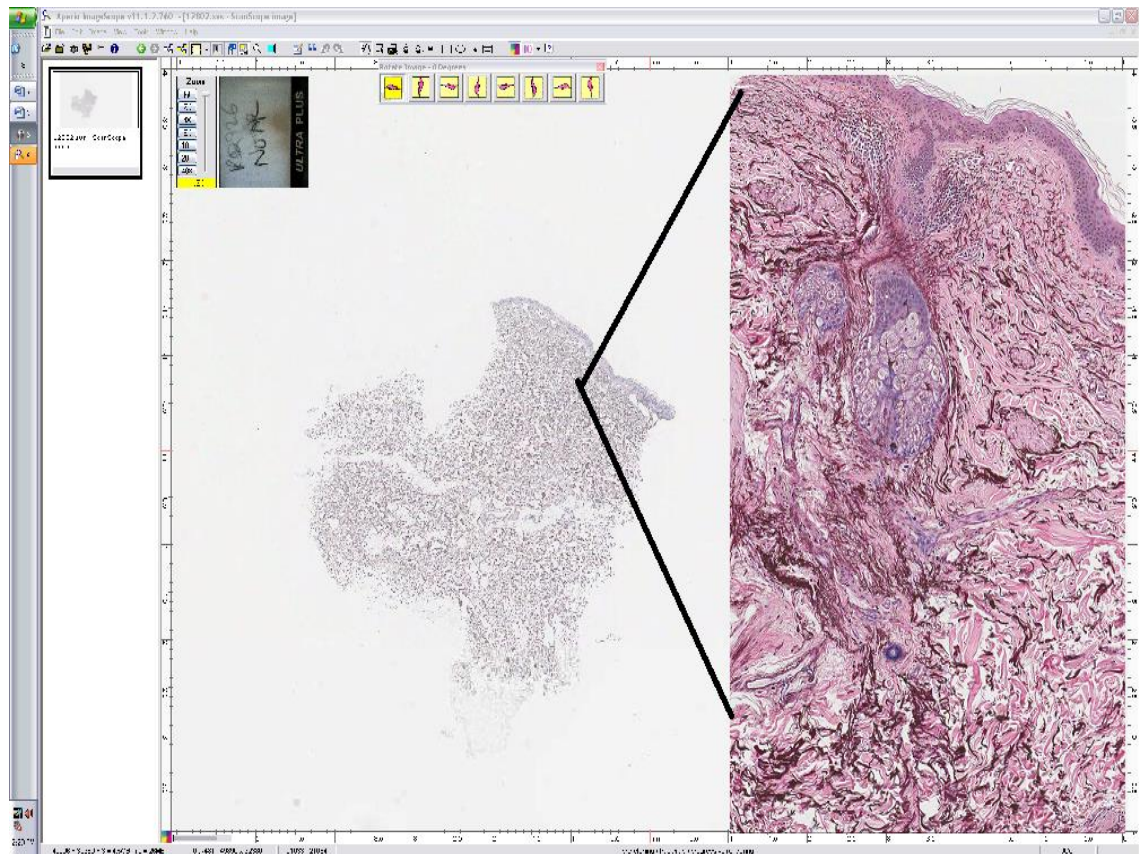


Figure 2-7 Human skin stained with G&O and scanned with the Aperio Imagescope™ software at 1x and 10x magnification.

This software enhances the analysis of skin morphology structure with the ability to discern the particular skin components (left panel) as well as the general structure.

2.5 Image capture and analysis

Whole-slide images were captured with an Aperio ScanScope CS scanner (Aperio, CA, USA) and additional fluorescent IHC images as well as picosirius red birefringence and fluorescent eosin under bright-field and cross-polar were captured using a Nikon TEi inverted microscope equipped with cross-polar optics (Nikon, Kingston, UK) and a QImaging CCD camera operated by Nikon NIS imaging software (version 4.10.01). Eosin fluorescence and other stains were assessed with the Nikon TEi instrument using a Nikon C-FL Epi-FI TRITC Filter Block (excitation wavelength 547nm, emission wavelength 572nm; Barrier Filter BA605/55). The grading of special stains and IHC images were completed with an ordinal scale Table 2.3.

Grading scale for especial stains and IHC images	
Grade index	Specific criteria
- (poor)	There is a lack of consistency and a disruption of key features as identified by the special stain, or lack of antigenic signal with IHC
† (satisfactory)	The main components highlighted by the special stain could be identified but a lack of consistency or disruption of features was still evident or variation in signal, both within and between samples in IHC
†† (good)	The desired features were identified following special staining or IHC, with consistency within and between samples
†††(Best)	indicates optimal staining consistency and feature visualisation for the individual special stain, or signal accuracy and strength in IHC

Table 2-3 Qualitative description of IHC images.

The scoring relates to the consistency of special stains or the level of IHC signal seen (rather than the general morphology of tissue).

2.6 Preparation of dermal fibroblasts

2.6.1 Explant culture of dermal fibroblast

The explant method grows dermal fibroblasts out of a skin specimen. Briefly, dorsally shaved skin samples were wiped with 70% alcohol before dissecting and under sterile conditions pieces were washed gently in PBS after removal of the connective tissue. Then each sample was incubated in 0.3% trypsin for 60-90 minutes at 37°C in a water bath under continuous shaking (350 cycles/per minute). The epidermis and the remaining connective tissue were removed and the dermal sheets were washed three times in PBS containing 1% penicillin/streptomycin prior to incubation in a petri dish with 10ml of DMEM supplemented with 10% bovine serum at 37C°/5% CO₂ incubator for 3-6 days.

2.6.2 Enzymatic isolation of fibroblasts

Dorsal skin was shaved, and wiped with 70% alcohol before dissecting a 4x4cm piece from each mouse model. Then the skin was incubated in 0.3% trypsin/2.5%/PBS for 50 minutes under continuous shaking in a 37°C water bath to aid epidermal dissociation. Each specimen was then transferred to a petri dish containing 5ml of 1% penicillin/streptomycin in PBS. Subsequently, using fine forceps, the dermis was peeled from the underlying subcutaneous fat (cleaning the dermis sheet from connective tissue). The dermal sheet was placed in a 20ml sterile tube containing 1ml PBS and then chopped into small (2-4mm) pieces prior to transferring 2.6ml of the cell mixture to 10.4ml of type IV collagenase (0.5mg/ml Lot 089K862) in a 50ml tube. The contents were incubated for 5 minutes under continuous shaking in a 37°C water bath and 13ml of ice cold complete DMEM, containing 10% foetal bovine serum added to stop further collagenase action. Fibroblasts were released by vortexing (1-2 minute) and debris was removed by passing the suspension through (80-100µm) a nylon mesh. The suspension was divided into four 10ml tubes and centrifuged at 150g for 10 minutes at 4°C. The supernatant was discarded and the pellets were resuspended in complete medium and seeded into collagen-coated tissue culture flasks (Cell Culture flask EZ flask collagen I coated, 25cm², Thermo Scientific Nunc). Fibroblasts were maintained in a 37°C/5% CO₂ incubator over 5-10 days until the cells were 70-90% confluent (passage 1). Primary dermal fibroblast cell lines from 3 *ob/ob* mice and 3 age-matched wild-type controls were cultured and expanded in supplemented DMEM (Chapter 5) and used in experiments at passages 1-5.

2.6.3 Western blotting

Primary dermal fibroblasts were isolated from 12 week old, male, *wt/wt*, *ob/ob*, misty, and *db/db* as well as 20 month old *wt/wt*. Cells were lysed in 150µL RIPA buffer (see Appendix 9) containing protease inhibitors. Lysates were shaken at 4°C for 15 minutes before centrifugation at 14,000g for 15 minutes at 4°C. 30µg protein was subjected to 10% SDS-PAGE before electrophoretic transfer onto nitrocellulose membranes. Blots were blocked in 5% BSA and probed with a polyclonal antibody to the insulin receptor β-subunit (IRβ, Cell Signaling Technologies, Danvers, MA, USA, 1:1000 dilution) overnight at 4°C. Following a one-hour incubation with an HRP-conjugated secondary antibody (goat anti-rabbit, 1:10000 dilution, Merck Millipore, Billerica, MA, USA),

blots were washed and developed with a chemiluminescent substrate (Supersignal West Pico, ThermoFisher, Rockford, IL, USA). Protein expression was quantified using Gelquant™ software (DNR Bioimaging Systems Ltd, version 2.7.0) and expression relative to GAPDH calculated.

2.6.4 Dermal fibroblast experiments

2.6.4.1 Cell viability

When dermal fibroblast cells reached the desired confluence, cell viability was measured by adding 0.4ml of the cell mixture to 0.1ml trypan blue with 0.01 ml of the mixture transferred to a haemocytometer. The percentage viable cells (with clear cytoplasm) to nonviable cells (blue cytoplasm) described cell viability (Strober, 2001). The dermal fibroblast cells viability were between 70-90%.

2.6.4.2 Proliferation

Proliferation was assessed using methylene blue uptake, as previously described (Olsson et al., 1982). Pre-confluent cells were assayed 2, 4, and 6 days post-plating. Cells were washed in PBS and fixed in 10% formaldehyde solution (v/v in PBS). After washing in borate buffer (10mM, pH8.4), cells were incubated with methylene blue (1% w/v, in borate buffer) for 10 minutes at room temperature. Cells were then washed under running water until no free dye persisted. After drying, methylene blue was eluted in 0.1N hydrochloric acid for 10 minutes at 50°C and the absorbance OD_{630nm} was measured.

2.6.4.3 Collagen production

Collagen synthesis was measured using a modified method of Heng et al (Heng et al., 2006). Pre-confluent culture plates were washed 3 times in PBS and fixed with Bouin's solution for one hour at room temperature before thorough rinsing in running water and air-drying overnight. Cells were stained for one hour at room temperature in picosirius solution (1mg/ml Direct Red 80 in saturated picric acid) with gentle agitation. Any free dye was removed with 4 washes in 0.01N HCl, before plates were dried for 20 minutes at 70°C. Incorporated dye was eluted in 0.1N NaOH with mild agitation for 30 minutes and the OD at 550nm determined by spectrophotometry. Values were normalised relative to total protein content measured using Bradford reagent (Bio-Rad Laboratories Ltd. Bio-Rad House Maxted Road) according to the manufacturer's recommendations. Briefly, the protein standards, 0.1-1.4mg/ml was prepared using bovine serum albumin

(BSA). Then 5µl of the protein standards and cell lysates were added to separate wells in a 96 well plate in duplicates, and 5µl of 1% Triton-X-100 was added to the blank wells. 250µl of Bradford reagent was then added to each well and mixed. Samples were incubated for 30 minutes and read at 595 nm.

$$\text{Protein (mg/ml)} = \frac{\text{A sample} \times \text{C standard}}{\text{A standard}}$$

Where A is absorbance at 595nm and C is concentration of standard mg/ml.

2.6.4.4 *Senescence- associated β-galactosidase assay*

Pre-confluent cells were washed twice in PBS and fixed for 15 minutes at room temperature in phosphate buffer (pH 7.3) containing 5mM EGTA, 2mM MgCl₂ and 0.2% glutaraldehyde. Following 2 washes in 2-3 ml of 0.1M phosphate buffer containing 2 mM MgCl₂, 1 mg/ml X-gal (in 0.1M phosphate buffer, 2mM MgCl₂, and 5mM potassium ferrocyanide) was added and the cells were incubated overnight at 37°C before thorough washing in PBS and analysis. Cells were visualized under a light microscope and the proportion of blue positively stained (senescent) cells was counted according to Bimri et al. The percentage area of β-galactosidase positive-cells was determined in 8 fields, from replicate cultures using VIS image analysis software (VisioPharm, Hoersholm, Denmark).

2.6.5 Statistical analysis

Statistical analysis was performed using GraphPad Prism™ 5 software (La Jolla, USA). All results are expressed as mean ± standard error of the mean (SEM) with a p<0.05 considered as statistically significant (*p<0.05, **p<0.01, ***p<0.001). Statistical differences were determined using an unpaired two-tailed Student's t-test or one- or two way ANOVA with a post-hoc Dunnett's test or followed by a Bonferroni post-test for selected data unless otherwise stated.

Chapter 3: Skin Histology of Mouse Models of Obesity and Type 2 Diabetes

3.1 Introduction

The majority of individuals diagnosed with type 2 diabetes mellitus will experience skin complications during the natural history of their disease, ranging from relatively benign epidermal manifestations, such as acanthosis nigricans, diabetic thick skin, through to potentially harmful delays in wound healing, and diabetic foot ulcers (Romano et al., 1998, Baloch et al., 2008). Addressing these sub clinical changes at the molecular level in order to understand the cutaneous complications and its pathogenesis in humans is difficult as there are many contributing factors in this disease and the skin presentation is complex. Furthermore there is a notable lack of skin donor availability, homogeneity as well as clear ethical constraints. These confounders have directed the researchers to rely on alternative experimental sources: including *in vitro* models, genetically engineered animal models, *ex vivo*, and xenotransplantation tools (Guerrero-Aspizua et al., 2010) to unravel the sophisticated aetiology and pathways (Treuting and Dintzis, 2011).

Mouse skin has been well acknowledged as an essential tool to study human skin diseases, including skin cancer, dermatological lesions, infections, hair loss and wound healing (Avci et al., 2013). Wild-type mice exposed to calorie-rich diets, or genetic mutants that lack the satiety regulator leptin (*ob/ob* mice) or its receptor (*db/db* mice), are widely used in the study of type 2 diabetes. These models are associated with weight gain, increasing plasma glucose levels and progressive insulin-resistance, and in the case of *db/db* mice, the eventual deterioration in pancreatic islet function modelling end-stage human disease (Hummel et al., 1966, Surwit et al., 1988). These animals also display the compromised re-epithelialisation and chronic inflammation, characteristic of non-healing diabetic wounds in man, and therefore, are widely used in wound healing studies (Frank et al., 2000). There is a lack of full knowledge of pathological changes in mouse models of obesity and type 2 diabetes skin in the literature. This might be due to the fact that mouse skin is much thinner, softer, and much more difficult to obtain good histological sections than human skin. Furthermore, the compressed anatomical structure in mouse skin (in comparison to human skin) characterised by thinner epidermis, poor vascularisation, the absence of rete ridges, clear boundary between reticular, and papillary dermis present many disadvantages if one seeking exploring these phenotypes.

Likewise, the major challenge in detecting the pathological changes in these mouse models was achieving good histological sections. Particularly, loss of architecture during processing, and other artefacts which has implications for later downstream applications.

3.2 Materials and methods

3.2.1 Histology of diabetic mouse skin

Dorsal skin sample from male from eight biological animal models; *wt/wt*, *ob/ob*, *misty*, *db/db*, *DIO*, lean (12 month), *ob/ob* with high fat diet, and ageing *wt/wt* at 20 month old (n=6). Three replicates from each mouse were cut into 5x10 mm and placed in plastic cassettes prior to be fixed in 10% NBF for 3 days at RT. Samples were processed for approximately 10 hours according to the long processing protocol (Appendix 3). Then 4µ paraffin embedded sections were generated using the softening agent (Appendix 4) prior to IHC analysis (as described in Chapter 2). A list of antibodies used in evaluating diabetic mouse skin phenotypes are detailed in (Appendix 5). Various procedures were employed including antigen retrieval, different primary antibodies (1Abs), and different incubation conditions to optimise the immunostaining results. Detailed below are the antibodies (which gave meaningful results), and the optimised dilutions and incubation conditions (Table 3.1).

Antibodies	1°Ab / Antigen Retrieval (AR)
PCNA	1:100 / 10 min pressure cooker/citrate buffer pH=6
Involucrin	1:50 / trypsin-EDTA
Profilaggrin	1:100 /10 min pressure cooker/ citrate buffer, pH6
CD31	1:200/10 min pressure cooker/ citrate buffer, pH6
CD68	1: 50 /10 min pressure cooker/ citrate buffer, pH6
keratin 14	1:2000/10 min pressure cooker/ citrate buffer pH=6
RAGE	1:500/ 10 min pressure cooker/ citrate buffer pH=6

Table 3-1 Primary antibody dilution and antigen revival (AR) method.

3.3 Results

3.3.1 Murine models of obesity and diabetes

Physiological measurements from various mouse models of insulin resistance, obesity and type 2 diabetes are described in Table 3.2. Ageing was associated with a small rise in fasting blood glucose in *wt/wt* animals, whilst those maintained on a high fat diet became mildly hyperglycaemic. Both genetically-obese models (*ob/ob* and *db/db*) showed hyperglycaemia. Circulating insulin acts to counter elevated plasma glucose and maintain a normoglycaemic state, and increased insulin levels were recorded in both obese (DIO) mice which were maintained on a high fat diet for 12 months, and in *ob/ob* mice. However, decreased insulin levels (even in the presence of high glucose levels) were measured in type 2 diabetic *db/db* animals.

Strain	Age (months)	Diet	Weight (g) (mean +SEM)	Glucose [mM]	Insulin [pM]
<i>wt/wt</i>	3	chow	26.6+/- 0.44	3.9+/-0.54	278+/-13
<i>wt/wt</i>	12	chow	39.6+/-0.9	6.2+/-0.3	298+/- 48
<i>wt/wt</i>	12 (DIO)	45% fat	44.5+/-0.6	7.2 +/- 0.6	2730 +/- 300
<i>ob/ob</i>	3	chow	46.5+/-5.5	8.7+/-3.3	4938+/- 1973
<i>ob/ob</i>	3	45% fat	52.6 +/- 4.2	10.7+/- 3.1	8800+/- 3852
Misty	3	chow	23.9+/-1.4	5.4+/-0.5	114+/-18
<i>db/db</i>	3	chow	45.3+/-3.6	14.8+/-2.6	1399+/-329

Table 3-2 Body weight, fasting blood glucose and plasma insulin levels in murine models of obesity and type 2 diabetes.

Mean values +/- SEM are shown from 6 animals per group.

3.3.2 Cutaneous organizations in insulin resistance, obesity, and old mice models

When comparing the morphological structure across these models I noticed that the structure of the dermis and subcutis changed with progressive insulin resistance, with the greatest disruption occurring in the dermis (Figure 3.1A). An increase in subcutaneous fat deposition relative to age-matched chow fed controls (12 months old) characterised the skin of *wt/wt* mice maintained on a high fat diet (DIO) (Buettner et al., 2007). Whereas tissue from *ob/ob* mice, which are a more severe model of obesity and insulin resistance showed both increased fat deposition and dermal erosion as compared to age-matched controls and this phenotype was exacerbated by a high fat diet as shown with H&E stained sections (Figure 3.1A). Complete loss of the reticular layer characterised tissue from *ob/ob* animals maintained on a high fat diet and the persisting sub-epidermal papillary dermis showed a loss of collagen integrity. Picrosirius staining

effectively demonstrated normal collagen organisation, and the well-organised “basketweave” of thick fibres characteristic of young lean skin, which was progressively lost with hyperinsulinaemia (Figure 3.1B). Loss of organisation was also seen to a lesser extent with age.

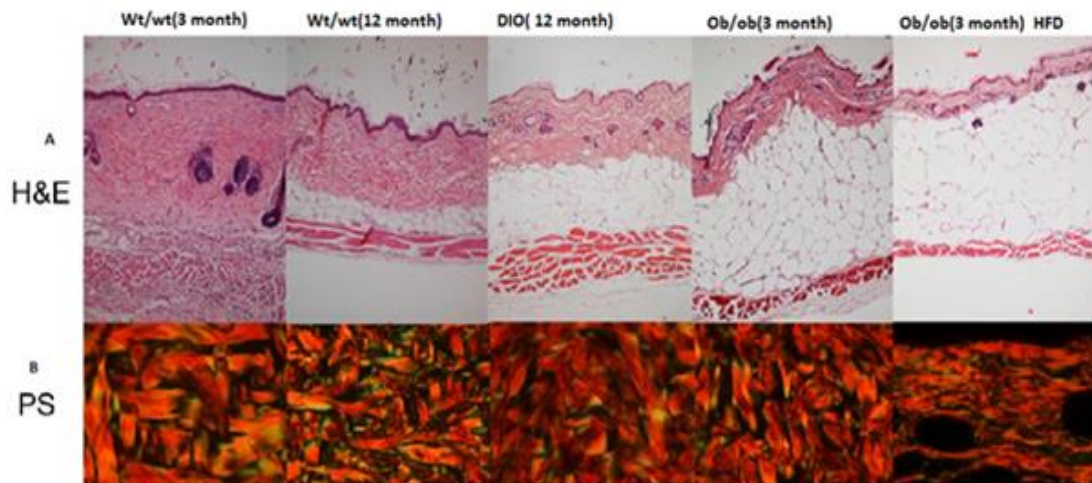


Figure 3-1 Skin compartments and collagen changes from different mouse models.

Representative images of H&E and PS stained sections from six mice per each group .(A) lean mice (*wt/wt*), and mouse models of obesity (DIO), insulin resistance (*ob/ob*) and age (12 month) with H&E and(B) with PicroSirious (under crossed-polar microscopy). Bright-field images were captured at 10x original magnification, and 50x under crossed-polar images.

3.3.3 Skin compartmental depth and body composition

Histological sections of skin from lean, insulin-resistant and ageing mice were used to measure dermal depth (Figure 3.2). Skin from 3 month old chow fed animals was characterised by a tightly packed dermis overlying a subcutis comprising one to two layers of adipocytes (Figure 3.2.A). In DIO mouse skin a slight increase in the subcutaneous layer (not significant) was not accompanied by a loss of dermis at 12 month of age (Figure 3.2.B). Fat deposition increased 3.6 fold in 12 month-old mice exposed to a high fat diet, when compared to lean controls at same age. However, while an increased space between collagen fibres characterised the dermis, there was no significant change in dermal depth (Figure 3.2I). Similar to previous reports, increased insulin resistance is a feature of ageing (Gkogkolou and Böhm, 2012, Osman et al., 2013a), and a slight reduction in dermal depth was recorded in wild-type mice maintained on chow at 20 months of age relative to 3 month *wt/wt* (Figures 3.2D and

3.2I). Insulin resistant *ob/ob* skin showed a 2.4 fold reduction in the size of the dermal compartment relative to controls, accompanied by a 6.3 fold subcutaneous expansion relative to wild-type controls (Figures 3.2E and 3.2I). This phenotype was exacerbated in *ob/ob* mice maintained on a high fat diet, and these animals displayed a 4.8 fold decrease in the dermis and an 8.8 fold adipose layer expansion relative to chow-fed wild-type controls (Figures 3.2F and 3.2J). Diabetic *db/db* animals displayed a 1.8 fold reduction in dermal depth and an 11 fold increase in adipose deposition compared to lean misty mice (Figures 3.2G, 3.2H and 3.2K). A significant increase in body weight, fat mass and % fat mass from 3 month old *ob/ob* and *db/db* as compared to their age matched controls was observed when measuring the body composition by DEXA (Dual Energy X-ray Absorptiometry) (Figure 3.3).

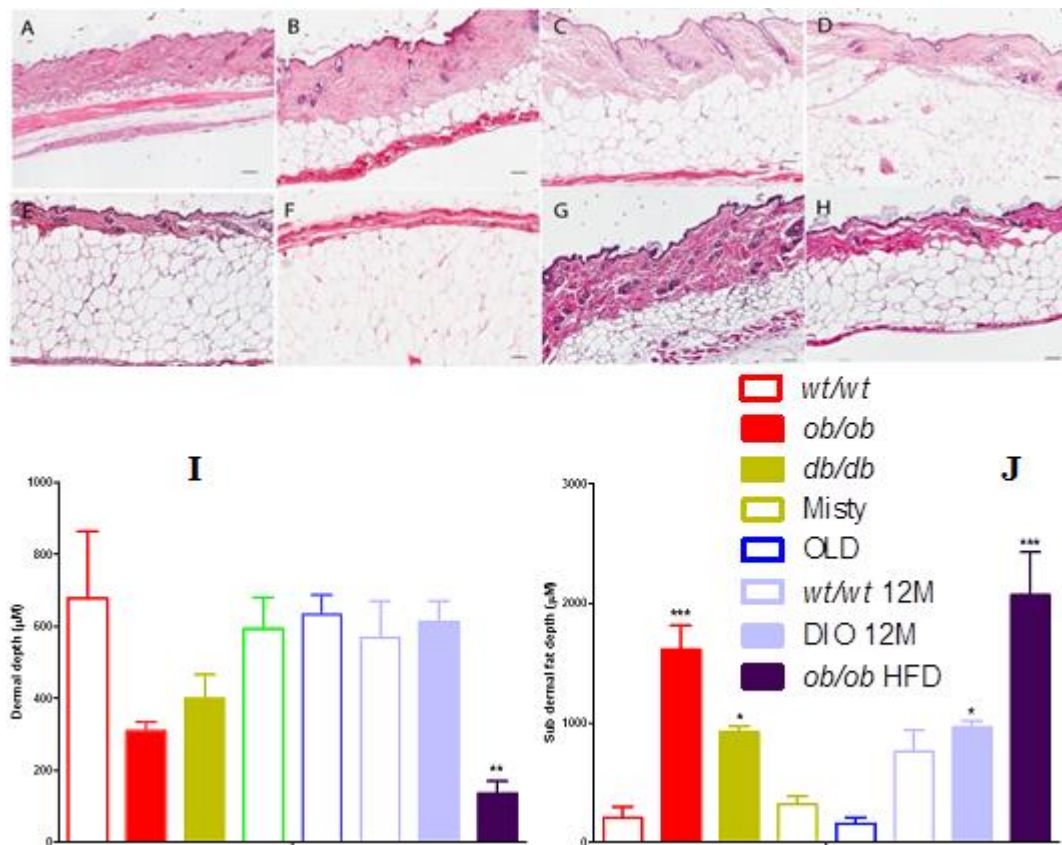


Figure 3-2. Cutaneous phenotypes in animal models of insulin resistance.

H&E stained paraffin sections representative images from 4-6 animals maintained on chow diet at 3 months (A) or 12 months without (B) or with fat diets (C), and from 20 month old mice on chow (D). Tissue from 3 month old *ob/ob* maintained on either chow or high fat diets are shown in E and F respectively. Finally, I studied tissue from 3 month old misty controls (G) and age matched *db/db* mice (H), both maintained on chow. Scale bars = 100 μm . I also quantified the dermal depth in (I), which revealed a significant loss of dermis with only *ob/ob* maintained on high fat diets. Dermal fat depth in showed a significant increase in *ob/ob* and *db/db* skin (J), which was exacerbated by a high fat diet. Significance was assessed by 1-way ANOVA with a post-hoc Dunnett's test. * $p < 0.05$, ** $p < 0.01$; *** $p < 0.001$.

Body composition (DEXA) 12 weeks of age

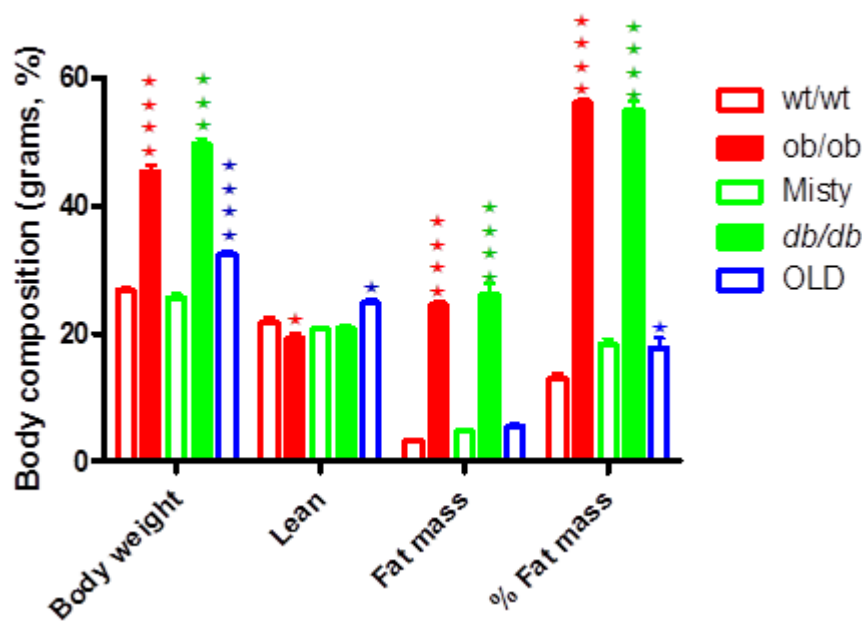


Figure 3-3 Body composition of mouse models of obesity and diabetes, and age.

By using DEXA (Dual Energy X-ray Absorptiometry) body weight, lean and fat mass, as well as the percentage of fat mass were measured from 6 animals at 3 month old *wt/wt*, *ob/ob*, *misty*, *db/db*, and 20 month old *wt/wt* (OLD) models. Significance was assessed by 1-way ANOVA followed by Dunnett's post-test. * $p < 0.05$,; *** $p < 0.001$, **** $p < 0.001$.

3.3.4 ECM structure and immune infiltration

The most abundant components of the extracellular matrix (ECM) of mouse skin are collagen fibres and elastic fibres to a lesser extent (Watt and Fujiwara, 2011). In wild type mouse skin, fine elastic fibres were difficult to discern from the relatively thick adnexal fibres in Giemsa and Orcein stained dermis (Figure 3.4A). Bundles of elastic fibres were observed in the upper layers of the dermis at 12 months of age, with an increased disorganisation in mice exposed to a high-fat diet. I did not observe any elastic areas in the skin from older mice, suggesting that localised elastosis may be a relatively stochastic phenomenon, rather than being specifically age-related. The considerable loss of dermis in the genetic models made it extremely difficult to assess the organisation of elastic fibres but no evidence of significant elastosis was detected.

Giemsa is an effective stain for immune cells, and mast cells are readily identified by their abundant cytoplasm that contains vivid purple-staining granules. Small numbers of mast cells are normally resident in the skin, but I did not observe a change in numbers in any of the models investigated. I did, however, observe an increase in CD68-positive macrophages in the dermis of 20 month old mice compared to young lean *wt/wt* mice (4-fold, $p=0.04$; Figure 3.7), but no significant change in any other state. Overall, there was no obvious significant evidence of inflammation in this study, nor was there evidence of angiogenesis in the CD31 stained sections in these models (Figure 3.7).

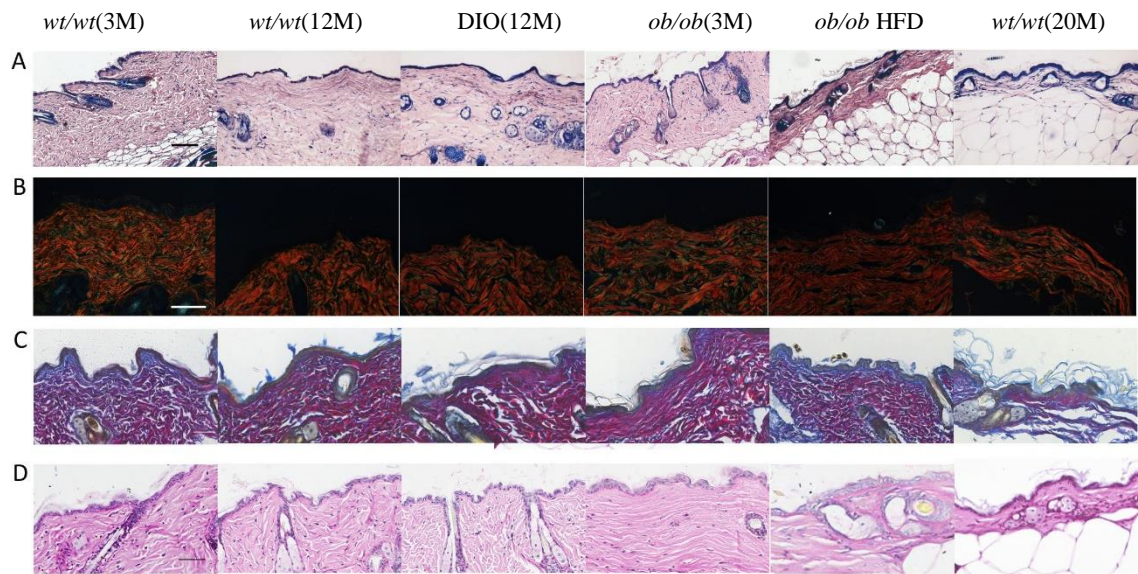


Figure 3-4 ECM organisation .

Representative images of 4-6 animals per each group. Tissues were stained with O&G (A), picrosirius (B), Herovici (C) and PAS (D) and viewed under bright-field, with the exception of cross-polar picrosirius images. (A) Elastic fibres appear dark purple/black, collagen rose pink, nuclei are dark blue, cytoplasm stains light blue and mast cells are characterised by purple cytoplasmic granules (difficult to discern at this magnification). Disorganised elastic fibre bundles can be seen in 12 month old animals. Scale bar =100 μ M. (B) shows the collagen basket-weave, revealed by picrosirius staining and cross-polar imaging. Scale bar =50 μ M. (C) Herovici staining identifies immature collagen as blue fibres and mature collagen as red fibres. Scale bar =50 μ M. (D) PAS staining highlights glycoproteins, predominantly in basement membranes and endothelial walls. Scale bar =100 μ M.

The birefringent property of picrosirius-stained collagen revealed a “basket-weave” conformation in young lean skin when viewed under polarised light (Figure 3.4.B) (Junqueira et al., 1979). The fine papillary and thicker reticular fibres meet approximately at the level of the sebaceous gland (seen as dark spaces) in picrosirius stained sections. Some relaxation of the basket-weave occurred in wild type chow-fed animals at 12 months of age, which was exacerbated by exposure to a high fat diet. Moreover, a loss of deeper reticular fibres was apparent in the latter group. A further loss of reticular fibres was detected in *ob/ob* mice, which was exacerbated in *db/db* skin. Strikingly, *ob/ob* animals maintained on a high fat diet retained only a thin layer of papillary dermis, which adopted a flattened, rather than basket-weave configuration. The deeper reticular dermis was all but lost in these tissues. Skin from an extreme-aged model also showed regions of basket-weave loss in the papillary dermis, as well as erosion of thicker reticular dermis.

Fiona Watt et al used Herovici’s polychrome to discern mature collagen fibres (red fibres) from immature fibres (blue fibres) (Collins et al., 2011a). This technique identified a layer of blue-staining collagen adjacent to the basement membrane in lean mice (Figure 3.4C). With increasing age, this pattern became discontinuous, and in the high fat-fed model, the blue layer was difficult to discern. The blue-staining layer was maintained in chow-fed *ob/ob* mice (albeit qualitatively reduced compared to controls), whereas exposure of these mice to a high-fat diet led to a loss of immature collagen fibres. In the extreme-aged model, collagen synthesis appeared to be discontinuous, and generally associated with epidermal ridges. PAS staining identified basement membranes and vasculature (Figure 3.4D). It is known that collagen and elastin in hyperglycaemic state undergo very slow non-enzymatic protein cross-linking and form heterogeneous group of protein-bound moieties called advance glycated end products (AGEs) which cause various complications in both diabetes and ageing (Nawale et al., 2006). Despite the increased levels of plasma glucose found in models of type 2 diabetes, increased glycation (except old mice skin) was not a prominent feature of any of the models studied. This confirmed by the lack of expression of RAGE IHC from the latest skin samples, and (Figure 3.6 left panel) shows a representative image from *db/db* skin(n=6). In contrast, the positive reaction of PAS materials (Figure 3.5), and RAGE immunoreactivity (Figure 3.6) were seen in the diabetic pancreas of *db/db* mice as evidence of glycation.

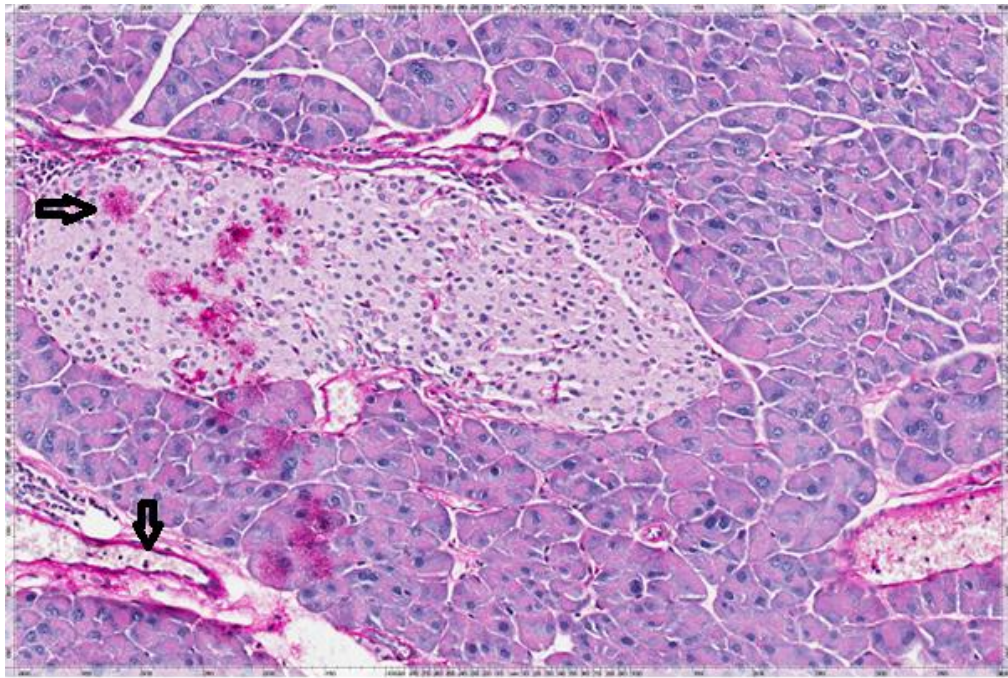


Figure 3-5 Representative image for positive PAS stain in diabetic pancreas.

PAS positive materials were detected in the pancreatic islet of diabetic mice (n=3), and blood vessel wall (arrows) from *db/db* mouse. Image was captured at 20x.

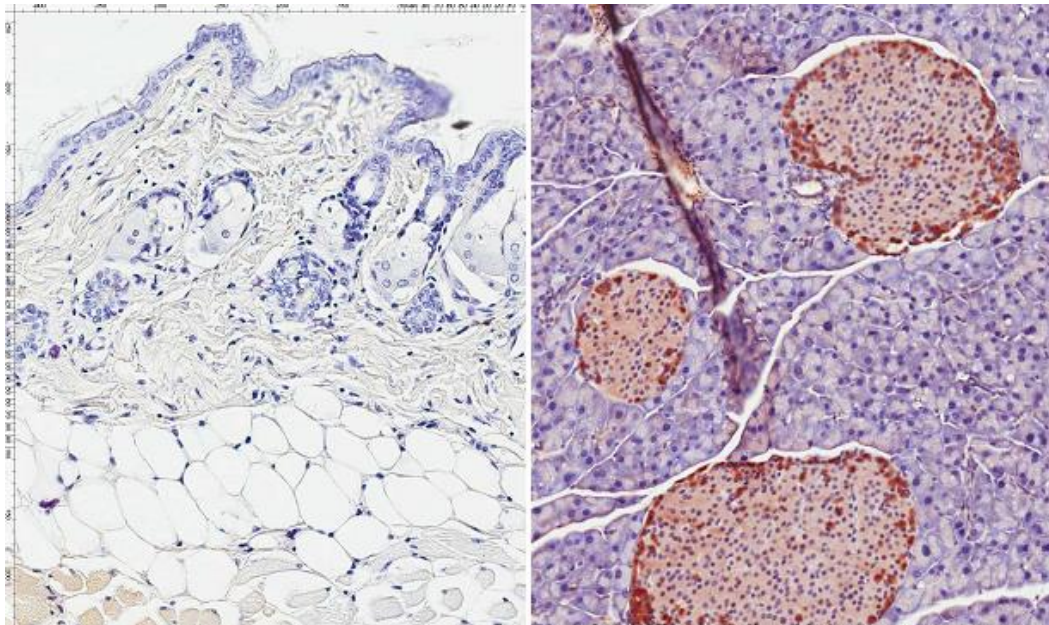


Figure 3-6 Representative images for expression of IHC with RAGE antibody.

Representative image in the left panel shows lack of expression RAGE IHC signal in skin from *db/db* animals (n=6). In the right panel refers to representative image of pancreas section from *db/db* mice (n=3) was stained with anti-RAGE antibody. The RAGE receptors were prominent in outer layer of the islet, where the alpha cells are localised. Image was captured at 20x.

3.3.5 Epidermal differentiation markers

Filaggrin expression normally decorates the upper spinous and granular epidermal layers, acting as an anchor for the assembly of keratin filaments in barrier formation (Dale and Holbrook, 1987). The expression of its precursor, profilaggrin, in normal and insulin-resistant states, as a marker of epidermal differentiation was detected (Figure 3.7), however, no gross changes in profilaggrin were seen in either DIO mice, or in chow-fed *ob/ob* or *db/db* mice relative to lean controls. Consistent with these results, no gross alterations were seen in the expression of involucrin, which is an earlier marker of epidermal differentiation, (Figure 3.8) (Gudjonsson et al., 2007). Interestingly, a qualitative reduction in PCNA immunoreactive cells was detected only in the most extreme obese group (high fat-fed *ob/ob* animals). Whilst no little changes were seen in the expression of the basal keratin K14 across any investigated models, with the exception of the high-fat fed *ob/ob* animals, which showed a lower level of immunoreactivity, although staining, remained continuous throughout the compartment.

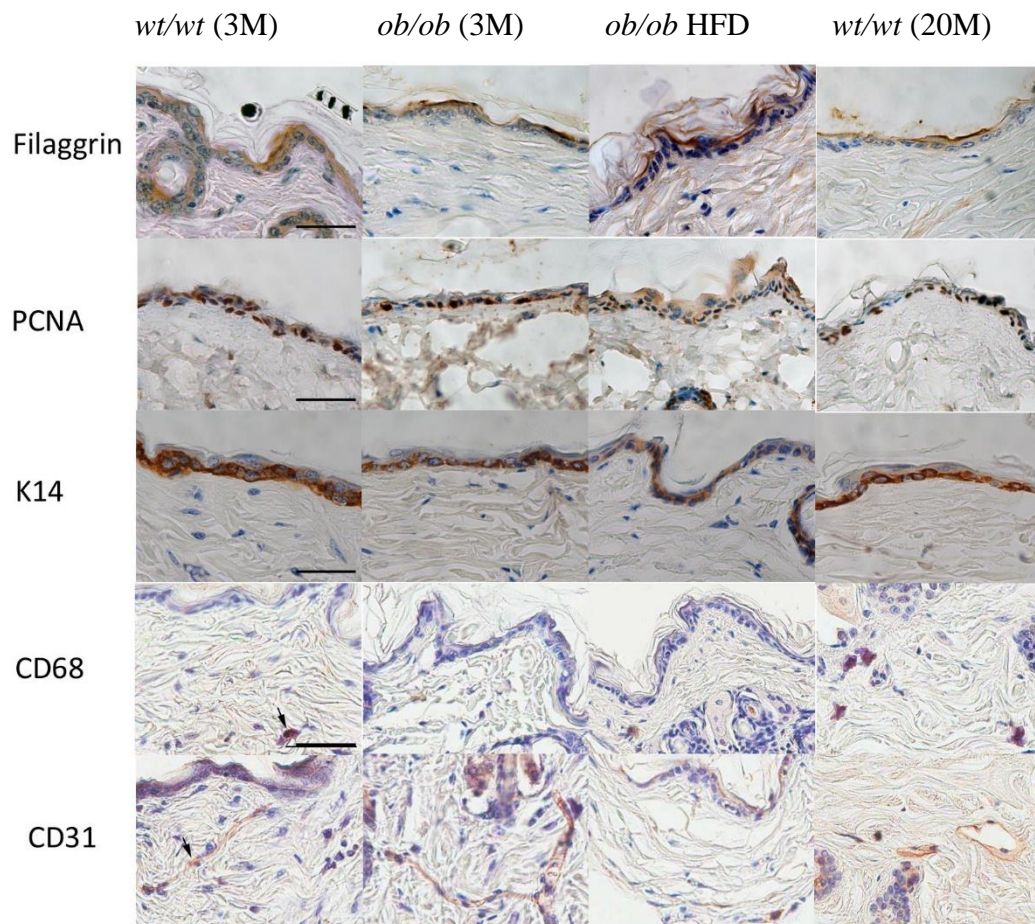


Figure 3-7 Macrophage infiltration, angiogenesis and epidermal maturation.

Representative images from 4-6 animals per each group. Macrophages were identified by CD68 expression in 4 μ M paraffin sections prepared from *wt/wt* mice at 3 month (M) old, age-matched *ob/ob* mice on chow and a high fat diet (HFD), and in 20 month old *wt/wt*. Scale bar =50 μ M. Endothelial cells were identified by CD31 immunoreactivity. Epidermal development was assessed by expression of filaggrin (decorating the outer stratum corneum), PCNA (mitotic cells, mainly located in the basal layer) and K14 (identifying basal keratinocytes). Images were captured at 20x magnification.

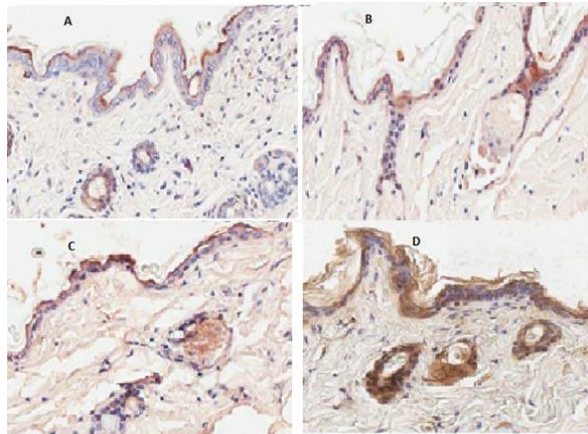


Figure 3-8 Involucrin as an early marker of epidermal differentiation immunoreactivity.

(A) *wt/wt* mice at 3 month old; (B) age-matched *ob/ob* mice on chow; and (C) on a high fat diet; (D) *wt/wt* mice, 20 month old. Representative images from 4-6 animals per each group. Images were captured at 20x magnification.

3.4 Discussion

Murine models of type 2 diabetes provide essential tools to unravel the aetiology of this disease. These models are used to study cutaneous disorders in increasingly hyperglycaemic and hyperinsulinaemic states (Lee-Kubli et al., 2014, Biessels et al., 2014). This chapter provides an evaluation of histological differences in mouse models of obesity and type 2 diabetes mellitus as well as a characterisation of cutaneous maturation and function through investigating various cutaneous markers.

The skin is an insulin-sensitive tissue (Shen et al., 2000) and in this study I described specific patterns of skin damage in animal models of obesity and type 2 diabetes, the most notable of which was the degradation of the deeper layers of the dermis. This attrition was accompanied by the loss of regular collagen organisation, which has implications for the physical integrity of the skin and its capacity for repair. In particular, the reticular layer of the dermis, adjacent to an expanded adipose depot, suffered the greatest insult, and this layer was all but lost in the most extreme phenotype (*ob/ob* animals maintained on a 60% fat diet). Moreover, the “basket weave” of the remaining papillary dermis adopted a more laminar organisation, coupled with a reduction in dense irregular fibrillar collagen topography. This is associated with

reduced mechanical strength, and consistent with a recent study (Delaine-Smith et al., 2014). Thus, insulin-resistance might be associated with the compromised ability of dermal fibroblasts to secrete and assemble collagen.

These pathological consequences previously were assumed to be the result of direct glycosylation of proteins exposed to hyperglycaemia (glycation, or browning) as the underlying cause of peripheral disease, but I have shown that tissue damage predates hyperglycaemia in DIO and old animals. This is, perhaps, unsurprising if one considers that many of the changes seen in diabetes are also seen (albeit in a less severe form) in ageing. This was supported by low expression of the receptor of advanced glycation end products (RAGE) antibody (Figure 3.6 left panel) in the skin from mouse models of obesity, type 2 diabetes and ageing (by applying IHC protocol with RAGE antibody as described in 2.3.11 and Table 2.1 in general method chapter). However, in agreement with other studies, the onset of advanced glycated end products, and positive the PAS staining in the diabetic pancreas suggests that the rate of glycation and oxidation reaction in skin is very slow and might only be presented in long term diabetes and ageing (Nawale et al., 2006). In accordance with previous studies, in ageing skin; the cutaneous collagen degradation, elastosis, and abnormal vasculature (slight CD31 and PAS up regulation diagnosed in our ageing mice skin) might result from collagen proteins cross-linking (glycation) (Nawale et al., 2006).

Changes in collagen organisation may reflect either the loss of thick fibres, revealing underlying collagens, or a more general loss of collagen integrity (or both). More interestingly, dermal layers show discrete responses to increasing insulin resistance, evidenced in the increasingly laminar organisation of papillary dermis and the loss of reticular dermis, as well as differences in elastin deposition. In particular, loosely packed collagen and altered elastin deposition characterises skin from diabetic animals compared to their controls suggesting that progressive loss of fibroblast function is inevitable in insulin resistant states. Thus, it is possible that *in vitro* studies of the dermal fibroblasts from *ob/ob* mice may provide a deeper insight into the dermal loss mechanism. Obesity and insulin resistance in humans is closely associated with ectopic fat deposition (Snel et al., 2012), particularly, the deep enlarged subcutaneous adipocyte that is considered as independent predictor for IR (Marinou et al., 2014). I observed an increase in both the size and the number of subcutaneous adipocytes in obese mice that correlated with a reduction in dermal tissue. Moreover, dermal erosion was extended to a loss of connective tissue in the adipose layer itself (the hypodermis). Elevated

adipokine signalling secreted from subcutaneous fat is emerging as a potential mediator of insulin-resistance (Karastergiou and Mohamed-Ali, 2010), thus it is possible that chronic exposure of fibroblasts to adipokines underlies their impaired function. Furthermore, peripheral damage in type 2 diabetes is traditionally considered to arise from prolonged exposure of tissues to elevated levels of reactive glucose molecules, but chronic hyperinsulinaemia, inflammation or hypoxia could also promote such damage (Aronson, 2008, Singh et al., 2014).

Why an increase in circulating adipokines characterises obesity remains unclear, although it was speculated that inflammation, and hypoxia arising from the relatively poor vascular supply within enlarged fat deposit could be the cause (Trayhurn and Wood, 2004). Macrophages are the most predominant immune cell in the inflammatory processes associated with obesity and diabetes; but no gross changes were seen in our insulin resistant and diabetic models using G&O staining (Drozdowski and Mehregan, 2005). Although there was little evidence of frank inflammation, as demonstrated by IHC analysis of CD68 (Chen et al., 2008) in this study elevated levels of CD68 expression were detected only in 20 month old mouse skin. Furthermore, by using HIF-1 α IHC detection (as mentioned in general chapter method 2.3.11 and according IHC protocol detailed in Table 2.1) there was no evidence of hypoxic condition in skin of mouse models used in this study, and no evidence of angiogenesis was seen (i.e. no changes in CD31 expression in our models with slight up regulation exception in ageing animal).

I also investigated skin integrity in ageing, as all tissues acquire some degree of insulin resistance over time (Varani et al., 2000), and I observed that many histological features of ageing, for example loss of collagen organisation and synthesis (Varani et al., 2006b), as well as abnormal elastic fibres in mid and lower dermis correlate with collagen degradation in these mouse models of obesity and diabetes (Seitz et al., 2011). A deeper understanding of the mechanisms underlying the commonality between insulin-resistant and ageing states (reviewed in (Seitz et al., 2011), and is essential to elucidate the appearance of an “accelerating ageing” skin phenotypes in mouse models of obesity and diabetes.

In contrast to the dermal and subcutaneous layers, I found little change in epidermal maturation (via profiling epidermal differentiation markers) with increasing insulin resistance. However, there was some disruption in the organisation and integrity of the epidermis with increasing insulin resistance. In particular, only the most insulin-resistant mouse models (*ob/ob* mice fed on high fat diets) showed a negative impact of differentiation through reduction in PCNA and K14 IHC expression. This was surprising as even relatively young *ob/ob* mice maintained on a chow diet are known to show impaired wound re-epithelialisation (Goren et al., 2006). Thus, the disrupted glucose homeostasis in insulin resistant states may have a greater effect on keratinocyte activation and migration, fibroblasts (in secreting, and remodelling ECM) and angiogenesis dysfunction (Berlanga-Acosta et al., 2012). Nevertheless, the epidermis may be a more protected site, perhaps as a consequence of higher cell densities (damage to the relatively sparse dermal fibroblast population will have a disproportionate outcome), or perhaps deleterious adipokines stimulation is mitigated by distance. However, severe insulin resistance is associated with impaired epidermal differentiation, and dermal disruption evidenced in the increasingly laminar organisation of papillary dermis and the loss of reticular dermis.

Although this study provided distinctive knowledge of many pathological sequelae of cutaneous damage in mouse models of obesity, type2 DM and ageing via histological, and IHC evaluation of skin structure and function, there were many histotechnological difficulties throughout this analysis. Mouse skin is very thin and the loss of architecture during processing has implications for downstream applications. In particular, obtaining good histology from diabetic mouse skin was the biggest challenge. However, detecting cutaneous phenotypes in mouse models of obesity and type 2 DM was difficult and required a deep understanding of the contributing factors and parameters that may affect the skin morphology, structure and quality that might confuse these phenotypes or cause misleading artefacts. Thus, by taking these issues to consideration, I went on to revise some histology methods in order to improve, and minimise artefacts of mouse skin morphological and IHC analysis in the next chapter.

Chapter 4: Optimising Histological Analysis of Normal Mouse Tissues

4.1 Introduction

It is well known that mouse skin is a useful tool to study human cutaneous diseases such as skin cancer, dermatological lesions and infections, hair loss and wound healing (Avci et al., 2013). This has been facilitated in part by innovation in both *in vivo* and *ex vivo* techniques such as histopathology, and cellular and molecular biology. Great care must be taken when translating data from mouse models of human disease to diagnose or elucidate mechanisms disease, or when investigating the effect of pharmaceuticals on specific pathogenic processes, by applying highly evaluated analysis protocols (Treuting and Dintzis, 2011). Histological analysis is a cornerstone of skin disease diagnosis, and the stratified nature of the skin presents many technical problems in the preparation of sections of acceptable quality. Furthermore, histological artefacts may be exacerbated in pathological states that compromise cutaneous integrity. Therefore, extra care must be taken when selecting the conditions, particularly fixative type, to ensure that meaningful conclusions may be drawn (Al-Habian et al., 2014). Although many reports describe the use of mouse skin to reveal insights into aspects of human pathology, it remains a challenge to find a standard protocol that retains the complex structure of mouse skin effectively. Researchers often report the use of human skin histology protocols when analysing mouse tissue and this is not necessarily acceptable when one considers the anatomical differences between human and mice. For example, mouse skin is thinner than human skin, thus it is much harder to achieve good sections. Moreover, this is exacerbated if tissues are compromised, for instance skin structure from obese and diabetic models shows a thickened subcutis and reduced dermis. Thus, getting acceptable sections from these models was extremely difficult, and many skin tissues were lost during preparation, and I spent a considerable amount of time adapting the best sectioning methods and conditions. Systematic analysis of histological methods in mouse are limited, and it is possible that fixatives that may provide outstanding morphology results could interfere with, for example, immunodetection techniques (Treuting and Dintzis, 2011). Problems related to incomplete fixation, or improper processing, cannot be remedied at a later stage, thus this is a crucial point when studying valuable tissues. Therefore, fixative and processing protocols must be decided upon at the outset (Srinivasan et al., 2002). The total impact of a particular fixative on tissue should be assessed after processing, sectioning and staining in order to demonstrate the adequacy of a specific fixative for any staining protocol (Taylor et al., 2002).

The term 'fixation' refers to chemical modification of a biological tissues to prevent autolysis and putrefaction. It is very important to understand the mechanism of fixation prior to histological or IHC applications. Fixation also helps in making the cellular elements more resistant to the rigorous processes of staining, and preserves antigenicity from cross-linking. Various types of fixation techniques are available to preserve tissue elements, and one must be aware that ineffective fixation (including over-fixation) may irreversibly degrade specimens and result in artefacts. Moreover, fixation not only causes chemical modification to stop degradation or bacterial decomposition, but also helps in the immobilisation of antigens and the arrest of other cellular processes (De Paul et al.). Thus, it is very important to understand the chemical actions of a fixative on tissues before embarking in any histopathology research (Treuting and Dintzis, 2011). Not all fixatives used in histopathology laboratories have similar properties. 10% neutral buffered formalin (NBF), a non-coagulating fixative, has been used widely for many decades, and continues to be the first choice for many pathologists (Grizzle, 2009b). However, the negative effects of 10% NBF include its propensity to mask antigenic sites, degrade certain antigens, promote tissue shrinkage and reduce nuclear detail. Moreover, the performance of NBF is inconsistent when a range of stains is compared (Howat and Wilson, 2014). Hence, selecting the appropriate processing conditions, particularly the fixative type and fixation time must be carefully considered to ensure that meaningful conclusions may be drawn. In this study, I sought to compare the ability of 10% NBF to preserve and retain cutaneous morphology and antigenicity with respect to three widely- used fixatives: Bouin's solution, zinc formalin (ZnF) and alcoholic formalin (AF) (Treuting and Dintzis, 2011) under various conditions to determine the optimal fixation methods for mouse skin histology. Time and temperature also play a key role, and I investigated each fixative with respect to these parameters. For example, 10% NBF has a propensity to mask antigenic sites, degrade certain antigens, promote tissue shrinkage, and reduce nuclear detail, and all these actions depend on cofactors such as time (which can determine the insufficient or sufficient cross-linking of polypeptide chains), and temperature (this reduces the time of action by increasing penetration) (Al-Habian et al., 2014). The literature provides little insight in to optimal fixation times in mouse skin tissue, and in most researchers fix for 24-72 hours with little consideration of ambient temperature and tissues thickness (Srinivasan et al., 2002).

Therefore, this chapter will focus on optimizing normal mouse skin histology methods through revising fixation and processing protocols. Skin sections from mouse models used in Chapter 3 were prepared according to existing best practice for skin in my laboratory were relatively good (10% NBF fixation for 3 days, followed by using routine processing protocols (Appendix 1), albeit at the cost of time in sectioning . I faced many problems in sectioning skin samples prepared under these condition, including folding and losing some parts of specimens (mainly from the loose packing of the dermis), and maintaining the organised adipocyte structure. On occasion there was a lack of clarity after staining the skin sections, possibly due to residual fixative. All these issues reduce the chance of getting good sections from paraffin blocks, and will influence to a certain extent histopathology analysis outcomes. Since the skin samples used in this thesis were collected from a variety of *in vivo* experiments, it was not feasible (or ethical) to repeat the entire study to revise the fixation and processing protocols. For this reason, from this point on I describe the optimisation histology protocols for prospective diabetic mouse tissue analyses. Firstly, before revising the fixative choice, I sought to compare the existing processing protocol with two customised ones, as dehydration, clearing, and wax infiltration play a critical role in maintaining tissue structure (Renshaw, 2007). To increase histological analysis throughput, and to minimise technical variation, I made use of tissue macroarrays (as described in the previous methods chapter). Various mouse organs were used to assess the efficiency and generalisability of different processing protocols. Secondly, I evaluated methods using normal mouse skin in order to achieve robust morphology and IHC analysis using a range of histological stains and the immunohistochemical analysis of key cutaneous proteins, as described in Chapter 3. Finally, I went on to evaluate fixation in either 10% neutral buffered formalin (NBF), alcoholic formalin (AF), Bouin's solution and zinc formalin (ZnF) under different temperatures and time.

4.2 Methods and results

4.2.1 Optimised processing of mouse tissues

4.2.1.1 Histological evaluation of processing time

Several critical variables need to be considered before processing specimens, including the type and concentration of dehydrating and clearing agents, paraffin infiltration, and operating temperature. For instance, specimens during processing may shrink by 20-30% of the original volume (Krekel et al., 2012). The skin tissues obtained with the

processing protocols previously used in my laboratory were relatively soft (particularly the fatty skin samples). This was most likely as a consequence of the alcohol dehydration steps and the subsequent clearing agent action. Thus, I evaluated histology results with an existing skin processing protocol, and customized long and short processing protocols with skin tissues fixed in 10% NBF for 3 days (detailed protocols are presented in Appendices 1, 2, 3). In order to investigate applicability not only to mouse skin but also to other mouse organs, I initially evaluated the influence of a new long processing protocol (described in detail in Appendix 3), as well as the protocol previously described, on the histological features of various mouse organs in tissue arrays.

The rationale was to maintain good epidermal, dermal and adipocyte integrity, when faced with sectioning fatty, fragile diabetic mouse skin. The short protocol was found not to be effective as tissues remained very soft, and difficult to cut. For that reasons, typical sections are not shown here. The extended processing protocol yielded sections that were much easier to cut compared to the standard protocol, and better maintained integrity, as shown in Figure 4.1.

To investigate the consistency of the new processing method, I sought to evaluate a range of mouse tissues. In order to minimize artefacts between experiments, I arrayed all mouse tissues on one slide (using a tissue macro arraying technique). Briefly, 12 different organs were collected from 3 month old *wt/wt* male mice (liver, small intestine, brain, lung, epididymal fat, kidney, heart, spleen, soleus muscle, skin, brown adipose tissue, and pancreas). Samples were fixed in 10% NBF for three days at room temperature, followed by processing with standard and extended protocols, prior to embedding in macroarray blocks.

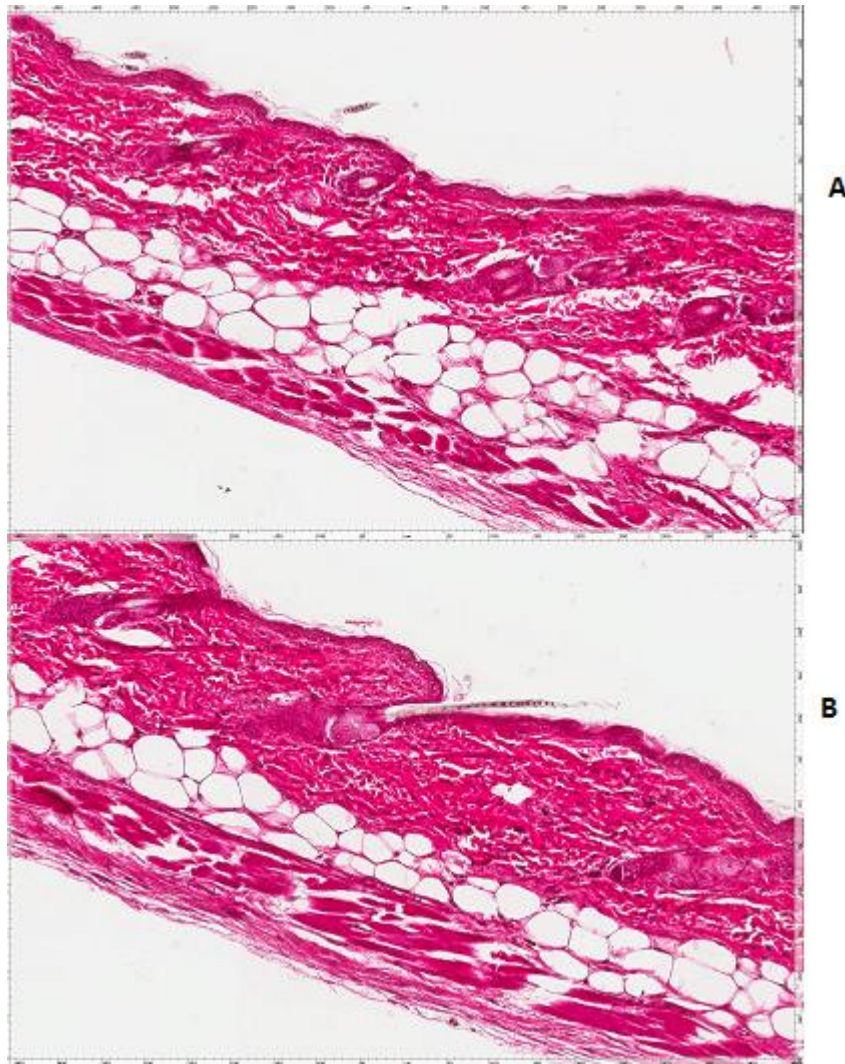


Figure 4-1 H&E staining of tissues with standard and extended processing protocols.

Representative images for each condition (n=4-6). *Wt/wt* skin tissue processed with routine processing (A), and a longer processing protocol (B). The skin structure was typically improved with the extended protocol. Images were captured with the Aperio Scanscope at 5x original magnification.

4.2.1.2 Staining and IHC

Routine H&E staining and CD31 immunostaining was used to assess morphology and antigenicity respectively (Pusztaszeri et al., 2006). CD31 identifies endothelium in all tissues, therefore, it represents a useful generic marker. It was outside the scope of this thesis to assess a broader range of antibodies. Whole-slide images were captured using an Aperio Scanscope CS scanner as discussed in Chapter 2. Chromogenic staining is shown when a larger field of view was informative. In some cases, CD31 immunofluorescence results are shown, in cases where more consistent results were

achieved compared to chromogenic staining. Fluorescent images were captured using a Nikon Eclipse 80i microscope equipped with fluorescent optics.

Various difficulties were associated with the routine protocol as discussed above (notably a hard cutting surface, tearing and reduced adhesion of sections to slides), which led to folding or tearing of tissues as seen in (Figure 4.2).

In general, microtomy was easier when the long processing protocol was used, providing consistent anatomical structure with reduced disruption in all of the mouse organs following an assessment by H&E staining (Figure 4.3). Sectioning 12 heterogeneous tissues was much easier when using the softening agent (as described in the general methods chapter). A key feature of the extended protocol was the removal of formaldehyde from the first step in order to reduce over-fixation. However, IHC signals were generally weak without antigen retrieval.

4.2.1.3 Antigen retrieval

Reduced immunostaining is more likely to occur with formalin fixed tissues compared to cryosections due to cross-linking of proteins (antigens) during the fixation process. This can render the epitopes (antibody-binding locations) inaccessible to antibodies (a process known as epitope masking), preventing detection by immunohistochemical methods. A number of methods were applied to unmask antigens, including enzymatic treatment (trypsin), heat-based (microwave) methods in citrate buffer of varying pH, or a combination of pressure and heating (using a domestic vegetable steamer or pressure cooker) (Figure 4.4). While pressure cooking revealed the strongest signal, it did lead to variable background with chromogenic detection. For this reason, fluorescent detection is shown in subsequent experiments.

The process of protein cross-linking is progressive i.e. the longer the fixation time, the stronger the cross-linking. This is exacerbated by increasing temperature, which also leads to a reduction in immunochemical detection (Webster et al., 2009). Enzymatic digestion by trypsin is a common method to uncover antigenic sites, however, for some antigens trypsin digestion could produce false positive results as a consequence of over digestion, or false negatives could result from insufficient retrieval of the antigenic site.

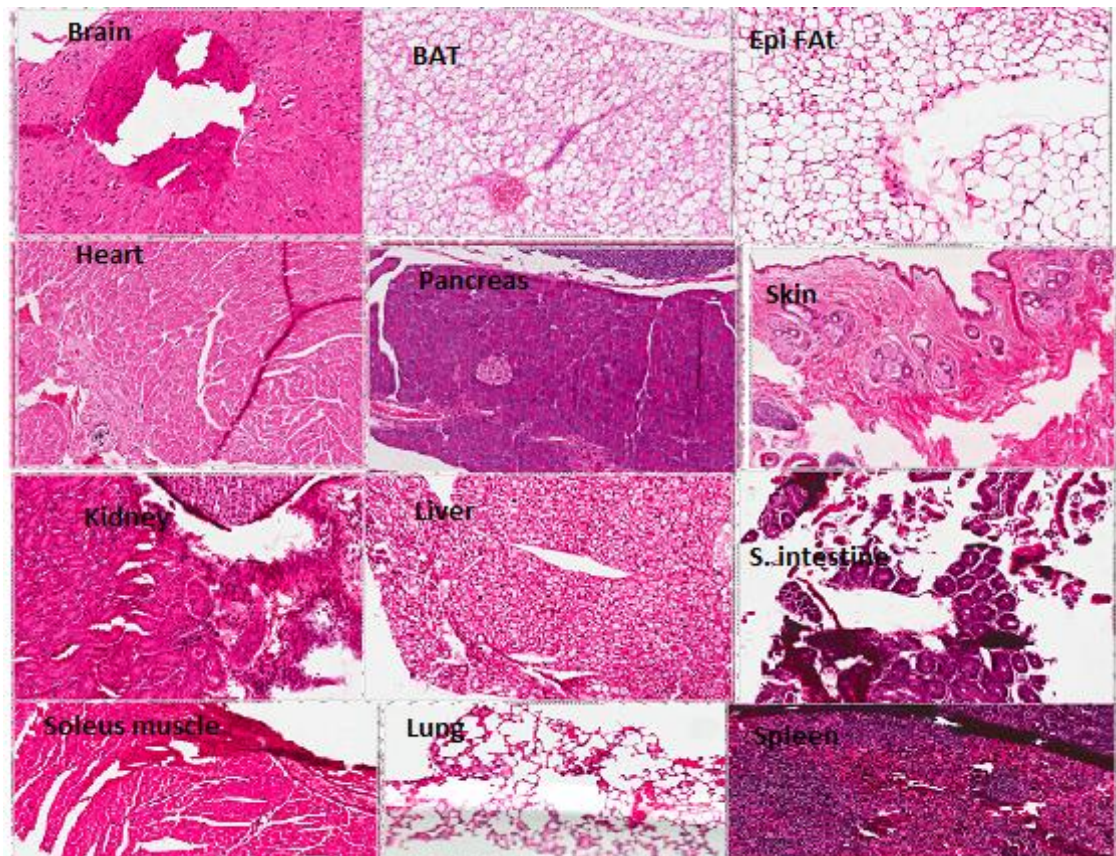


Figure 4-2 H&E staining of tissues prepared using the standard processing protocol.

12 different tissues from 3 month old male *wt/wt* mice were processed using the routine processing protocol. Morphological features of many tissues were disrupted (tissue folding and loss). Representative images from three mice. Images were captured with the Aperio Scanscope at 15x original magnification.

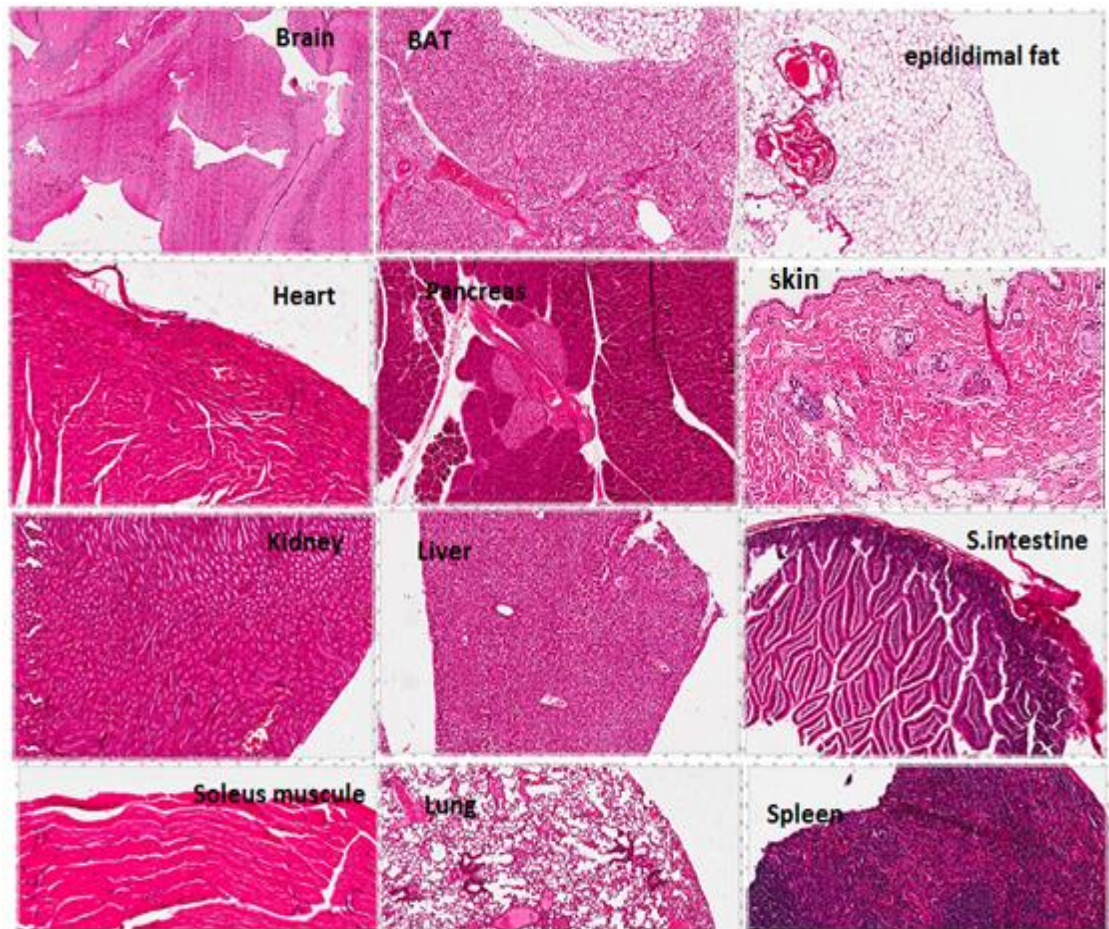


Figure 4-3 H&E staining of tissues prepared with an extended processing protocol.

12 different tissues from 3 month old male *wt/wt* mice were processed using a long processing protocol. Representative images from three mice. Images were captured with the Aperio Scanscope at 15x original magnification.

The results depend on digestion time and enzyme concentration, and these need to be adjusted for individual antibodies, and fixation time and type. For other retrieval results, temperature and pH must be optimized to produce acceptable, and consistent IHC staining. Other factors, such as section thickness, dewaxing, and rehydration of tissues yield certain nuclear antigens may require longer treatment. Moreover, the IHC protocol choice (chromogenic or fluorescent) can favour particular antibodies. I found that immunofluorescent detection of CD31 expression with heat-induced antigen retrieval by pressure cooking in citrate buffer provided the most consistent signal/ noise ratio across a range of tissues (Figure 4.5).

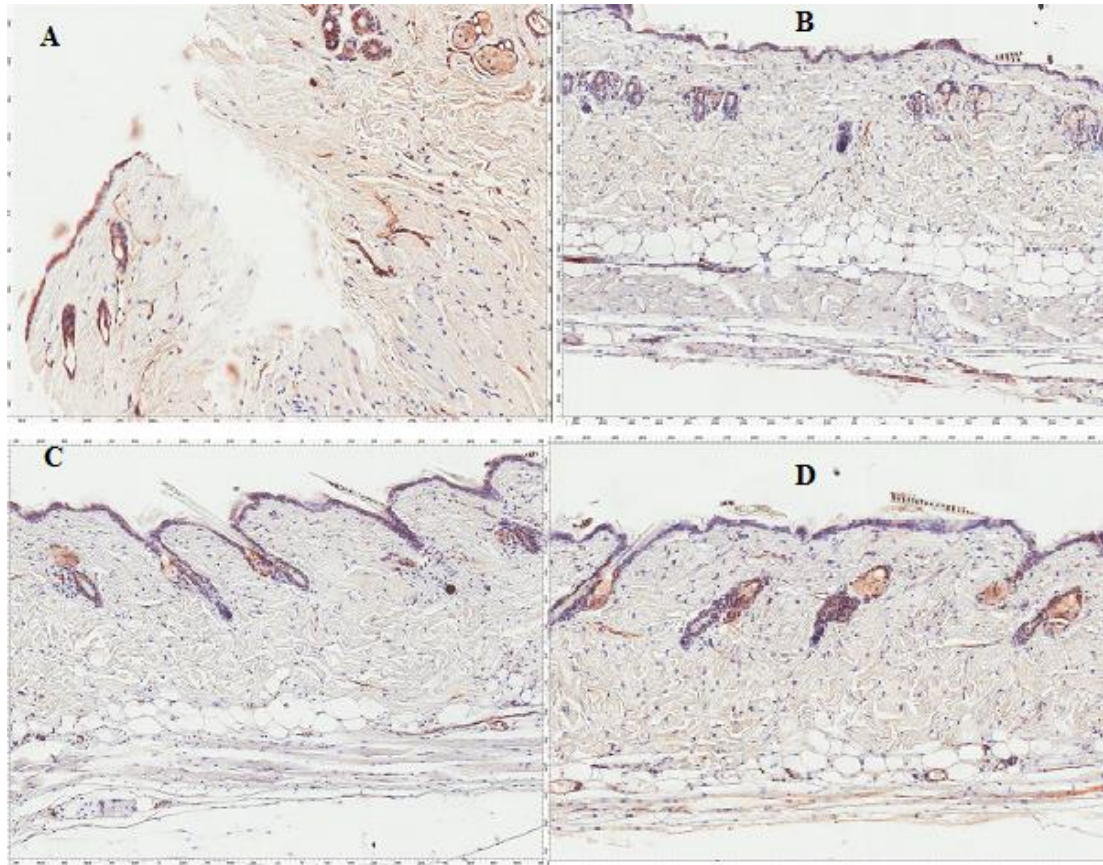


Figure 4-4 Antigen retrieval methods to reveal CD31 immunoreactivity in *wt/wt* skin with chromogenic detection. Representative images for each condition (n=4-6)

No qualitative differences were observed in CD31 immunodetection between skin specimens fixed in 10% NBF for 3 days, and retrieved with enzymatic treatment with trypsin (B), microwaving (C), and steaming (D). Pressure cooking did enhance antigen retrieval outcomes, although there was some increase in tissue disruption and background (A). Images were scanned using the Aperio Scanscope at 10x magnification.

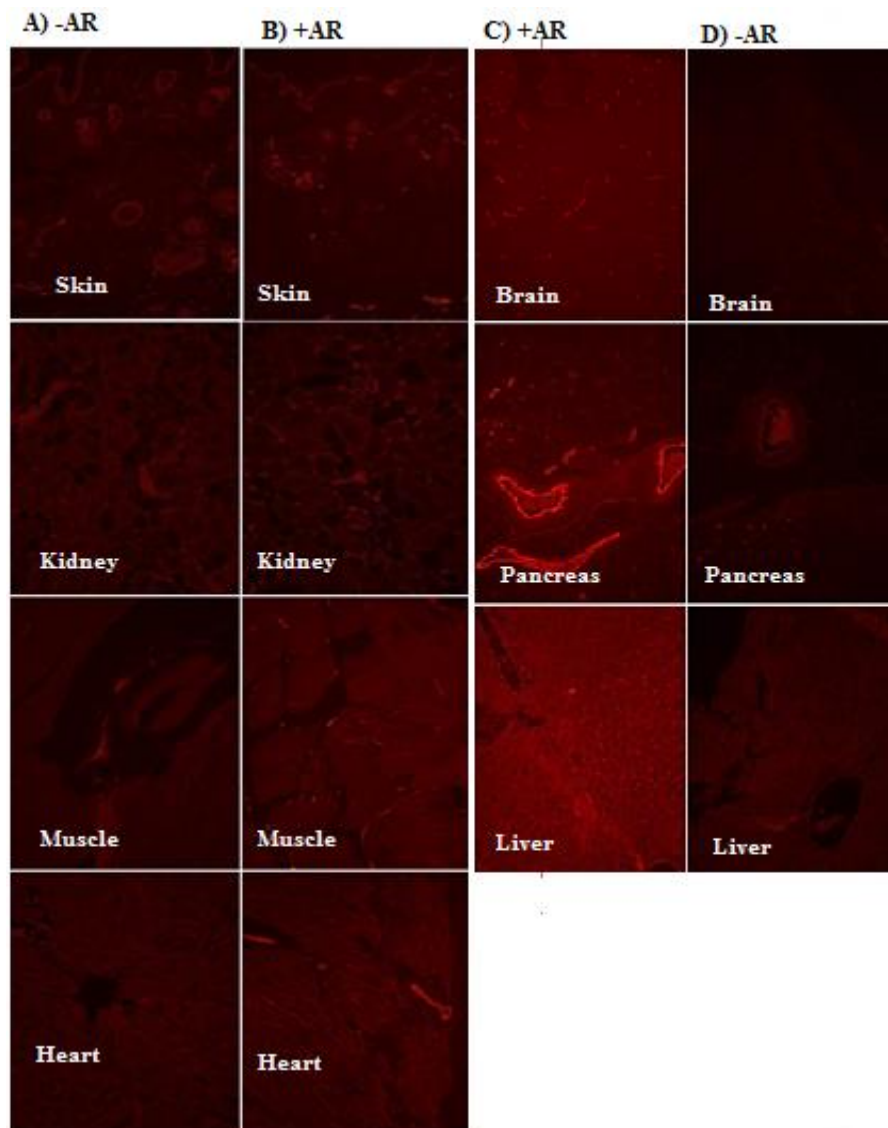


Figure 4-5 Representative images of immunofluorescent detection of CD31 expression in mouse tissues. Representative images for each condition (n=3)

Sections were fixed in 10% NBF for 3 days and processed with the long processing protocol without antigen retrieval (-AR) and with antigen retrieval (+AR). Antigen retrieval consistently reveals CD31 staining in endothelium. Images were captured at 20x original magnification.

Tissue loss from slides is an issue in histology, made worse by relatively harsh antigen retrieval during IHC. Figure 4.6A shows H&E stained TMAs with tissues prepared with the standard protocol. Use of the extended protocol promotes tissue adherence, even following heat-based antigen retrieval (Figure 4.6B).

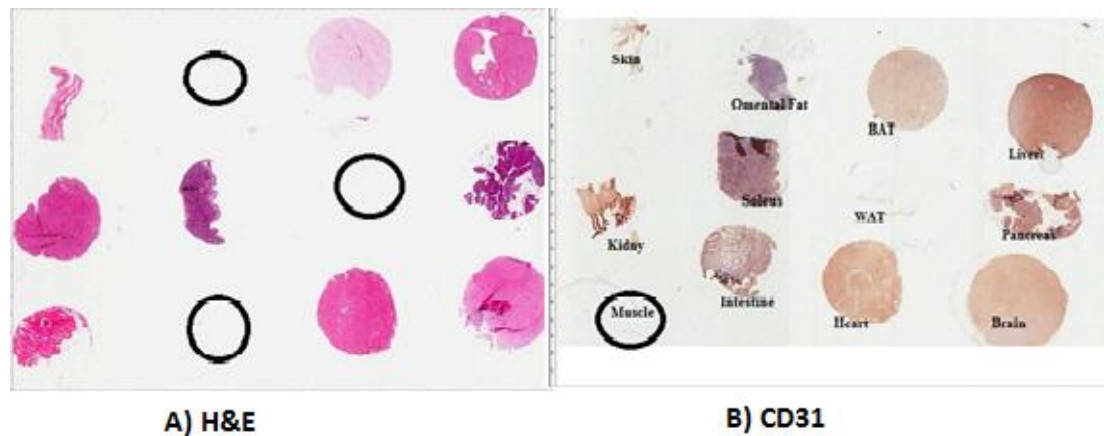


Figure 4-6 Loss of sections from organ tissue arrays prepared with standard and extended processing protocols. Representative images for each condition (n=3)

A) H&E stained TMA with tissue prepared using the short protocol. Missing tissues are circled. B) CD31 immunostained TMA showing retention of tissue, even following antigen retrieval. Image were captured using the Aperio Scanscope at 1x magnification.

Overall, the extended processing protocol improved the histology of multiple tissue types compared to the routinely used one. Thus, I went on to assess this protocol on CD31 IHC across different organ arrays.

Without antigen retrieval, the IHC signal for CD31 was inconsistent across tissues. With heat induced antigen retrieval, signals were improved in pancreas, heart, kidney and brain, with a small improvement in skin (which gave a good signal without retrieval). Weak signal were achieved in heart and muscle, suggesting that these tissues could be relatively over-fixed. Rather than go on to vary the numerous parameters relevant to processing, I was satisfied that the extended protocol provided a significant advantage over the previous method across a range of tissues. I then sought to focus on skin, and investigate the effect of different fixatives on histological analysis, starting with 10%NBF. In particular, I wanted to investigate the relationship between fixative and a broader range of downstream histological techniques.

4.2.2 Effect of fixation time and temperature

4.2.2.1 Tissue Preparation

Three male *wt/wt* mice were obtained at 5-6 weeks of age and maintained on a chow diet. At 3 months of age the dorsal skin was shaved and 5cm by 5cm pieces of skin specimens were dissected from three separate animals and sliced into multiple 5mm x 10mm x 2mm thick samples. Skin samples from each of three different mice were prepared in triplicate and placed in a histological cassette prior to fixation. Skin samples in each fixative were treated with 3 different conditions: 1) short fixation time (6 hours) at room temperature; 2) short fixation time (6 hours) at 40°C; and 3) long fixation time (32 hours) at room temperature. All tissues were then processed using to the extended processing protocol described above. Three TMAs were created, one for each fixation condition as described in Chapter 2 (Figure 4.7). Each TMA had three biological replicates of mouse skin fixed with each fixative.

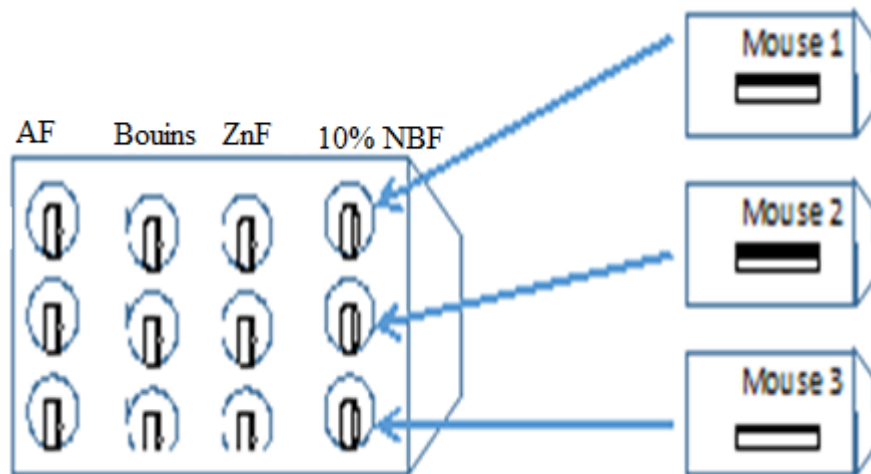




Figure 4-7 Tissue macroarray overview

Recipient Block (left diagram) consists of four replicated skin samples from each mouse fixed with four different fixatives (rows), and three biological replicates from different mice (columns). The four samples were generated from single piece of mouse skin embedded in a donor block.  Hole with 4mm punch biopsy from  Donor skin.

4.2.2.2 Effect of short fixation time at RT and 40°C with 10%NBF

H&E staining revealed improved morphology in skin fixed with 10%NBF for 6 hours at 40°C compared to RT (Figure 4.8). For example, dermal collagen organisation disruption seen in skin samples fixed at RT (Figure 4.8 A) can be contrasted with the tightly-packed organisation seen when tissues were fixed at a higher temperature (Figure 4.8B). Consistent detection of PCNA immunoreactivity in skin is difficult, and this antibody was used as a sensitive test of antigenicity, and good signals were obtained when fixation was performed at both temperatures for short periods of time (Figure 4.9). Notably, no antigen retrieval was required.

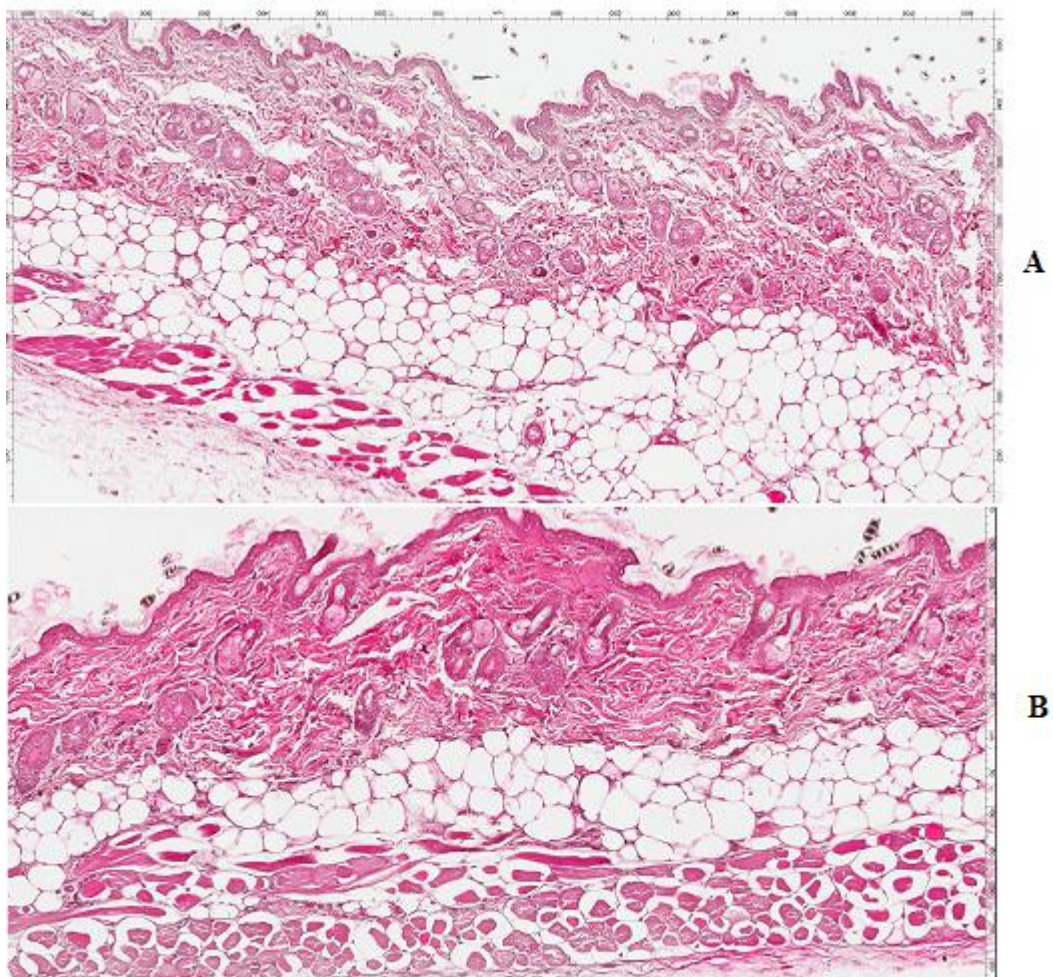


Figure 4-8 H&E staining of wt/wt skin fixed for 6 hours in 10%NBF at RT and 40°C.

Dermal collagen structure was typically characterised by many spaces when skin tissue was fixed at RT in 10%NBF (A) in comparison to fixation at 40°C (B). Images were captured at 5x magnification with an Aperio scanner. Representative images for each condition (n=3)

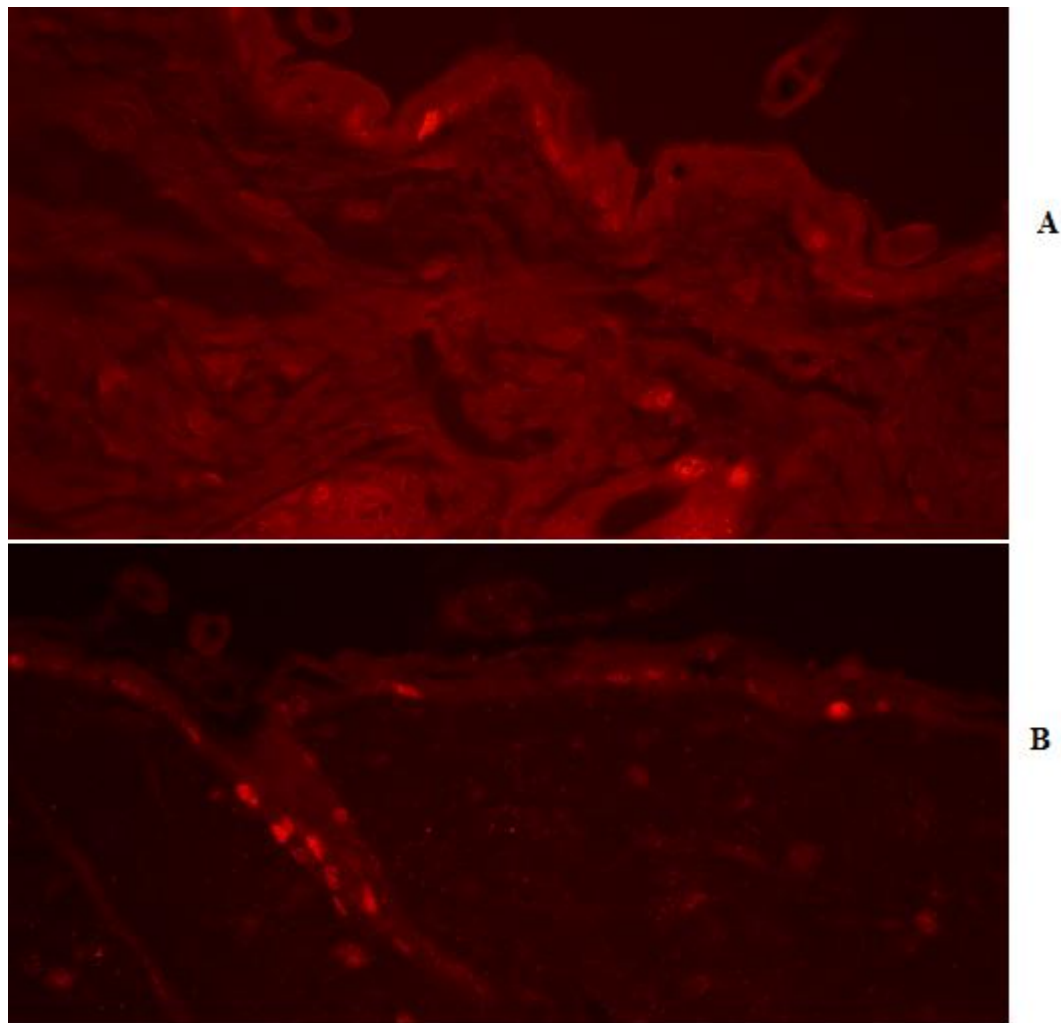


Figure 4-9 PCNA immunoreactivity in *wt/wt* skin

Tissues were fixed for 6 hours in 10%NBF at 40°C (A) and at RT (B). . **Representative images for each condition (n=3).** Images were captured using a 40x objective lens.

4.2.2.3 Effect of short fixation with 10%NBF at 40°C to long fixation at RT

Having established that 6 hours at 40°C gave good results, I went on to compare tissue preservation achieved with longer fixation (32 hours) at room temperature. It has been suggested that fixation up to 48 hours provides a good compromise between effective tissue preservation and antigenicity (Grizzle, 2009a). For pragmatic reasons, I selected 32 hours to allow for consistent timing in tissue preparation and transfer to the processor. An initial finding was that extended fixation time was associated with a hard cutting surface, tissue loss and over-staining (Figure 4.10). Better morphology, reduced shrinkage, and better contrast were associated with shorter fixation (Figure 4.11).



Figure 4-10 Disrupted organisation in H&E stained *wt/wt* skin with 32 hour fixation.

A typical image is shown. . Representative images for each condition (n=3). Image was captured at 20X original magnification.

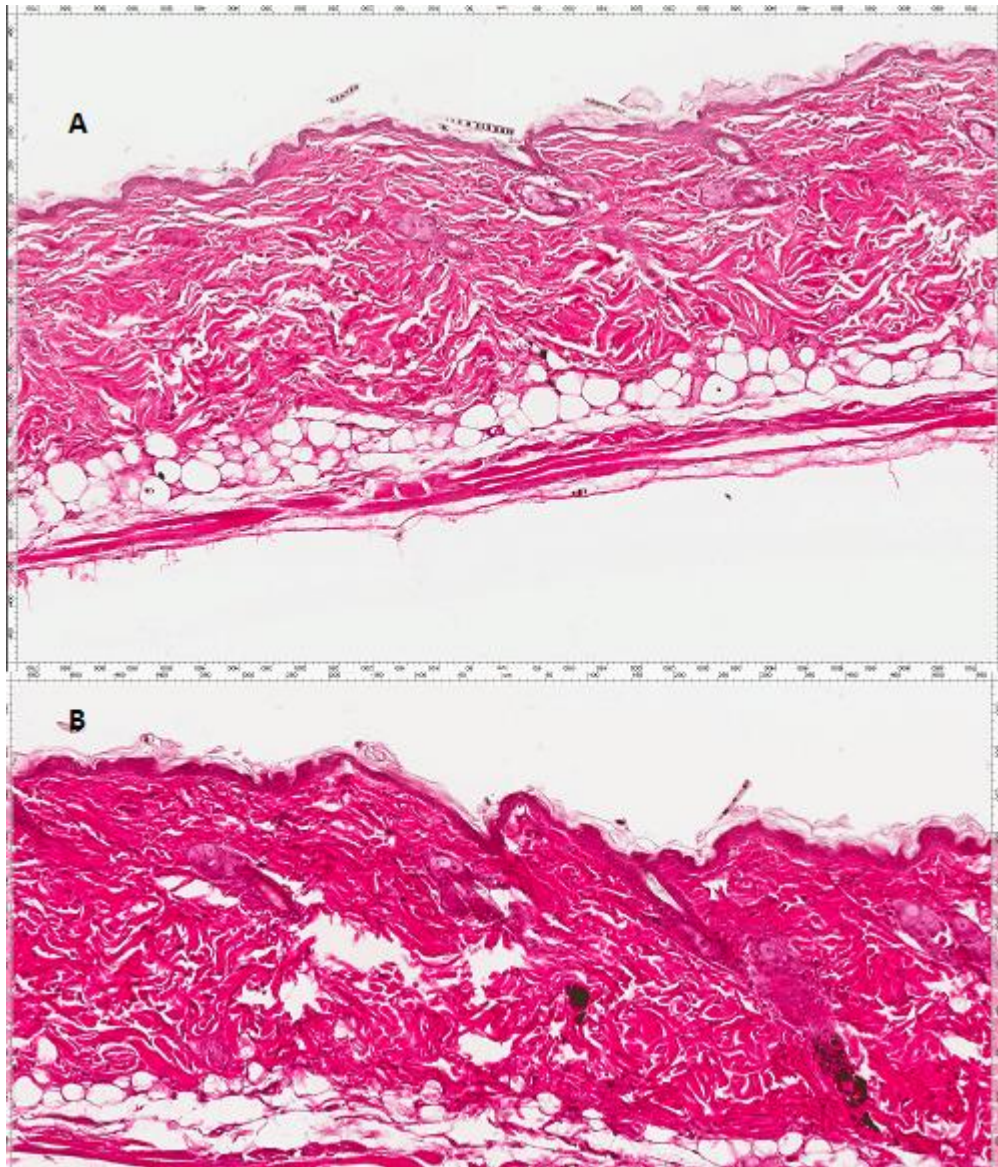


Figure 4-11 Effect of fixation time.

Better histology of skin tissues fixed at 40°C for 6 hours in 10%NBF are shown in A, compared to 32 hours fixation (B). Representative images for each condition (n=3). Images were captured at 10x.

4.2.3 Reduction of endogenous peroxidases

Any changes in fixation will influence histology and immunostaining outcomes, and IHC methods must be optimised empirically (Moelans et al., 2011). Both direct and indirect approaches were used to detect target antigens, through either chromogenic or fluorescent means (as described previously in Chapter 2). While I described quenching endogenous peroxidases earlier, I had to re-evaluate these methods in light of shorter fixation times when chromogenic IHC methods were used.

Endogenous peroxidases may react with chromogenic substrates and contribute to background signals that may compromise subsequent analysis. A solution of 3% hydrogen peroxide is commonly used to block such endogenous peroxidases. Skin tissues were incubated in 3% H₂O₂ v/v in methanol for 30 and 60 minutes prior to a 3 minutes PBS-T wash and incubation with ImmPact DAB substrate (Vector Laboratories) for 5 minutes at RT in order to determine appropriate conditions.

It was noteworthy that skin fixed for 6 hours required a longer incubation period (up to one hour) to block the endogenous peroxidase activity as shown in Figure 4.12B. In comparison, a 30 minutes incubation with 3% H₂O₂ was enough to reduce the non-specific substrate deposition with long-fixed tissues (Figure 4.12A).

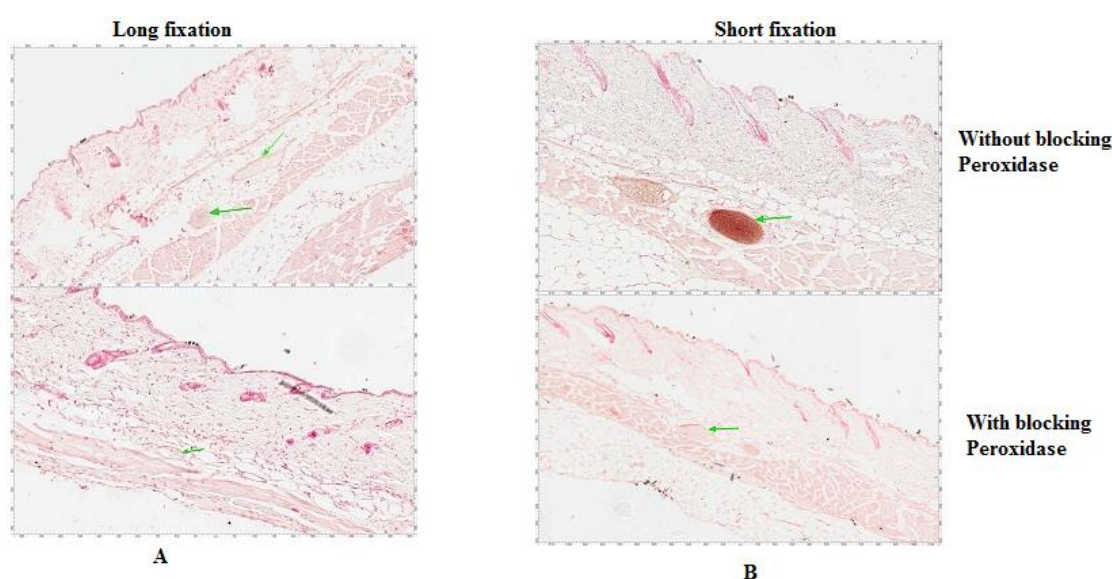


Figure 4-12 Endogenous peroxidase reduction skin from *wt/wt* mouse skin.

Sections fixed in 10% NBF for 32 hours (A), and 6 hours (B) were evaluated with and without blocking. In particular, high levels of endogenous peroxidase persisted with short fixation (upper panel B, arrow). Images were captured at 10x original magnification. . Representative images for each condition (n=3)

4.2.4 Optimisation of primary antibody concentrations

A range of cutaneous antigens were investigated by IHC. Again, primary antibody concentrations had to be titred in light of adapted fixation protocols (table 4.1). Secondary antibodies were either FITC or TRTC conjugated for immunofluorescent detection. All were used at a 1:200 dilution in PBS-T containing 2% relevant serum. Routinely, primary antibodies incubations were performed for one hour at either RT

with short fixed tissues, or with varying conditions with longer fixation. Generally, long fixed skin samples required more optimisation compared to short fixation. In contrast, the short fixed samples retained good antigenicity with all biomarkers used in this study, with lower primary antibody concentrations, fewer optimisation steps, and more importantly, without the need for antigen retrieval (Figure 4.13).

4.2.5 Antigen retrieval

Without antigen retrieval, immunoreactivity of most biomarkers was weak with fixation for 32 hours. To unmask the cross-linking of proteins, I used various antigen retrieval methods including enzymatic antigen retrieval and heat induced retrieval using pressure cooker and microwaving. A summary of optimal dilutions of primary antibodies and best antigen retrieval methods is shown in Table 4.1.

Antibody	Primary antibody dilution/incubation 6hr fixation	Primary antibody dilution/antigen retrieval/incubation 32hr fixation
involucrin	1:500/1hr at 37 ⁰ C	1:100/ trypsin-EDTA/ 1hr at 37 ⁰ C
profilaggrin	1:500/overnight at 4 ⁰ C	1:200/10 min microwave in citrate buffer pH6 / overnight at 4 ⁰ C
keratin 14	1:2000/1hr at RT	1:500-1000/10 min pressure cooker in citrate buffer pH6/1hr at RT
PCNA	1:400/overnight at 4 ⁰ C	1:200/ 10 min pressure cooker in citrate buffer pH6/ overnight at 4 ⁰ C

Table 4-1 Optimised primary antibody dilutions, incubation conditions and antigen retrieval methods.

No antigen retrieval was required to give a good signal with all antibodies used when a short fixation time was used (Figure 4.13). With long fixation, antigen retrieval was

required to obtain signals with involucrin, profilaggrin and PCNA. K14 yielded a robust signal under all conditions.

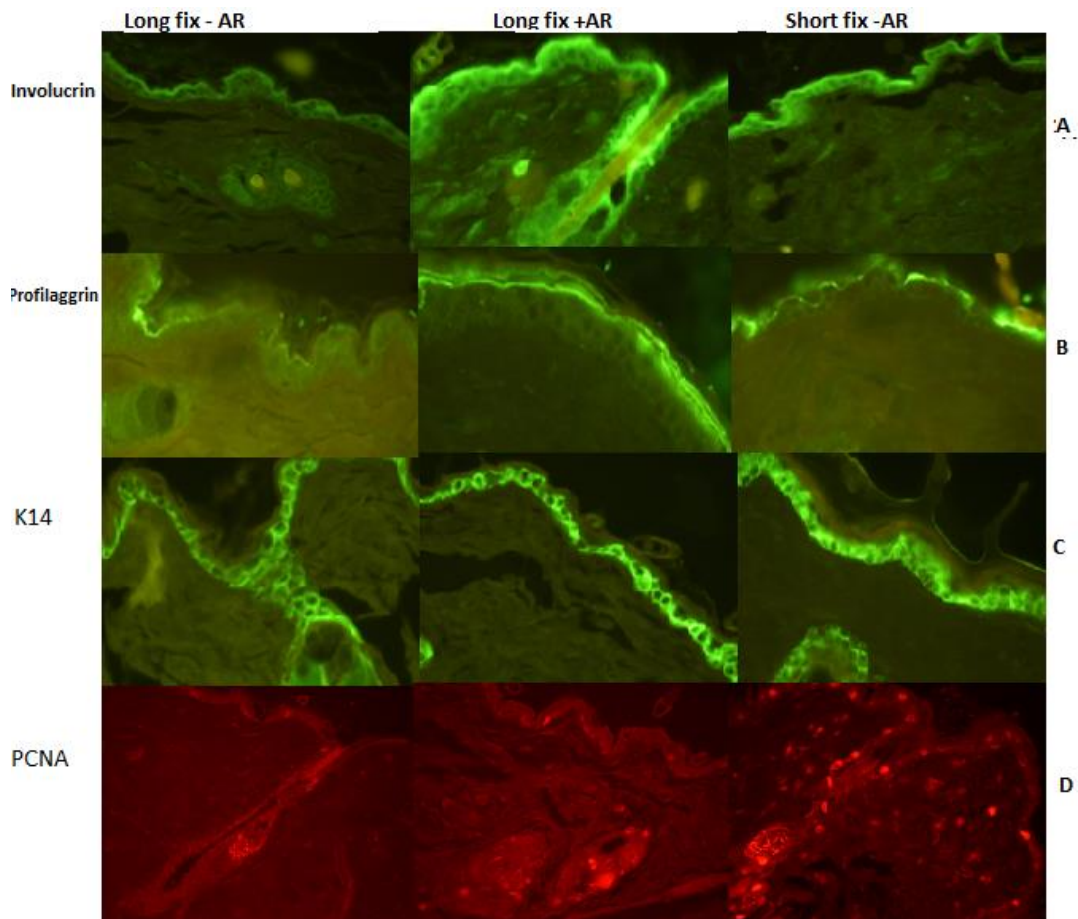


Figure 4-13 IHC detection of cutaneous markers.

Representative images of *wt/wt* skin sections fixed in 10%NBF for 32 hours without antigen retrieval (AR, left panel), and with AR (centre panel), and for 6 hours at 40°C without AR (right panel). . Representative images for each condition (n=4-6). Images were captured at 50x original magnification.

Overall, 6 hours fixation in 10%NBF at 40°C gave better results than 32 hours fixation at RT. However, I was still not satisfied that I was achieving optimal results and wished to investigate other fixatives, in the first instance using 32 hour incubations.

4.2.6 Effect of fixatives type on histological analysis

4.2.6.1 Special Histological Stains

4µm TMA paraffin sections were stained using a variety of special histological stains to evaluate cutaneous organisation as described in Chapter 2.

4.2.6.2 Preservation of Morphology

H&E staining is routinely used to make a general assessment of tissue organisation. Basic haematoxylin in the presence of a mordant (aluminium) distinctively stains the

acid content of the cell, giving nuclei a bluish-purple colour. Eosin stains cytoplasm and connective tissue varying shades of pink. Whole-slide image evaluation confirmed large variation in hue and intensity when identical tissues were stained following preparation with different fixatives (Figure 4.14). Bouin's, AF and ZnF fixation led to superior preservation of skin morphology with limited shrinkage of the tissue compared to 10% NBF fixation and this was particularly revealed in the separation of collagen fibres, seen in (Figure 4.14A-D). Despite the maintenance of overall skin morphology, Bouin's fixative led to disruption of nuclear detail and tissue were brittle while sectioning (Figure 4.14.B), whilst ZnF was associated with a reduced intensity of colour hue (Figure 4.14D). Overall AF fixation most effectively preserved skin morphology (Figure 4.14C), sharpness of nuclear detail (Figure 4.14C, inset) and contrast in colour. I also studied skin morphology revealed under eosin auto-fluorescence, a technique that provides increased resolution relative to bright-field microscopy (Kiernan, 1990). In this way, collagen fibres were easily discerned from other tissue components (for example the epidermis) with all fixatives, but this distinction was most apparent with AF and ZnF fixation (Figure 4.14E-H). The use of these two fixatives yielded enhanced clarity in resolving fibre bundles compared to the commonly used 10% NBF fixation.

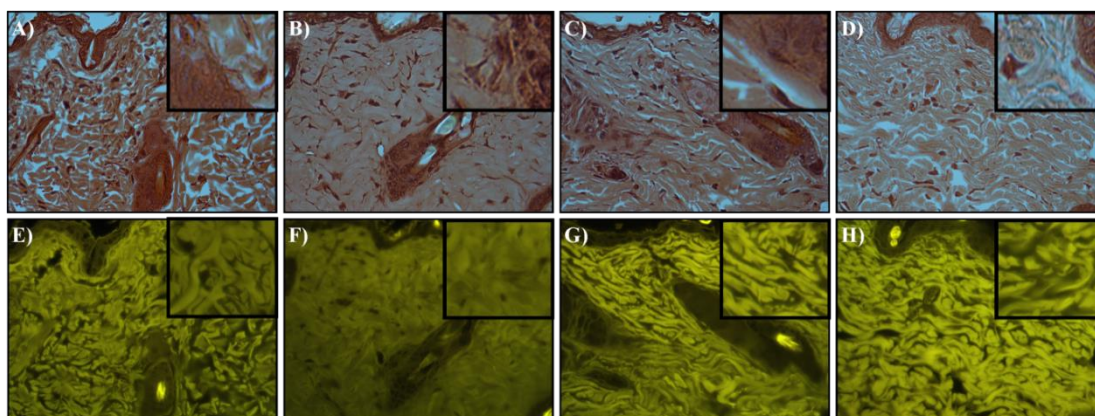


Figure 4-14 H&E stained sections of mouse skin prepared with four different fixatives.

Top panel images were captured under bright-field microscopy and the lower panels show matched images obtained under eosin auto fluorescence. Inset images illustrate nuclear detail (top panel) or collagen fibre resolution (lower panels). A, E: 10% NBF; B, F: Bouin's solution; C, G: AF; D, H: ZnF. Images are representative of three experiments, and were captured at 60X original magnification (inset 180X magnification). .Representative images for each condition (n=4-6)

4.2.6.3 Basement membranes and vasculature

Periodic acid oxidises polysaccharide moieties to create aldehyde groups whose reaction with Schiff reagent yields a deep red/magenta colour. Therefore, PAS staining readily identifies glycoproteins such as those constituting basement membranes and blood vessel walls, but it should be noted that both of these structures are much thinner in mouse than in human skin. Under normal conditions, PAS-stained collagen appears light pink, thus good contrast is extremely important in discriminating skin features. However, weak staining was obtained with both 10% NBF and ZnF fixation and typical PAS staining of NBF-fixed material is shown in Figure 4.15A. Better results were obtained when either Bouin's or AF fixed tissues were examined; with which sufficient contrast to discriminate basement membranes and blood vessels was obtained (typical PAS staining of Bouin's fixed material is shown in Figure 4.15B). PAS staining of Bouin's fixed material is shown in Figure 4.15B).

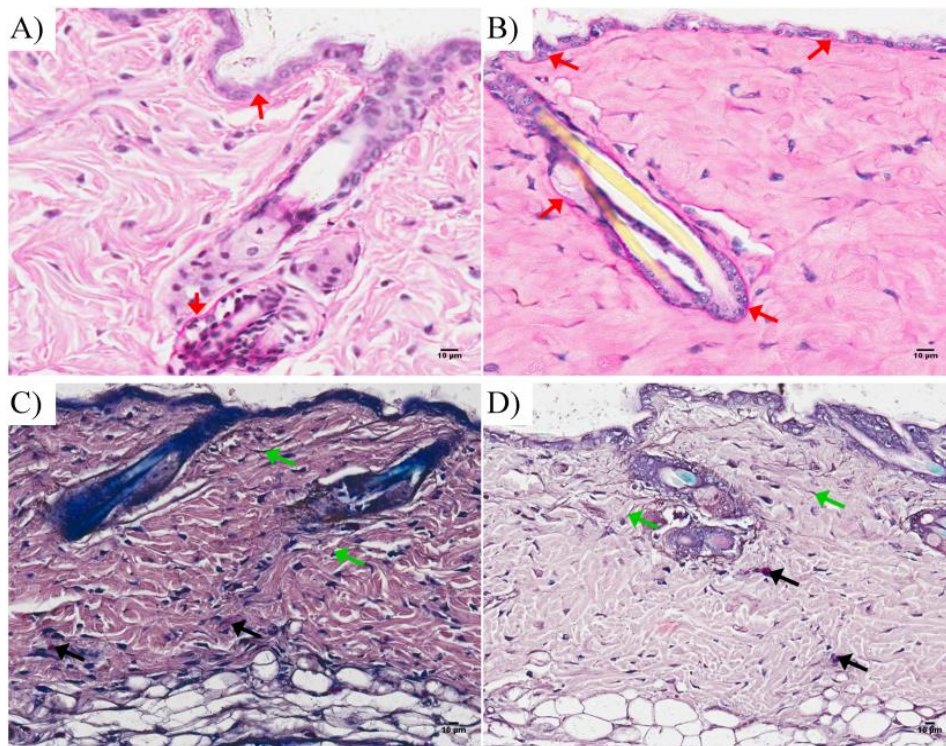


Figure 4-15 Representative images of normal skin with PAS and G&O stained sections.

PAS (A and B) and G&O stained specimens (C and D) in mouse skin processed with different fixatives. A and C were fixed in 10% NBF, panel B was fixed in Bouin's solution and panel D was fixed in ZnF. Red arrows highlight the basement membrane distinguished in PAS staining; green arrows indicate fine elastic fibres (C); black arrows indicate purple granule-bearing mast cells (D) identified with G&O staining. Representative images for each condition (n=4-6). Images representative of skin from three different animals is shown. Images were captured at 15x magnification.

4.2.7 Elastic fibres and immune cells

Giemsa is composed of a mixture of methylene blue, azure B and eosin, and provides an excellent stain for identifying leucocytes in blood smears, as well as red blood cells and platelets (García and Bruckner, 1988, García and Standards, 2000). In particular, methylene blue has metachromatic properties in that a reaction with mast cell granules yields a colour (purple) other than the colour of the dye itself (blue). Orcein is a synthetic dye that identifies elastin. I used a combined G&O stain for multiple skin feature identification and found that although Bouin's fixation yielded excellent discrimination of mast cells, it was to a lesser extent capable of identifying elastic fibres. However, both 10% NBF and ZnF fixation gave good discrimination of mast cells (arrowed, Figure 4.15C and D), and better discrimination of elastic fibres compared to other fixatives.

4.2.8 Collagen fibre organisation

The polychromatic Herovici stain distinguishes young, newly formed collagen fibres, which appear blue, from the mature, dense collagen fibres, which appear red, making this stain very useful in the investigation of collagen organisation and dynamics. Possibly due to tissue shrinkage induction obtained with Bouin's (and to some extent with ZnF), blue fibres were difficult to discern in skin preserved with either of the fixatives used. However, use of both 10% NBF (Figure. 4.16 A) and AF fixation (Figure. 4.16B) revealed distinct blue and red stained collagen fibres.

Picrosirius red (PS) is a strong anionic dye that enhances the normal birefringent property of collagen (Constantine and Mowry, 1968). Under cross-polar microscopy, collagen fibres show a "basket-weave" conformation and fibres of different size and type may be discriminated by hue (Montes and Junqueira, 1991). Fixation with AF and ZnF, and to some extent 10% NBF (Figure.4.16C), revealed a distinct collagen basket-weave structure in these images. However, AF fixation yielded the broadest spectrum of colours compared to the other fixatives (Figure 4.16D), thus AF may be preferred to distinguish thick type I collagen fibres (red or orange) from thin type III fibres (yellow or green) if this type of collagen discrimination is required (Ren et al., 2013). Bouin's was not an effective fixative to reveal structure under cross-polar microscopy. PS, van Gieson (VG) and Masson's trichrome (MT) staining are commonly used histological stains for collagen identification (Manne et al., 2013). Collagen was readily identified with all stains and all fixatives, but I could not readily discriminate fine murine elastic

fibres under any of the conditions used (Figures 4.16E and F). However, in tissues fixed in 10% NBF, Masson's trichrome revealed thick red-staining reticular fibres, while finer fibres appeared blue (Figure 4.16E). Red staining is generally associated with erythrocytes, muscle, cytoplasm and cross-linked keratins, but in this case tightly-packed collagen bundles also stained red, as did keratins in the cornified layer of the epidermis (Bancroft and Gamble, 2008b).

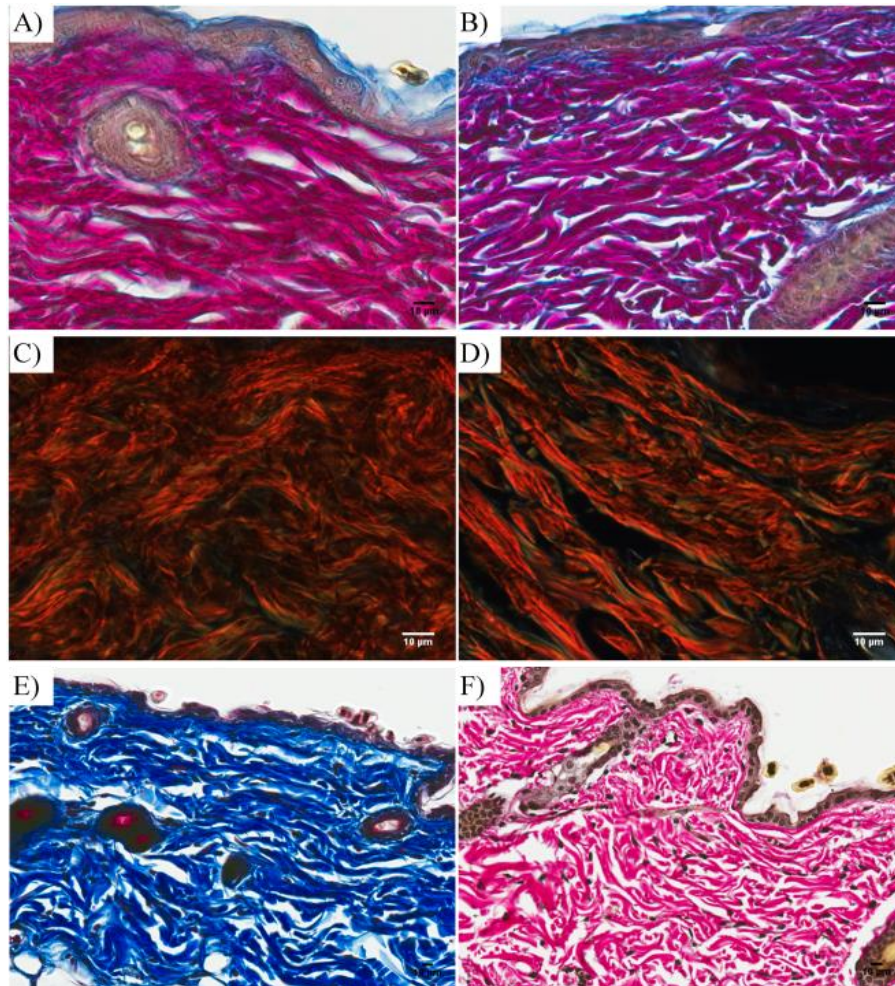


Figure 4-16 Collagen fibre organisation with different stains.

The collagen fibres were identified using Herovici (A, B), picrosirius (C, D), Masson's trichrome (E) and van Geison stains (F) in mouse skin processed with different fixatives. Representative images are shown for 10% NBF fixed specimens (A, C, E, and F) and AF (B, D). Representative images for each condition (n=4-6). Images representative of skin from three different animals and captured at 20x original magnification.

4.2.9 Immunostaining

In order to assess the effects of different fixatives on antigen recognition, I evaluated the detection of three key epidermal proteins by applying IHC: involucrin, K14, and PCNA. Cytoplasmic involucrin expression decorates the cornified layers of the epidermis (Crish et al., 1993), K14 is expressed at high levels in the cytoplasm of basal keratinocytes (Moll et al., 2008), whilst nuclear PCNA localisation characterises proliferating cells of the (predominantly) basal layer of the epidermis (Furukawa et al., 1992).

K14 immunoreactivity was detected in all skin specimens irrespective of the fixative. The detection of this antigen was most easily discerned with ZnF fixation (Figure 4.17A) but was also effectively discerned with Bouin's fixative (Figure 4.17 B).

Involucrin antigenicity was retained to some extent with 10% NBF and AF fixation (Figure 4.17C), whilst the signal was weak in ZnF fixed skin, and diffuse when Bouin's solution was used. Antigen retrieval with trypsin-EDTA digestion led to an improvement in ZnF fixed skin specimens (Figure 4.17 D).

PCNA antigenicity was both weak and inconsistent in 10% NBF fixed tissue (Figure 4.17E). The level of background signal also varied between fixatives, most noticeably in ZnF and Bouin's fixed skin. The best signal to noise ratio was achieved with AF fixation (Figure 4.17F). However, when tissues underwent antigen retrieval in citrate buffer with heat, PCNA antigenicity was improved relatively with all fixatives.

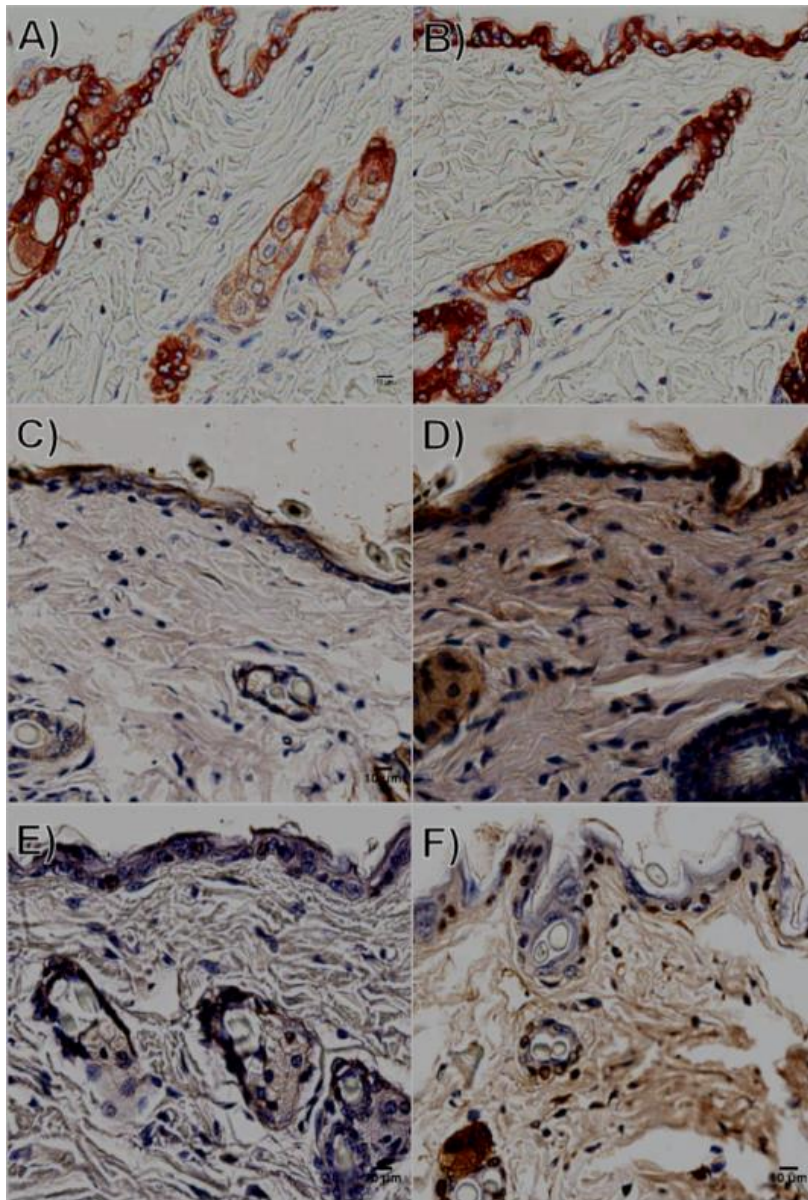


Figure 4-17 Immunodetection of K14 (A, B), involucrin (C, D) and PCNA (E, F) in mouse skin prepared with different fixatives.

Specimens were fixed with AF, and Bouin's without antigen retrieval (A, B), and AF (C), and ZnF with antigen retrieval (D), and 10%NBF without antigen retrieval (E) and ZnF with heat-mediated antigen retrieval (F). Representative images for each condition (n=4-6). Images representative of skin from three different animals were captured at 20x magnification.

The previous results were quantified and scored according to the consistency of special stains or the level of IHC signal (rather than the general morphology of tissues as described in table 2.3 in general methods) and summarized in Table 4.2 and 4.3. In summary, no single fixative provided optimal results with both histological and IHC analysis and each fixative have a particular advantage or disadvantage. Therefore, I went on to evaluate skin preservation and antigenicity with the four fixatives using the short fixation time in a subset of conditions as it is beyond the scope of this thesis to systematically evaluate every possible parameter.

Fixatives		10% NBF		Bouin’s			AF			ZnF			
H&E	Histology stains	†	Tissue shrinkage	†			††			†††			
			the separation of collagen fibres, seen in eosin auto-fluorescence										
PAS		††	Fair contrast	†††			†††			†	Weak discrimination		
				Sufficient contrast to discriminate basement membranes and blood vessels was good with AF									
G&O		†††	Good discrimination of both mast cells and elastic fibres	††	excellent discrimination of mast cells, it was poor at identifying elastic fibres		†		Good observation of (immune cell)		†††	good discrimination of both mast cells and elastic fibres	
VG		††		-			†				-		
			Difficult to detect fine murine elastic fibres under any conditions										
MT		†††		††			††				†		
		Good collagen and cross-linked keratins identification											
Herovici		††	Good discrimination blue and red	†	blue fibres were difficult to discern		††		Good discrimination blue and red		††	blue fibres were difficult to discern	
PicroSirius	††	Distinct collagen basket-weave.	-	Poor distinction		†††		Good distinct collagen basket-weave		††	Distinct collagen basket-weave.		

Table 4-2 Summary of special staining for 32 hour fixation.Key for grade index - (poor) † (satisfactory)†† (good) †††(Best)

		10% NBF		Bouin's		AF		ZnF	
Involucrin	IHC	†	Good antigenicity	-	Weak	††	Good antigenicity	-	Antigen retrieval with trypsin-EDTA Figure
K14		†		-	Epidermal shrinkage resulting in the loss of keratinocyte nuclear detail.	†† †		††	
PCNA		-	weak inconsistent	-	Weak inconsistent.	††	Best signal to noise ratio was achieved with AF fixation	-	Antigen retrieval with heat improved (for all)

Table 4-3 Summary of IHC results for 32 hours fixation. Key for grade index - (poor) † (satisfactory) †† (good) ††† (Best)

4.2.10 Comparison of four fixatives for short and long time

Normal skin samples exposed to the four fixatives for 6 hours at 40°C were evaluated using some of the histological stains and antibodies described earlier. Overall, the microscopic evaluation of skin morphology with H&E staining following fixation at 40°C for six hours in all solutions was characterised by better structure, reduced shrinkage, and better contrast compared to sections from skin samples fixed for 32 hours at room temperature (Figure 4.18). Particularly, AF achieved good morphology with fewer artefacts with short fixation (Figure 4.18 C) when compared to other fixatives at longer time (Figure 4.18G). Longer fixation was consistently associated with artefacts such as poor contrast, tissue shrinkage, abnormal collagen fibre organisation, lack of nuclear details and compromised epidermal structure. Another advantage of short fixation was enhanced antigenicity, exemplified in K14 immunostaining, with only AF not showing evidence of over fixing by 32 hours (Figure 4.19).

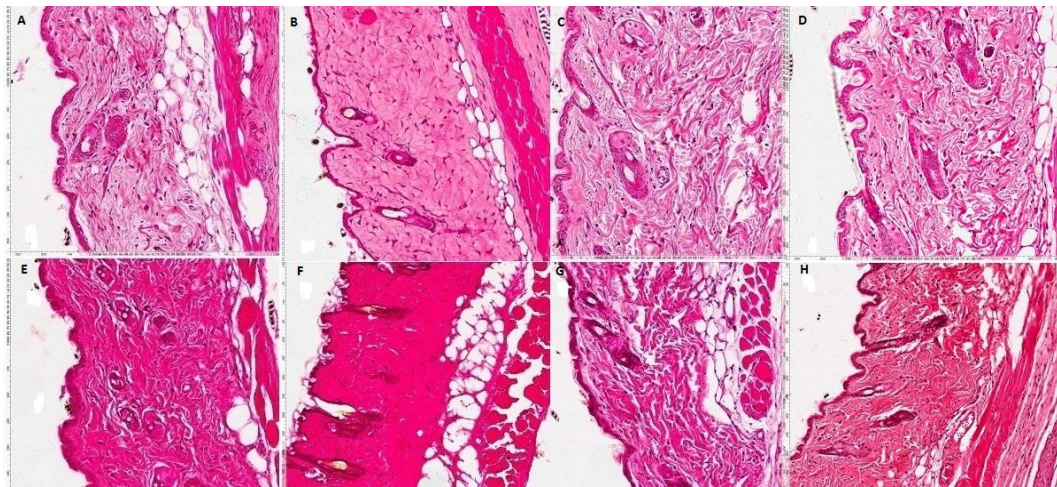


Figure 4-18 H&E staining of wild-type mouse skin with four fixatives.

Top panels, skin fixed for 6 hours at 40°C, and lower panel skin samples fixed for 32 hours at RT: A, E 10% NBF, B, F Bouin's, C, G AF and D, H ZnF. Lower panel, fixation for 32 hours at RT. The 6 hour fixed skin samples were characterised by better contrast with which to discern the skin layers. AF fixative with short (C), and long fixation (G) improves overall morphology. Representative images for each condition (n=4-6). Images were captured at 10x magnification using the Aperio scanner.

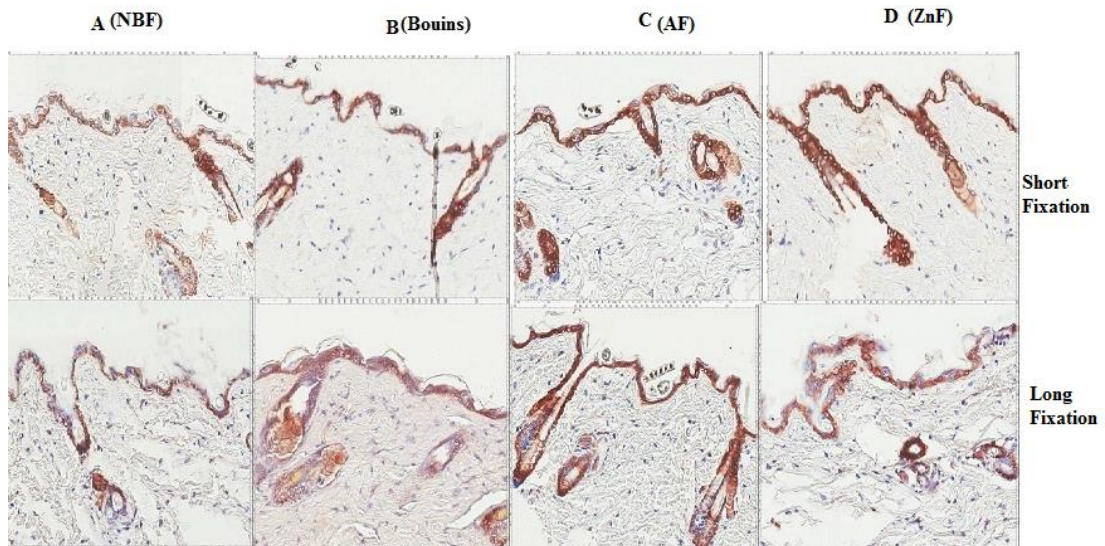


Figure 4-19 Representative images of K14 immunohistochemistry after 6 hours (40°C) and 32 hour fixation in various solutions.

Representative images for each condition (n=4-6). Images were captured 20x magnification.

PCNA IHC results were also consistently better with short fixation (especially 10% NBF and AF) compared to long fixation. (Figure 4.20). Best results were obtained with short AF staining. This could be as a consequence of the chemical properties of the various formulations, notably pH, osmolality, and coefficient of diffusability. For example, the diffusability for ethanol (1.0) is higher than that for 10%NBF (0.79) (Bancroft and Gamble, 2008c). Thus, it is very important to be aware of these parameters, and the nature of the tissue under study, when selecting fixative for any study (Treuting and Dintzis, 2011).

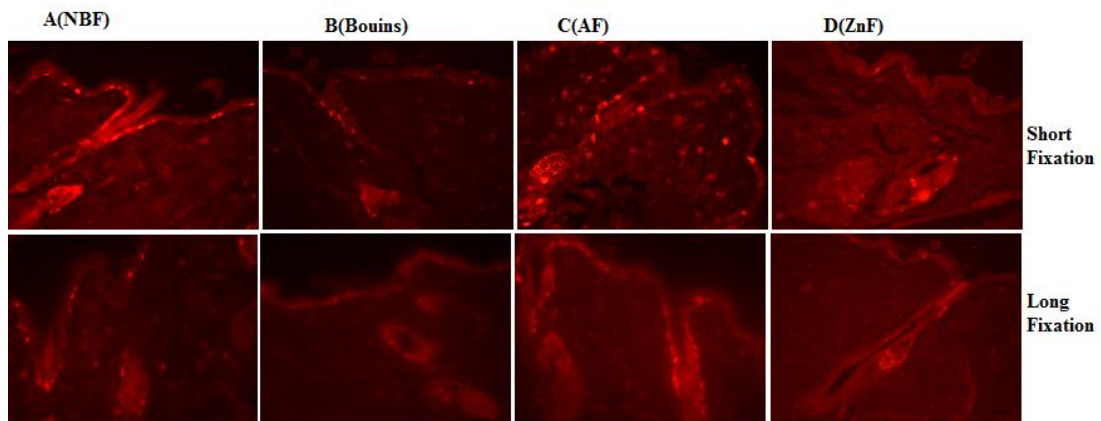


Figure 4-20 Representative images of PCNA immunohistochemistry after 6 hours (40°C) and 32 hours fixation in various fixatives.

Representative images without the use of antigen retrieval are shown. Representative images for each condition (n=4-6). Images were captured at 20x magnification.

All fixatives used in histopathology have different chemical properties and characteristics. Therefore, there is no universal fixative for all tissues due to the fact that certain fixatives might be appropriate for specific tissue components or certain IHC applications. The sectioning procedures and overall morphology of normal mouse tissues obtained using the four fixatives with six hour incubations at 40°C were better than those achieved using longer conditions when comparing the morphology of mouse skin using a range of histological stains. As well as revealing the expression of key cutaneous proteins, I found that prolonged tissue exposure to any of the four fixatives (32 hours) will increase the masking of antigen's epitopes, so requiring antigen retrieval, which can promote tissue damage. However, AF and 10% NBF fixed tissues tolerate this reasonably well. With short fixation, both AF, and 10% NBF provided good retention of morphology and structure of normal skin with special histological staining. AF was more effective in maintaining antigenicity for the cutaneous markers investigated in this study.

However, the rationale of these experiments was to identify optimal conditions for the histological evaluation of tissues including fragile mouse skin. I went on to study the effect of AF fixation on diabetic mouse skin organisation with a selective range of histology stains, compared with the method used in Chapter 3.

4.2.11 Histological analysis of diabetic mouse skin fixed with AF

Mouse skin tissues from three male *wt/wt*, *ob/ob*, *db/db*, and misty animals were fixed for 6 hours at 40°C before processing with the long processing protocol (Appendix 3). Three biological replicates from each model were used to establish TMAs to ensure consistency between skin sections, and minimise artefacts that might confuse downstream analysis of skin phenotypes in obese and insulin resistant mouse models.

4.2.11.1 Sectioning diabetic mouse skin from different fixations

TMA sections skin fixed in 10% NBF for 3 days (the previous standard) were compared to tissues fixed in AF for 6 hours at 40°C. A hard cutting surface, missing or folded regions, as well as artefact including abnormal nuclei, collagen deposition, and adipocyte architecture were only associated with TMA obtained from the 10%NBF fixed tissues Figure 4.21 4.22, and 4.23)

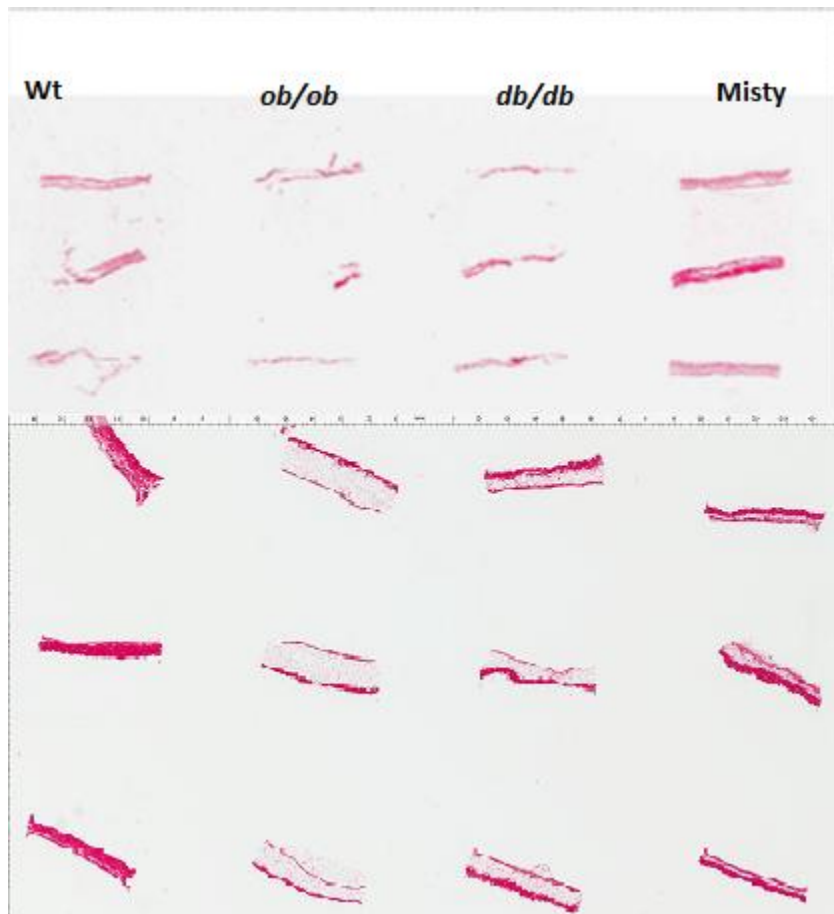


Figure 4-21 Gross organisation of TMA sections with old and revised histological methods.

Skin TMAs prepared from different mouse models at 3 month of age (*wt/wt*, *ob/ob*, *db/db* and *misty*) are shown. Typical structure obtained with fixation in 10% NBF for 3 days is shown in upper panel. Improved section quality achieved by fixation in AF for 6 hours is shown in the lower panel. Representative images for each condition (n=4-6). Images were captured at 1x magnification with the Aperio Scanscope.

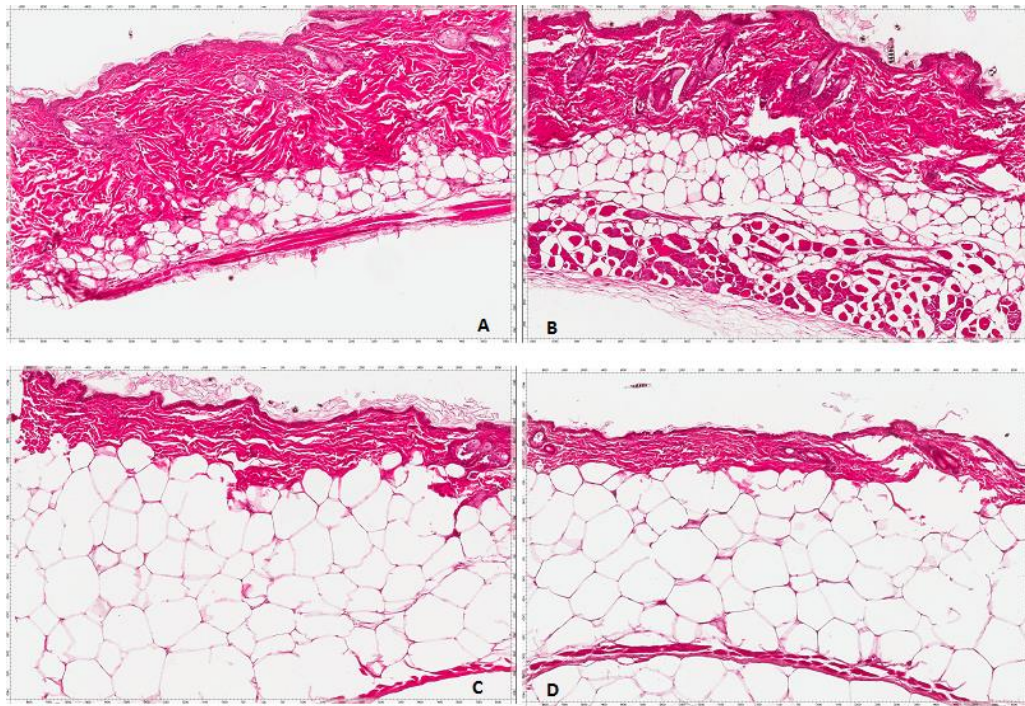


Figure 4-22 H&E stained sections of mouse skin.

Skin samples fixed in 10%NBF for 3 days: *wt/wt* skin (A), *misty* (B), *ob/ob* (C) and *db/db* (D). Representative images for each condition (n=4-6). Images were captured at 10x magnification with the Aperio scanner

While it was possible to achieve good sections using the method described earlier, this was at the cost of sectioning time, and the need to cut more sections due to tissue loss. In future studies, the use of AF fixation gives consistent morphology, with considerable time saving in preparation (Figure 4.23). Moreover, the contrast achieved with H&E staining was very good.

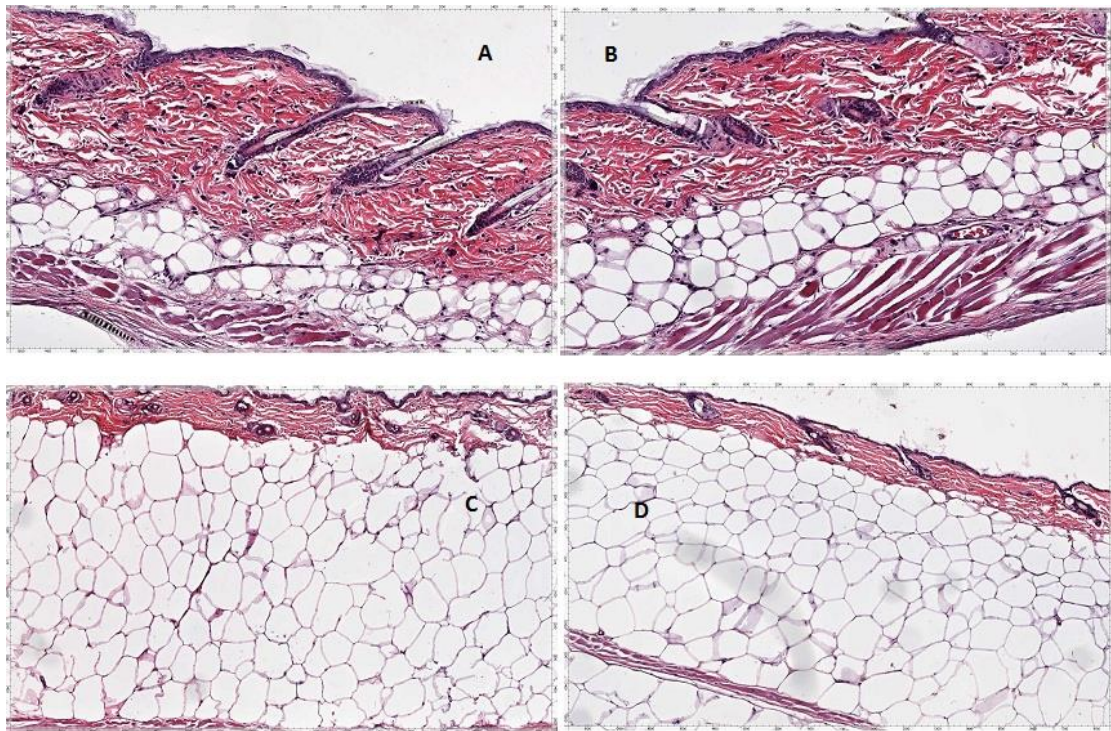


Figure 4-23 Different mouse models skin fixed in AF and stained with H&E.

Tissue organisation following AF fixation: *wt/wt* skin (A), *misty* (B), *ob/ob* (C) and *db/db* (D). Representative images for each condition (n=4-6). Images were captured at 10x magnification with the Aperio scanner

4.3 Discussion

It is critical in histopathology that researchers are aware of the range of fixatives and processing parameters that may impact the tissue's morphology under investigation (Srinivasan et al., 2002). This is more difficult in mouse tissues as histology texts focus on human material, which tends to be more robust than murine counterparts (Glasø and Hovig, 1987), and extra care must be taken to avoid protein denaturing or masking due to poor or over fixation (Srinivasan et al., 2002, Treuting and Dintzis, 2011). Problems are exacerbated when tissue integrity is impacted by a pathological state, and to my knowledge there are no methods that describe preserving diabetic mouse skin tissue. These models are characterised by an expanded subcutis (and cutting fatty tissue is difficult) and a loosely packed dermis.

One of the aims of this thesis is to identify cutaneous pathology in mouse model of diabetes. Tissue processing is central to this, and the choice of fixative is, therefore,

crucial if one is to preserve fine cutaneous structures (Glasø and Hovig, 1987, Al-Habian et al., 2014). Also fixation has various affects at the molecular level that can retain or destroy key structural details, and mask some antigens (Treuting and Dintzis, 2011). In most pathology laboratories, formalin based processing protocols (particularly 10% NBF) are considered the first choice fixatives (Tang et al., 2013, Khan et al., 2009, Kunder et al., 2007). Previous studies have considered the influence of fixatives on mouse skin with particular respect to the immunoreactivity of various antibodies (Mikaelian et al., 2003). However, to my knowledge no previous studies have investigated time and temperature systematically (and certainly no use was made of TMAs) for both histology and IHC experiments. The Table 4.4 provides a brief outline of the steps relevant to developing optimal mouse skin histology and IHC methods and problems solving process.

PROBLEM	SOLUTION	OUTCOME
Brittle sections	Adapt processing	Improved sections
Inconsistent staining		Improved special staining
Antigen masking		Unmasking still required
Throughput low preparing TMAs	Softening agent	Reduced loss of tissue and good TMA histology
Tissue disruption with antigen unmasking	Evaluate antigen retrieval methods	Inconsistent IHC and tissue damage
Inconsistent IHC	Adapt fixation time	Reduced fixation improves antigenicity
Lack of contrast with special staining	Evaluate fixative type	Consistent staining with 10% NBF. Improved staining with AF
Poor signal/noise ratio with IHC	Evaluate antibody conditions and detection methods	Unambiguous IHC
Loss of diabetic skin tissue organisation	Short fixation in AF, long processing protocol	Retention of diabetic skin integrity

Table 4-4 Optimisation of diabetic mouse skin histology and IHC

Fixation time is very important and tissues are routinely exposed to fixative for one hour per millimetre depth using non-coagulative fixatives (Medawar, 1941, Bancroft and Gamble, 2008d). Other studies have recommended 25 hours to fix a 4x4x4 mm piece of mouse tissue (Treuting and Dintzis, 2011). Therefore, the size of skin samples is one of the major factors in the fixation process, and the use of thin skin slices in this

study ensures effective penetration and faster action of fixatives. However, when using 10% NBF, fixation is not complete until cross-linking has occurred and so samples are usually left for at least 24 hours to ensure complete fixation (Tellyesnicky, 1926, Baker, 1958). Thus, thin specimens might be fixed sufficiently in 10% NBF in 5- 6 hours, and rapid fixation is acceptable as long as histochemical staining is effective (Bancroft and Gamble, 2008c). However, increasing the ambient temperature of fixative enhances its action. This is supported by recent studies on Bouin's, AF and ZnF, which demonstrated that fixation is completed by 6 hours at 37°C (Coscia et al., 2014, Elzabbal et al., 2013), and that skin is effectively fixed after 18 hours at room temperature. Whilst under-fixation is associated with tissue degradation and underperformance in histological assays, over fixation is associated with problems including loss of antigenicity (Werner et al., 2000, Bancroft and Gamble, 2008a). However, I observed no "edge effects" with either special staining or IHC that might indicate incomplete tissue fixation with any fixatives employed with different conditions in this study, whereas long fixation was associated with over-staining and tissue shrinkage and limited retention of cutaneous antigens and loss of nuclear detail, as reported previously (Ananthanarayanan et al., 2005). For IHC analysis of skin tissues, I would recommend AF as this provided a good signal to noise ratio and the robust retention of antigenicity. These findings are intriguing as 10% NBF is the most widely used fixative in histology laboratories (Grizzle, 2009b). In agreement with previous studies, ZnF enhanced staining and nuclear details, but I saw no deleterious effects of alcohol on nuclear or cytoplasmic detail, as has been previously suggested (Eltoum et al., 2001, Rolls, 2012).

My rationale for evaluating mouse skin histology was informed by two considerations; firstly, the widespread use of mouse as a disease model and secondly, that this tissue provides a challenging experimental environment that has yet to be assessed systematically for histological artefacts arising from fixation. Mouse skin is thinner and more fragile than human skin, and so loss of architecture during processing has implications for downstream applications. In particular, obtaining good histology from diabetic mouse skin (the most fragile) such as maintaining subcutaneous adipocyte architecture and the discrimination of components such as fine elastic fibres presents a considerable challenge. Moreover, this study provides many insights via comparison of the effects of processing protocols and fixatives under two different conditions (time

and temperature) on the detection of cutaneous features. Finally, I suggest that these observations are applicable to tissue derived from a variety of tissues, and are relevant to human material when considering downstream applications. A summary of key technical steps and the main findings of this study provide guidelines for preparing skin samples from mouse models of insulin resistance (*ob/ob*), obese (DIO), and diabetic (*db/db*) for prospective histological and IHC analysis. These are listed in (Table 4.5).

Tissue harvesting	Shave the skin and cut into 2-5x5-10mm slices before fixation
Pre-fixation	Use fresh fixative with the correct tissues to fixative's volume ratio (1 to 20)
Fixative	Alcoholic formalin for 6 hours at 40°C (histology) or (IHC) works well across a range of experiments.
Processing	Use extended processing protocol with fresh reagents, without delay in starting or removing from the processor
Sectioning	Use TMAs, softening agent, and keep the temperature in the sectioning room below 15°C
IHC	Consider utility of both chromogenic and fluorescent methods. Investigate different chromogens and fluorescent labels (FITC, TRITC). Short fixation may remove need for antigen retrieval.
Antigen retrieval	Retrieval with trypsin preserves tissue structure, but may not suffice. More aggressive heat-based methods disrupt tissue, but 10 minutes of pressure cooking in citrate buffer at pH6 was satisfactory.
Primary antibody	Short fixation times may allow for reduced primary antibody concentrations and better signal to noise ratios. Investigate incubation time and temperature.

Table 4-5 Recommended guidelines for diabetic mouse skin histology and IHC application

Chapter 5: Cytokine Profiling and Dermal Fibroblast Culture

5.1 Introduction

There is growing evidence in the literature about the relationship between white adipose tissue metabolism, insulin resistance, diabetes, hypertension, and cardiovascular disease (Bjørndal et al., 2011, Trayhurn and Wood, 2004). Fat distribution, adipose gene expression profiles, adipokine secretion and lipolytic capacity are among the major determinants of metabolic disease (Snel et al., 2012). For example, the metabolic activity of white adipose tissue varies depending upon its location, with visceral adipose tissue (VAT) having a higher metabolic activity, mitochondrial and free fatty acid (FFA) content, and sensitivity to insulin stimulated glucose uptake than subcutaneous fat depots (Bjørndal et al., 2011, Goran and Alderete, 2012b). Both systemic and local inflammatory agents impact peripheral tissue function, and I wanted to investigate an association with cutaneous pathophysiology in the models described in this thesis.

Using the range of histological techniques developed in the previous chapters, I investigated different cutaneous phenotypes including dermal damage, disorganisation, and increased fat accumulation in animal models of insulin resistance, type 2 diabetes, and ageing. Interestingly, I was able to distinguish subcutaneous (the deep layer) from subdermal fat (the superficial layer) in mouse skin. There are several terms used for the third layer of the skin, which is located beneath the dermis. These terms include the hypodermis, subcutaneous adipose tissue (SAT) and subcutis, and are used in both humans and mice (Avram, 2004, Trottier et al., 2008). However, there is emerging evidence that the SAT in humans can be anatomically divided into two distinct layers by Scarpa's fascia; the superficial subcutaneous adipose tissue (panniculus adiposus), and a deeper subcutaneous adipose tissue (panniculus carnosus) (Abu-Hijleh et al., 2006). Recently, the deeper layer of SAT has been linked to features of insulin resistance, unlike the superficial layer which acts more likely as a buffering fat depot for excess energy intake (Marinou et al., 2014). In this chapter, I chose to investigate the upper layer as other researchers have recently shown that the more superficial fat layer (also called the intra dermal layer) influences whole body physiology, potentially via a thermoregulatory response (Kasza et al., 2014). Other researchers were able to differentiate the dermal adipose tissue in mature mouse skin from deeper subcutaneous tissue (Wojciechowicz et al., 2013). However, I found that the more superficial layer was difficult to discern in young adult mice, but that it could be discerned in obese models. The topography is displayed in Figure 5.1, showing the location of sub-dermal

fat, which lies above the muscle layer, and the deeper subcutaneous fat layer, which is beneath the dermal fascia and muscle in mature and obese mouse skin. It is likely that each layer has distinct physiological and biochemical properties, but physically isolating each fat layer was very difficult. In the first instance, I looked at the inflammatory cytokine profile of plasma (which is considered to be relatively non-inflammatory) and epididymal fat depots (a visceral depot, also considered to be relatively protective), both of which contribute to some extent to peripheral diabetic pathophysiology in insulin resistant and ageing states. I then went on to look at the local cytokine profiles of the skin compartments (including both adipose depots) in wild type and *ob/ob* mice as there is evidence that deeper subcuticular adipose depots have a relatively pathogenic effect. To my knowledge, however, no group is yet to report the biochemical properties of the divisions of this depot.

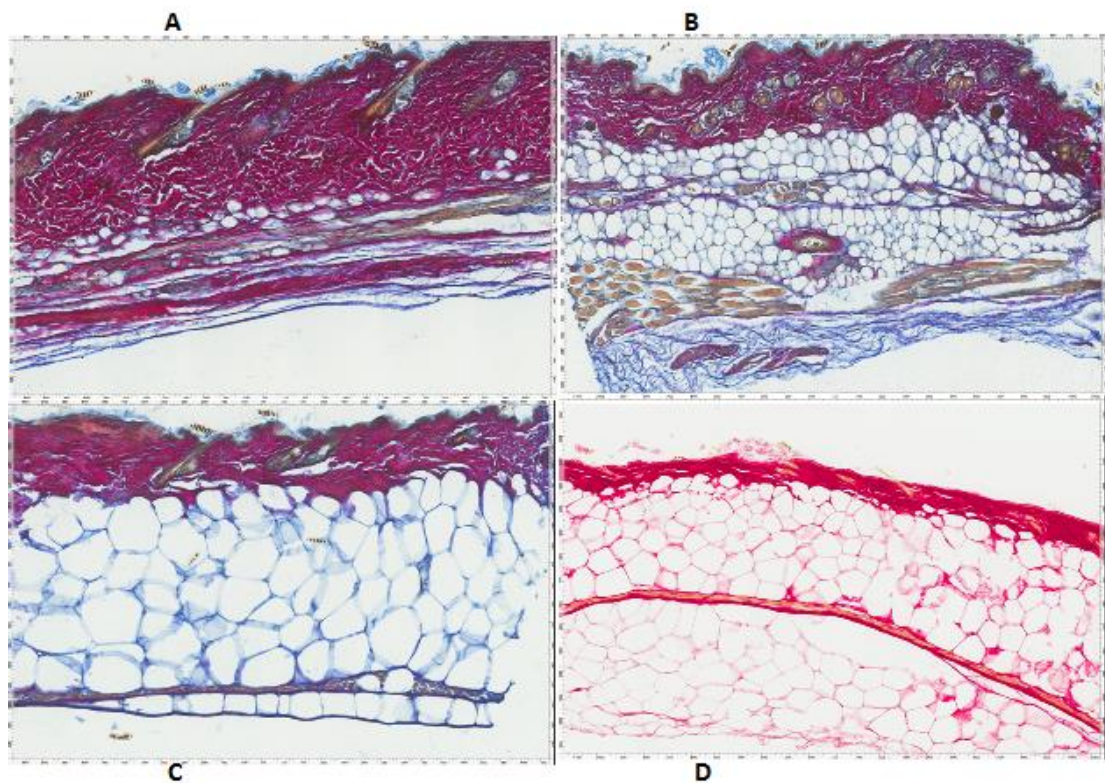


Figure 5-1 Mouse skin adipose tissue layers.

The topography of mouse skin sub dermis above the panniculus carnosus layer, was distinguishable from the deep SAT (beneath panniculus carnosus layer) in 20 month B, *db/db* C, and *ob/ob* D and was difficult to discern in 3 month old *wt/wt* mice skin stained with herovici in A, B ,and C, and H&E in D. . Representative images form three mice. Images were scanned Aperio™ Scan Scope and captured at 10x magnification.

An understanding of the mechanisms underlying the disruption of dermal collagen structure and function in murine models of obesity and type 2 diabetes will provide insight into human disease. Previous *in vitro* studies of dermal fibroblasts have identified impairments related to fibroblast function arising from reduced vasculature, and the local inflammatory impact of adipokines (Lerman et al., 2003b, Schmidt and Horsley, 2013). These effects may provoke downstream cascades of altered ECM remodelling (Berlanga-Acosta et al., 2012). I wanted to investigate if fibroblasts from a model of insulin resistance (*ob/ob* mice) maintained a “diabetic” phenotype if maintained *ex vivo* by studying proliferation, collagen synthesis, and senescence. I also wanted to evaluate if insulin signalling mechanisms were impacted by determining the expression in the β -subunit of the insulin receptor, which is known to be down-regulated in insulin resistant and ageing states.

Previous studies have shown that insulin resistance in various adipose tissues from obese subjects (both subcutaneous and visceral fat) influences systemic insulin sensitivity via both paracrine and endocrine mechanisms (Virtanen et al., 2002, Khan et al., 2009). Therefore, my hypothesis was to investigate the possible relation between dermal damage and local or systemic cytokine action from expanded fat depots by profiling candidate cytokines from both adipose tissue and plasma of mouse models of obesity, type 2 DM and ageing.

5.2 Methods

5.2.1 Optimisation of dermal fibroblast culture protocol

Methods to culture dermal fibroblasts were described in detail in the general methods chapter, but preparing viable cells from *ob/ob* mice proved challenging, and herein I highlight some important technical considerations. Culture methods for primary dermal fibroblasts in both human and rodents are well established (Takashima, 2001, Seluanov et al., 2010). However, these are not optimised to produce fibroblasts of impaired function, and yields of *ob/ob* fibroblasts were low. As access to *ob/ob* fibroblasts was limited, I initially optimised methods using *wt/wt* cells. Two methods (explants and isolation of cells following enzymatic digestion) were assessed using young, lean *wt/wt* mouse skin to maximise yields of dermal fibroblasts. I found explant methods to be unsatisfactory, producing a very low number of dermal fibroblast after 48 hours in culture. By day 6, growth had consistently ceased (Figure 5.2).

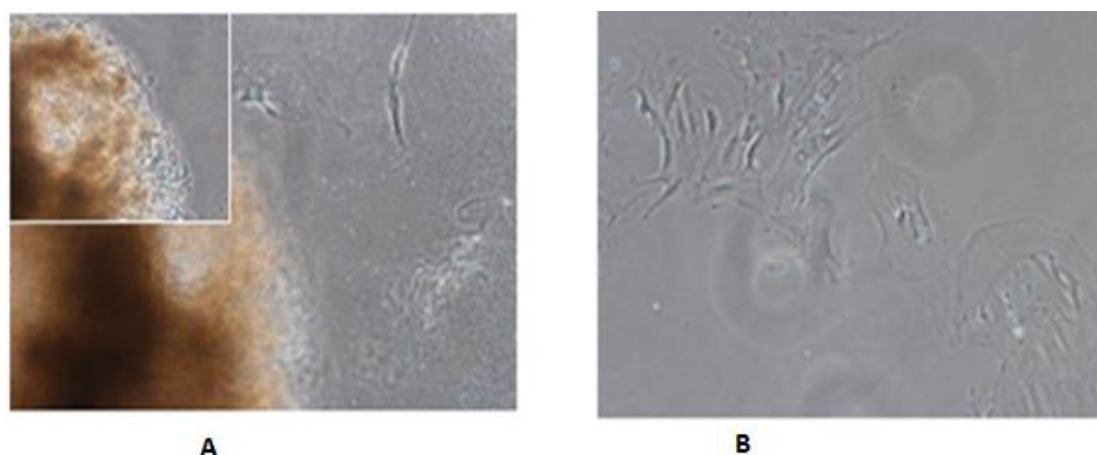


Figure 5-2 Explant culture of dermal fibroblasts from *wt/wt* mouse.

A typical skin explant releasing few cells after 2 days is seen in panel A. By day 6, there was little evidence of proliferating fibroblasts (B). Images captured under phase contrast at 10x original magnification

The second technique used enzymatic digestion of skin to release fibroblasts followed by seeding in culture flasks, as described by Takashima (Takashima, 2001). This requires the removal of extraneous tissue such as hair and fat. Table 5.1 summarises the key factors investigated to improve collagenase treatment.

Collagen type	Type II or type IV
Concentration	0.5 and 1.0%
Incubation time/ temperature	5min-30 minutes (RT), or on 4°C
Shaker speed	200 or 350 cycles per minute
Substrate	Collagen coated plates

Table 5-1 Critical parameters in primary dermal fibroblast culture

There was relatively difference in yields obtained with collagenase type, concentration or incubation conditions (not shown). The most dramatic improvement was found with shaker speed (Figure 5.3). Enzymatic incubation at 200 cycle per minute yielded a relatively intact dermal sheet from which many fibroblasts were released (indicated by pellet size (Figure 5.3.B) in comparison to over-digested dermal sheet under 350 cycle per minute (Figure 5.3 A). The other critical parameter was the use of collagen-coated

flasks, which promoted cell attachment and growth (Figure 5.4). In this way, I was able to prepare viable cultures of both *wt/wt* and *ob/ob* fibroblasts.

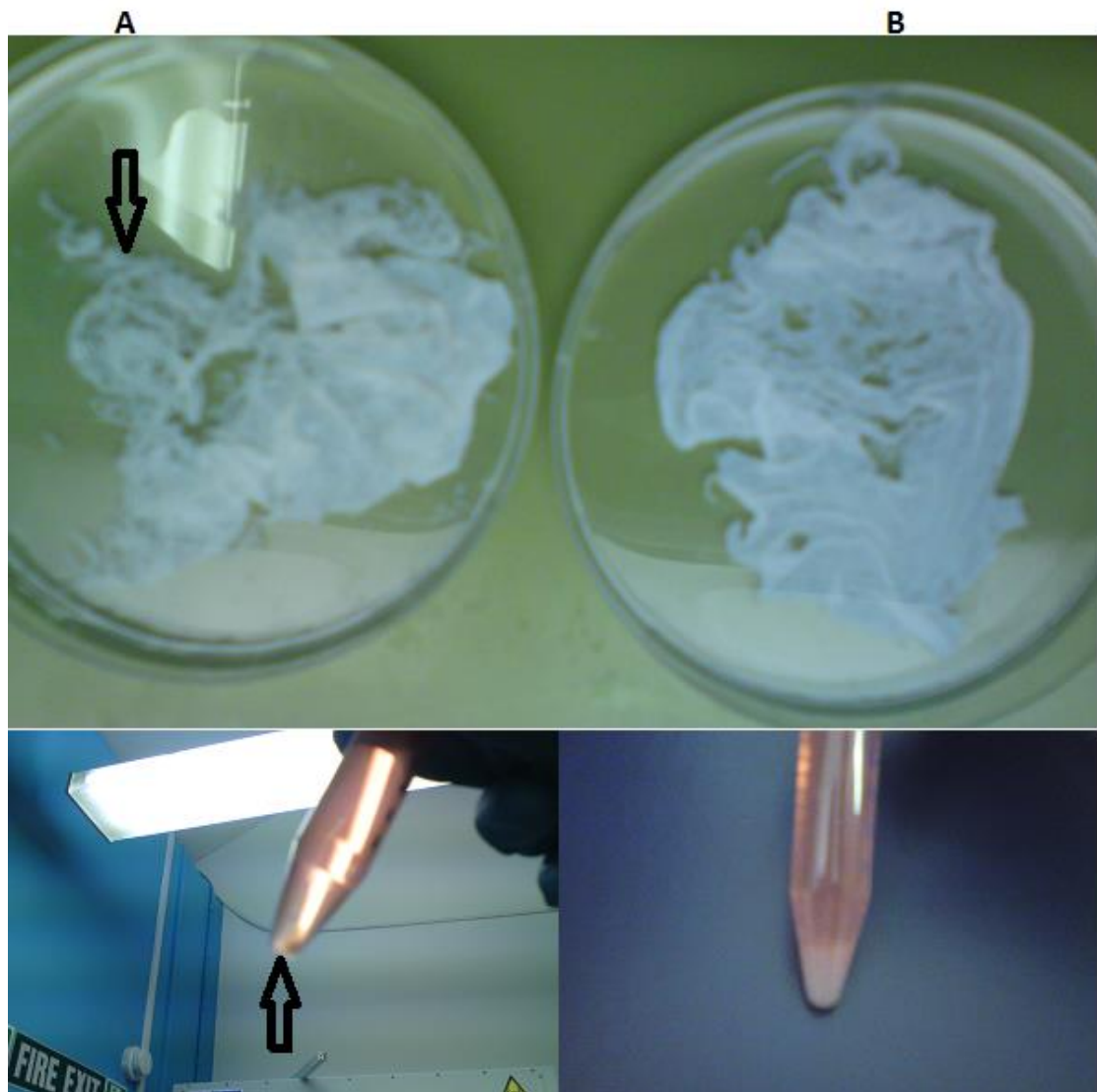


Figure 5-3 Preparation of dermal fibroblasts..

A. The higher shaking speed (350 cycles per minute) resulted in an over-digested dermal sheet. The arrow in (A) top panel highlights damage. Panel B shows an intact sheet resulting from the slower shaking speed. The lower left panel shows that very few cells were recovered with high shaker speed (arrow), in comparison to 200 cycles per minute (lower right panel).

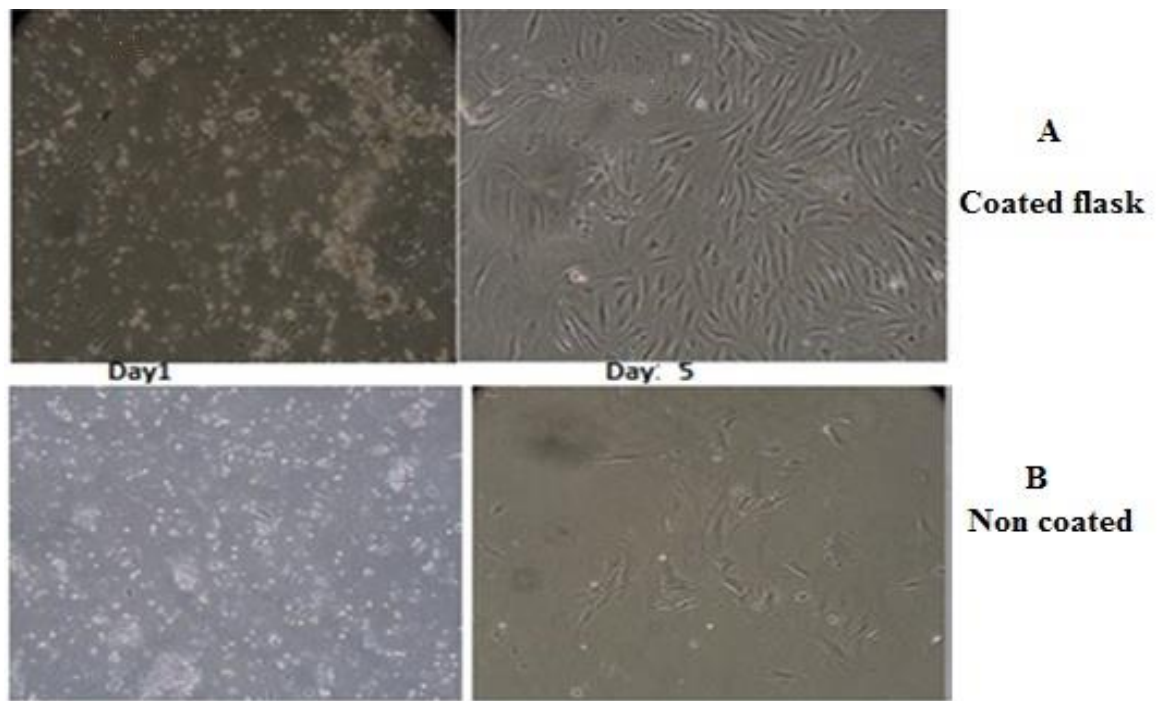


Figure 5-4 Use of collagen coated flasks to promote dermal fibroblast attachment and proliferation.

Representative images from normal dermal fibroblasts from three mice. Cells were cultured in collagen coated flasks (row A), and non-coated flasks (row B) at days one and 5 in culture. Images were captured at 10x original magnification.

5.3 Results

5.3.1 Plasma cytokine levels

Cytokine levels were quantified in plasma obtained from young (3 month old) lean *wt/wt* and ageing (12 month old *wt/wt*), KS/J (misty), *ob/ob* and *db/db* mice (all at 3 months of age and maintained on chow diets; (Table 5.2). A 2.4 fold up-regulation in TNF α was seen with age, but not in insulin-resistant *ob/ob* or diabetic *db/db* plasma. Furthermore, IL10 and IL12 showed 2.3 and 2.0 fold increases respectively in old mice in comparison to young. Both MCP1 and RANTES were up-regulated significantly (* $p < 0.01$, ** $p < 0.001$) in *ob/ob* animals only compared to controls (3.2 and 1.7 fold respectively). Overall, there was no strong inflammatory profile in the plasma of *ob/ob* or *db/db* mice and only ageing mice showed a mild inflammatory profile.

Plasma cytokines pg/ml	<i>wt/wt</i>		<i>ob/ob</i>		Old	
	Mean	SEM	Mean	SEM	Mean	SEM
IFN	3	2	7	6	5.8	2
IL10	48	13	64	16	111	59
IL12	128	5	108	5	267	128
IL1-β	3	1	2.4	0.7	5.6	0.6
IL6	38	12	28	5	79	36
MKC	111	20	125	5	102	26
TNF-α	2	1	3	0.5	4.8	0.9
GMCSF	0.3	0.1	0.19	0.009	0.2	0.2
MCP1	32	12	104*	3	21	4.8
RANTES	42	4	73**	6	5	2.2
Plasma cytokines	Misty(n=4)		<i>db/db</i> (n=4)			
	Mean	SEM	Mean	SEM		
IFN	6	4	3	0.8		
IL10	58	19	81	7.2		
IL12	124	42	225	53		
IL1-β	4	1.2	5	0.9		
IL6	40	6	64	11		
MKC	125	29	137	35		
TNF-α	2	1.6	3	0.7		
GMCSF	0.8	0.4	1.1	1		
MCP1	53	16	51	12		
RANTES	84	7.9	96	11		

Table 5-2 Plasma levels of cytokines from 3-4 animals per each group. Significant analysis was performed using unpaired two-tailed Student's t-test for each parameter

5.3.2 Subcutaneous adipose conditioned medium

In Table 5.3 there was significant up-regulation in IFN γ (39 fold), IL1 β (17 fold), IL6 (35 fold), TNF α (13 fold), and RANTES (13 fold) in the conditioned medium from *ob/ob* mice compared to age-matched lean controls. While there was no distinct inflammatory phenotype in *db/db* and ageing models (with exception of IL12, IL6, and MCP1 in ageing)*ob/ob* SAT characterised by higher level of various cytokines..

SC cytokines pg/ml	<i>wt/wt</i>		<i>ob/ob</i>		Old	
	Mean	SEM	Mean	SEM	Mean	SEM
IFN	0.3	0.06	14***	2	1.7	0.2
IL10	661	88	2760	887	529	135
IL12	56	15	1042	98	155	19
IL1- β	3	0.4	53	7	12	6
IL6	633	44	22207***	5735	2634	254
MKC	1843	247	47947	3042	6655	798
TNF- α	55	7	726***	141	75	13
GMCSF	1	0.3	26	2.7	3	2
MCP1	246	40	6816	522	932	190
RANTES	38	7.9	394	155	19	6
SC cytokines	Misty		<i>db/db</i>			
	Mean	SEM	Mean	SEM		
IFN	1.7	0.2	0.4	0.02		
IL10	238	62	210	62		
IL12	229	99	N/A	N/A		
IL1- β	7	3.2	2	0.5		
IL6	1246	275	465	135		
MKC	2939	822	1465	384		
TNF- α	32	6.4	32	10		
GMCSF	1.8	1	4	4		
MCP1	286	150	387	78		
RANTES	192	92.	66	53		

Table 5-3 Cytokine profile from subcutaneous adipose conditioned medium (ACM) from 4 animals per each group. Significant analysis was performed using unpaired two-tailed Student's t-test for each parameter

5.3.3 Epididymal adipose conditioned medium

Table 5.4 shows the cytokine profile from epididymal fat isolated from young (3 month old) lean *wt/wt*, and ageing (12 month old), KS/J, *ob/ob* and *db/db* mice (3 month of age on chow). There was a significant up regulation in MCP-1 with 47 fold induction, and MKC, TNF- α , and GMCSF (18, 7.4, and 40) fold induction respectively from *ob/ob* mice compared to their lean age-matched controls. Slight changes in *db/db* and ageing epididymal fat cytokines profile were detected in IL6, M κ C, TNF- α , and MCP1 mainly in ageing.

Epididymal cytokines pg/ml	<i>wt/wt</i>		<i>ob/ob</i>		Old	
	Mean	SEM	Mean	SEM	Mean	SEM
IFN	1.4	0.91	12	2.9	2	1.6
IL10	1819	231	2710	636	689	0.3
IL12	107	22	1298	174	24	2.2
IL1- β	6.8	3.7	55	7	6	0.9
IL6	1117	262	17203	2135	2866	2.5
MKC	2944	616	54496. ***	2857	9795	3.3
TNF- α	90	6	668***	106	114	1.2
GMCSF	0.9	0.1	36***	7	5	6.3
MCP1	247	64	11738***	1881	915	3.7
RANTEs	70	11	207.	37	11	0.1
Epidi cytokines	Misty		<i>db/db</i>			
	Mean	SEM	Mean	SEM		
IFN	1.3	0.8	1.4	1.1		
IL10	421	228	864	2		
IL12	282	111	159	0.56		
IL1- β	8	2.8	6	0.8		
IL6	1939	1006	1583	0.8		
MKC	5944	3248	5224	0.8		
TNF- α	159	61	95	0.6		
GMCSF	4.7	2.9	4.8	1		
MCP1	645	376	607	0.9		
RANTEs	26.7	22	28	1		

Table 5-4 Cytokine profile from epididymal adipose conditioned medium (ACM) from 4 animals per each group. Significant analysis was performed using unpaired two-tailed Student's t-test for each parameter

5.3.4 Comparing cytokines profile from different cutaneous layers in *ob/ob* mice

Having established an inflammatory profile in SAT and VAT depots, I went on to investigate local levels of a subgroup of key cytokines (IL-10, IL-6, IL-1 β , MKC, TNF- α) in the skin layers of *ob/ob* mice compared to lean controls. In particular, I was able to micro dissect the dermal adipose layer in order to contrast the cytokine profile with that of deeper subcuticular fat analysed above (Figure 5.5). It was not possible to retain a cytokine signal upon the enzymatic separation of epidermis from dermis, and so these layers were profiled together. No changes were seen in plasma cytokine levels, while, a consistent reduction in levels of both anti-inflammatory (IL-10) and pro-inflammatory

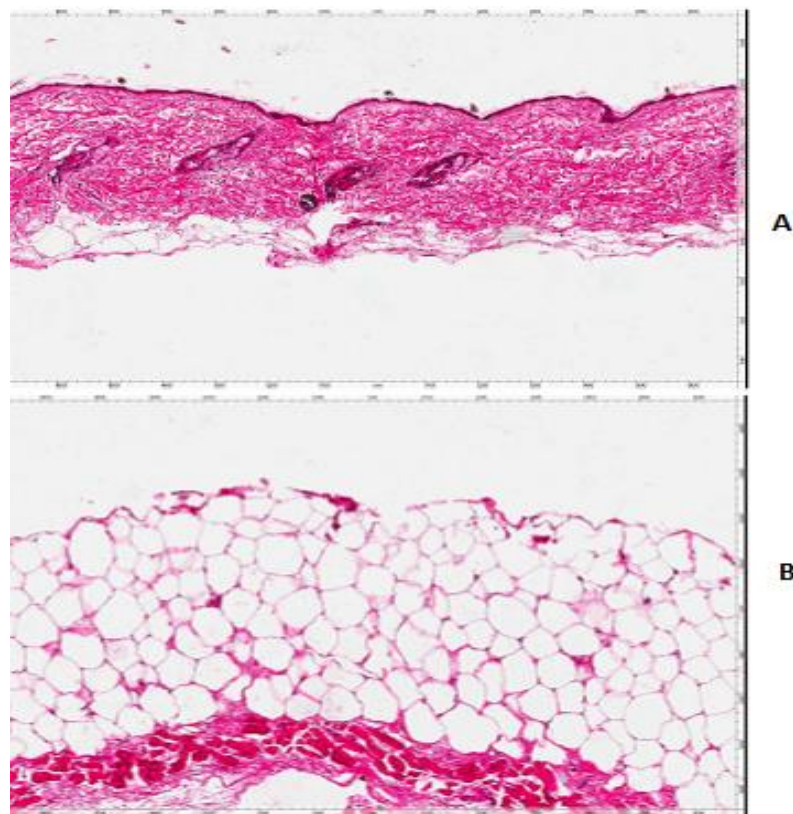


Figure 5-5 Illustrative figure of inner and outer layers separation

The dermis adipose tissue B from *ob/ob* mouse skin has been anatomically separated from the outer layer (epidermis and dermis) A and stained with H&E in image A, and B. Images were scanned AperioTM Scan Scope and captured at 10x magnification

factors (IL-1 β , IL6, TNF- α , and MKC) were down regulated in subdermal. A significant increase was seen in the non-adipose layers of *ob/ob* skin. Thus, local TNF α action could be a critical mediator of cutaneous damage in insulin resistant states. The inflammatory profile of each compartment is summarised in Table 5.5.

Cytokine pg/ml	Plasma	VAT	SAT	Subdermal fat	Non-adipose Skin
IL10	1.3	1.4	4	0.2	0.3
IL6	0.8	15	35	0.3	0.5
IL1-β	0.9	8	17	0.6	0.6
MKC	1.2	18.5	26	0.3	0.2
TNF-α	1.5	7	13	1	10

Table 5-5 Summary of key cytokines in plasma, skin and adipose depots of *ob/ob* mice. Fold-change values compared to control animals are shown.

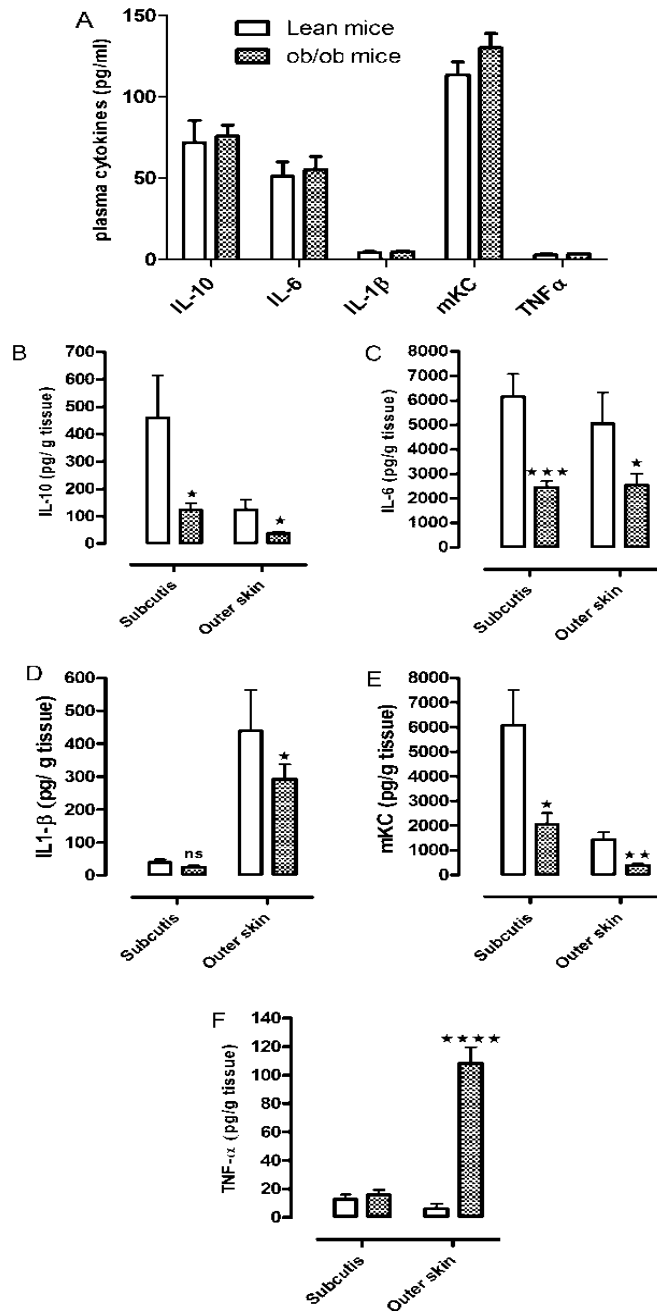


Figure 5-6 Cytokine profiles from plasma and deferent skin compartment of *ob/ob* mice.

(A) Plasma cytokine levels were investigated in age-matched chow fed wild type *wt/wt* and *ob/ob* mice (n=4). Expression of individual cytokines in conditioned medium prepared by exposure to different skin compartments is shown in B-F. Significance was assessed by student unpaired t test, and *p<0.05, and **p<0.01; ***p<0.001, ****p<0.0005.

5.3.5 Insulin receptor expression in normal and diabetic fibroblasts

Western blotting analysis showed that the β -subunit of the insulin receptor is down-regulated in dermal fibroblasts from *db/db* and 20 month old mice (Figure 5.7). An even greater suppression was observed in freshly-isolated 3 month old *ob/ob* fibroblasts, compared to age-matched wild-type controls.

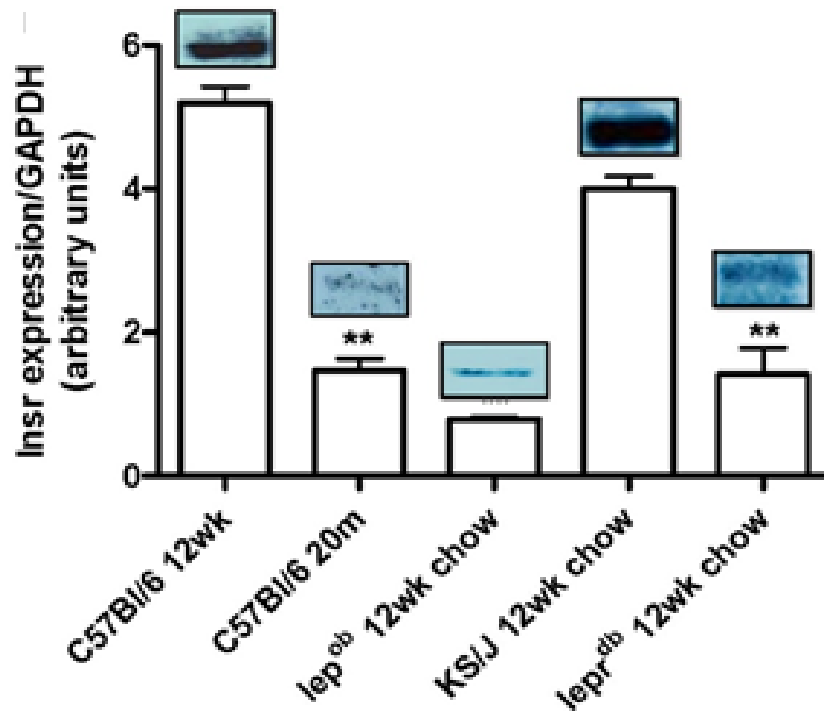


Figure 5-7 Insulin receptor (β -chain) expression in dermal fibroblasts.

Dermal fibroblasts were isolated from lean C57Bl/6 at 3 month (12 week) and 20 month, along with KS/J, *ob/ob* and *db/db* mice (3 month of age on chow) is shown, normalised relative to GAPDH expression. Representative blots for each group are shown. Significance was assessed by 1-way ANOVA with post-hoc Dunnett's tests to compare the groups in the C57BL/6 background, and a Student's unpaired t-test was used to compare the mice on a KS/J (misty) background. ** indicates $p < 0.01$. All experiments were performed in triplicate (cells prepared from 3 different mice per group).

5.3.6 Proliferation of *wt/wt* and *ob/ob* fibroblasts

Dermal fibroblast cell morphology and growth in tissue culture was measured. The growth curves indicate that *ob/ob* fibroblasts had a reduced proliferative capacity compared to controls as shown in Figure 5.8. Representative images were captured at

days 2, 4, 7 showing a reduction in refractile, spindle shaped fibroblasts in *ob/ob* cells compared to controls (Figure 5.9).

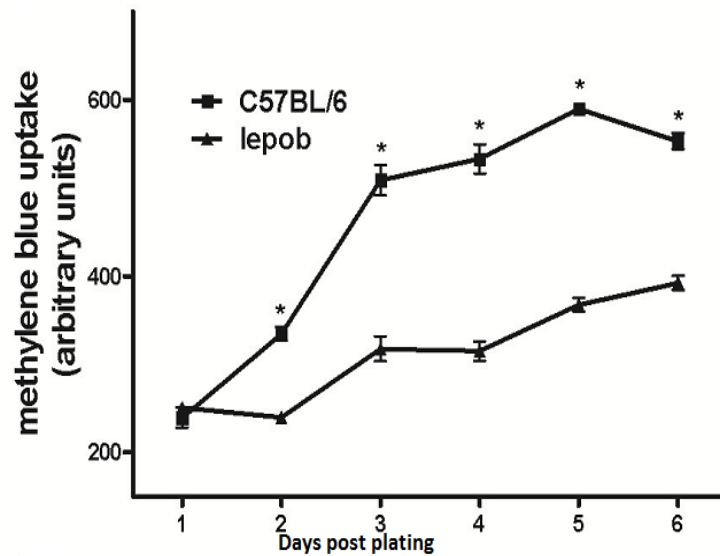


Figure 5-8 Proliferation of normal and insulin resistance fibroblasts.

Growth curves were generated from wild type and *ob/ob* cell lines (n=3). Experiments were performed on cells from 3 different mice per group.* indicates $P<0.001$.

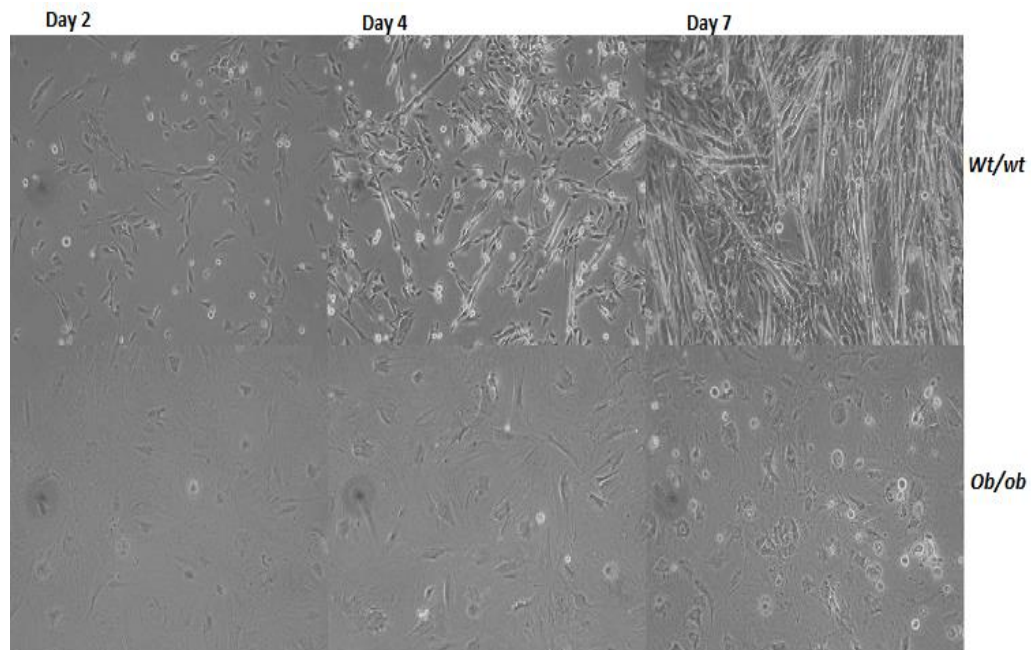


Figure 5-9 Proliferation of normal and insulin resistant fibroblasts.

Representative images from three phases of proliferation at day 2, 4, 7 from *wt/wt* and *ob/ob* dermal fibroblasts (n=3). Images were captured at 10x original magnification.

5.3.7 Collagen production by *wt/wt* and *ob/ob* fibroblasts

Total collagen deposition was assessed by picrosirius uptake once cultures reached confluence. Deposition was found to be reduced by 38% ($P < 0.001$) in *ob/ob* fibroblasts relative to age-matched lean controls as seen in Figure 5.10.

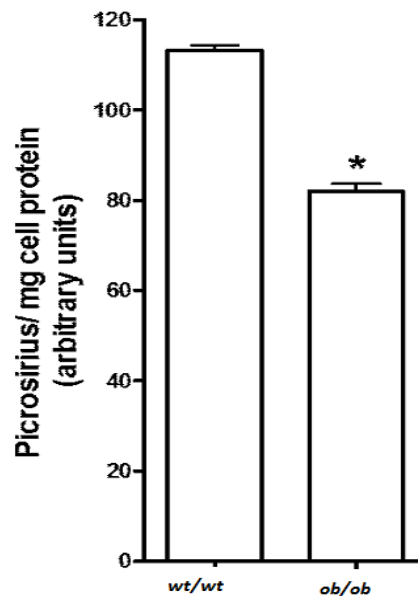


Figure 5-10 Collagen production by *wt/wt* and *ob/ob* mice fibroblasts .

Quantitative measures of collagen deposition normalised to total cellular protein using a picrosirius assay (** $p < 0.0001$) ($n=3$).

5.3.8 Senescence in *wt/wt* and *ob/ob* fibroblasts

Elevated β -galactosidase expression is a feature of senescent cells (Tchkonia et al., 2010), and levels were assayed in primary fibroblast cell lines prepared from lean and *ob/ob* mice (Figure 5.11). Quantitative histomorphometry revealed that β -galactosidase-positive cells accounted for 1.1% (SEM ± 1.0) of the total surface area in confluent *wt/wt* cultures, in contrast to *ob/ob* derived fibroblasts in which 11.6% (SEM ± 2.4) of the surface area stained blue.

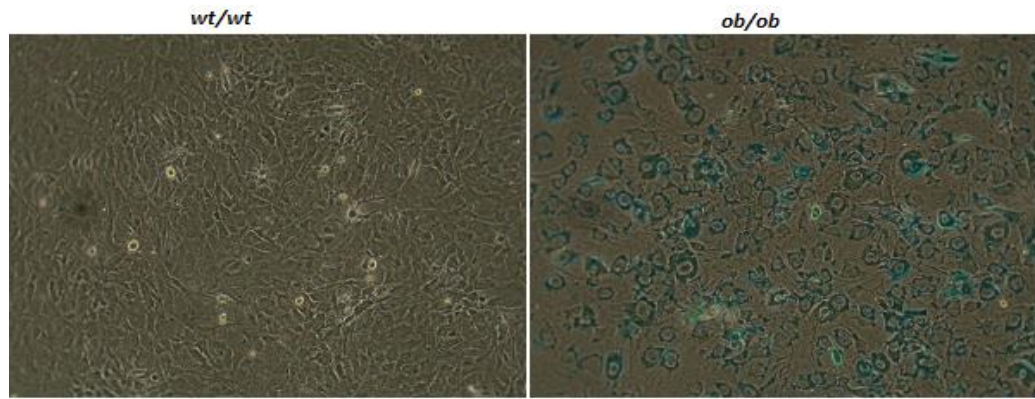


Figure 5-11 Senescence assay in normal and insulin resistant fibroblasts.

Typical fields of β -galactosidase stained *wt/wt* (left panel), *ob/ob* primary dermal fibroblasts (right panel) (n=3) are shown at 10x original magnification. Cells with blue staining cytoplasm prevalent in the right panel are senescent.

5.4 Discussion

The skin is an insulin sensitive tissue, and so the integrity of skin will be impacted by insulin resistance and obesity (Shen et al., 2000). In the healthy state, collagen comprises 50-70% of the skin's connective tissue, with dermal collagen organisation presenting as dense perpendicular “basket-weave” like bundle of fibres to provide mechanical strength (Delaine-Smith et al., 2014). In Chapter 3 I discussed patterns of skin damage seen in animal models of IR and obesity. Specifically, the reticular layer of the dermis, adjacent to the expanded subcutaneous fat layer, was progressively degraded with increasing insulin resistance. Moreover, the reticular layer was all but lost in the most extreme obese phenotype, while the “basket-weave” organisation of the surviving papillary dermis adopted a predominantly “flattened” organisation in the most hyperglycaemic groups.

There are a number of possible mechanisms to explain these pathological sequelae, including but not limited to: 1) intrinsic deficiencies in insulin signalling in dermal fibroblasts; 2) chronic exposure of insulin-sensitive fibroblasts to supra-physiological levels of insulin and glucose; and 3) chronic adipokine insult originating from an expanded subcutis. These mechanisms are discussed below.

The disappearance of the reticular layer relative to papillary dermis with increasing insulin-resistance may be as consequence of proximity to the subcutis, or intrinsic differences in papillary and reticular fibroblast physiology (reviewed in (Sorrell and Caplan, 2004b). Papillary fibroblasts display a faster rate of cell division compared to those in the reticular layer, and each compartment also secretes distinct collagens: mainly type III in the papillary layer, compared with type I in the reticular dermis (Rook et al., 1986). Parallel studies suggest that elevated glucose concentrations (hyperglycaemia) resulting from diabetes are associated with perturbed fibroblast physiology, ECM degradation, and impaired re-epithelialisation (Berlanga-Acosta et al., 2012, Schmidt and Horsley, 2013). Traditionally, the peripheral tissue damage associated with diabetic states is assumed to result from the modification of proteins exposed to high levels of glucose (Kennedy and Baynes, 1984), but I found that the tissue damage in DIO mice at 12 months, and *ob/ob* mice (increased fat deposition and dermal erosion) occurred prior to the onset of frank diabetes. Furthermore, as discussed in Chapter 3, I did not observe evidence for increased collagen glycation in hyperglycaemic states (manifested as either RAGE immunoreactivity or PAS positivity).

Previous studies of Lerman and colleagues, who investigated mechanisms of insulin resistance in dermal fibroblasts from young and adult *db/db* mice showed that a reduction in proliferation and collagen deposition was associated with endothelial dysfunction arising from hypoxic conditions rather than leptin deficiency (Lerman et al., 2003a). This is consistent with my findings of compromised physiological function in *ob/ob* dermal fibroblasts, which showed a reduced proliferative capacity when compared to the age-matched lean controls. These *ob/ob* dermal fibroblasts also synthesise lower levels of collagen and were highly senescent in comparison to age-matched wild type controls. However, there was no evidence of hypoxic condition in our models, in that no expression of the hypoxia marker HIF-1 was detected in paraffin embedded sections, and nor was there evidence of angiogenesis that hypoxia would promote.

Any perturbation in normal dermal fibroblast function will have myriad pathological sequelae, as these cells secrete all of the structural components of this compartment, including fibrillar type I and III collagens, elastic fibres and the enzymes that control

their turnover. These cells are also capable of releasing a range of the pro- and anti-inflammatory cytokines that make a critical contribution to wound healing and, potentially, fibrosis (Falanga, 2005). Underlying the dermis is a layer of highly-metabolically active adipose tissue, the subcutis, which acts as an energy store for excess energy intake (in the form of triglyceride) (Rook et al., 1986). An increase in subcutaneous fat in obese subjects is known to be linked to metabolic complications to a greater extent than visceral fat (Marinou et al., 2014). Indeed, SAT was associated with increased inflammatory cytokine release (notably TNF α and IL1 β), which promote tissue damage (Trayhurn and Wood, 2004, Trayhurn, 2013b). Thus, exposure to cytokines released under hypoxic condition from the subcutis could impair adjacent skin function. In my studies, deeper subcutaneous fat was characterised by the highest levels of pro-inflammatory factors (IL-1 β , IL-6 and MKC, TNF- α) compared to other depots, and these cytokines may initiate inflammatory processes in the skin, and promote the secretion of other proinflammatory cytokines that could impair insulin sensitivity in dermal fibroblasts.

The cells of the skin are insulin sensitive and any defects in insulin signalling could provoke further cutaneous complications, arising from a decrease in the number of insulin receptors, or from impairments in down-stream tyrosine kinase signalling cascades (Caro et al., 1986, Olefsky, 1976, Rook et al., 1986). Indeed, insulin receptor null mice show impaired insulin signalling, and disrupted keratinocyte and fibroblast function (LeRoith et al., 2004). LeRoith and colleagues also reported that the pathogenesis of dermatological complications in diabetes resulting from hyperglycaemia was linked to impaired insulin signalling, and remodelling the ECM. This might explain the reduction in the levels of the β 1 subunit of the insulin receptor in both *ob/ob* and aged fibroblasts, and may indicate that acquired deficiencies in fibroblasts impair their capacity to produce collagen in insulin resistance and ageing.

Elevated adipokine signalling is emerging as a mediator of insulin-resistance, possibly stimulated by hypoxia (Trayhurn, 2013a). Both adipocyte hypertrophy and hyperplasia characterise the expanded subcutaneous fat depots in mouse models of obesity and type two diabetes mellitus (Osman et al., 2013a). Moreover, insulin resistance and obesity are associated with chronic low-grade inflammation as a result of increased levels of pro-inflammatory cytokines including IL-1 β , IL-6, IL-10, IL-12, TNF- α , MCP-1, RANTES, which are secreted from both adipocytes and immune cells such macrophages

and lymphocytes that infiltrate adipose (Plambeck Hansen et al., 2010) (Ramachandrapa and Farooqi, 2011, Finucane et al., 2012). My studies of plasma cytokine levels suggest a lack of systemic inflammation in comparison to strong pro-inflammatory profile from deep (SAT) and not in the superficial (sub dermal fat) (as shown in table 5.5). While the SAT is a source of inflammatory cytokines, which are commonly associated with immune cells infiltrations. But these were not associated with the presence of monocytic infiltrates that the local release of pro-inflammatory cytokines such as IL-6 and TNF- α might elicit in the dermis. High local levels of TNF α is known to promote insulin resistance, however, and this factor may drive impairment fibroblast function and dysregulated ECM remodelling. Elevated levels of circulating FFAs or cellular stress may also induce inflammatory processes (Trayhurn, 2013a). It was suggested that enhanced production of chemo- attractive cytokines such as MCP-1 by hyperplastic adipocytes leads to the recruitment of M1 macrophages to adipose tissue, in turn producing the majority of pro-inflammatory cytokines and stimulating the creation of reactive oxygen species (Wu et al., 2011). Pro-inflammatory macrophages form crown-like structures around necrotic or apoptotic adipocytes initiate the removal of non-functional cells (Murano et al., 2008). Other studies have shown that the stimulation of T helper (Th-1) lymphocytes by IFN γ in adipose tissue leads to the generation of M1 macrophages (Wu et al., 2011). However, I did not see evidence for either increased macrophage infiltration or the presence of crown structures (other than a slight increase in macrophages in ageing only). Recent studies of human abdominal subcutaneous fat has shown that the deeper SAT layer possesses a more pro-inflammatory, lipolytic, and lipogenic profile compared to more superficial SAT, and is strongly associated with obesity related pathology (such as insulin resistance and cardiovascular disease) (Marinou et al., 2014). Interestingly, in this study I confirmed that the deep SAT in the insulin resistant mouse had a more inflammatory profile than both the superficial (subdermal) depot and VAT (epididymal fat).

This provides strong evidence about the influence of local inflammatory factors, rather than systemic effects, on skin in insulin resistant states. Dissecting the roles of cytokines is complex, for example, IL-10 is known to improve insulin sensitivity and counteract the pathological effects of IL-6, IL1- β , MKC and TNF- α (Lumeng et al., 2007, Esposito et al., 2003, Ha et al., 2014), but it is tempting to speculate that while the subdermal

layer has a protective effect (evidenced by the lack of immune cell infiltration), local TNF α levels promote insulin resistance in dermal fibroblasts.

Finally, although a relationship between insulin resistance and skin complications is well recognized, the mechanism underlying dermal pathogenesis remains poorly understood. This study shows that dermal damage in obese and diabetic states may occur as consequence of local factors that influence dermal fibroblast physiology. Exposure of healthy dermal fibroblasts to inflammatory cytokines in culture may yield useful insights into the contribution of adipose tissue to cutaneous damage.

Chapter 6: General Discussion and Future Work

6.1 General discussion

Mouse models provide powerful tools for the investigation of many human skin diseases and associated mechanisms. This is made possible by both physiological and anatomical similarities between man and mouse, and the availability of genetic models carrying spontaneous or induced mutations that model human disease (e.g. knockout or transgenic mice) (Wikramanayake et al., 2014). Great care, however, must be taken when translating data from mice in the elucidation of various human disease mechanisms. Another concern is that researchers must carefully validate experimental methods to ensure sensitivity and accuracy when investigating pathological phenotypes seen in mouse tissues to ensure the detection of subtle changes, and mitigate the influence of artefacts (Treuting and Dintzis, 2011). In pathology, for example, artefacts arising from incomplete fixation or improper processing protocols cannot be remedied if problems are seen at later histology stages, and so considerable thought must be given at the outset to experimental design (Srinivasan et al., 2002). My rationale for the rigorous evaluation of mouse skin histology was informed by two considerations; firstly, the widespread use of mouse as a disease model and secondly, the lack of standard histochemical protocols for mouse skin. This tissue provides a challenging environment for histopathological investigation that has yet to be assessed systematically for histological artefacts arising from fixation (Al-Habian et al., 2014). Moreover, mouse skin is much thinner and more fragile than human skin, and so loss of architecture during histology procedures has implications for downstream applications. In particular, obtaining good histology from diabetic mouse skin (which is extremely fragile) presented a considerable challenge. Moreover, these problems were compounded as I decided to use a tissue macroarray approach that could increase throughput and reduce technical variation if it could be implemented across a range of mouse models. However, optimising histological methods to find effective fixation, processing, and IHC protocols for mouse skin was complicated, and many difficulties were faced during the sectioning and downstream analysis process, which necessitated constant rounds of refinement. My initial studies of skin phenotypes in a range of mouse tissues used skin material made available from investigation of other organs systems, and tissues were prepared using protocols standard in the laboratory at the time. These yielded adequate sections, but it was clear that further optimisation was necessary for prospective analyses. It was not feasible, or ethical to repeat the full range of mouse studies. Therefore, I chose to evaluate the improved histological methods on a representative

subset of skin samples. These techniques more effectively preserved diabetic skin tissues, achieved better sections, and gave superior histological results for the characterisation of various skin compartments. This included the maintenance of good subcutaneous adipocyte architecture and the retention of collagen basket weave organisation (as seen in cross-polar imaging of picrosirius stained sections in Figure 6.1 and Figure 6.2). The revised histological methods also improved other special stains by providing better discrimination of various skin components such as fine elastic fibres. The concept of this study was not to develop histological techniques as an end in itself, but rather to detect with sensitivity features associated with diabetic murine skin (Ibuki et al., 2012). Achieving consistent histology also facilitated the development of novel bioimaging techniques in parallel by colleagues in my laboratory, in particular those to count adipocytes (which requires the maintenance of fragile adipocyte cell membranes to ensure accurate counting), and the use of mathematical algorithms to quantify collagen basket weave in cross-polar captures of picrosirius stained tissue, and so measure incremental changes in skin structure with ageing (Osman et al., 2013a) (Osman et al., 2013b). Colleagues were also able to develop methods to quantify collagen dynamics in Herovici stained images (Osman 2014, *Proceedings of the 1st International Conference on Bioimaging*, pp41-48).

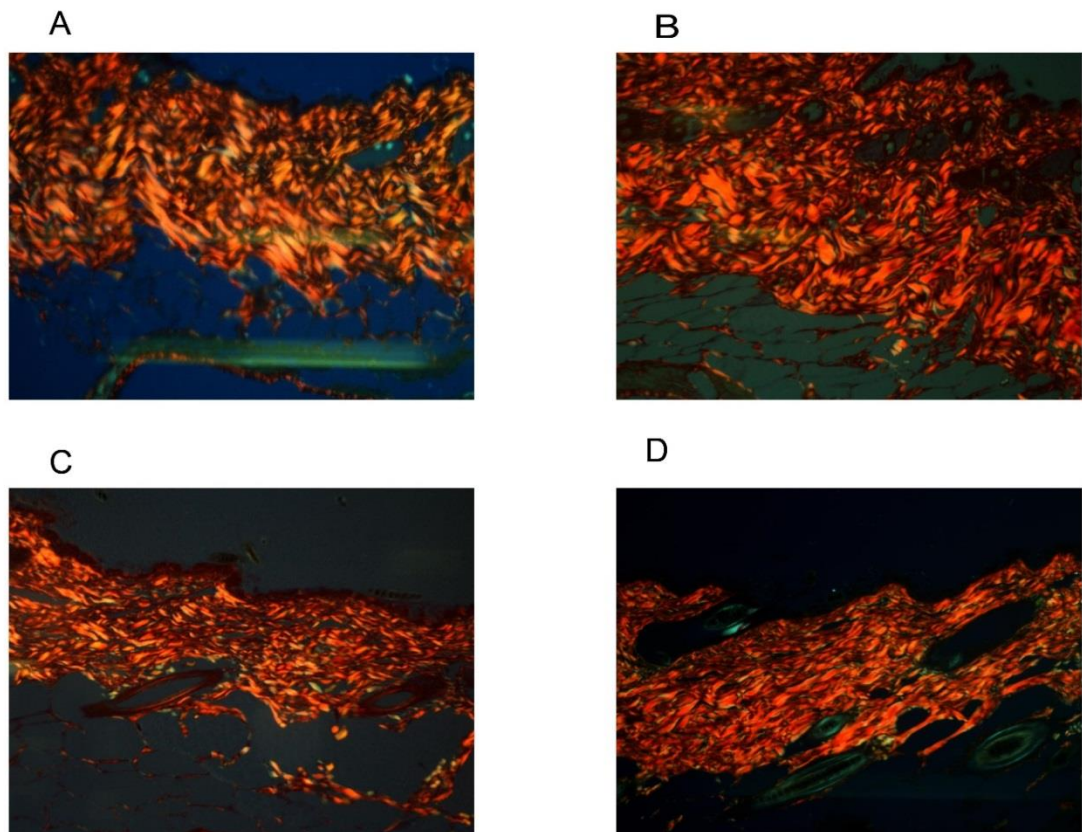


Figure 6-1 Mouse collagen basket-weave structure prior to optimisation.

Skin samples stained with picrosirious were captured using cross-polar microscopy at 20x original magnification. Loss of thicker reticular fibres can be seen in *ob/ob* mice (C) relevant to controls (A), and in *db/db* mice (D) relative to lean controls (B) (n=3)..

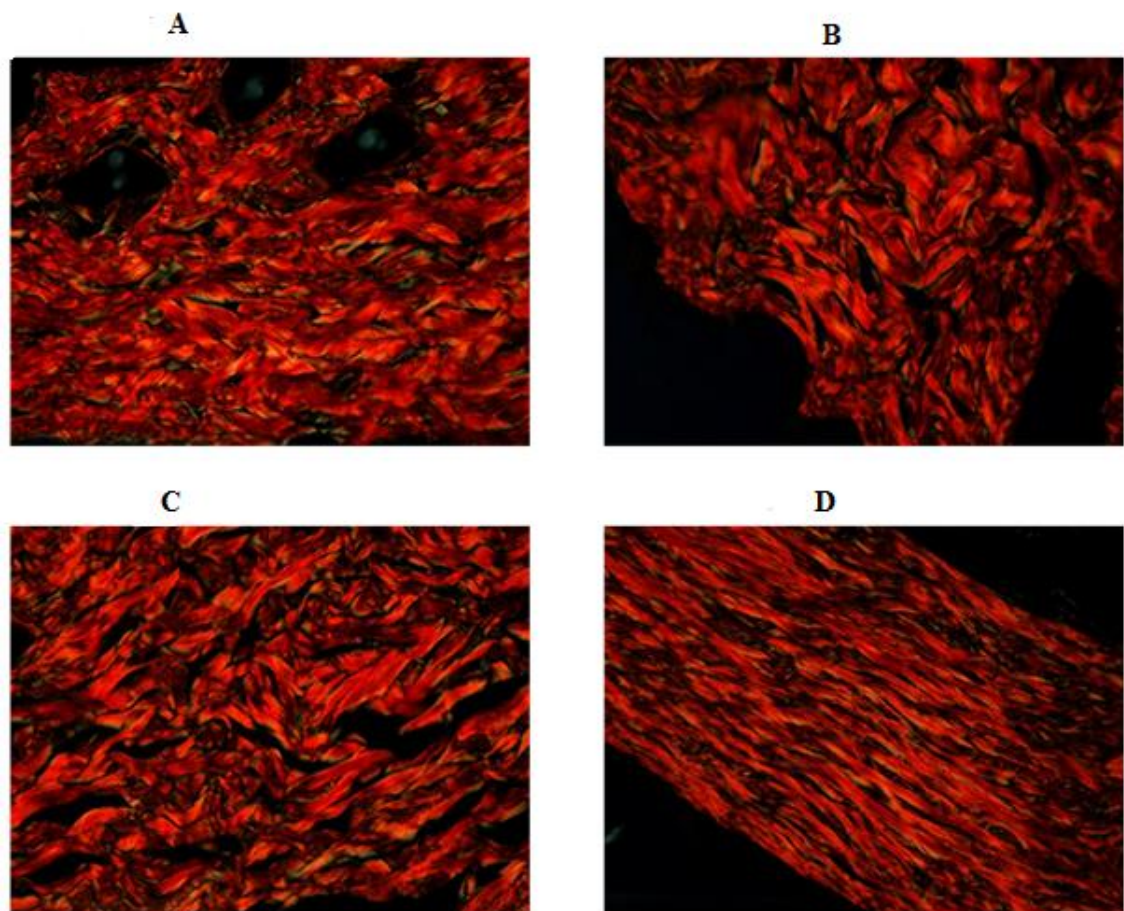


Figure 6-2 Improved collagen basket weave structure from mouse skin processed with the optimised techniques.

Skin samples stained with picosirious were captured using cross-polar microscopy at 90x original magnification. Greater retention of fibre structure can be seen in *ob/ob* mice (C) relevant to controls (A). Loss of reticular fibres and increasing loss of basket-weave is prominent in *db/db* mice (D) relative to lean controls (B) (n=3).

Skin displays many pathological changes in type 2 diabetes, including various forms of dermopathy such as bullosis diabeticorum, necrobiosis liboidiea diabeticorum and scleroderma diabeticorum (Jelinek, 1993). However, the greatest clinical problems are impaired wound healing and diabetic foot ulcers.

Cutaneous manifestations of type 2 diabetes must be considered in the context of other risk factors linked to this disease such as obesity, CVS defects, hypertension and peripheral neuropathy (Olcucu et al., 2014). For instance, impaired wound healing might be linked to reduction in blood supply as result of vasculature damage, and frequent cutaneous infections secondary to immune system disruption. Both of these are

exacerbated if protective action is not taken as a consequence of nerve damage. Type 2 diabetes is chronic and multifactorial disease, involving complex interactions between genetic and environmental factors. Impaired skin homeostasis could arise from compromised cellular function during the insulin resistant state that predates frank diabetes and the associated abnormalities of metabolism such as dysregulation of glucose, insulin and lipids. Uncontrolled type 2 diabetes will lead to permanent, irreversible functional changes such as glycation of proteins, vasculopathy and neuropathy (Baloch et al., 2008). Thus, early diagnosis of diabetes is critical, even if its aetiology remains unclear. Many researchers rely on rodent models because of accessibility, shorter life-cycle, anatomical similarity, and similarity of genomes and gene regulatory pathways with humans in order to unravel the mechanisms of dermatological changes in insulin resistance, obesity, and type 2 diabetes (Wikramanayake et al., 2014). An improved understanding of these mechanisms may help in early diagnosis, before the frank (and damaging) progression of these complications, perhaps by an assessment of early cutaneous presentations. It could also provide a mechanism to evaluate innovative treatment strategies to remediate diabetic tissue damage.

The skin is comprised of insulin sensitive tissues (Shen et al., 2000), and in this study I describe specific patterns of skin damage in animal models of obesity, type 2 DM, and ageing (the latter provides a model of very mild insulin resistance). Unlike changes in the fat and dermis, epidermal homeostasis was sustained in our skin models, confirmed by the lack of quantitative changes of late differentiation markers of cornified cell envelope formation (profilaggrin and involucrin). A very slight down regulation of basal keratin K14 and the proliferation marker PCNA was only seen in the most obese group (*ob/ob* mouse maintained on high fat diets).

The most striking finding was that the reticular layer of the dermis adjacent to an expanded subcutis, was progressively degraded with increasing insulin resistance. The reticular layer was all but lost in the most extreme obese phenotype, while the “basket-weave” organisation of the surviving papillary dermis adopted a predominantly “flattened” organisation in the most hyperglycaemic groups. Peripheral tissue damage associated with diabetic states is assumed to result from the modification of proteins exposed to high levels of glucose (Kennedy and Baynes, 1984), but I found that tissue

damage in DIO mice predated hyperglycaemia, and I did not observe evidence for increased collagen glycation in hyperglycaemic states. There are a number of possible mechanisms that could explain type 2 diabetes complications, including: 1) primary endothelial dysfunction caused by hyperglycaemia, hypoxia, non-enzymatic glycosylation of proteins (glycation) and cytokine insult to the cutaneous vascular system; 2) loss of fibroblast function associated with acquired insulin resistance; 3) chronic exposure of fibroblasts to elevated levels of insulin and glucose; 4) chronic cytokine exposure; 5) oxidative stress; and 6) hypoxia, all of which will impact the dermal compartment and ECM remodelling. Although I did not investigate reactive oxygen species in this study, or identify an effective IHC marker of matrix metalloproteases, Ibuki *et al* reported that diabetic skin fragility in obese mice (seen in disrupted dermal collagen organisation and impaired tensile strength) correlates with a dramatic increase in oxidative stress and MMP expression originating from the expanded subcutaneous adipose tissue (Ibuki et al., 2012).

Much commonality exists between insulin-resistant and ageing states. Loss of fibrillar collagens in ageing (as result of an increase in matrix metalloprotease [MMP] activity) has long been known (Varani et al., 2000), while Varani *et al* also reported that the well-organised collagen structure characteristic of young human subjects (aged 18 to 29 years) becomes disrupted in skin from older subjects (mean age greater than 80) (Varani et al., 2006b). Moreover, other reports have detailed the appearance of parallel collagen bundles and disorganised elastin in the papillary dermis (Nawale et al., 2006). Varani *et al* also reported a 75% reduction in collagen synthesis by fibroblasts derived from ageing individuals (which is a greater reduction compared to my observations in *ob/ob* mice), consistent with inherent differences in fibroblast physiology contributing to impaired skin phenotypes. Fibroblasts are commonly studied in ageing, and Schneider showed in 1979 that those isolated from a young cohort (20 to 35 years of age) were less senescent and faster growing than those isolated from an older group of individuals (aged 65 years or more), also mirroring my observations in *ob/ob* mice derived dermal fibroblasts, which showed an accelerating age phenotype (i.e. senescent, low proliferation, reduced collagen synthesis profile and irregular morphology) (Schneider, 1979). It is tempting to speculate, therefore, that one mechanism underlying the age-related decay in cutaneous function is that of increasing insulin-resistance, a process common to all insulin sensitive tissues including the skin (Shen et al., 2000). Glycation

is the non-enzymatic reaction between reducing sugars, such as glucose, and proteins, lipids or nucleic acids, and has been implicated in various pathological changes in humans including age and diabetes (Nawale et al., 2006, Gkogkolou and Böhm, 2012). Indeed, the peripheral tissue damage in diabetic states is generally assumed to result from the modification of proteins exposed to high levels of glucose (Kennedy and Baynes, 1984). I investigated this phenomenon with PAS staining, which identifies oxidised sugar moieties in various tissues including basement membranes and blood vessel walls (which are known to have a glycoprotein component). Neither this, nor immunostaining for advanced glycation end-products (AGE) highlighted frank glycation of collagen. In the absence of collagen glycation, one cannot ignore the impact of hyperglycaemia on endothelial cell function, ECM physiology and downstream remodelling cascades in diabetic skin (reviewed in (Seitz et al., 2011)). Furthermore, it is well known that hyperinsulinaemia and AGEs in diabetic animal correlate positively with the production of ROS via the reduced form of nicotinamide adenine dinucleotide (NADH), which is likely to play an important role in the development of type 2 diabetes and the promotion of vascular damage (Kaneto et al., 2010). In the diabetic models studied herein, local rather than systemic pro-inflammatory cytokines are more likely to impact ECM physiology as the deeper subcuticular fat layer appeared to be the source of inflammatory cytokines, rather than plasma. Interestingly, the more superficial dermal fat layer might serve as protective barrier from increased levels of cytokines in subcutaneous layer. In contrast, the highest levels of TNF α were seen in the deeper subcutaneous layer, and this cytokine could promote insulin resistance, possibly amplified by agonistic interaction with AGE/RAGE and the generation of ROS (Wu et al., 2011).

Inflammatory cytokines, free fatty acids (FFAs) and high glucose concentrations can also attenuate insulin signalling in endothelial cells and stimulate formation of superoxide and hydroxyl reactive groups (Kolluru et al., 2012). Disrupted fibroblast and endothelial cell function in diabetic mouse skin could also impact epidermal homeostasis (Schmidt and Horsley, 2013), and this may explain mild alterations in epidermal markers in very obese mice (i.e. *ob/ob* mice maintained on high fat diets). Thus, it would seem that there is relatively little impact on normal keratinocyte maturation in diabetic states although the response to a challenge (i.e. wounding) was not investigated in this study. Further studies of the properties of diabetic keratinocytes

maintained *ex vivo* could be of interest. Similarly, pericytes, which are essential to a number of processes including angiogenesis and inflammation, are sensitive to elevated free fatty acid (FFA) levels, hypoxia, adipokine stimulation (particularly TNF α) and macrophage infiltration (Klötting and Blüher, 2014). Impaired pericyte function was reported to drive to adipocyte apoptosis, endothelial dysfunction and collagen degradation (Seitz et al., 2011, Berlanga-Acosta et al., 2012).

More generally, increased levels of cytokines (released from both adipose and immune cells) is emerging as a mediator of insulin-resistance, possibly stimulated by hypoxia (Trayhurn et al., 2008). While plasma levels of a range of cytokines remained stable in *ob/ob* mice compared to lean controls, deeper SAT depots expressed an inflammatory profile. I consistently observed a local reduction in these cytokines in dermal fat and non-fat skin tissues, with the exception of TNF α . TNF α levels are known to rise in hypoxic states, but I found an increase in the dermal/epidermal compartment, and not in the proximal fat compartment (the sub- or intra-dermal fat), suggesting that this rise was not in response to hypoxia. Consistent with this was a lack of monocytic infiltrates in diabetic dermis. Thus, it seems unlikely that increased cytokine exposure from an expanded subcutis, or from the circulation, promotes the degradation of reticular fibres. Previous studies have documented a reduction in insulin receptor levels in the fat and muscle of type 2 DM subjects in rodents and humans (Caro et al., 1986, Olefsky, 1976, Kerouz et al., 1997), which results in compromised insulin signalling and impaired glucose handling (Goodyear et al., 1995, Kerouz et al., 1997, Krook et al., 1998). Consistent with this, I found a reduction in the levels of the $\beta 1$ subunit of the insulin receptor in dermal fibroblasts in *ob/ob*, *db/db* (as well as in ageing) mice. Thus, another possible contributing factor is that insulin-resistant dermal fibroblasts are impaired in their ability to secrete and organise collagen.

Neonatal *ob/ob* fibroblasts do not display reduced growth characteristics (Lerman et al., 2003b), and I observed impaired fibroblast physiology following the onset of hyperglycaemia, thus an insulin-resistant phenotype is acquired following exposure to elevated levels of insulin and glucose. Other supporting evidence from *in vitro* studies of normal and diabetic fibroblast confirms that hyperglycaemia was associated with increased ROS production, impaired cell polarization, decreased migration speed, adhesion and maturation (Lamers et al., 2011).

However, one cannot ignore the possibility that the capacity of skin to repair damage sustained in hyperinsulinaemic states is compromised by elevated cytokines from the expanded subcutis, and further research is needed to profile these cytokines and study their impact on dermal fibroblasts isolated from a spectrum of hyperinsulinaemic states (from lean through DIO to *ob/ob* and *db/db*) to elucidate the influence of hypoxia, endothelial dysfunction, hyperglycaemia and adipokine signalling on cellular physiology.

Diabetic skin damage represents a “perfect storm” of intrinsic, extrinsic, genetic and environmental factors. Figure 6.3 provides an overview of the complex pathways underlying cutaneous sequelae of hyperinsulinaemia and hyperglycaemia, adapted from the literature using the results presented in this thesis.

6.2 Conclusion

Although murine models of human disease are widely studied, one must recognise physiological and anatomical differences. All layers of mouse skin are much thinner than human counterparts and some features, notably elastic fibres, can be difficult to discern in mice. However, while mouse skin does not necessarily model the full range of cutaneous sequelae observed in human type 2 diabetic subjects, it is likely that underlying cellular mechanisms are shared. An improved understanding of the contribution of the layers of the skin, particularly the dermis, to ageing and pathological processes may provide new insights into the mitigation of damage. In particular, improving insulin sensitivity and glucose utilisation in the dermal layers could have important consequences for cutaneous health.

6.3 Future work

6.3.1 Dermal fibroblast physiology in insulin resistant models

It is known that diabetic fibroblasts maintain a compromised phenotype *in vitro* (for example in reduced collagen synthesis) (Ren et al., 2013, Varani et al., 2002). Investigations of insulin responsiveness of normal human dermal fibroblasts in culture, and the effects on glucose uptake, proliferation, and ECM synthesis (collagen and elastin) in response to increasing concentrations of insulin will enrich our understanding of insulin resistance and obesity effects on skin physiology. Another interesting experiment would be to look at compartmental glucose uptake in the layers of the skin (including the reticular and papillary dermis). This could be performed by feeding mice a labelled glucose analogue that was sufficiently stable to be detected in histological preparations (for example the fluorescent 2-deoxyglucose analogue 2-NBDG). Any differences observed between lean and diabetic mice would provide considerable mechanistic insight into glucose utilisation by different skin layers.

6.3.2 The restoration of cutaneous insulin sensitivity and diabetic skin function

The restoration of glycaemic control reverses many of the peripheral effects of diabetes (Lu et al., 2010). It would be worthwhile to investigate whether intervention to improve local insulin sensitivity in the skin would act to reduce diabetes associated phenotypes, and so improve cutaneous health. For example, thiazolidinediones (TZDs), via their

main target peroxisome proliferator-activated receptor gamma (PPAR γ), improve peripheral insulin sensitivity and are of potential utility in dermatology. PPAR γ is expressed in many cutaneous compartments, including keratinocytes (Mao-Qiang et al., 2004b) and dermal fibroblasts (Ghosh et al., 2004a), and TZDs have many effects on diabetic skin, including the restoration of abnormal epidermal differentiation markers (lorocrin, filaggrin), reducing fibrosis and inflammation, and protecting endothelial cells (Han et al., 2009, Tian et al., 2012, Shi-wen et al., 2010). Moreover, they may also act to suppress adverse effects of fat by reducing adipocyte hyperplasia through promotion of the proliferation of small adipocytes (Ezure and Amano, 2011) (Goossens, 2008). Systematic studies of the restoration of dermal integrity by TZDs in diabetic mice have yet to be performed, and in a pilot study I investigated *db/db* skin histology in sections prepared from mice treated centrally with the TZD Rosiglitazone (Figure 6.4). It is clear that intervention to improve systemic insulin sensitivity in my models promoted a restoration of subcutaneous adipose structure, and I am now investigating dermal organisation. Rosiglitazone does have some CVS contra-indications, and evaluation of local action, by either topical application *in vivo* or exposure in culture, will allow the study of the therapeutic benefits of local restoration of glucose control to be studied. In particular, the use of bespoke image analysis algorithms in concert with optimised TMA skin preparation will allow incremental improvements to be identified.

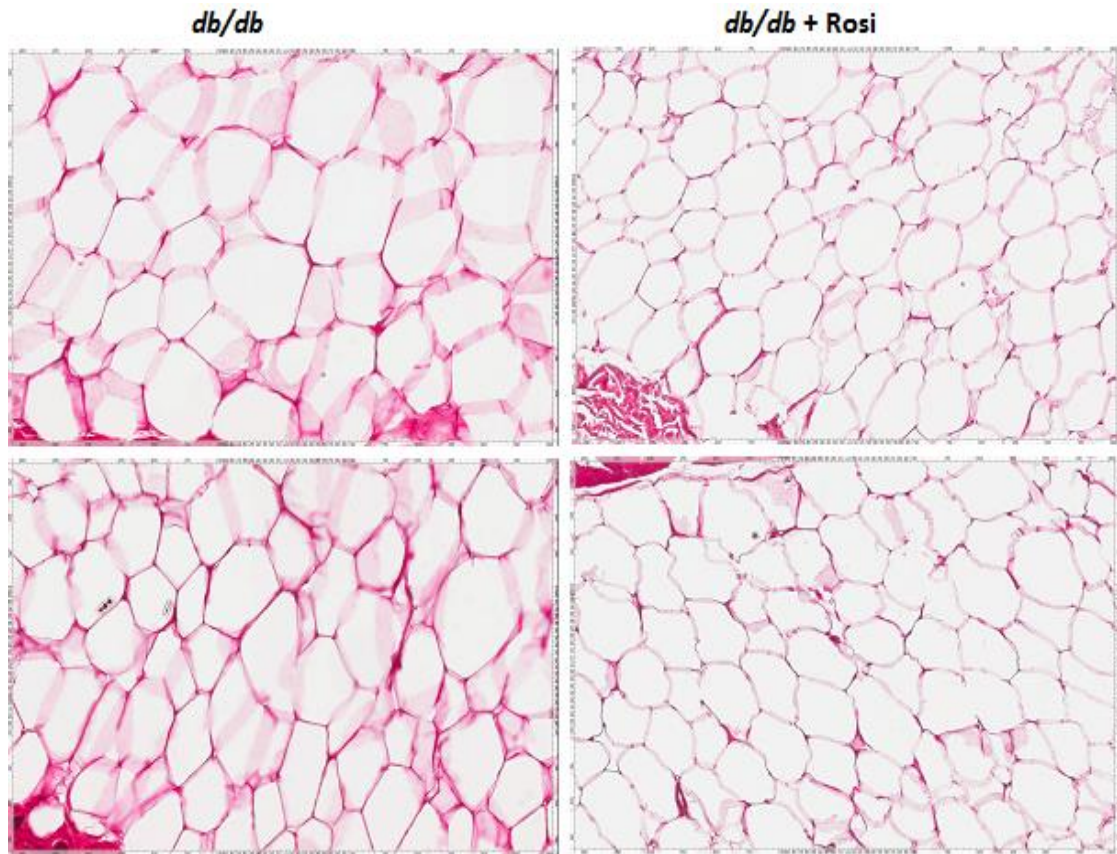


Figure 6-4 The effect of rosiglitazone on adipocyte size

Representative images from six animals to show subcutaneous adipocytes section stained with H&E from 3 month *db/db* mice skin. Higher number of small adipocytes in subcutaneous tissue were observed from *db/db* mice treated with rosiglitazone for 35 days at 30mg/KG right panel) and in comparison to control (left panel). Images were captured at 20x.

6.3.3 Investigation of fibroblast/ keratinocyte interactions

While most studies have focused on the fibroblast function in isolation, cellular cross-talk between keratinocytes, fibroblasts and endothelial cells is undoubtedly important (Egles et al., 2008, Schmidt and Horsley, 2013). Living skin equivalent models could be used to study the influence of, for example, diabetic fibroblasts on insulin-sensitive keratinocyte homeostasis (and vice versa). In fact, one could manipulate a number of parameters in this system (for example cytokine exposure), so this would provide a very powerful model to dissect underlying pathological mechanisms.

6.3.4 Role of adipokine signalling in skin damage.

The influence of the expanded SAT is highly damaging in obesity and type 2 diabetes. Adipocytes serve as a buffer to prevent excess lipid being shunted to other tissues such as liver, muscle, heart, and pancreas, and insulin resistance in these organs occurs via various mechanisms (notable dysregulated insulin signalling) once this buffering capacity is exceeded. Recent studies found that the expansion of deep SAT correlates with metabolic disorders and insulin resistance more than the superficial SAT (Kamolka et al., 2013, Marinou et al., 2014). Thus, it would be of much interest to more fully understand the consequences of dysregulated insulin signalling in different depots of subcutaneous adipose tissue. In the first instance, techniques such as microarrays (or next generation sequencing) could identify candidate genes or processes discriminating the two SAT depots in insulin resistant states. Any mechanisms isolated could then be tested on cultures of human dermal fibroblasts, for example by determining the effects of exposing cells to panels of cytokines. Microarrays could also be used to reveal fibroblast processes impacted by exposure to exogenous agents such as cytokines.

I believe that the future work results will enhance our understanding of cutaneous damage in murine models of obesity, and type two diabetes mellitus, and ageing. Likewise, help in detecting an early signs of cutaneous insulin resistance correlated phenotypes and more likely offer better approaches to prevent or at least cure the dermatological sequelae of type two diabetes mellitus.

6.3.5 Studies of vasculature and epithelial appendages

Superficial blood vessels in mouse skin can be difficult to discriminate, even when highlighted by a marker such as CD31. Indeed, I found little evidence of significant perturbations in diabetic vasculature. A broader panel of endothelial markers may provide insight into vascular pathology. I did not systematically investigate hair follicle or sebaceous gland structure. Anecdotal evidence suggests that diabetic mice do not have a frank hair phenotype, but this is worth of further study.

References

2007. *Shimizu's Textbook of Dermatology*, 中山書店.
- ABU-HIJLEH, M., ROSHIER, A., AL-SHBOUL, Q., DHARAP, A. & HARRIS, P. 2006. The membranous layer of superficial fascia: evidence for its widespread distribution in the body. *Surgical and Radiologic Anatomy*, 28, 606-619.
- AL-HABIAN, A., HARIKUMAR, P. E., STOCKER, C. J., LANGLANDS, K. & SELWAY, J. L. 2014. Histochemical and immunohistochemical evaluation of mouse skin histology: comparison of fixation with neutral buffered formalin and alcoholic formalin.
- ANANTHANARAYANAN, V., PINS, M. R., MEYER, R. E. & GANN, P. H. 2005. Immunohistochemical assays in prostatic biopsies processed in Bouin's fixative. *J Clin Pathol*, 58, 322-4.
- ANSEL, J., PERRY, P., BROWN, J., DAMM, D., PHAN, T., HART, C., LUGER, T. & HEFENEIDER, S. 1990. Cytokine modulation of keratinocyte cytokines. *J Invest Dermatol*, 94, 101S-107S.
- ARCHER, C. 2004. Functions of the skin. *Rook's Textbook of Dermatology, Seventh Edition*, 129-140.
- ARONI, K., TSAGRONI, E., KAVANTZAS, N., PATSOURIS, E. & IOANNIDIS, E. 2008. A study of the pathogenesis of rosacea: how angiogenesis and mast cells may participate in a complex multifactorial process. *Archives of dermatological research*, 300, 125-131.
- ARONSON, D. 2008. Hyperglycemia and the pathobiology of diabetic complications. *Adv Cardiol*, 45, 1-16.
- AVCI, P., SADASIVAM, M., GUPTA, A., DE MELO, W. C., HUANG, Y.-Y., YIN, R., CHANDRAN, R., KUMAR, R., OTUFOWORA, A. & NYAME, T. 2013. Animal models of skin disease for drug discovery. *Expert opinion on drug discovery*, 8, 331-355.
- AVRAM, M. M. 2004. Cellulite: a review of its physiology and treatment. *Journal of Cosmetic and Laser Therapy*, 6, 181-185.
- AZFAR, R. S. & GELFAND, J. M. 2008. Psoriasis and metabolic disease: epidemiology and pathophysiology. *Curr Opin Rheumatol*, 20, 416-22.
- BADEN, H., ROTH, S., GOLDSMITH, L., BADEN, S. & LEE, L. 1974. Keratohyalin protein in disorders of keratinization. *Journal of Investigative Dermatology*, 62, 411-414.
- BAKER, J. R. 1958. Principles of biological microtechnique. A study of fixation and dyeing. *Principles of biological microtechnique. A study of fixation and dyeing*.
- BALAJI, A., JAMIL, K., MARUTHIRAM, G. & HABIBULLA, C. 2010. Isolation of a novel population of multipotent stem cells from epidermal layer of human skin. *Biology and Medicine*, 2, 57-66.
- BALLOCH, G. H., MEMON, N. M., DEVRAJANI, B. R., IQBAL, P. & THEBO, N. K. 2008. Cutaneous manifestations of type-II diabetes mellitus. *JLUMHS*, 7, 67-70.
- BANCROFT, J. D. & GAMBLE, M. 2008a. Theory and Practice of Histological Techniques. *Churchill Livingstone Elsevier*, 53-54.
- BANCROFT, J. D. & GAMBLE, M. 2008b. Theory and Practice of Histological Techniques. *Churchill Livingstone Elsevier*, 146-148.
- BANCROFT, J. D. & GAMBLE, M. 2008c. *Theory and practice of histological techniques*, Elsevier Health Sciences.

- BANCROFT, J. D. & GAMBLE, M. 2008d. Theory and Practice of Histological Techniques. *Churchill Livingstone Elsevier*, 62.
- BANDARU, P., RAJKUMAR, H. & NAPPANVEETIL, G. 2013. The impact of obesity on immune response to infection and vaccine: an insight into plausible mechanisms. *Endocrinology & Metabolic Syndrome*, 2, 113.
- BARNESS, L. A., OPITZ, J. M. & GILBERT-BARNESS, E. 2007. Obesity: genetic, molecular, and environmental aspects. *Am J Med Genet A*, 143A, 3016-34.
- BARRIENTOS, S., STOJADINOVIC, O., GOLINKO, M. S., BREM, H. & TOMIC-CANIC, M. 2008. Growth factors and cytokines in wound healing. *Wound Repair and Regeneration*, 16, 585-601.
- BASKIN, D. G., FIGLEWICZ LATTEMANN, D., SEELEY, R. J., WOODS, S. C., PORTE, D., JR. & SCHWARTZ, M. W. 1999. Insulin and leptin: dual adiposity signals to the brain for the regulation of food intake and body weight. *Brain Res*, 848, 114-23.
- BENNETT, M. F., ROBINSON, M. K., BARON, E. D. & COOPER, K. D. Skin immune systems and inflammation: protector of the skin or promoter of aging? *Journal of Investigative Dermatology Symposium Proceedings*, 2008. Nature Publishing Group, 15-19.
- BENNETT, R. 2009. 1 Anatomy and Physiology of the Skin. *Facial Plastic and Reconstructive Surgery*.
- BERLANGA-ACOSTA, J., SCHULTZ, G. S., LÓPEZ-MOLA, E., GUILLEN-NIETO, G., GARCÍA-SIVERIO, M. & HERRERA-MARTÍNEZ, L. 2012. Glucose toxic effects on granulation tissue productive cells: the diabetics' impaired healing. *BioMed research international*, 2013.
- BERNAT-KARPINSKA, M. & PIATKIEWICZ, P. 2014. Prevalence of Impaired Fasting Glucose and Type 2 Diabetes with its Chronic Complications in Warsaw and Mazovia Province of Poland. *Journal of Endocrinology and Diabetes Mellitus*, 2, 8-15.
- BIESSELS, G., BRIL, V., CALCUTT, N., CAMERON, N., COTTER, M., DOBROWSKY, R., FELDMAN, E., FERNYHOUGH, P., JAKOBSEN, J. & MALIK, R. 2014. Phenotyping animal models of diabetic neuropathy: a consensus statement of the diabetic neuropathy study group of the EASD (Neurodiab). *Journal of the Peripheral Nervous System*.
- BISCHOF, M., KNECHTLE, B., C, A. R., KNECHTLE, P. & ROSEMAN, T. 2013. Changes in Skinfold Thicknesses and Body Fat in Ultra-endurance Cyclists. *Asian J Sports Med*, 4, 15-22.
- BITTER, P. H. 2000. Noninvasive rejuvenation of photodamaged skin using serial, full-face intense pulsed light treatments. *Dermatologic surgery*, 26, 835-843.
- BJØRNDAL, B., BURRI, L., STAALESEN, V., SKORVE, J. & BERGE, R. K. 2011. Different adipose depots: their role in the development of metabolic syndrome and mitochondrial response to hypolipidemic agents. *Journal of obesity*, 2011.
- BODEY, B., SIEGEL, S. E. & KAISER, H. E. 2004. Antigen presentation by dendritic cells and their significance in antineoplastic immunotherapy. *in vivo*, 18, 81-100.
- BONAMIGO, R. R., RAZERA, F. & OLM, G. S. 2011. Neutrophilic dermatoses: part I. *An Bras Dermatol*, 86, 11-25; quiz 26-7.
- BOUDKO, S., FRANK, S., KAMMERER, R. A., STETEFELD, J., SCHULTHESS, T., LANDWEHR, R., LUSTIG, A., BACHINGER, H. P. & ENGEL, J. 2002. Nucleation and propagation of the collagen triple helix in single-chain and trimerized peptides: transition from third to first order kinetics. *J Mol Biol*, 317, 459-70.

- BOZA, J., TRINDADE, E., PERUZZO, J., SACHETT, L., RECH, L. & CESTARI, T. 2012. Skin manifestations of obesity: a comparative study. *Journal of the European Academy of Dermatology and Venereology*, 26, 1220-1223.
- BRAVERMAN, I. M. The cutaneous microcirculation. *Journal of Investigative Dermatology Symposium Proceedings*, 2000. Nature Publishing Group, 3-9.
- BROHEM, C., CARVALHO, C., RADOSKI, C., SANTI, F., BAPTISTA, M., SWINKA, B., A URBAN, C., ARAUJO, L., GRAF, R. & FEFERMAN, I. 2013. Comparison between fibroblasts and mesenchymal stem cells derived from dermal and adipose tissue. *International journal of cosmetic science*, 35, 448-457.
- BUCKINGHAM, E. M., GOLDMAN, F. D. & KLINGELHUTZ, A. J. 2012. Dyskeratosis Congenita Dermal Fibroblasts are Defective in Supporting the Clonogenic Growth of Epidermal Keratinocytes. *Aging Dis*, 3, 427-37.
- BUETTNER, R., SCHÖLMERICH, J. & BOLLHEIMER, L. C. 2007. High-fat diets: Modeling the metabolic disorders of human obesity in rodents. *Obesity*, 15, 798-808.
- BUMASCHNY, V. F., YAMASHITA, M., CASAS-CORDERO, R., OTERO-CORCHON, V., DE SOUZA, F. S., RUBINSTEIN, M. & LOW, M. J. 2012. Obesity-programmed mice are rescued by early genetic intervention. *J Clin Invest*, 122, 4203-12.
- BURNS, T., BREATHNACH, S., COX, N. & GRIFFITHS, C. 2010. *Rook's Textbook of Dermatology, 4 Volume Set*, Wiley.
- BURNS, T., BREATHNACH, S., COX, N. & GRIFFITHS, C. 2013. *Rook's Textbook of Dermatology*, Wiley.
- CAMERON, N., PETTIFOR, J., WET, T. & NORRIS, S. 2003. The relationship of rapid weight gain in infancy to obesity and skeletal maturity in childhood. *Obesity research*, 11, 457-460.
- CARO, J. F., ITTOOP, O., PORIES, W. J., MEELHEIM, D., FLICKINGER, E. G., THOMAS, F., JENQUIN, M., SILVERMAN, J. F., KHAZANIE, P. G. & SINHA, M. K. 1986. Studies on the mechanism of insulin resistance in the liver from humans with noninsulin-dependent diabetes. Insulin action and binding in isolated hepatocytes, insulin receptor structure, and kinase activity. *J Clin Invest*, 78, 249-58.
- CASES, C. 2006. French health system reform: recent implementation and future challenges. *Eurohealth*, 12, 10.
- CHANTRAIN, C. F., FERON, O., MARBAIX, E. & DECLERCK, Y. A. 2008. Bone marrow microenvironment and tumor progression. *Cancer Microenviron*, 1, 23-35.
- CHEN, L., TREDGET, E. E., WU, P. Y. & WU, Y. 2008. Paracrine factors of mesenchymal stem cells recruit macrophages and endothelial lineage cells and enhance wound healing. *PloS one*, 3, e1886.
- CHEN, M., MARINKOVICH, M. P., VEIS, A., CAI, X., RAO, C. N., O'TOOLE, E. A. & WOODLEY, D. T. 1997. Interactions of the amino-terminal noncollagenous (NC1) domain of type VII collagen with extracellular matrix components. A potential role in epidermal-dermal adherence in human skin. *J Biol Chem*, 272, 14516-22.
- CHUGUNOVA, E. 2004. *Biological Function of Mast Cell Chymase*.
- CLEE, S. M., NADLER, S. T. & ATTIE, A. D. 2005. Genetic and genomic studies of the BTBR ob/ob mouse model of type 2 diabetes. *American journal of therapeutics*, 12, 491-498.

- COLLINS, C. A., KRETZSCHMAR, K. & WATT, F. M. 2011a. Reprogramming adult dermis to a neonatal state through epidermal activation of beta-catenin. *Development*, 138, 5189-99.
- COLLINS, C. A., KRETZSCHMAR, K. & WATT, F. M. 2011b. Reprogramming adult dermis to a neonatal state through epidermal activation of β -catenin. *Development*, 138, 5189-5199.
- CONSTANTINE, V. 1969. A Combined Tissue Stain for the Selective Staining of Collagen, Elastic Fibers and Acidic Carbohydrates 1. *Journal of Investigative Dermatology*, 52, 353-356.
- CONSTANTINE, V. S. & MOWRY, R. W. 1968. Selective staining of human dermal collagen. II. The use of picosirius red F3BA with polarization microscopy. *J Invest Dermatol*, 50, 419-23.
- CONTROL, C. F. D., PREVENTION, CONTROL, C. F. D. & PREVENTION 2011. National diabetes fact sheet: national estimates and general information on diabetes and prediabetes in the United States, 2011. *Atlanta, GA: US Department of Health and Human Services, Centers for Disease Control and Prevention*, 201.
- CORK, M. J., DANBY, S. G., VASILOPOULOS, Y., HADGRAFT, J., LANE, M. E., MOUSTAFA, M., GUY, R. H., MACGOWAN, A. L., TAZI-AHNINI, R. & WARD, S. J. 2009. Epidermal barrier dysfunction in atopic dermatitis. *J Invest Dermatol*, 129, 1892-908.
- CORNIER, M.-A., MARSHALL, J. A., HILL, J. O., MAAHS, D. M. & ECKEL, R. H. 2011. Prevention of overweight/obesity as a strategy to optimize cardiovascular health. *Circulation*, 124, 840-850.
- COSCIA, M. R., SIMONIELLO, P., GIACOMELLI, S., ORESTE, U. & MOTTA, C. M. 2014. Investigation of immunoglobulins in skin of the Antarctic teleost *Trematomus bernacchii*. *Fish & shellfish immunology*.
- CRISH, J. F., HOWARD, J. M., ZAIM, T. M., MURTHY, S. & ECKERT, R. L. 1993. Tissue-specific and differentiation-appropriate expression of the human involucrin gene in transgenic mice: an abnormal epidermal phenotype. *Differentiation*, 53, 191-200.
- DALE, B. A. & HOLBROOK, K. A. 1987. Developmental expression of human epidermal keratins and filaggrin. *Curr Top Dev Biol*, 22, 127-51.
- DAS, C., NORO, M. G. & OLMSTED, P. D. 2009. Simulation studies of stratum corneum lipid mixtures. *Biophys J*, 97, 1941-51.
- DAULTREY, H., GOODAY, C. & DHATARIYA, K. 2011. Increased length of inpatient stay and poor clinical coding: audit of patients with diabetes. *JRSM short reports*, 2, 83.
- DE PAUL, A. L., MUKDSI, J. H., PETITI, J. P., GUTIÉRREZ, S., QUINTAR, A. A., MALDONADO, C. A. & TORRES, A. I. Immunoelectron microscopy: a reliable tool for the analysis of cellular processes.
- DEFRONZO, R. A., BONADONNA, R. C. & FERRANNINI, E. 1992. Pathogenesis of NIDDM: a balanced overview. *Diabetes care*, 15, 318-368.
- DEFRONZO, R. A., ELDOR, R. & ABDUL-GHANI, M. 2013. Pathophysiologic approach to therapy in patients with newly diagnosed type 2 diabetes. *Diabetes Care*, 36 Suppl 2, S127-38.
- DELAINE-SMITH, R. M., GREEN, N. H., MATCHER, S. J., MACNEIL, S. & REILLY, G. C. 2014. Monitoring Fibrous Scaffold Guidance of Three-Dimensional Collagen Organisation Using Minimally-Invasive Second Harmonic Generation. *PloS one*, 9, e89761.

- DESPRES, J. P. 2012. Body fat distribution and risk of cardiovascular disease: an update. *Circulation*, 126, 1301-13.
- DIVOUX, A. & CLEMENT, K. 2011. Architecture and the extracellular matrix: the still unappreciated components of the adipose tissue. *obesity reviews*, 12, e494-e503.
- DROSTE, M. S. 2007. Determining Factors of Skin Colouration: A Light and Electron Microscopic Study of the Distribution of Melanin and Its Degradation in the Human Epidermis.
- DROZDOWSKI, B. & MEHREGAN, D. 2005. Acid-Orcein Giemsa: A Multifunctional Stain. *Journal of Cutaneous Pathology*, 32, 86-86.
- DUNTON, G. 2011. Using real-time data capture methods to investigate children's physical activity and eating behaviors. *Childhood Obesity: Risk Factors, Health Effects and Prevention*, 105-114.
- EGLES, C., SHAMIS, Y., MAUNEY, J. R., VOLLOCH, V., KAPLAN, D. L. & GARLICK, J. A. 2008. Denatured collagen modulates the phenotype of normal and wounded human skin equivalents. *Journal of Investigative Dermatology*, 128, 1830-1837.
- EL-KHALAWANY, M. A. & MAHMOUD, A. M. 2014. The spectrum of cutaneous infection in diabetic patients with hepatitis C virus infection: A single-center study from Egypt. *Indian Journal of Dermatology*, 59, 247.
- ELTOUM, I., FREDENBURGH, J. & GRIZZLE, W. E. 2001. Advanced Concepts in Fixation: 1. Effects of Fixation on Immunohistochemistry, Reversibility of Fixation and Recovery of Proteins, Nucleic Acids, and other Molecules from Fixed and Processed Tissues. 2. Developmental Methods of Fixation. *Journal of Histotechnology*, 24, 201-210.
- ELZABBAL, M. H., AHMED, H., ABDELLAZIZ, M., SADIK, I. & ABDALHMEED, M. 2013. *Effect of Fixatives Temperatures on Subsequent Histochemical Staining*. Sudan University of Science and Technology.
- ESPOSITO, K., PONTILLO, A., DI PALO, C., GIUGLIANO, G., MASELLA, M., MARFELLA, R. & GIUGLIANO, D. 2003. Effect of weight loss and lifestyle changes on vascular inflammatory markers in obese women: a randomized trial. *Jama*, 289, 1799-1804.
- EZURE, T. & AMANO, S. 2011. Negative regulation of dermal fibroblasts by enlarged adipocytes through release of free fatty acids. *Journal of Investigative Dermatology*, 131, 2004-2009.
- FAKHOURI, T. H. & STATISTICS, N. C. F. H. 2012. *Prevalence of obesity among older adults in the United States, 2007-2010*, US Department of Health and Human Services, Centers for Disease Control and Prevention, National Center for Health Statistics.
- FALANGA, V. 2005. Wound healing and its impairment in the diabetic foot. *The Lancet*, 366, 1736-1743.
- FARAGE, M. A., MILLER, K. W., BERARDESCA, E. & MAIBACH, H. I. 2009. Clinical implications of aging skin: cutaneous disorders in the elderly. *Am J Clin Dermatol*, 10, 73-86.
- FERNANDEZ-FLORES, A. 2009. Irritated seborrheic keratosis with coarse keratohyalin granules. *Rom J Morphol Embryol*, 50, 583-7.
- FINUCANE, O. M., REYNOLDS, C. M., MCGILLICUDDY, F. C. & ROCHE, H. M. 2012. Insights into the role of macrophage migration inhibitory factor in obesity and insulin resistance. *Proceedings of the Nutrition Society*, 71, 622-633.
- FRANK, S., STALLMEYER, B., KAMPFER, H., KOLB, N. & PFEILSCHIFTER, J. 2000. Leptin enhances wound re-epithelialization and constitutes a direct function of leptin in skin repair. *J Clin Invest*, 106, 501-9.

- FRIEND, W. G. 1963. A polychrome stain for differentiating precollagen from collagen. *Stain Technology*, 38, 204-206.
- FURUKAWA, F., IMAMURA, S., FUJITA, M., KINOSHITA, K., YOSHITAKE, K., BROWN, W. R. & NORRIS, D. A. 1992. Immunohistochemical localization of proliferating cell nuclear antigen/cyclin in human skin. *Arch Dermatol Res*, 284, 86-91.
- GAMBLE, M. 2008. Hematoxylin and Eosin. In: BANCROFT, J. D. & GAMBLE, M. (eds.) *Theory and Practice of Histological Techniques*. Churchill Livingstone Elsevier.
- GARCIA-MENENDEZ, L., KARAMANLIDIS, G., KOLWICZ, S. & TIAN, R. 2013. Substrain specific response to cardiac pressure overload in C57BL/6 mice. *American Journal of Physiology-Heart and Circulatory Physiology*, 305, H397-H402.
- GARCÍA, L. S. & BRUCKNER, D. A. 1988. *Diagnostic medical parasitology*, University of Michigan, Elsevier.
- GARCIA, L. S. & STANDARDS, N. C. F. C. L. 2000. *Laboratory Diagnosis of Blood-Borne Parasitic Diseases, M15-A: Approved Guideline*, National Committee for Clinical Lab Standards.
- GAUGLITZ, G. G. & SCHAUER, J. 2013. Skin: Architecture and Function. *Dermal Replacements in General, Burn, and Plastic Surgery*. Springer.
- GHADIALLY, R. 2012. 25 years of epidermal stem cell research. *J Invest Dermatol*, 132, 797-810.
- GHADIALLY, R., BROWN, B. E., SEQUEIRA-MARTIN, S. M., FEINGOLD, K. R. & ELIAS, P. M. 1995a. The aged epidermal permeability barrier. Structural, functional, and lipid biochemical abnormalities in humans and a senescent murine model. *J Clin Invest*, 95, 2281-90.
- GHADIALLY, R., BROWN, B. E., SEQUEIRA-MARTIN, S. M., FEINGOLD, K. R. & ELIAS, P. M. 1995b. The aged epidermal permeability barrier. Structural, functional, and lipid biochemical abnormalities in humans and a senescent murine model. *Journal of Clinical Investigation*, 95, 2281.
- GHOSH, A. K., BHATTACHARYYA, S., LAKOS, G., CHEN, S. J., MORI, Y. & VARGA, J. 2004a. Disruption of transforming growth factor beta signaling and profibrotic responses in normal skin fibroblasts by peroxisome proliferator-activated receptor gamma. *Arthritis Rheum*, 50, 1305-18.
- GHOSH, A. K., BHATTACHARYYA, S., LAKOS, G., CHEN, S. J., MORI, Y. & VARGA, J. 2004b. Disruption of transforming growth factor β signaling and profibrotic responses in normal skin fibroblasts by peroxisome proliferator-activated receptor γ . *Arthritis & Rheumatism*, 50, 1305-1318.
- GHOSH, M. M., BOYCE, S., LAYTON, C., FREEDLANDER, E. & MAC NEIL, S. 1997. A comparison of methodologies for the preparation of human epidermal-dermal composites. *Ann Plast Surg*, 39, 390-404.
- GIACCO, F. & BROWNLEE, M. 2010. Oxidative stress and diabetic complications. *Circulation research*, 107, 1058-1070.
- GKOGKOLOU, P. & BÖHM, M. 2012. Advanced glycation end products.
- GLASØ, M. & HOVIG, T. 1987. The influence of fixation on the morphology of mouse epidermis. *Virchows Archiv B*, 54, 73-88.
- GOODYEAR, L. J., GIORGINO, F., SHERMAN, L. A., CAREY, J., SMITH, R. J. & DOHM, G. L. 1995. Insulin receptor phosphorylation, insulin receptor substrate-1 phosphorylation, and phosphatidylinositol 3-kinase activity are decreased in intact skeletal muscle strips from obese subjects. *J Clin Invest*, 95, 2195-204.

- GOOSSENS, G. H. 2008. The role of adipose tissue dysfunction in the pathogenesis of obesity-related insulin resistance. *Physiology & behavior*, 94, 206-218.
- GORAN, M. I. & ALDERETE, T. 2012a. Targeting adipose tissue inflammation to treat the underlying basis of the metabolic complications of obesity.
- GORAN, M. I. & ALDERETE, T. L. 2012b. Targeting adipose tissue inflammation to treat the underlying basis of the metabolic complications of obesity. *Nestle Nutr Inst Workshop Ser*, 73, 49-60; discussion p61-6.
- GOREN, I., MULLER, E., PFEILSCHIFTER, J. & FRANK, S. 2006. Severely impaired insulin signaling in chronic wounds of diabetic ob/ob mice: a potential role of tumor necrosis factor- α . *Am J Pathol*, 168, 765-77.
- GORMAN, A. E. 2011. *Obesity and diet quality predict periodontal disease development in men*, Boston University.
- GRICE, E. A., SNITKIN, E. S., YOCKEY, L. J., BERMUDEZ, D. M., LIECHTY, K. W., SEGRE, J. A., MULLIKIN, J., BLAKESLEY, R., YOUNG, A. & CHU, G. 2010. Longitudinal shift in diabetic wound microbiota correlates with prolonged skin defense response. *Proceedings of the National Academy of Sciences*, 107, 14799-14804.
- GRIZZLE, W. E. 2009a. Models of fixation and tissue processing. *Biotechnic & histochemistry: official publication of the Biological Stain Commission*, 84, 185.
- GRIZZLE, W. E. 2009b. Special symposium: fixation and tissue processing models. *Biotech Histochem*, 84, 185-93.
- GUDJONSSON, J. E., JOHNSTON, A., DYSON, M., VALDIMARSSON, H. & ELDER, J. T. 2007. Mouse models of psoriasis. *Journal of Investigative Dermatology*, 127, 1292-1308.
- GUERRERO-ASPIZUA, S., GARCÍA, M., MURILLAS, R., RETAMOSA, L., ILLERA, N., DUARTE, B., HOLGUÍN, A., PUIG, S., HERNÁNDEZ, M. I. & MEANA, A. 2010. Development of a bioengineered skin-humanized mouse model for psoriasis: dissecting epidermal-lymphocyte interacting pathways. *The American journal of pathology*, 177, 3112-3124.
- HA, V. T., BEAK, H. S., KIM, E., BAEK, K.-S., HOSSEN, M. J., YANG, W. S., KIM, Y., KIM, J. H., YANG, S. & KIM, J.-H. 2014. NF- κ B/AP-1-Targeted Inhibition of Macrophage-Mediated Inflammatory Responses by Depigmenting Compound AP736 Derived from Natural 1, 3-Diphenylpropane Skeleton. *Mediators of inflammation*, 2014.
- HAAKE, A., SCOTT, G. A. & HOLBROOK, K. A. 2001. Structure and function of the skin: overview of the epidermis and dermis. *The Biology of the skin*, 2001, 19-45.
- HAN, G., WILLIAMS, C. A., SALTER, K., GARL, P. J., LI, A. G. & WANG, X.-J. 2009. A role for TGF β signaling in the pathogenesis of psoriasis. *Journal of Investigative Dermatology*, 130, 371-377.
- HARIKUMAR, P. E., SELWAY, J. L., CHU, A. & LANGLANDS, K. 2014. Collagen remodeling and peripheral immune cell recruitment characterizes the cutaneous Langerhans cell histiocytosis microenvironment. *International journal of dermatology*.
- HAYASHI, K., CAO, T., PASSMORE, H., JOURDAN-LE SAUX, C., FOGELGREN, B., KHAN, S., HORNSTRA, I., KIM, Y., HAYASHI, M. & CSISZAR, K. 2004. Progressive hair loss and myocardial degeneration in rough coat mice: reduced lysyl oxidase-like (LOXL) in the skin and heart. *Journal of investigative dermatology*, 123, 864-871.
- HEIB, V., BECKER, M., TAUBE, C. & STASSEN, M. 2008. Advances in the understanding of mast cell function. *Br J Haematol*, 142, 683-94.

- HENG, E. C., HUANG, Y., BLACK, S. A., JR. & TRACKMAN, P. C. 2006. CCN2, connective tissue growth factor, stimulates collagen deposition by gingival fibroblasts via module 3 and alpha6- and beta1 integrins. *J Cell Biochem*, 98, 409-20.
- HEROVICI, C. 1963. Polychrome stain for differentiating precollagen from collagen. *Stain Technology*, 38, 204-205.
- HODAK, E., GOTTLIEB, A. B., ANZILOTTI, M. & KRUEGER, J. G. 1996. The insulin-like growth factor 1 receptor is expressed by epithelial cells with proliferative potential in human epidermis and skin appendages: correlation of increased expression with epidermal hyperplasia. *J Invest Dermatol*, 106, 564-70.
- HOLST, J. J. & GROMADA, J. 2004. Role of incretin hormones in the regulation of insulin secretion in diabetic and nondiabetic humans. *American Journal of Physiology-Endocrinology And Metabolism*, 287, E199-E206.
- HOOKERMAN, B. J. 2014. Dermatopathology: An abridged compendium of words. A discussion of them and opinions about them. Part 3. *Dermatology practical & conceptual*, 4, 3.
- HOWARD, B. V., MOTT, D. M., FIELDS, R. M. & BENNETT, P. H. 1979. Insulin stimulation of glucose entry in cultured human fibroblasts. *J Cell Physiol*, 101, 129-38.
- HOWAT, W. J. & WILSON, B. A. 2014. Tissue fixation and the effect of molecular fixatives on downstream staining procedures. *Methods*.
- HU, F. B. 2011. Globalization of diabetes: the role of diet, lifestyle, and genes. *Diabetes Care*, 34, 1249-57.
- HUMMEL, K. P., DICKIE, M. M. & COLEMAN, D. L. 1966. Diabetes, a new mutation in the mouse. *Science*, 153, 1127-8.
- IBUKI, A., AKASE, T., NAGASE, T., MINEMATSU, T., NAKAGAMI, G., HORII, M., SAGARA, H., KOMEDA, T., KOBAYASHI, M. & SHIMADA, T. 2012. Skin fragility in obese diabetic mice: possible involvement of elevated oxidative stress and upregulation of matrix metalloproteinases. *Experimental dermatology*, 21, 178-183.
- INZUCCHI, S. E., BERGENSTAL, R. M., BUSE, J. B., DIAMANT, M., FERRANNINI, E., NAUCK, M., PETERS, A. L., TSAPAS, A., WENDER, R., MATTHEWS, D. R., AMERICAN DIABETES, A. & EUROPEAN ASSOCIATION FOR THE STUDY OF, D. 2012. Management of hyperglycemia in type 2 diabetes: a patient-centered approach: position statement of the American Diabetes Association (ADA) and the European Association for the Study of Diabetes (EASD). *Diabetes Care*, 35, 1364-79.
- JAIN, S. 2012. *Dermatology: Illustrated Study Guide and Comprehensive Board Review*, Springer.
- JAMES, W. D., BERGER, T. & ELSTON, D. 2011. *Andrew's diseases of the skin: clinical dermatology*, Elsevier Health Sciences.
- JANOVSKA, J., ZAVORINS, A., VOICEHOVSKA, J., KLEINA, R., KISIS, J., KARLS, R. & VOICEHOVSKA, A. SKIN CHANGES AND PECULIARITIES IN PATIENTS WITH METABOLIC SYNDROME. CBU International Conference Proceedings, 2013. pp. 264-271.
- JONES, M. L., BANCROFT, J. & GAMBLE, M. 2002. Connective tissues and stains. *Theory and Practice of Histological techniques*, 153.
- JUNQUEIRA, L. C., BIGNOLAS, G. & BRENTANI, R. R. 1979. Picrosirius staining plus polarization microscopy, a specific method for collagen detection in tissue sections. *Histochem J*, 11, 447-55.

- KAMPF, C., OLSSON, I., RYBERG, U., SJÖSTEDT, E. & PONTÉN, F. 2012. Production of Tissue Microarrays. *Immunohistochemistry Staining and*.
- KANASAKI, K. & KOYA, D. 2011. Biology of obesity: lessons from animal models of obesity. *BioMed Research International*, 2011.
- KANETO, H., KATAKAMI, N., MATSUHISA, M. & MATSUOKA, T.-A. 2010. Role of reactive oxygen species in the progression of type 2 diabetes and atherosclerosis. *Mediators of inflammation*, 2010.
- KANITAKIS, J. 2002. Anatomy, histology and immunohistochemistry of normal human skin. *Eur J Dermatol*, 12, 390-9; quiz 400-1.
- KARASTERGIOU, K. & MOHAMED-ALI, V. 2010. The autocrine and paracrine roles of adipokines. *Molecular and cellular endocrinology*, 318, 69-78.
- KASZA, I., SUH, Y., WOLLNY, D., CLARK, R. J., ROOPRA, A., COLMAN, R. J., MACDOUGALD, O. A., SHEDD, T. A., NELSON, D. W. & YEN, M.-I. 2014. Syndecan-1 Is Required to Maintain Intradermal Fat and Prevent Cold Stress. *PLoS genetics*, 10, e1004514.
- KELESIDIS, T., KELESIDIS, I., CHOU, S. & MANTZOROS, C. S. 2010. Narrative review: the role of leptin in human physiology: emerging clinical applications. *Annals of internal medicine*, 152, 93-100.
- KEMPF, W., HANTSCHKE, M., KUTZNER, H. & BURGDORF, W. H. 2008. *Dermatopathology*, Springer.
- KENNEDY, A. J., ELLACOTT, K. L., KING, V. L. & HASTY, A. H. 2010. Mouse models of the metabolic syndrome. *Disease models & mechanisms*, 3, 156-166.
- KENNEDY, L. & BAYNES, J. W. 1984. Non-enzymatic glycosylation and the chronic complications of diabetes: an overview. *Diabetologia*, 26, 93-8.
- KEROUZ, N. J., HORSCH, D., PONS, S. & KAHN, C. R. 1997. Differential regulation of insulin receptor substrates-1 and -2 (IRS-1 and IRS-2) and phosphatidylinositol 3-kinase isoforms in liver and muscle of the obese diabetic (ob/ob) mouse. *J Clin Invest*, 100, 3164-72.
- KHAN, T., MUISE, E. S., IYENGAR, P., WANG, Z. V., CHANDALIA, M., ABATE, N., ZHANG, B. B., BONALDO, P., CHUA, S. & SCHERER, P. E. 2009. Metabolic dysregulation and adipose tissue fibrosis: role of collagen VI. *Molecular and cellular biology*, 29, 1575-1591.
- KHAVARI, P. A. 2006. Modelling cancer in human skin tissue. *Nature Reviews Cancer*, 6, 270-280.
- KIERNAN, J. A. 1990. *Histological & histochemical methods: theory and practice*, Pergamon Press.
- KITAMURA, T. 2013. The role of FOXO1 in β -cell failure and type 2 diabetes mellitus. *Nature Reviews Endocrinology*, 9, 615-623.
- KLEINMAN, N., ABOUZOID, S., ANDERSEN, L., WANG, Z. & POWERS, A. 2014. Cohort analysis assessing medical and nonmedical cost associated with obesity in the workplace. *J Occup Environ Med*, 56, 161-70.
- KLÖTING, N. & BLÜHER, M. 2014. Adipocyte dysfunction, inflammation and metabolic syndrome. *Reviews in Endocrine and Metabolic Disorders*, 1-11.
- KOCH, C. E., LOWE, C., PRETZ, D., STEGER, J., WILLIAMS, L. M. & TUPS, A. 2014. High-Fat Diet Induces Leptin Resistance in Leptin-Deficient Mice. *Journal of neuroendocrinology*, 26, 58-67.
- KOLLURU, G. K., BIR, S. C. & KEVIL, C. G. 2012. Endothelial dysfunction and diabetes: effects on angiogenesis, vascular remodeling, and wound healing. *International journal of vascular medicine*, 2012.

- KOMOLKA, K., ALBRECHT, E., WIMMERS, K., MICHAL, J. & MAAK, S. 2013. Molecular heterogeneities of adipose depots-potential effects on adipose-muscle cross-talk in humans, mice and farm animals. *J Genomics*, 2, 31-44.
- KREKEL, N. M., VAN SLOOTEN, H. J., BARBÉ, E., DE KLERK, E. S. D. L., MEIJER, S. & VAN DEN TOL, M. P. 2012. Is breast specimen shrinkage really a problem in breast-conserving surgery? *Journal of clinical pathology*, 65, 224-227.
- KROOK, A., ROTH, R. A., JIANG, X. J., ZIERATH, J. R. & WALLBERG-HENRIKSSON, H. 1998. Insulin-stimulated Akt kinase activity is reduced in skeletal muscle from NIDDM subjects. *Diabetes*, 47, 1281-6.
- KUNDER, S., CALZADA-WACK, J., HÖLZLWIMMER, G., MÜLLER, J., KLOSS, C., HOWAT, W., SCHMIDT, J., HÖFLER, H., WARREN, M. & QUINTANILLA-MARTINEZ, L. 2007. A comprehensive antibody panel for immunohistochemical analysis of formalin-fixed, paraffin-embedded hematopoietic neoplasms of mice: analysis of mouse specific and human antibodies cross-reactive with murine tissue. *Toxicologic pathology*, 35, 366-375.
- LAMERS, M. L., ALMEIDA, M. E., VICENTE-MANZANARES, M., HORWITZ, A. F. & SANTOS, M. F. 2011. High glucose-mediated oxidative stress impairs cell migration. *PLoS one*, 6, e22865.
- LATEEF, H., STEVENS, M. J. & VARANI, J. 2004. All-*trans*-Retinoic Acid Suppresses Matrix Metalloproteinase Activity and Increases Collagen Synthesis in Diabetic Human Skin in Organ Culture. *The American journal of pathology*, 165, 167-174.
- LAVKER, R. M., ZHENG, P. S. & DONG, G. 1987. Aged skin: a study by light, transmission electron, and scanning electron microscopy. *J Invest Dermatol*, 88, 44s-51s.
- LEE-KUBLI, C. A., MIXCOATL-ZECUATL, T., JOLIVALT, C. G. & CALCUTT, N. A. 2014. Animal Models of Diabetes-Induced Neuropathic Pain.
- LEGRO, R. S. Obesity and PCOS: implications for diagnosis and treatment. *Seminars in reproductive medicine*, 2012. NIH Public Access, 496.
- LEHNERT, T., SONNTAG, D., KONNOPKA, A., RIEDEL-HELLER, S. & KONIG, H. H. 2013. Economic costs of overweight and obesity. *Best Pract Res Clin Endocrinol Metab*, 27, 105-15.
- LEI, Y., SINHA, A., NOSOUDI, N., GROVER, A. & VYAVAHARE, N. 2014. Hydroxyapatite and calcified elastin induce osteoblast-like differentiation in rat aortic smooth muscle cells. *Exp Cell Res*, 323, 198-208.
- LERMAN, O. Z., GALIANO, R. D., ARMOUR, M., LEVINE, J. P. & GURTNER, G. C. 2003a. Cellular dysfunction in the diabetic fibroblast: impairment in migration, vascular endothelial growth factor production, and response to hypoxia. *The American journal of pathology*, 162, 303-312.
- LERMAN, O. Z., GALIANO, R. D., ARMOUR, M., LEVINE, J. P. & GURTNER, G. C. 2003b. Cellular dysfunction in the diabetic fibroblast: impairment in migration, vascular endothelial growth factor production, and response to hypoxia. *Am J Pathol*, 162, 303-12.
- LEROITH, D., TAYLOR, S. I. & OLEFSKY, J. M. 2004. *Diabetes Mellitus: A Fundamental and Clinical Text*, Lippincott Williams & Wilkins.
- LEVY, L. & ZEICHNER, J. A. 2012. Dermatologic manifestation of diabetes. *Journal of diabetes*, 4, 68-76.
- LIPPENS, S., KOCKX, M., KNAAPEN, M., MORTIER, L., POLAKOWSKA, R., VERHEYEN, A., GARMYN, M., ZWIJSEN, A., FORMSTECHE, P. &

- HUYLEBROECK, D. 2000. Epidermal differentiation does not involve the pro-apoptotic executioner caspases, but is associated with caspase-14 induction and processing. *Cell Death & Differentiation*, 7.
- LOWE, J. R. 2009. Skin integrity in critically ill obese patients. *Critical care nursing clinics of North America*, 21, 311-322.
- LU, S., TRAN, T. A., JONES, D. M., MEYER, D. R., ROSS, J. S., FISHER, H. A. & CARLSON, J. A. 2009. Localized lymphedema (elephantiasis): a case series and review of the literature. *Journal of cutaneous pathology*, 36, 1-20.
- LU, X., GUO, X., KARATHANASIS, S. K., ZIMMERMAN, K. M., ONYIA, J. E., PETERSON, R. G. & KASSAB, G. S. 2010. Original investigation Rosiglitazone reverses endothelial dysfunction but not remodeling of femoral artery in Zucker diabetic fatty rats.
- LUMENG, C. N., BODZIN, J. L. & SALTIEL, A. R. 2007. Obesity induces a phenotypic switch in adipose tissue macrophage polarization. *The Journal of clinical investigation*, 117, 175-184.
- MAKRANTONAKI, E., GANCEVICIENE, R. & ZOUBOULIS, C. 2011. An update on the role of the sebaceous gland in the pathogenesis of acne. *Dermatoendocrinol*, 3, 41-9.
- MAKSIMOVIC, S., NAKATANI, M., BABA, Y., NELSON, A. M., MARSHALL, K. L., WELLNITZ, S. A., FIROZI, P., WOO, S.-H., RANADE, S. & PATAPOUTIAN, A. 2014. Epidermal Merkel cells are mechanosensory cells that tune mammalian touch receptors. *Nature*.
- MANNE, J., MARKOVA, M., SIRACUSA, L. D. & JIMENEZ, S. A. 2013. Collagen Content in Skin and Internal Organs of the Tight Skin Mouse: An Animal Model of Scleroderma. *Biochemistry research international*, 2013.
- MAO-QIANG, M., FOWLER, A. J., SCHMUTH, M., LAU, P., CHANG, S., BROWN, B. E., MOSER, A. H., MICHALIK, L., DESVERGNE, B. & WAHLI, W. 2004a. Peroxisome-proliferator-activated receptor (PPAR)- γ activation stimulates keratinocyte differentiation. *Journal of Investigative Dermatology*, 123, 305-312.
- MAO-QIANG, M., FOWLER, A. J., SCHMUTH, M., LAU, P., CHANG, S., BROWN, B. E., MOSER, A. H., MICHALIK, L., DESVERGNE, B., WAHLI, W., LI, M., METZGER, D., CHAMBON, P. H., ELIAS, P. M. & FEINGOLD, K. R. 2004b. Peroxisome-proliferator-activated receptor (PPAR)-gamma activation stimulates keratinocyte differentiation. *J Invest Dermatol*, 123, 305-12.
- MAO, H. Z., ROUSSOS, E. T. & PÉTERFY, M. 2006. Genetic analysis of the diabetes-prone C57BLKS/J mouse strain reveals genetic contribution from multiple strains. *Biochimica et Biophysica Acta (BBA)-Molecular Basis of Disease*, 1762, 440-446.
- MARINOU, K., HODSON, L., VASAN, S. K., FIELDING, B. A., BANERJEE, R., BRISMAR, K., KOUTSILIERIS, M., CLARK, A., NEVILLE, M. J. & KARPE, F. 2014. Structural and functional properties of deep abdominal subcutaneous adipose tissue explain its association with insulin resistance and cardiovascular risk in men. *Diabetes care*, 37, 821-829.
- MARUYAMA, K., ASAI, J., II, M., THORNE, T., LOSORDO, D. W. & D'AMORE, P. A. 2007. Decreased macrophage number and activation lead to reduced lymphatic vessel formation and contribute to impaired diabetic wound healing. *The American journal of pathology*, 170, 1178-1191.
- MAXWELL, M. A. & COLE, D. A. 2012. Development and initial validation of the Adolescent Responses to Body Dissatisfaction measure. *Psychol Assess*, 24, 721-37.

- MCGRATH, J., EADY, R. & POPE, F. 2010. Anatomy and organization of human skin. *Rook's textbook of dermatology*, 1.
- MCKLEROY, W., LEE, T.-H. & ATABAI, K. 2013. Always cleave up your mess: targeting collagen degradation to treat tissue fibrosis. *American Journal of Physiology-Lung Cellular and Molecular Physiology*, 304, L709-L721.
- MCMILLAN, J. R. & SHIMIZU, H. 2001. Desmosomes: structure and function in normal and diseased epidermis. *J Dermatol*, 28, 291-8.
- MEDAWAR, P. B. 1941. III.—THE RATE OF PENETRATION OF FIXATIVES. *Journal of the Royal Microscopical Society*, 61, 46-57.
- MERCATI, F., PASCUCI, L., CECCARELLI, P., DALL'AGLIO, C., PEDINI, V. & GARGIULO, A. 2009. Expression of mesenchymal stem cell marker CD90 on dermal sheath cells of the anagen hair follicle in canine species. *European journal of histochemistry: EJH*, 53.
- MIKAELIAN, I., NANNEY, L. B., PARMAN, K. S., KUSEWITT, D. F., WARD, J. M., NÄF, D., KRUPKE, D. M., EPPIG, J. T., BULT, C. J. & SEYMOUR, R. 2003. Antibodies that label paraffin-embedded mouse tissues: a collaborative endeavor. *Toxicologic pathology*, 32, 181-191.
- MINE, S., FORTUNEL, N. O., PAGEON, H. & ASSELINEAU, D. 2008. Aging alters functionally human dermal papillary fibroblasts but not reticular fibroblasts: a new view of skin morphogenesis and aging. *PLoS One*, 3, e4066.
- MITHIEUX, S. M. & WEISS, A. S. 2005. Elastin. *Advances in protein chemistry*, 70, 437-461.
- MOELANS, C. B., TER HOEVE, N., VAN GINKEL, J.-W., FIEBO, J. & VAN DIEST, P. J. 2011. Formaldehyde substitute fixatives analysis of macroscopy, morphologic analysis, and immunohistochemical analysis. *American journal of clinical pathology*, 136, 548-556.
- MOLL, R., DIVO, M. & LANGBEIN, L. 2008. The human keratins: biology and pathology. *Histochem Cell Biol*, 129, 705-33.
- MONTES, G. S. & JUNQUEIRA, L. C. 1991. The use of the Picrosirius-polarization method for the study of the biopathology of collagen. *Mem Inst Oswaldo Cruz*, 86 Suppl 3, 1-11.
- MORRIS, M., XU, J., CASKEY, R., URENCIO, M., ZGHEIB, C., SMITH, E., BEASON, D., DORSETT-MARTIN, W. W., MITCHELL, M. & SOSLOWSKY, L. 2013. The Progressive Decline in the Biomechanical Properties of Diabetic Skin is Associated With Dysregulation of MicroRNA-29a Gene Expression and Collagen Protein Production. *Journal of Surgical Research*, 179, 343-343.
- MURANO, I., BARBATELLI, G., PARISANI, V., LATINI, C., MUZZONIGRO, G., CASTELLUCCI, M. & CINTI, S. 2008. Dead adipocytes, detected as crown-like structures, are prevalent in visceral fat depots of genetically obese mice. *Journal of lipid research*, 49, 1562-1568.
- MURIS, D. M., HOUBEN, A. J., SCHRAM, M. T. & STEHOUWER, C. D. 2013. Microvascular dysfunction: an emerging pathway in the pathogenesis of obesity-related insulin resistance. *Reviews in Endocrine and Metabolic Disorders*, 14, 29-38.
- NAWALE, R., MOURYA, V. & BHISE, S. 2006. Non-enzymatic glycation of proteins: a cause for complications in diabetes. *Indian Journal of Biochemistry and Biophysics*, 43, 337.
- NGUYEN, D. M. & EL-SERAG, H. B. 2010. The epidemiology of obesity. *Gastroenterol Clin North Am*, 39, 1-7.

- NIGRO, E., SCUDIERO, O., MONACO, M. L., PALMIERI, A., MAZZARELLA, G., COSTAGLIOLA, C., BIANCO, A. & DANIELE, A. 2014. New Insight into Adiponectin Role in Obesity and Obesity-Related Diseases. *BioMed Research International*, 2014, 14.
- NIKOLAKIS, G., MAKRANTONAKI, E. & ZOUBOULIS, C. C. 2013. Skin mirrors human aging. *Hormone Molecular Biology and Clinical Investigation*, 16, 13-28.
- NONG, Z., O'NEIL, C., LEI, M., GROS, R., WATSON, A., RIZKALLA, A., MEQUANINT, K., LI, S., FRONTINI, M. J. & FENG, Q. 2011. Type I collagen cleavage is essential for effective fibrotic repair after myocardial infarction. *The American journal of pathology*, 179, 2189-2198.
- O'HARA, A., LIM, F.-L., MAZZATTI, D. J. & TRAYHURN, P. 2009. Microarray analysis identifies matrix metalloproteinases (MMPs) as key genes whose expression is up-regulated in human adipocytes by macrophage-conditioned medium. *Pflügers Archiv-European Journal of Physiology*, 458, 1103-1114.
- OKA, M., LINK, C. L. & KAWACHI, I. 2013. Area-Based Variations in Obesity Are More than a Function of the Food and Physical Activity Environment. *Journal of Urban Health*, 90, 442-463.
- OLCUCU, S. O. B., BURKAN, S. & TIRYAKI-SONMEZ, G. 2014. Effect of Acute Resistance Exercise on Appetite in Healthy Men. *Life Science Journal*, 11.
- OLEFSKY, J. M. 1976. Decreased insulin binding to adipocytes and circulating monocytes from obese subjects. *J Clin Invest*, 57, 1165-72.
- OLSON, A. H. 2013. Image analysis using the Aperio ScanScope.
- OLSSON, N. O., LECLERC, A., JEANNIN, J. F. & MARTIN, F. 1982. A simple photometric microassay for the quantitative evaluation of macrophage-mediated cytotoxicity on adherent cancer cells. *Ann Immunol (Paris)*, 133D, 245-54.
- ORGANIZATION, W. H. 2009. *Global health risks: mortality and burden of disease attributable to selected major risks*, World Health Organization.
- ORGEL, J. P., SAN ANTONIO, J. D. & ANTIPOVA, O. 2011. Molecular and structural mapping of collagen fibril interactions. *Connect Tissue Res*, 52, 2-17.
- OSHIMA, H., ROCHAT, A., KEDZIA, C., KOBAYASHI, K. & BARRANDON, Y. 2001. Morphogenesis and renewal of hair follicles from adult multipotent stem cells. *Cell*, 104, 233-45.
- OSMAN, O. S., SELWAY, J. L., HARIKUMAR, P. E., STOCKER, C. J., WARGENT, E. T., CAWTHORNE, M. A., JASSIM, S. & LANGLANDS, K. 2013a. A novel method to assess collagen architecture in skin. *BMC bioinformatics*, 14, 1-10.
- OSMAN, O. S., SELWAY, J. L., KĘPCZYŃSKA, M. A., STOCKER, C. J., O'DOWD, J. F., CAWTHORNE, M. A., ARCH, J. R., JASSIM, S. & LANGLANDS, K. 2013b. A novel automated image analysis method for accurate adipocyte quantification. *Adipocyte*, 2, 160.
- PIERAGGI, M., NEJJAR, I., JULIAN, M. & BOUISSOU, H. Staining of elastic tissue by Verhoeff's iron hematoxylin. *Annales de pathologie*, 1985, 74-77.
- PINKUS, H. 1944. Acid orcein-giemsa stain (modification of unna-taenzer method): A useful routine stain for dermatologic sections. *Archives of Dermatology and Syphilology*, 49, 355-356.
- PINKUS, H. & HUNTER, R. 1960. Simplified acid orcein and Giemsa technique for routine staining of skin sections. *Arch Dermatol*, 82, 699-700.
- PLAMBECK HANSEN, C., BERENTZEN, T. L., NAUTRUP ØSTERGAARD, J., DAHM, C. C., HELLGREN, L. I., SCHMIDT, E. B., TJØNNELAND, A., SØRENSEN, T. I., OVERVAD, K. & JAKOBSEN, M. U. 2010. Adipose tissue trans fatty acids and changes in body weight and waist circumference. *ECO*.

- PLASCENCIA GÓMEZ, A., VEGA MEMIJE, M., TORRES TAMAYO, M. & RODRÍGUEZ CARREÓN, A. 2014. Skin Disorders in Overweight and Obese Patients and Their Relationship With Insulin. *Actas Dermo-Sifiliográficas (English Edition)*, 105, 178-185.
- PLONKA, P., PASSERON, T., BRENNER, M., TOBIN, D., SHIBAHARA, S., THOMAS, A., SLOMINSKI, A., KADEKARO, A., HERSHKOVITZ, D. & PETERS, E. 2009. What are melanocytes really doing all day long...? *Experimental dermatology*, 18, 799-819.
- POBLET, E., JIMÉNEZ, F. & ORTEGA, F. 2004. The contribution of the arrector pili muscle and sebaceous glands to the follicular unit structure. *Journal of the American Academy of Dermatology*, 51, 217-222.
- POUDEL, R. R. 2013. Renal glucose handling in diabetes and sodium glucose cotransporter 2 inhibition. *Indian journal of endocrinology and metabolism*, 17, 588.
- PUCHTLER, H., WALDROP, F. S. & VALENTINE, L. S. 1973. Polarization microscopic studies of connective tissue stained with picro-sirius red FBA. *Beitr Pathol*, 150, 174-87.
- PUSZTASZERI, M. P., SEELENTAG, W. & BOSMAN, F. T. 2006. Immunohistochemical expression of endothelial markers CD31, CD34, von Willebrand factor, and Fli-1 in normal human tissues. *Journal of Histochemistry & Cytochemistry*, 54, 385-395.
- RAINS, J. L. & JAIN, S. K. 2011. Oxidative stress, insulin signaling, and diabetes. *Free Radic Biol Med*, 50, 567-75.
- RAMACHANDRAPPA, S. & FAROOQI, I. S. 2011. Genetic approaches to understanding human obesity. *The Journal of clinical investigation*, 121, 2080-2086.
- RASI, A., SOLTANI-ARABSHAHI, R. & SHAHBAZI, N. 2007. Skin tag as a cutaneous marker for impaired carbohydrate metabolism: a case-control study. *International journal of dermatology*, 46, 1155-1159.
- REDDI, S., JAIN, A. K., YUN, H.-B. & REDDI, L. N. 2012. Biomimetics of stabilized earth construction: Challenges and opportunities. *Energy and Buildings*, 55, 452-458.
- REN, M., HAO, S., YANG, C., ZHU, P., CHEN, L., LIN, D., LI, N. & YAN, L. 2013. Angiotensin II regulates collagen metabolism through modulating tissue inhibitor of metalloproteinase-1 in diabetic skin tissues. *Diabetes and Vascular Disease Research*, 10, 426-435.
- RENSHAW, S. 2007. Immunochemical staining techniques.
- REQUENA, L. & SANGUEZA, O. P. 1997. Cutaneous vascular anomalies. Part I. Hamartomas, malformations, and dilatation of preexisting vessels. *Journal of the American Academy of Dermatology*, 37, 523-549.
- RICH, L. & WHITTAKER, P. 2005. Collagen and picrosirius red staining: a polarized light assessment of fibrillar hue and spatial distribution. *Braz J Morphol Sci*, 22, 97-104.
- RICHTER, E. A. & HARGREAVES, M. 2013. Exercise, GLUT4, and skeletal muscle glucose uptake. *Physiol Rev*, 93, 993-1017.
- RIVERA-GONZALEZ, G., SHOOK, B. & HORSLEY, V. 2014. Adipocytes in Skin Health and Disease. *Cold Spring Harbor perspectives in medicine*, 4, a015271.
- ROBINSON, P. N., ARTEAGA-SOLIS, E., BALDOCK, C., COLLOD-BÉROUD, G., BOOMS, P., DE PAEPE, A., DIETZ, H. C., GUO, G., HANDFORD, P. A. & JUDGE, D. P. 2006. The molecular genetics of Marfan syndrome and related disorders. *Journal of medical genetics*, 43, 769-787.

- ROCKEN, M., SCHALLER, M., SATTLER, E. & BURGDORF, W. 2012. *Color Atlas of Dermatology*, Thieme.
- ROLLS, G. 2012. Fixation and Fixatives (3)–Fixing Agents Other than the Common Aldehydes. Wetzlar: Leica Biosystems.
- ROMANO, G., MORETTI, G., DI BENEDETTO, A., GIOFRE, C., DI CESARE, E., RUSSO, G., CALIFANO, L. & CUCINOTTA, D. 1998. Skin lesions in diabetes mellitus: prevalence and clinical correlations. *Diabetes Res Clin Pract*, 39, 101-6.
- ROOK, A., WILKINSON, D. S., EBLING, F. J. G., CHAMPION, R. H. & BURTON, J. L. (eds.) 1986. *Textbook of Dermatology*, Oxford: Blackwell Scientific Publications.
- ROSEN, E. D. & SPIEGELMAN, B. M. 2006. Adipocytes as regulators of energy balance and glucose homeostasis. *Nature*, 444, 847-853.
- SAKAI, S., ENDO, Y., OZAWA, N., SUGAWARA, T., KUSAKA, A., SAYO, T., TAGAMI, H. & INOUE, S. 2003. Characteristics of the epidermis and stratum corneum of hairless mice with experimentally induced diabetes mellitus. *Journal of investigative dermatology*, 120, 79-85.
- SAKAI, S., KIKUCHI, K., SATOH, J., TAGAMI, H. & INOUE, S. 2005. Functional properties of the stratum corneum in patients with diabetes mellitus: similarities to senile xerosis. *British Journal of Dermatology*, 153, 319-323.
- SALTON, S. R., HAHM, S. & MIZUNO, T. M. 2000. Of mice and MEN: what transgenic models tell us about hypothalamic control of energy balance. *Neuron*, 25, 265-268.
- SAMS, W. M. & SMITH, J. G. 1961. The histochemistry of chronically sun-damaged skin. *Journal of Investigative Dermatology*, 37, 447-453.
- SCHEINFELD, N. 2005. Infections in the elderly. *Dermatology online journal*, 11.
- SCHMIDT, B. A. & HORSLEY, V. 2013. Intradermal adipocytes mediate fibroblast recruitment during skin wound healing. *Development*, 140, 1517-1527.
- SCHNEIDER, E. L. 1979. Aging and cultured human skin fibroblasts. *J Invest Dermatol*, 73, 15-8.
- SCHWARTZ, M. W., SEELEY, R. J., TSCHÖP, M. H., WOODS, S. C., MORTON, G. J., MYERS, M. G. & D'ALESSIO, D. 2013. Cooperation between brain and islet in glucose homeostasis and diabetes. *Nature*, 503, 59-66.
- SEITZ, O., SCHÜRMANN, C., HERMES, N., MÜLLER, E., PFEILSCHIFTER, J., FRANK, S. & GOREN, I. 2011. Wound healing in mice with high-fat diet-or ob gene-induced diabetes-obesity syndromes: a comparative study. *Experimental diabetes research*, 2010.
- SELUANOV, A., VAIDYA, A. & GORBUNOVA, V. 2010. Establishing primary adult fibroblast cultures from rodents. *Journal of visualized experiments: JoVE*.
- SHEN, S., WERTHEIMER, E., SAMPSON, S. R. & TENNENBAUM, T. 2000. Characterization of glucose transport system in keratinocytes: insulin and IGF-1 differentially affect specific transporters. *J Invest Dermatol*, 115, 949-54.
- SHERRATT, M. J. 2009. Tissue elasticity and the ageing elastic fibre. *Age*, 31, 305-325.
- SHERWOOD, E. R. & TOLIVER-KINSKY, T. 2004. Mechanisms of the inflammatory response. *Best Pract Res Clin Anaesthesiol*, 18, 385-405.
- SHI-WEN, X., EASTWOOD, M., STRATTON, R. J., DENTON, C. P., LEASK, A. & ABRAHAM, D. J. 2010. Rosiglitazone alleviates the persistent fibrotic phenotype of lesional skin scleroderma fibroblasts. *Rheumatology*, 49, 259-263.

- SHIMIZU, H. 2007. *Shimizu's Textbook of Dermatology* [Online]. Available: <http://books.google.co.uk/books?id=sM0cPQAACAAJ> [Accessed September 2014].
- SHIRAKI, Y., ISHIBASHI, Y., HIRUMA, M., NISHIKAWA, A. & IKEDA, S. 2006. Cytokine secretion profiles of human keratinocytes during *Trichophyton tonsurans* and *Arthroderma benhamiae* infections. *J Med Microbiol*, 55, 1175-85.
- SIMON, M. & GREEN, H. 1984. Participation of membrane-associated proteins in the formation of the cross-linked envelope of the keratinocyte. *Cell*, 36, 827-34.
- SINGH, V. P., BALI, A., SINGH, N. & JAGGI, A. S. 2014. Advanced glycation end products and diabetic complications. *The Korean Journal of Physiology & Pharmacology*, 18, 1-14.
- SMITH, K. & THIBOUTOT, D. 2008. Thematic review series: skin lipids. Sebaceous gland lipids: friend or foe? *Journal of lipid research*, 49, 271-281.
- SNEL, M., JONKER, J. T., SCHOONES, J., LAMB, H., DE ROOS, A., PIJL, H., SMIT, J., MEINDERS, A. & JAZET, I. 2012. Ectopic fat and insulin resistance: pathophysiology and effect of diet and lifestyle interventions. *International journal of endocrinology*, 2012.
- SOLANO, F. 2014. Melanins: Skin Pigments and Much More—Types, Structural Models, Biological Functions, and Formation Routes. *New Journal of Science*, 2014, 1-28.
- SORRELL, J. M. & CAPLAN, A. I. 2004a. Fibroblast heterogeneity: more than skin deep. *Journal of cell science*, 117, 667-675.
- SORRELL, J. M. & CAPLAN, A. I. 2004b. Fibroblast heterogeneity: more than skin deep. *J Cell Sci*, 117, 667-75.
- SPENCE, P. 1999. From genome to drug—optimising the drug discovery process. *Progress in drug research*. Springer.
- SRINIVASAN, M., SEDMAK, D. & JEWELL, S. 2002. Effect of fixatives and tissue processing on the content and integrity of nucleic acids. *The American journal of pathology*, 161, 1961-1971.
- STROBER, W. 2001. Trypan blue exclusion test of cell viability. *Current protocols in immunology*, A. 3B. 1-A. 3B. 2.
- STURM, R. A., BOX, N. F. & RAMSAY, M. 1998. Human pigmentation genetics: the difference is only skin deep. *Bioessays*, 20, 712-721.
- SURWIT, R. S., KUHN, C. M., COCHRANE, C., MCCUBBIN, J. A. & FEINGLOS, M. N. 1988. Diet-induced type II diabetes in C57BL/6J mice. *Diabetes*, 37, 1163-7.
- SWEAT, F., PUCHTLER, H. & ROSENTHAL, S. I. 1964. Sirius Red F3ba as a Stain for Connective Tissue. *Arch Pathol*, 78, 69-72.
- TAKASHIMA, A. 2001. Establishment of fibroblast cultures. *Current Protocols in Cell Biology*, 2.1. 1-2.1. 12.
- TANG, Y., ZHANG, M. J., HELLMANN, J., KOSURI, M., BHATNAGAR, A. & SPITE, M. 2013. Proresolution therapy for the treatment of delayed healing of diabetic wounds. *Diabetes*, 62, 618-627.
- TAYLOR, C. R., SHI, S.-R., BARR, N. & WU, N. 2002. Techniques of immunohistochemistry: principles, pitfalls, and standardization. *Diagnostic immunohistochemistry*, 2, 3-44.
- TAYLOR, K. R., COSTANZO, A. E. & JAMESON, J. M. 2011. Dysfunctional $\gamma\delta$ T cells contribute to impaired keratinocyte homeostasis in mouse models of obesity. *Journal of Investigative Dermatology*, 131, 2409-2418.

- TAYLOR, S. E., REPETTI, R. L. & SEEMAN, T. 1997. Health psychology: what is an unhealthy environment and how does it get under the skin? *Annual review of psychology*, 48, 411-447.
- TCHKONIA, T., MORBECK, D. E., VON ZGLINICKI, T., VAN DEURSEN, J., LUSTGARTEN, J., SCRABLE, H., KHOSLA, S., JENSEN, M. D. & KIRKLAND, J. L. 2010. Fat tissue, aging, and cellular senescence. *Aging cell*, 9, 667-684.
- TCHORSH-YUTSIS, D., ZLOTNIKOV KLIONSKY, Y., BACHAR-LUSTIG, E., ARONOVICH, A., FEINE, I., SHEZEN, E., ROSEN, C., BITCOVER, R., EVENTOV-FRIEDMAN, S., KATCHMAN, H., ZANGI, L., TAL, O., COHEN, S. & REISNER, Y. 2011. Embryonic pig pancreatic tissue for the treatment of diabetes: potential role of immune suppression with "off-the-shelf" third-party regulatory T cells. *Transplantation*, 91, 398-405.
- TELLYESNICKSKY, K. 1926. Article on 'Fixation'. In: KRAUSE'S, R. (ed.) *Enzyklopädie der mikroskopischen Technik*. Berlin (Urban & Schwarzenberg).
- TERASHI, H., IZUMI, K., DEVECI, M., RHODES, L. M. & MARCELO, C. L. 2005. High glucose inhibits human epidermal keratinocyte proliferation for cellular studies on diabetes mellitus. *International wound journal*, 2, 298-304.
- TERSTAPPEN, K. 2008. *Aspects on in vivo imaging techniques for diagnostics of pigmented skin lesions*, Institute of Clinical Sciences. Department of Dermatology and Venereology.
- THOENES, M. M. 2012. Acanthosis nigricans: An opportunity for intervention. *The Journal for Nurse Practitioners*, 8, 621-625.
- THOMPSON, D., KARPE, F., LAFONTAN, M. & FRAYN, K. 2012. Physical activity and exercise in the regulation of human adipose tissue physiology. *Physiol Rev*, 92, 157-91.
- TIAN, X. Y., WONG, W. T., WANG, N., LU, Y., SAN CHEANG, W., LIU, J., LIU, L., LIU, Y., LEE, S. S.-T. & CHEN, Z. Y. 2012. PPAR δ activation protects endothelial function in diabetic mice. *Diabetes*, 61, 3285-3293.
- TISDALE, P. 2011. *The regulation of metabolic gene expression in humans*. University of Nottingham.
- TRAYHURN, P. 2013a. Hypoxia and adipose tissue function and dysfunction in obesity. *Physiological Reviews*, 93, 1-21.
- TRAYHURN, P. 2013b. Hypoxia and adipose tissue function and dysfunction in obesity. *Physiol Rev*, 93, 1-21.
- TRAYHURN, P., WANG, B. & WOOD, I. S. 2008. Hypoxia in adipose tissue: a basis for the dysregulation of tissue function in obesity? *Br J Nutr*, 100, 227-35.
- TRAYHURN, P. & WOOD, I. S. 2004. Adipokines: inflammation and the pleiotropic role of white adipose tissue. *Br J Nutr*, 92, 347-55.
- TREUTING, P. M. & DINTZIS, S. M. 2011. *Comparative Anatomy and Histology: A Mouse and Human Atlas (Expert Consult)*, Academic Press.
- TROTTIER, V., MARCEAU-FORTIER, G., GERMAIN, L., VINCENT, C. & FRADETTE, J. 2008. IFATS Collection: Using Human Adipose-Derived Stem/Stromal Cells for the Production of New Skin Substitutes. *Stem Cells*, 26, 2713-2723.
- TROUSDALE, R. K., JACOBS, S., SIMHAEE, D. A., WU, J. K. & LUSTBADER, J. W. 2009. Wound Closure and Metabolic Parameter Variability in a *db/db* Mouse Model for Diabetic Ulcers. *Journal of Surgical Research*, 151, 100-107.
- TUOMILEHTO, J. 2013. The emerging global epidemic of type 1 diabetes. *Current diabetes reports*, 13, 795-804.

- VAN HATTEM, S., BOOTSMA, A. H. & THIO, H. B. 2008. Skin manifestations of diabetes. *Cleveland Clinic Journal of Medicine*, 75, 772-787.
- VARANI, J., DAME, M. K., RITTIE, L., FLIGIEL, S. E., KANG, S., FISHER, G. J. & VOORHEES, J. J. 2006a. Decreased collagen production in chronologically aged skin: roles of age-dependent alteration in fibroblast function and defective mechanical stimulation. *The American journal of pathology*, 168, 1861-1868.
- VARANI, J., DAME, M. K., RITTIE, L., FLIGIEL, S. E., KANG, S., FISHER, G. J. & VOORHEES, J. J. 2006b. Decreased collagen production in chronologically aged skin: roles of age-dependent alteration in fibroblast function and defective mechanical stimulation. *Am J Pathol*, 168, 1861-8.
- VARANI, J., PERONE, P., MERFERT, M. G., MOON, S. E., LARKIN, D. & STEVENS, M. J. 2002. All-trans retinoic acid improves structure and function of diabetic rat skin in organ culture. *Diabetes*, 51, 3510-3516.
- VARANI, J., WARNER, R. L., GHARAEI-KERMANI, M., PHAN, S. H., KANG, S., CHUNG, J. H., WANG, Z. Q., DATTA, S. C., FISHER, G. J. & VOORHEES, J. J. 2000. Vitamin A antagonizes decreased cell growth and elevated collagen-degrading matrix metalloproteinases and stimulates collagen accumulation in naturally aged human skin. *J Invest Dermatol*, 114, 480-6.
- VARGHESE, B., VERHAGEN, R., HUSSAIN, A., BOUDOT, C., TAI, Q., DING, S., HOLZ, J. A. & UZUNBAJAKAVA, N. E. 2013. Quantitative Assessment of Birefringent Skin Structures in Scattered Light Confocal Imaging Using Radially Polarized Light. *Sensors*, 13, 12527-12535.
- VIRTANEN, K. A., LÖNNROTH, P., PARKKOLA, R., PELTONIEMI, P., ASOLA, M., VILJANEN, T., TOLVANEN, T., KNUUTI, J., RÖNNEMAA, T. & HUUPPONEN, R. 2002. Glucose uptake and perfusion in subcutaneous and visceral adipose tissue during insulin stimulation in nonobese and obese humans. *The Journal of Clinical Endocrinology & Metabolism*, 87, 3902-3910.
- WAGNER, E. F., SCHONTHALER, H. B., GUINEA-VINIEGRA, J. & TSCHACHLER, E. 2010. Psoriasis: what we have learned from mouse models. *Nature Reviews Rheumatology*, 6, 704-714.
- WALLER, J. M. & MAIBACH, H. I. 2005. Age and skin structure and function, a quantitative approach (I): blood flow, pH, thickness, and ultrasound echogenicity. *Skin Research and Technology*, 11, 221-235.
- WALLI, R. 2009. *The role of lipid rafts in UVA radiation-induced signal transduction in human keratinocytes*. Düsseldorf, Univ., Diss., 2010.
- WANG, J., DODD, C., SHANKOWSKY, H. A., SCOTT, P. G. & TREDGET, E. E. 2008. Deep dermal fibroblasts contribute to hypertrophic scarring. *Laboratory investigation*, 88, 1278-1290.
- WANG, Y.-I. & SANDERS, J. 2005. Skin model studies. *Pressure ulcer research*. Springer.
- WARGENT, E., ZAIBI, M., SILVESTRI, C., HISLOP, D., STOCKER, C., STOTT, C., GUY, G., DUNCAN, M., DI MARZO, V. & CAWTHORNE, M. 2013. The cannabinoid Δ^9 -tetrahydrocannabinavarin (THCV) ameliorates insulin sensitivity in two mouse models of obesity. *Nutrition & diabetes*, 3, e68.
- WATT, F. M. & FUJIWARA, H. 2011. Cell-extracellular matrix interactions in normal and diseased skin. *Cold Spring Harbor perspectives in biology*, 3, a005124.
- WEIGHT, W. Overweight and Obesity Statistics.
- WERNER, M., CHOTT, A., FABIANO, A. & BATTIFORA, H. 2000. Effect of Formalin Tissue Fixation and Processing on Immunohistochemistry. *The American Journal of Surgical Pathology*, 24, 1016-1019.

- WIKRAMANAYAKE, T. C., STOJADINOVIC, O. & TOMIC-CANIC, M. 2014. Epidermal Differentiation in Barrier Maintenance and Wound Healing. *Advances in wound care*, 3, 272-280.
- WILHELM, K.-P., ZHAI, H. & MAIBACH, H. I. 2010. *Dermatotoxicology*, CRC Press.
- WOJCIECHOWICZ, K., GLEDHILL, K., AMBLER, C. A., MANNING, C. B. & JAHODA, C. A. 2013. Development of the mouse dermal adipose layer occurs independently of subcutaneous adipose tissue and is marked by restricted early expression of FABP4. *PloS one*, 8, e59811.
- WONG, V. W., SORKIN, M., GLOTZBACH, J. P., LONGAKER, M. T. & GURTNER, G. C. 2010. Surgical approaches to create murine models of human wound healing. *BioMed Research International*, 2011.
- WOOD, A. & KELLY, D. 2010. Skin microbiology, body odor, and methylotrophic bacteria. *Handbook of Hydrocarbon and Lipid Microbiology*. Springer.
- WU, C.-C., SYTWU, H.-K., LU, K.-C. & LIN, Y.-F. 2011. Role of T cells in type 2 diabetic nephropathy. *Experimental diabetes research*, 2011.
- XU, H., BARNES, G. T., YANG, Q., TAN, G., YANG, D., CHOU, C. J., SOLE, J., NICHOLS, A., ROSS, J. S. & TARTAGLIA, L. A. 2003. Chronic inflammation in fat plays a crucial role in the development of obesity-related insulin resistance. *The Journal of clinical investigation*, 112, 1821-1830.
- YAMAMOTO, Y., SOUSSE, L. E., ENKHBAATAR, P., KRAFT, E. R., DEYO, D. J., WRIGHT, C. L., TAYLOR, A., TRABER, M. G., COX, R. A. & HAWKINS, H. K. 2012. Gamma-Tocopherol Nebulization Decreases Oxidative Stress, Arginase Activity, and Collagen Deposition after Burn and Smoke Inhalation in the Ovine Model. *Shock (Augusta, Ga.)*, 38, 671.
- YE, X., TONG, Z., DANG, Y., TU, Q., WENG, Y., LIU, J. & ZHANG, Z. 2010. Effects of blood glucose fluctuation on skin biophysical properties, structure and antioxidant status in an animal model. *Clinical and experimental dermatology*, 35, 78-82.
- YOSIPOVITCH, G., DEVORE, A. & DAWN, A. 2007. Obesity and the skin: skin physiology and skin manifestations of obesity. *Journal of the American Academy of Dermatology*, 56, 901-916.
- ZGRAGGEN, S., OCHSENBEIN, A. M. & DETMAR, M. 2013. An important role of blood and lymphatic vessels in inflammation and allergy. *Journal of allergy*, 2013.
- ZHANG, P., ZHANG, X., BROWN, J., VISTISEN, D., SICREE, R., SHAW, J. & NICHOLS, G. 2010. Global healthcare expenditure on diabetes for 2010 and 2030. *Diabetes Res Clin Pract*, 87, 293-301.

Appendices

APPENDIX 1: Routinely used processing protocol

STATION	REAGENT	TIME (mins)
1	Formalin + 70 % EtOH	30
2	70% EtOH	30
3	80%	90
4	90%	60
5	100%	60
6	100%	90
7	100%	120
8	Xylene (Histoclear)	30
9	Xylene (Histoclear)	90
10	Xylene (Histoclear)	60
11	Wax	90
12	Wax	60

APPENDIX 2: Short processing protocol

STATION	REAGENT	TIME (min)
1	50% EtOH , 10% Formalin	10
2	70% EtOH(40°C)	10
3	80% EtOH(40°C)	10
4	90% EtOH(40°C)	10
5	100% EtOH(40°C)	10
6	100% EtOH(40°C)	10
7	100% EtOH(40°C)	10
8	Histoclear(40°C)	10
9	Histoclear(40°C)	10
10	Histoclear(40°C)	10
11	Paraffin wax (80°C)	10
12	Paraffin wax (80°C)	10

APPENDIX 3: Long processing protocol

STATION	REAGENT	TIME (min)
1	50% EtOH	60
2	70% EtOH	30
3	80% EtOH	30
4	90% EtOH	60
5	100% EtOH	60
6	100% EtOH	60
7	100% EtOH	60
8	Histoclear	15
9	Histoclear	30
10	Histoclear	60
11	Paraffin wax (60°C)	15
12	Paraffin wax (60°C)	90

Tissue samples undergo automated processing during 12 steps involving dehydration (50%-100% ethanol), clearing (xylene) and paraffin impregnation in preheated (60°C) paraffin in the Leica TP1020 tissue processor (Leica Microsystems, Germany). The vacuum function was used during processing to accelerate the speed of tissue processing (10mM sodium citrate, 0.05% Tween 20, pH6.0).

APPENDIX 4 : Softening agent formula

REAGENT	PERCENTAGE IN PBS
Glycerol	10%
Methanol	20 %
Phenol	5%
Acetone	5%
Triton-X100	0.5%

APPENDIX 5: list of antibodies used in the thesis

ANTIBODIES	COMPANY\CAT#
PCNA (Anti-proliferating Cell Nuclear Antigen)	Sigma p8825 Abcam, ab2426 Santacruz, sc9857
Involucrin	Covance, prb140c
Profilaggrin	Covance, PRB-417P ZYMED S1-2100
CD31	TCS Cellwork, zha-1225 R&D AF 3628
VEGF (Vascular endothelial growth factor)	Abcam ab/1316-100
HIF1-α	Santa Cruz, USA, 1:50
TIMP-1	Santa Cruz, sc-5538 R&D,AF980
CD68	Santa Cruz, sc 9139
Keratin 14	Covance, PRB-155P
RAGE	IHCWorld, IW-PA1069
α-Smooth Muscle antibody	Sigma, A2547

APPENDIX 6: H&E staining protocol

STAGE	REAGENT	DURATION	NOTES
1	Xylene	2x 2 min	Dewaxing
2	100% EtOH	2x 1 min	Rehydration
	90% EtOH	1 min	
	75% EtOH	1 min	
	Running water	1 min	
3	Hematoxylin	10 min	Overstaining
4	Running water	5 min	Rinsing
5	Acid alcohol	30 s	Differentiation
6	Running water	1 min	Rinsing
7	0.1% sodium bicarbonate	30 s	Bluing
8	Running water	5 min	Rinsing
9	Eosin Y	3 min	Counterstaining
10	Running water	5 min	Rinsing
11	90% EtOH	30 s	Dehydration
	100% EtOH	30 s	
12	Xylene 1	2x1 min	Clearing
13	Mountant		Permanent mounting

APPENDIX 7: Sirius Red staining protocol

STAGE	DESCRIPTION	DURATION	NOTE
1	Xylene (2x), x/e, EtOH 100%(2x), EtOH 90% to 70% EtOH	2 min each stage	Rehydration tissues
2	Rinse in distilled H ₂ O	Few seconds	
3	0,1% Sirius Red	60 min at RT	Staining
4	Acid water 2 times (fresh a.w)		
5	100% EtOH (2x), e/x to xylene (2x)	30 s each	Dehydration
6	Permanent mount	As quick as possible	Mounting

Sirius Red (Direct Red 80) in saturated picric acid (0.1%picrosirius:1g Sirius red per 1l of saturated picric acid). Acid water: 5ml glacial acetic acid in 1l distilled water.

APPENDIX 8: Giemsa and Orcein protocol

Stage	REAGENTS	DURATION	NOTE
1	Xylene (2x), x/e, EtOH 100% (2x), EtOH 90% to 70% EtOH	2 min each stage	Dehydration
2	0,1% Orcein in acid alcohol	1 h at 25°C	Staining the elastic fibres
3	Running tap water	5 min	
4	Acid alcohol	30 s	Destaining/ differentiation
5	Running tap water	Few s	
6	Giemsa	1 h at 56°C	Staining immune cells
7	Running tap water	5 min	
8	95% EtOH/Eosin Y	1 min	Staining collagen fibres
9	100% EtOH to xylene	30 s each stage	Dehydration
10	Mountant	2 min each stage	mounting

Giemsa stock solution: dissolve 7.36g Giemsa in 500ml warm glycerol (~50°C) for 30 minutes with occasional mixing. Cool, add 500ml methanol. Filter before use. Store at RT. Dilute 1ml stock solution in 45ml H₂O.

APPENDIX 9: RIPA buffer

50mM	Tris-HCl, pH 7.4	25 ml of 1M
1%	NP-40	5ml
0.5%	Na-deoxycholate	2.5 g
0.1%	SDS	0.5 g
150mM	NaCl	15 ml of 5M
2mM	EDTA	2 ml of 0.5M
50mM	NaF	1.05 g

Final volume 500 ml. Store at 4°C. Add the protease/phosphatase inhibitors immediately prior use.